MONITORING OF BIOMOLECULAR INTERACTIONS FOR NUCLEIC ACIDS RESEARCH

DOCTORAL DISSERTATION

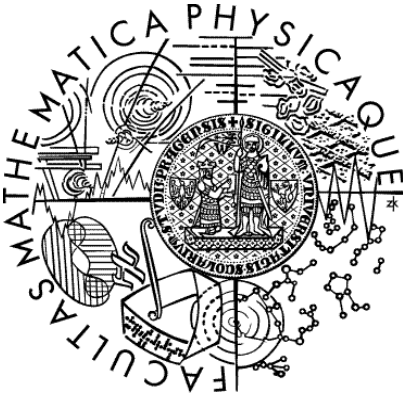

Hana Vaisocherová

Supervisor: **Prof. Josef Štěpánek, PhD.**

Charles University in Prague,
Faculty of Mathematics and Physics
Institute of Physics

Associate Supervisor: **Assoc. Prof. Jiří Homola, PhD.**

Institute of Radio Engineering and Electronics,
Academy of Sciences of the Czech Republic, Prague

2006

ACKNOWLEDGEMENTS:

I would like to express my gratitude to my supervisor Prof. Josef Štěpánek from the Institute of Physics of the Charles University for his continuous help, encouragement and kind understanding. My appreciation goes to Dr. Jiří Homola from the Institute of Radio Engineering and Electronics of the Academy of Sciences of the Czech Republic for his support and encouragement during the course of my doctoral work.

I would like to thank those I have worked with during the course of my research activities. At the Institute of Radio Engineering and Electronics: Kateřina Hegnerová, Markéta Lochmanová, Marek Piliarik, Jakub Dostálek, Jan Habr, Dr. Kamila Moquin, Alice Zítová, Dr. Radan Slavík, Dr. Petr Tobiška and others. At the Institute of Macromolecular Chemistry of the Academy of Sciences of the Czech Republic: Dr. Eduard Brynda. At the Faculty of Sciences of the Charles University: Dr. Jiří Škvor. At the University of Washington in Seattle: Dr. Christina Boozer, John Ladd. At the Institute of Organic Chemistry and Biochemistry of the Academy of Sciences of the Czech Republic: Dr. Ivan Rosenberg and Dr. Jan Snášel. I am also grateful to Dr. Ivan Rosenberg for helpful discussions during the course of biosensor experimental work.

I give a note of gratitude to my high school teachers, especially Dr. Zdenko Ternbach (physics and chemistry), Dr. Truda Kopková (mathematics), Dr. Karel Sobota (biology and geography) for motivating me to study biophysics.

Special thanks to my family for their continued encouragement.

TABLE OF CONTENTS:

1. Introduction

1.1 Nucleic Acids Interactions

The genetic information essential for life functions, reproduction and development of organisms is stored in base sequences of polynucleotide molecules. Transfer of the genetic information is carried out in the processes of deoxyribonucleic acid (DNA) replication and transcription into ribonucleic acid (RNA) (Figure 1). Hybridization of complementary nucleotide sequences is a crucial step in these processes.

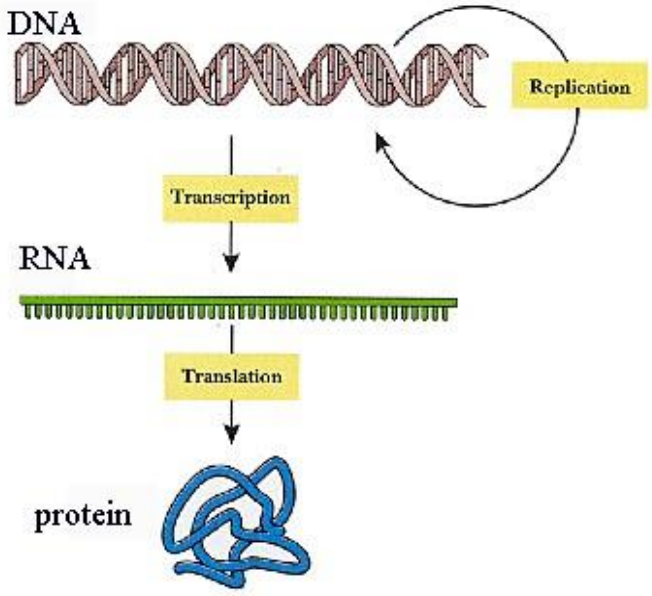

Fig. 1 Scheme of gene transfer processes in living cells.

The skeleton of NA strand is formed by a sugar-phosphate backbone and heterocyclic bases that are attached to the sugar moiety (ribose and 2'-deoxyribose for RNA and DNA, respectively) via an N-glycosidic bond. Four major bases are present in the DNA structure: adenine (A), thymine (T), guanine (G) and cytosine (C). In RNA structure, the thymine is replaced with uracil (U). The specific base pairing is a key to storage and transfer of genetic information. As it was revealed by James Watson and Francis Crick in 1953 [1], adenine forms a pair only with thymine (by two hydrogen bonds) while guanine binds by three hydrogen bonds cytosine in DNA double-helix (duplex), Figure 2.

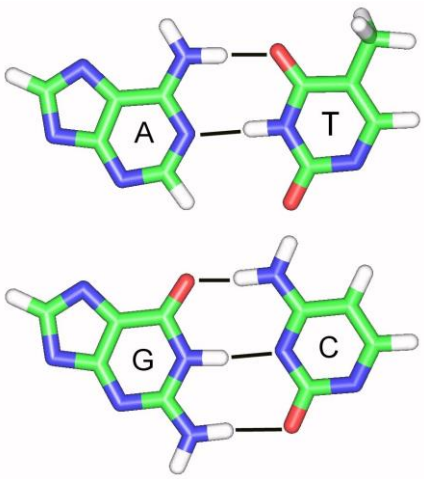

Fig. 2 Scheme of the adenine (A) - thymine (T) and guanine (G) - cytosine (C) specific Watson-Crick base-pairing concept.

Besides the standard Watson-Crick base-pairing found in NA duplexes, other pairing schemes can occur in the multi-strand complexes, e.g., Hoogsteen base pairing. Hoogsteen pairing is present in NA triple helices (triplexes) that are often considered to regulate the gene transcription [2-4]. Triplexes are formed exclusively between homopurine and homopyrimidine strands and can have parallel or antiparallel structures according to the composition and orientation of the third strand [4]. Potential schemes of DNA or RNA triplexes include triplets such as T:A*T, U:A*U or $C:G*C^+$ (Figure 3). Formation of triplexes depends on temperature, pH, concentrations of particular cations and other factors [5, 6]. For example, the parallel-motif triplexes (for instance $C:G*C^+$) require protonation at the N3 position of cytosine residues and are stabilized by low pH and high ionic strength [7].

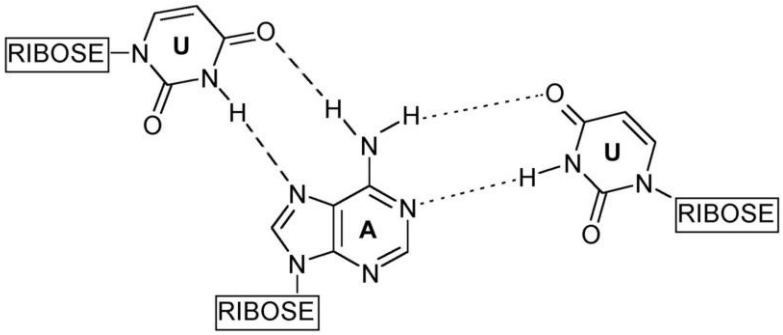

Fig. 3 Base triplet (U:A*U) occurring in RNA triplex structure; dotted lines represent hydrogen bonds of Watson-Crick base-pairing, dashed lines those of Hoogsteen pairing

Hydrogen bonds occurring in the base pairs play a fundamental role in the functionality of nucleic acids (NA), but they are not the main stabilizing factor of the NA three-dimensional structure. Their structure is stabilized mainly by the base stacking, and by ionic and hydrophobic interactions with the aqueous environment. The geometry of nucleic

acids in solution is though not rigid and it is influenced by numerous factors like the base sequence, NA concentration, length of the NA strands, temperature, ionic strength, *etc* [5, 6, 8]. In general, we distinguish several basic canonical forms of NA duplexes: prevailing is the right-handed B-form for DNA and A-form for RNA, respectively (Figure 4).

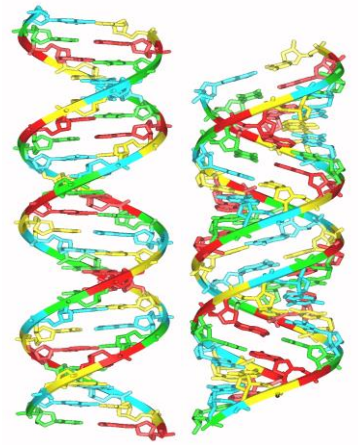

Fig. 4 Basic canonical forms of nucleic acid duplexes: B-DNA (left) and A-RNA (right).

Under particular conditions the organized structure completely disappears and the NA complex is denatured. In particular, NA complexes can be destroyed with increasing temperature leading to a complete separation of single strands. This process has features of a phase transition hence it is referred to as "melting" of NA complexes. Melting temperature (T_m) of complexes is defined as the temperature at which half of the complexes are disintegrated. Melting temperature is commonly employed as a basic parameter characterizing the stability of NA complexes [9].

The hybridization reaction is nowadays routinely exploited in numerous molecular biology techniques such as polymerase chain reaction (PCR) or blotting techniques [10, 11]. These methods rely on highly sensitive and specific detection of hybridization between short synthetic oligonucleotide (ON) probe and target nucleic acid sequence. Using common instruments applied in such techniques, only the final NA complex is detected and the actual process of hybridization cannot be monitored. Moreover for a majority of such assays, a radioactive or fluorescent labeling is required within the read-out system. This increases the cost and the time of the analyzing procedure. Some labels can also interfere with the interaction under study and thus lead to less correct or even false results. Further development of NA techniques obligates detailed knowledge of the hybridization reaction. There is still a search for sensitive real-time methods that enable monitoring of the hybridization process without need of any additive labeling.

1.2 Gene targeting therapies

High research interest has recently been focused on the development of strategies for gene therapy that basically rely on oligonucleotide hybridization. The standard drugs nowadays act at the protein level. The mechanism of their action is based on interrupting the target disease-specific protein functionality. As the 3D structure and function of proteins are very complex, the mechanism of therapeutic effect of many current drugs is still unclear [12]. Current methods for potential drugs development such as combinatorial chemistry or parallel synthesis generate tens of thousands of probable protein-target drug molecules per particular viral, bacterial or malignant disease. Thus the libraries of compounds must be screened to select potential candidates for further development. This process is time consuming and prolongs the costs [13].

Opposite to that, gene-targeting therapies utilizing short synthetic oligonucleotides (ONs) could be more efficient, sensitive, and more universal in combating viral and malignant diseases [14]. The principle of such therapies is to block the synthesis of protein that is essential for growth of malignant cell or for particular virus reproduction at the early stage of this protein synthesis - at the nucleic acids level. The most common concepts of gene-targeting therapy include antigene and antisense therapies. Antigene strategies pursue the gene targeting by triple-helix-forming oligonucleotides (TFOs) [15]. Anti-messenger RNA conceptions comprise the use of artificial ribozymes [16] and so-called antisense oligonucleotides [17] with a complementary base sequence to the target mRNA region (Figure 5). The aptamers are short DNA or RNA oligomers that can bind to a protein with high affinity and specificity and thus can disable the protein function as well [18].

Since the first observations of the antiviral effect of selected oligonucleotides against Rous sarcoma virus in the work of Zamecnik et al. two decades ago [19], the antisense approach has become the most popular one [17, 20] among these strategies and the research has been focused on that. The successful antisense oligonucleotides must meet the requirements as follows: (i) the ability to hybridize with the target sequence, (ii) satisfactory resistance against nucleases, (iii) the ability to penetrate into the cells through cell membranes to the target, and (iv) the ability to elicit RNase H activity [14, 17]. As the natural phosphodiester ONs cannot meet the requirement for intracellular stability, the modification of ON structure is necessary. The chemists have offered a variety of the ON analogs whereas the modifications of internucleotide linkage have been shown to be the most promising [12]. The phosphorothioate oligomers as the first generation of antisense oligonucleotides [17, 21, 22] have reached the clinical trials level and practical use [20, 23]. But the lower specificity in comparison with the natural ONs, and some other unwanted side effects of phosphorothioate analogs have been reported [24, 25]. Other ON analogs such as the compounds consisting of both 2'-*O*-methyl and phosphorothioate units have reached the

clinical trials level as the antisense oligonucleotides of the second or the third generation [20, 26, 27]. However, there is still a continuous search for another antisense oligonucleotide with novel chemical composition that will be optimal for wide clinical use.

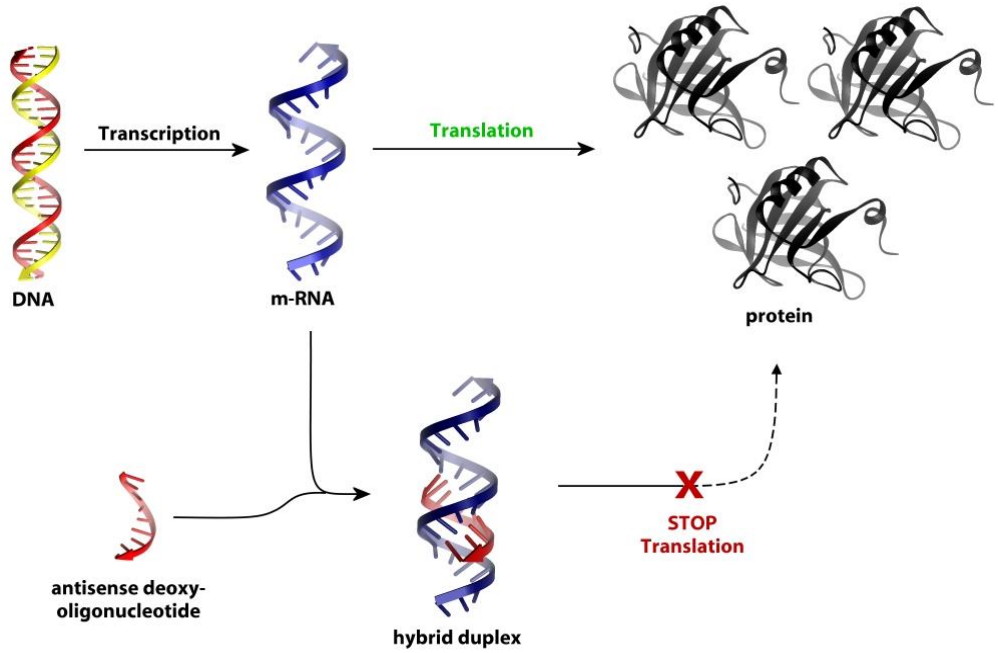

Fig. 5 Principle of the antisense strategy: binding of a short antisense ON to target mRNA sequence blocks the gene expression.

1.3 Surface Plasmon Resonance Method

Oligonucleotide (ON) hybridization can be in principle studied in solution or using solid-phase based methods. The common approaches investigating ON hybridization in solution such as optical spectroscopy (ultra-violet UV [28, 29], circular dichroism CD [30], fluorescence [31, 32] and Raman spectroscopy [8]), or other methods, e.g., calorimetry [30] or molecular modeling [28, 33] can either provide an useful information on the structural features of formed complexes [8] or enable to predict the complex stability. Nevertheless it is not possible to monitor the actual process of the hybridization and thus to determine kinetic parameters of the reactions by using standard devices.

The hybridization has been studied in solid phase using different matrices such as polyacrylamide gel [34], nylon membranes [10] or glass [35]. The interest in a solid-phase detection of ONs, particularly in reaction between the single-stranded oligonucleotide probe immobilized on the surface and the complementary target strand in solution has significantly

increased since the development of the first DNA chip [36]. This technology enables simultaneous detection of hundreds to thousands hybridization reactions in an array format. Nowadays, the advances in photolithographic, spotting and other array techniques allow for parallel monitoring of up to thousands of DNA hybridization reactions with the lowest concentration limit of ON detection (LOD) at femtomolar level [37]. However, such sensitive DNA or RNA microarrays still require fluorescent or radioactive labeling [31, 32].

Biosensor technology can meet the requirements for sensitive specific real-time and label-free monitoring of biomolecular interactions involving hybridization reaction and thus it is of a huge interest of current research. In past years, many examples of use of biosensor technology for detection of biological or chemical analytes and for studying various biomolecular interactions can be found [38-41]. Among other sensor technologies, e.g., those based on electrochemical [42] or piezoelectric principle of action [43], the optical biosensors are advantageous because of their high sensitivity. Next advantage of optical sensor measurements is that they do not require any electrical signal in a sensing area and cannot be perturbed by electric or magnetic fields [44-46]. Optical biosensors offer a universal platform for study of various biological or chemical molecules and their interactions.

Surface plasmon resonance (SPR) biosensors have been significantly improved within the family of label-free optical biosensors in many aspects including the detection limit, microfluidics, immobilization methods, sample handling, and data analysis. Nowadays, SPR biosensors represent the most widely used label-free optical biosensors; numerous commercial SPR instruments have been extensively produced and sold. Various platforms of SPR biosensors such as array-format based SPR imaging for parallel monitoring of many reactions or portable SPR sensors for the field use have been developed and optimized for particular applications [47, 48]. Overwhelming amount of research papers prove that modern SPR biosensors enable highly sensitive, rapid, and label-free detection of various biomolecules [49-51]. Moreover, the kinetics of interaction can be monitored due to real-time regime of the measurement [52, 53]. These advantages make SPR biosensors excellent candidates for investigating NA interactions such as oligonucleotide hybridization processes or NA-enzyme interactions.

The surface plasmon resonance biosensors are based on measuring changes in properties of an optical wave excited at a metal-dielectric interface. This wave represents a special mode of electromagnetic field - surface plasmon polariton (SPP) – that propagates along the surface of a thin metal film. The commonly used metal is gold due to its chemical stability. Intensity of the SPP electromagnetic field decays exponentially from the metal surface to an adjacent medium. A change of the refractive index due to the binding of analyte molecules to biomolecular recognition elements immobilized on the metal surface influence the SPP propagation constant [54]. SPR biosensor measures the changes in the propagation

constant of the SPP and thus it determines the relative amount of bound analyte on the biosensor surface.

The SPR biosensor utilizes measurement of one of the characteristics of SPP-exciting light wave that is modified by the changes in the SPP propagation constant. Depending on the particular measured parameter, the SPR sensors are classified as sensors with angular, wavelength, intensity, phase, or polarization modulation [54].

One of the successful strategies of SP excitation is based on attenuated total reflection (ATR) in a prism coupler, Figure 6 [54]. In SPR sensors with wavelength modulation, a beam of polychromatic light incidents on the metal film under a fixed angle of incidence and excites an SPP (Figure 6). The propagation constant of the SPP is characterized by measuring the intensity of reflected light at various wavelengths and determining the wavelength at which the strongest coupling with SPP occurs (mode of highest attenuation of the total reflection).

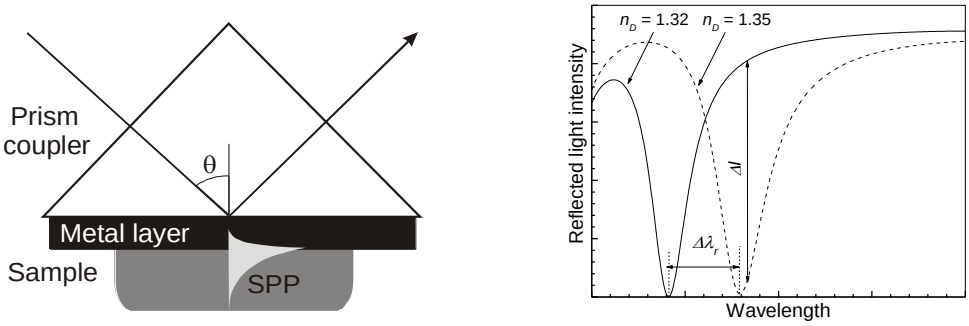

Fig. 6 Left: Excitation of the surface plasmons via prism coupler. Right: Intensity of reflected light as a function of wavelength for a fixed angle of incidence (curves for two different refractive indices of the sample).

The shift in resonant wavelength is proportional to the refractive index change at the sensor surface. An SPR-sensorgram of the analyte binding to receptor immobilized on the sensor surface is shown in Figure 7 as a typical plot of the shift in sensor response nanometers versus time. Three phases of the single measurement can be distinguished: (1) washing the sensor surface with buffer till the stable baseline is achieved (Fig. 7, phase I.), (2) flowing with solution of analyte over the sensor surface - complex formation with immobilized biomolecular partner is monitored (Fig. 7, phase II.), (3) washing the sensor surface with the same buffer as before the analyte injection – dissociation of complexes can be measured (Fig 7, phase III.). The amount of bound analyte at the sensor surface is determined as the difference in the sensor response nanometers between the equilibrium level after washing the bound surface with buffer (at the end of phase III.) and the baseline level

obtained when the same buffer was flowed before the injection of the analyte solution (at the end of phase I.).

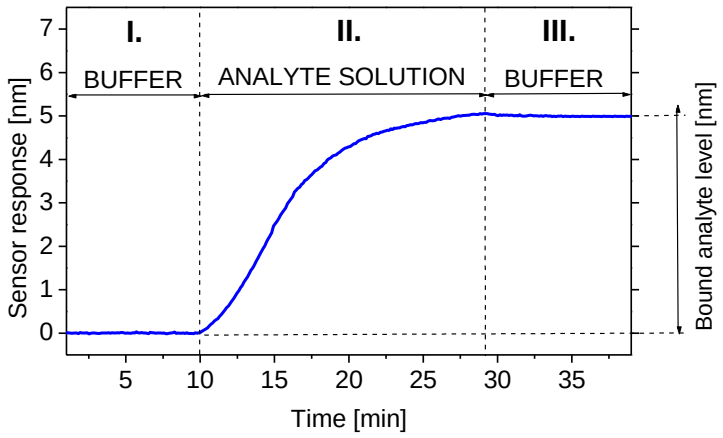

Fig. 7 Typical SPR sensorgram corresponding to real-time measurement of analyte binding to functionalized sensor surface. In the first phase, the functionalized sensor surface is washed with buffer (I.), then the solution of analyte is injected and the biomolecular complex formation is monitored (II.), washing the solution with the same buffer as it was used in the phase I. to measure potential dissociation of complexes and to determine the level of tightly bound analyte.

The sensor response can be calibrated to provide the surface concentration of bound molecules. The calibration coefficient is proportional to their molar weight [55] and depends on the resonant wavelength.

For the majority of experiments mentioned in this dissertation, four-channel or eight-channel SPR sensors based on wavelength modulation [56] and wavelength division multiplexing (WDM) [57, 58], were used. These sensors were developed at the Department of Optical Sensors of the Institute of Radio Engineering and Electronics of the Academy of Sciences of the Czech Republic. The eight-channel SPR sensor combined wavelength division multiplexing of two serially ordered sensing channels in a special sensing element with four parallel light beams (Figure 8) to yield the total of eight sensing channels.

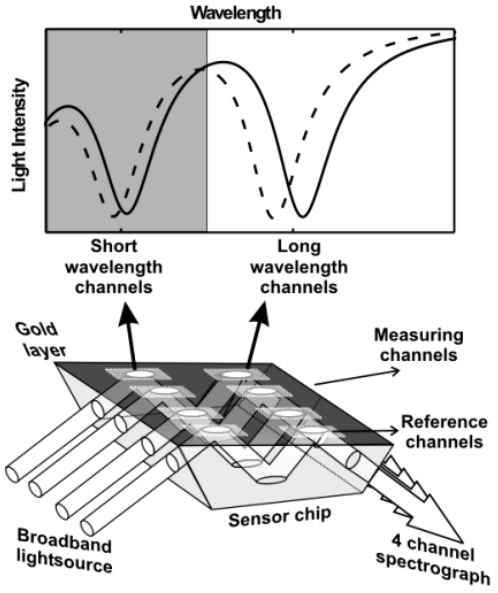

Fig. 8 Scheme of an eight-channel SPR sensor with four parallel light beams and the wavelength division multiplexing (WDM) of sensing channels (lower graph); Spectrum of transmitted light with two SPR dips before (dashed line) and after the binding (solid line) (upper graph).

Broadband light from a halogen lamp was collimated, polarized and then introduced into the WDM-SPR sensing element interfaced with a chip made of a glass coated by an adhesion-promoting titanium film (thickness - 2 nm) and a gold film (thickness - 55 nm). Upon the first incidence on a thin gold film, each light beam excited a surface plasmon at a certain wavelength (~ 650 nm and ~ 750 for eight-channel and four-channel system, respectively). In the eight-channel system, the reflected light was redirected towards the gold film at a different angle of incidence and excited a surface plasmon at another wavelength (~800 nm). The sequential excitation of the surface plasmons generated two narrow dips in the spectrum of light leaving the sensing element (Figure 8). Finally the reflected light was collected into a four optical fibers and coupled to a four-channel spectrograph. Acquired spectra were analyzed in real time by an home-made software package that allowed determination of the resonant wavelength for each sensing channel [59]. A flow-cell with four or eight separate flow chambers facing each sensing spot was interfaced with the chip to confine the sample during the experiment. The flow chambers were precisely aligned with the zones where the surface plasmons were excited in each sensing channel. The depth of each flow cell was about 50 μm and the volume of each flow-cell chamber was 1-3 μl with respect to the particular flow cell design. A peristaltic pump was used to flow liquid samples over the sensing spots. The overall scheme of the eight-channel SPR instrument is shown in Figure 9.

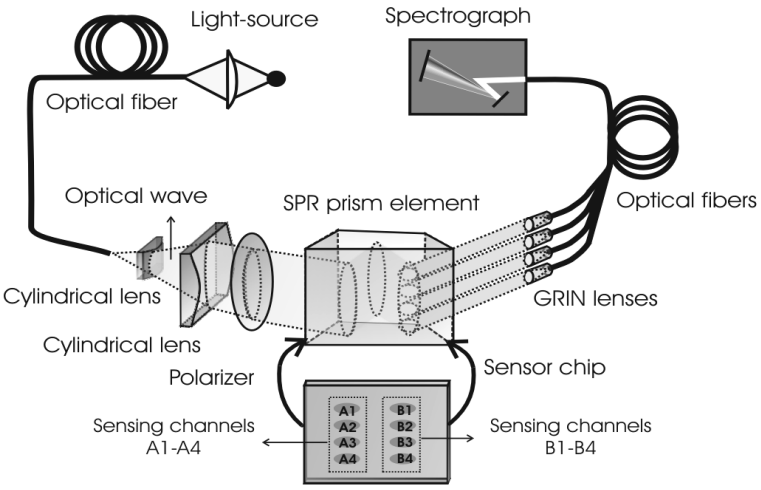

Fig. 9 The eight-channel SPR sensor combining parallel architecture with the wavelength division multiplexing of serially arranged channels.

Within the four-channel SPR biosensor instrument, it was possible to control the temperature at which we monitored the molecular interactions. The temperature was stabilized by a Peltier's thermoelectric element installed into a thermally stabilized body and a precision temperature controller (ILX Lightwave, USA). Liquid samples in thin-walled Peek tubing were flowed across the thermally stabilized body. The optical prism and the sensor chip were also in contact with the stabilized body (Figure 10). The accuracy of the temperature setting was 0.2°C (limited by the accuracy of the thermistor calibration); the range of temperatures used for various experiments was 5-40°C.

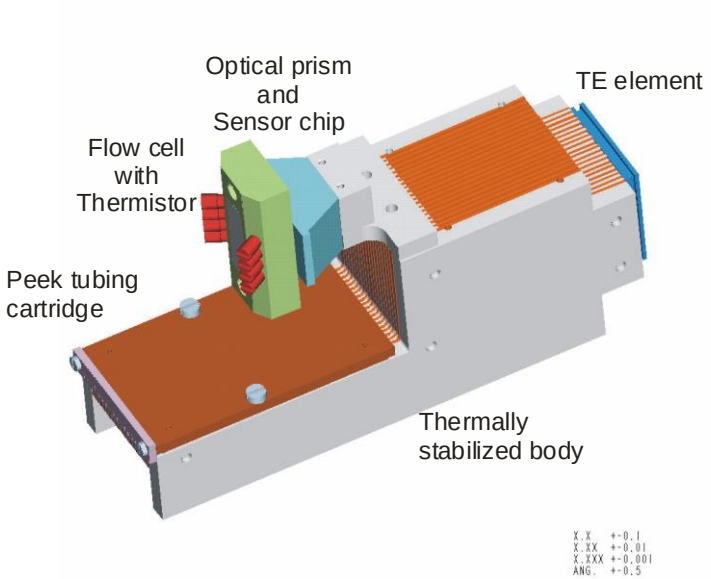

Fig. 10 Scheme of the temperature stabilization set-up used in four-channel SPR sensor

1.4 Art of Immobilization

Besides the optical transducer, a biomolecular recognition element that is attached to the sensor surface makes a heart of the SPR biosensor. Various biomolecules such as antibodies [60], peptides [61], oligonucleotides [62, 63], or molecularly imprinted polymers [64] have been used as the biomolecular recognition elements (receptors). The immobilization of receptors on the sensor surface is a fundamental step of the particular biosensor development because it influences significantly the resulting sensor sensitivity and specificity of the target analyte detection. The important requirements that the immobilization procedures have to fulfill are the defined and sufficiently high density of immobilized receptors with preservation of their biological activity and non-fouling background of the sensor chip surface.

In general, methods of immobilization of biomolecular recognition elements on gold films exploit physico-chemical interactions such as chemisorptions [65], covalent binding [66, 67], hydrophobic and electrostatic interactions [68], and high-affinity biomolecular linker systems (e.g., streptavidin–biotin [69, 70], proteins A or G [71], and complementary oligonucleotides [72]).

The first reports on using SPR technology for (bio) analytical applications were based on simple physical adsorption of protein ligands to the SPR metal surfaces [73]. However, it was soon realized that a more sophisticated approach was needed in order to meet the challenges demanded by the range of sensing applications. Commonly used gold substrate for SPR shows a high tendency for spontaneous adsorption of proteins and other molecules. This passive binding to the metal substrate can result in a loss of the sensor bioactivity. Studies on antibody binding activities in ELISA-type assays after their adsorption on plastic surfaces have shown bioactive levels as low as 2-10 % of the adsorbed amount [74]. These effects can be explained by a reorganization of the ligand to reach the most favorable thermodynamic state. For example, adsorption to hydrophobic surfaces is driven by rearrangement in the ligand conformation that optimizes contact of hydrophobic segments with the substrate. Passive binding to the surface substrate also opens the possibilities for uncontrolled exchange of the ligands during the measurement.

One of the most remarkable techniques in surface chemistry is the spontaneous self-organization of *n*-alkylthiols or disulfides on gold substrate enabling formation of well-ordered arrays. Self-assembled monolayers (SAMs) have been employed in many immobilization methods for spatially controlled attachment of biomolecular recognition elements to surfaces of sensors [50], Figure 11. To achieve a desired surface density of receptors, SAMs mixed of long-chained (n=12 and higher) *n*-alkylthiols terminated with functional group for further attachment of receptors and of short-chained alkylthiols for a non-fouling background have been utilized [75].

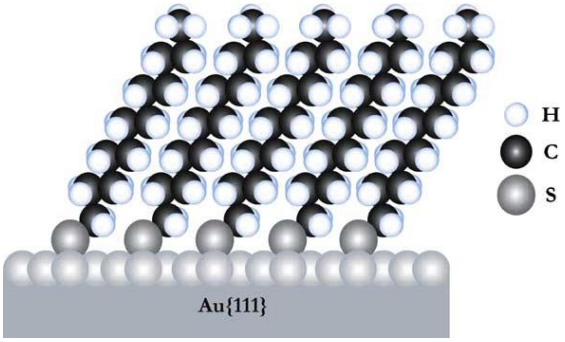

Fig. 11 Scheme of n-dodecanethiolate self-assembled on gold substrate. The assembly is held together by bonds between the sulfur head groups and the gold surface as well as by van der Waals and hydrophobic interactions between neighboring hydrocarbon chains (from [76]).

Several approaches for oligonucleotide immobilization onto gold sensor surface have been suggested. Two most common strategies are as follows: (1) assembly of thiol-terminated oligonucleotide probes directly on the gold surface [63, 77, 78], and (2) coupling of biotinylated probes to the streptavidin assemblies via a non-covalent highly affinitive streptavidin-biotin interaction [50, 79, 80]. Disadvantage of the first type of the immobilization is a need of expensive chemical modification of the immobilized oligonucleotides and a limited length of immobilized probes [63]. Further comparison of immobilization procedures on gold surfaces is available for instance in [70].

An immobilization approach employing the streptavidin – biotin system reaches a good stability due to an extremely high binding affinity ($K_d \sim 10^{-15}$ M) between streptavidin and biotin [81]; each streptavidin molecule contains four equivalent binding pockets for biotin [82], Figure 12.

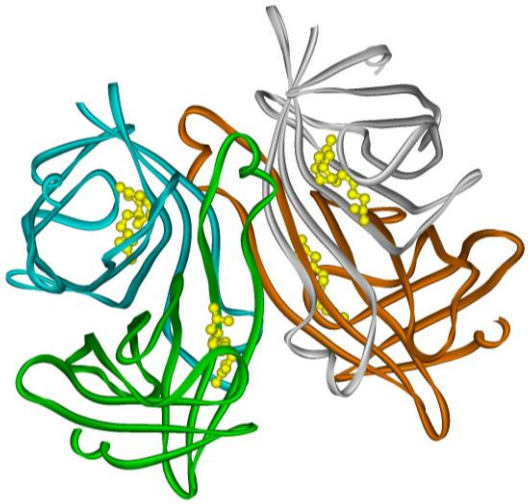

Fig. 12 Scheme of streptavidin tetramer with four biotin molecules (yellow-colored) bound in its four binding pockets.

In the most widespread commercial SPR biosensors (BIAcore™), streptavidin coating is prepared using "amine coupling chemistry" based on covalent attachment of streptavidin by primary amines to activated carboxylate groups of a carboxymethyl group-terminated hydrogel (dextran) matrix [67, 83]. This method (if it starts from the bare gold substrate) is rather laborious and problems with stability [84], non-specific binding [85] and reproducibility [86] were reported. This method is also less suitable for kinetic studies due to undesired additive effect of analyte penetration through the hydrogel matrix that influences the resulting binding kinetics [87-89].

1.5 Kinetic Aspects of SPR Method

The interaction of biomolecules makes a heart of biology. Much research effort has been focused on biomolecular interactions analysis in the areas such as antibody engineering, drug development research or functional protein analysis; these interactions are also vital in industrial applications where manufacture and purification of biomolecules is performed. One of fundamental characteristics of these interactions relies on the kinetics of association and dissociation processes. An interaction between two molecules (A and R) can be described as reaction:

$$A + R \underset{k_d}{\overset{k_a}{\rightleftharpoons}} AR \qquad (1)$$

where AR is the product of their association and k_a, k_d are association and dissociation kinetic rate constants. In this chapter it is assumed that A and R are homogeneous species that interact each other in a monovalent manner. If A and R are mixed, only the association (forward) reaction initially occurs. The AR complex is formed and concentrations of A and R decrease. As a time proceeds and the concentration of AR increases, the reverse reaction (dissociation) becomes significant. After some time (this can take as little as a few seconds or as long as overnight depending on the kinetics and the biological system under study) the rates of the two reactions (forward and reverse) come into equilibrium when overall concentrations of A, R, and AR become stable. These equilibrium concentrations ([A], [R], and [AR]) are related by the Law of Mass Action:

$$[AR]=K_a[A][R] \qquad (2)$$

K_a is termed as an association equilibrium constant. The reciprocal form of K_a is referred to as a dissociation equilibrium constant K_d. The relationship between the equilibrium and the rate constants is given by

$$K_d = 1/K_a = k_d/k_a \quad (3)$$

The equilibrium constant K_d or K_a can in most cases be readily determined. On the opposite, the majority of methods that are today used to determine the kinetic rate constants k_d and k_a are too laborious, too specialized or too inaccurate for a common use. This situation has changed since the advent of new biosensor technologies; the potential for kinetic rate constants determination has thus become one of the greatest advantages of the SPR biosensor technique.

Current kinetic analysis of biosensor data is based on the concept that interaction between monovalent analyte A in solution and immobilized receptor binding site R can be described by the Eq. 1. We further assume that reaction scheme of the interaction between the A and R may be described by pseudo-first-order kinetics in situations where constancy of the analyte concentration is maintained as the result of either continual replenishment by flowing analyte solution along the sensor surface or by the use of a sufficiently high analyte concentration [90].

SPR biosensors measure in time the relative changes in the molecular mass in the close proximity of the sensor surface. The sensor response ξ is directly proportional to the concentration of the bound analyte. To analyze quantitatively the sensor response to interactions between the studied biomolecular analyte and the surface bound receptors, it is necessary to employ a relevant mathematical model [Appendix XII]. Kinetic equation that describes how the amounts of formed/dissociated complexes depend on the local concentrations of the free analyte and the free binding sites of the receptors is for the binding stoichiometry of 1:1 given by [91, 92]

$$\frac{d\gamma}{dt} = k_a \alpha_0 (\beta - \gamma) - k_d \gamma \quad (4)$$

where γ is the amount of the complexes formed per unit time, α_0 is the injected concentration of the analyte [A], and β is the concentration of the receptors on the sensor surface. Thus $\beta - \gamma$ is the concentration of free unbound receptors. Both quantities β and γ are expressed in the same way in terms of local density. Equation (4) was originally derived by Langmuir for interactions at a surface in contact with reactants in solution. In real molecular systems, the processes in the active sensor layer may be more complicated and the sensor response is a superposition of several parallel or consecutive reactions. In these cases it is necessary to employ relevant (and more difficult) kinetic models to achieve a desired accuracy of kinetic rate constants determination.

Although in ideal cases an appropriate kinetic model of molecular interaction is able to completely describe the SPR biosensor response, in reality the effect of hydrodynamic conditions need to be taken into account [91]. In flow cell-based biosensor experiments, the free analyte transport from bulk to the sensor surface is always limited by diffusion. The extent of effect of mass transport limitations on the reactions at the sensor surface is given by comparing the transport throughput to the kinetic rates. Slow analyte transport causes a decrease in its concentration when it is consumed during the association phase and an increase when it is produced during the dissociation phase. As a result, both reactions are slowed down. Rigorous approach to modeling the reaction kinetics at the sensor surface, including the mass transport effects, requires solving of the fundamental partial differential equation (PDE) coupled with the relevant kinetic equations (full model) [93]. This equation can be solved only numerically. The enormously time-consuming computation of full model hampers the use of this approach for routine fits of experimental data. It has been more employed to verify simpler models and/or to confirm the reasonability of rate constants by comparison with experimental data. To enable more convenient and routine analysis of measured sensorgrams, simpler models of mass transport effects have been proposed and implemented into commercial SPR data analyzing software [94, 95].

2. Objectives

The hybridization reaction analysis that is nowadays routinely exploited in molecular biology techniques relies on highly sensitive and specific detection of hybridization between short synthetic oligonucleotide probes and target nucleic acid sequences. Commonly used instruments detect, however, only the final NA complex but cannot monitor the actual process of the hybridization. In addition to that, great majority of current hybridization-based assays require radioactive or fluorescent labeling to visualize the hybridization reaction. Missing detailed information about hybridization reaction of short oligonucleotides still hampers development of NA techniques. For example, the general rules accounting for the NA duplex stability based solely on the relative occurrence of guanine-cytosine base pairs and buffer conditions are not sufficient for short NA chains since the local sequence dependences are not averaged out as in longer sequences [9]. An approach based on nearest neighbor model has been proposed as a promising idea to predict stability of various types of short oligonucleotide complexes [96-98]. The complex stability prediction is though still complicated for systems of hybrid (RNA-DNA) complexes as well as for complexes formed by oligonucleotide analogs with modified chemical structure [8, 28, 99, 100]. Therefore, further development of experimental techniques is desirable with the aim to obtain detailed knowledge of the hybridization reaction. Detailed knowledge of hybridization could benefit many areas such as medical diagnostics, environmental monitoring, food safety or biological warfare detection [101]. Real-time label-free surface plasmon resonance biosensors bring a new insight into these issues and are of growing research interest.

The objective of my PhD work in general was to improve and optimize methodology of SPR bioexperiments for various sensor platforms to set up routine SPR measurements. The goal was to develop robust methods for SPR sensors to be capable of highly sensitive, specific and reproducible detection of biomolecules from pure and complex samples as well as precise analysis of various biomolecular interactions. The experimental work has mainly been carried out at the Department of Optical Sensors of the Institute of Radio Engineering and Electronics of the Academy of Sciences of the Czech Republic, where advanced platforms of SPR sensors have been designed (see part 1.3). In this research, I have also utilized previous experience with investigation of oligonucleotide interactions by methods of optical spectroscopy, performed at the Division of Biomolecular Physics (Institute of Physics, Charles University).

The primary aim of my dissertation work was to design surfaces of receptors including oligonucleotides, antibodies, antigens or other proteins with further potential of sensitive detection of target analytes and kinetic analysis performance. During the first two years of the doctoral study, a systematic work was carried out to improve and optimize procedures of SPR biosensor functionalization. The goal was to immobilize various receptors

on a gold sensor surface with optimal density and reproducibility with preservation of their specific affinity to biomolecular targets. Sensor biomolecular surfaces should also resist the possible non-specific binding of other molecules from analyte solutions.

Next goal of this work was using the developed biomolecular sensor surfaces to detect target analytes with the sensitivity, specificity and reproducibility as high as possible and then to study various biomolecular interactions, mainly those of the NA-NA and NA-enzyme types. The optimized procedure of DNA/RNA chips preparation was employed for study of hybridization properties of synthetic modified oligonucleotides with potential application in antisense therapy. By means of the optimized SPR biosensor chip and

in situ monitoring of the enzyme activity (in particular HIV-1 integrase strand transfer activity) has also been performed.

Due to the comprehensive description of both the methodology research and the obtained results of interaction studies in publications attached to this work, the following section is composed mainly of short comments to the publications with emphasized the novel improvements to previously reported results. The contribution of the own author's work to individual publications is specified.

3. Results

3.1 Immobilization of Proteins on the Surface of SPR Sensor

As mentioned in the Introduction Section, biomolecules can be attached to the gold sensor surface by using different physico-chemical principles. Various immobilization methods of immobilization of biomolecular ligands has been proposed, tested and described in literature [66-68, 74, 83, 102, 103]. While DNA chip technology has been nowadays routinely exploited at the research level as well as in the clinical laboratories, protein chip technology is in the beginning of common laboratory use. The major reason for that is a high complexity of protein molecule (e.g., antibody, antigen, enzyme) that makes requirements for stability, biological activity and orientation of protein receptor layer difficult to meet.

Recent trends in the field of protein immobilization techniques are as follows: (1) full resistance to non-specific binding of other molecules from analyzed solution and thus a formation of non-fouling background on the sensor chip, (2) increasing of the affinity and stability of protein receptors, (3) higher robustness and reproducibility of biomolecular recognition element purification or synthesis, (4) higher robustness and reproducibility of immobilization procedure with respect to its potential application in robot microarrays.

During the course of this doctoral work, a set of functionalization procedures have been investigated for immobilization of various protein ligands such as antibodies, antigens or peptide-albumin conjugates. They included dextran-based "amine coupling chemistry" that is nowadays mostly utilized in commercial SPR sensors (BIAcore™), methods utilized self-assembled monolayers (SAM) of varied composition, method based on electrostatic coupling, protein A or protein G-based immobilization, and others. The method based on formation of mixed self-assembled monolayer (SAM) followed with covalent attachment of ligands via amide bond formation was found to be the most suitable for majority of tested biomolecular systems. Schematic description of the procedure is shown in Figure 13.

Each step of this alkanethiol attachment chemistry was optimized for individual biomolecules. For antibody (IgG typed) immobilization, this method was optimized as follows: The sensor chip slides were first cleaned in UV ozone cleaner for 15 minutes, then washed with milliQ water and dried with nitrogen stream. A molar 7:3 mixture of C_{11}-chained and C_{16}-chained alkanethiols was dissolved in degassed absolute ethanol with a total thiol concentration of 1 mM. These alkanethiols formed a self-assembled monolayer (SAM) on clean gold surface. The C_{16} alkanethiols terminated with a carboxylic group were used to anchor antibody by amide bond formation; C_{11} alkanethiols terminated with a di(ethylene glycol) group were used to form a stable non-fouling background. Sensor chips were immersed in the solution of alkanethiols at temperature of 40°C and then stored in a dark place at room temperature for up to 2 days.

After, the chips were rinsed with ethanol, dried under nitrogen stream, rinsed with water and dried with nitrogen again. The carboxylic terminal groups on the sensor surface were transformed into reactive *N*-hydroxysuccinimidyl esters with N,N,N',N'-Tetramethyl-O-(N-succinimidyl)uronium tetrafluoroborate (TSTU) as follows. A sensor chip was immersed in solution of TSTU in argon degassed DMF (2 mg/ml), then it was sonicated for 5 minutes and shaken for 1 h. The sensor chip was rinsed with water, dried with nitrogen and immediately mounted into the SPR instrument. Antibody attachment was performed *in situ* by flowing sodium acetate buffer (SA) of pH 5.0, which was about one point lower than typical isoelectric point of an antibody molecule. When the baseline was achieved, the SA buffer solution with 10-50 µg/ml of antibody was brought into contact with the sensor surface and the coupling by amide bond formation was occurred.

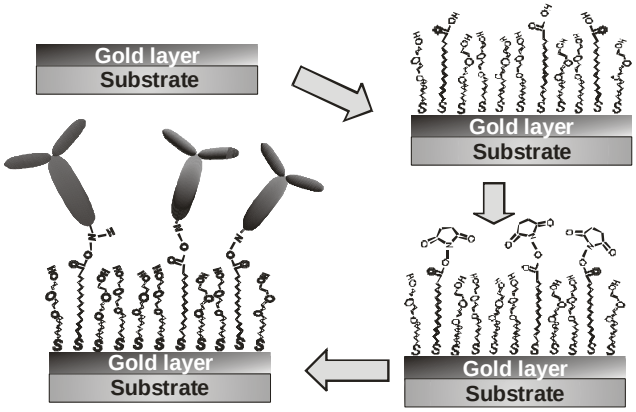

Fig. 13 Immobilization of antibodies to the sensor surface based on mixed SAM and covalent coupling: Clean gold surface was first covered with mixture of carboxylic group and oligo(ethyleneglycol) terminated alkanethiols to form a tight SAM. After activating the carboxylic group by hydroxysuccindiimide, antibody molecules were attached to the SAM by amide bond formation.

This optimized alkanethiol attachment chemistry was employed for immobilization of antibody against human immunoglobulin E on the sensor chip of special design (**Appendix II**, *Measurement Science and Technology* 2006) exploiting simultaneous excitation of two different surface plasmons in a single sensing spot. Four different antibodies (antibody against Immunoglobulin E, antibody against Immunoglobulin G, antibody against horseradish peroxidase, and antibody against human choriogonadotropin) were immobilized using this method with the aim of multianalyte detection (**Appendix III**, *Sensors and Actuators* 2004 and **Appendix IV**, *Methods* 2005).

This immobilization method was also employed to validate applicability of a new high-throughput surface plasmon resonance (SPR) sensor based on combination of SPR imaging with polarization contrast and of a spatially patterned multilayer SPR structure, for detection of bioanalyte, especially for detection of human choriogonadotropin (hCG) with

antibody against hCG immobilized on the sensor surface (**Appendix V**, *Biosensors & Bioelectronics* 2005).

An effort in immobilization methods improvements for protein attachment to the sensor surface came to a head with the work concerning immobilization of peptides for highly sensitive detection of antibody against Epstein-Barr virus (anti-EBNA) in human serum (**Appendix VII**, *Biosensors & Bioelectronics* 2006). Three different immobilization methods were investigated for the attachment of EBNA-1 conjugated with bovine serum albumin (BSA) to obtain high ligand density and minimal loss of peptide immunoactivity: alkanethiol attachment chemistry with covalent coupling of BSA-EBNA conjugates (CHEM I), electrostatic and hydrophobic interactions-based methods (CHEM II and CHEM III, respectively). For purpose of this work, the eight-channel SPR sensor was used. It was found that non-polar amino acids composition of EBNA peptide influenced significantly level of immobilized BSA-EBNA receptors. Optimized alkanethiol attachment chemistry resulting in slightly hydrophilic layer showed the lowest ligand density in contrast with attachment of BSA-EBNA on clean gold via mostly hydrophobic interactions. Although the highest amount of immobilized receptors was obtained using the electrostatic coupling-based immobilization method (CHEM II), the highest immune-activity of EBNA-1 was achieved when immobilized by using chemistry based on physical adsorption of BSA-EBNA conjugates on clean gold surface in physiological conditions (CHEM III). Thus, the hydrophobic interactions-based coupling was the most compatible with the non-polar EBNA structure and preserved the EBNA biological activity. A reference-compensated sensor response to anti-EBNA binding for the series of different antibody concentrations for different immobilization methods is shown in Figure 14.

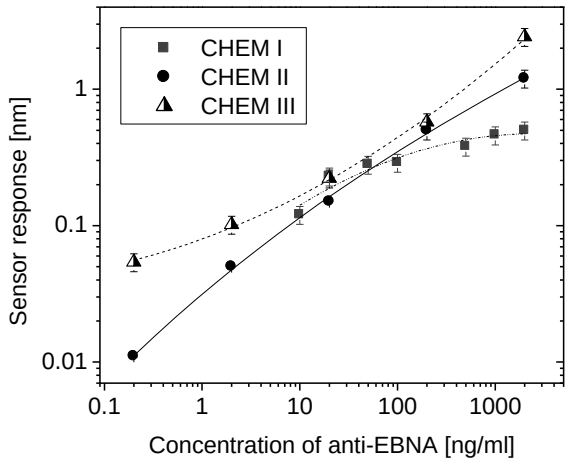

Fig. 14 Sensor response to anti-EBNA binding to EBNA-1 surface in dependence on anti-EBNA concentration that was obtained from spots functionalized with BSA-EBNA conjugates using CHEM I, II and III, respectively.

3.2 Detection of Protein Target Analytes

The sensor chips functionalized with protein receptors using optimized methods of immobilization were used for detection of respective analytes using different platforms of SPR sensors that were developed in the Institute of Radio Engineering and Electronics.

The eight-channel SPR sensor based on spectroscopy of surface plasmons and wavelength division multiplexing was mainly used for the purpose of this doctoral work. This sensor was described in details in the Introduction Section. A model experiment demonstrating potential of this multi-channel sensor for multi-analyte detection was carried out (**Appendix III**, *Sensors and Actuators* 2004). Four different antibodies (antibody against Immunoglobulin E, antibody against Immunoglobulin G, antibody against horseradish peroxidase, and antibody against human choriogonadotropin) with respective antigens were used as a model system. Each type of antibody was immobilized into two sensing spots. It was shown, that sensor responses to the target analyte when it was present alone in the injected solution were fully comparable with those obtained from a complex solution containing also the other three antigens. Our results showed a great potential of the developed eight-channel sensor for simultaneous detection of a series of analytes from complex samples. Figure 15 shows sensor response to different concentrations of analytes when they were detected from pure buffer and from the mixture of all antigens. The binding data for selected antibody-antigen (IgE) system are shown in Figure 16. Results of these experiments are discussed in more details in **Appendix IV**, *Methods* 2005. My contribution to this publication, dealing with description of the currency and future of multi-channel SPR platforms, was in writing the review of immobilization methods as well as in performance of the above mentioned model bioexperiments.

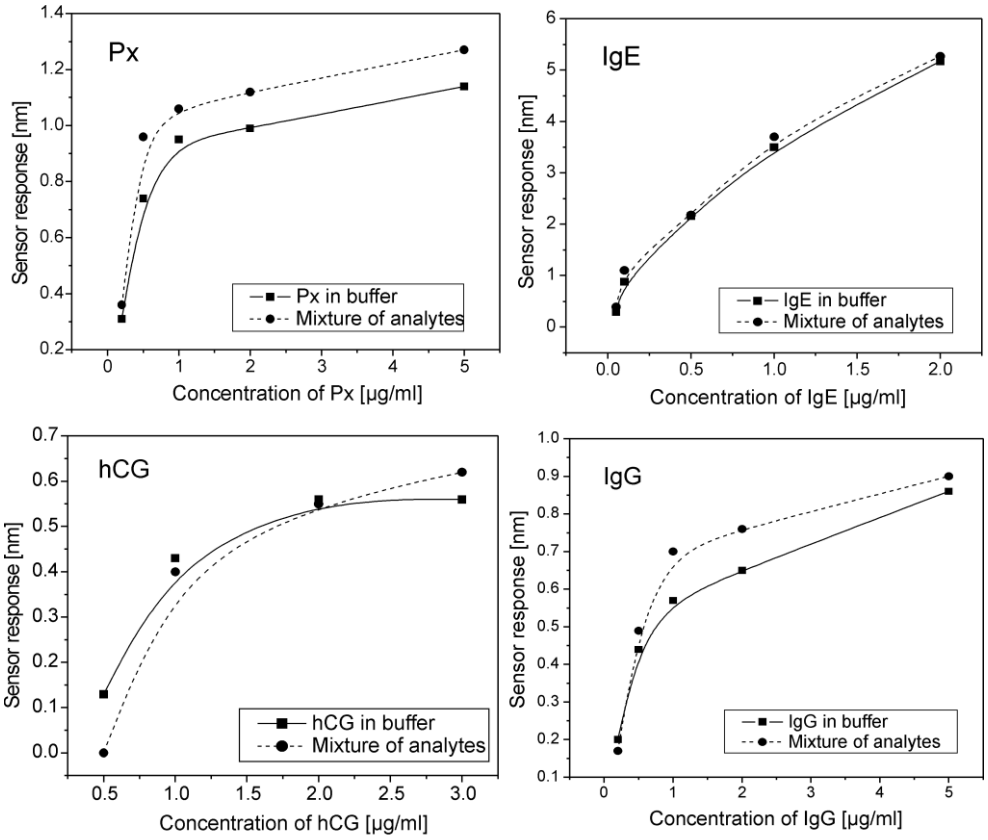

Fig. 15 Sensor response as a function of analyte concentration for Px, IgE, hCG and IgG measured in pure buffer and mixture of all antigens.

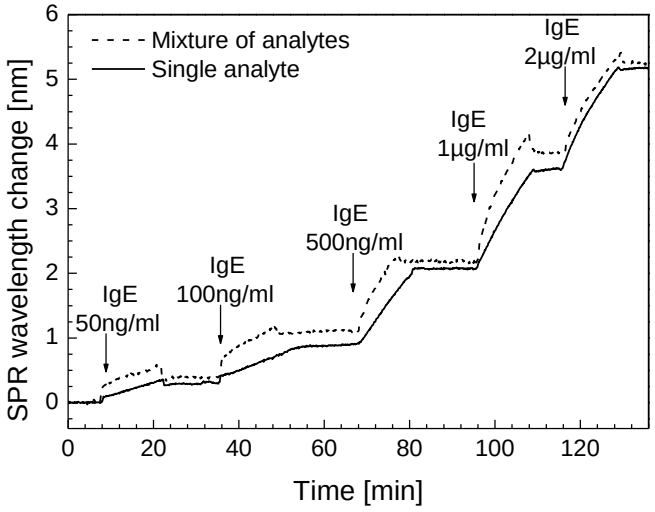

Fig. 16 Sensorgrams corresponding to IgE binding for solutions containing either only IgE or mixture of all four model antigens (IgE, Px, hCG, IgG); antigen solutions were injected sequentially with increasing antigen concentrations.

Sensor for highly sensitive detection of antibody against Epstein-Barr virus (anti-EBNA) in diluted human serum was developed (**Appendix VII**, *Biosensors & Bioelectronics* 2006). Short synthetic peptide (EBNA-1) conjugated with bovine serum albumin (BSA) was used as a biomolecular recognition element and immobilized on the sensor surface via previously optimized method based on hydrophobic interactions. Resulting sensor calibration curve performed high chip-to-chip reproducibility (standard deviation less than 18%). The detection limit for the direct detection of anti-EBNA was found to be 0.2 ng/ml. This detection limit was lower by a factor of five when compared to detection limit obtained using widely used indirect ELISA assay. The procedure for the regeneration of sensor chip was developed and no significant loss in sensor sensitivity was observed after more than 10 regeneration/measurement cycles. It was demonstrated as well that the reported peptide-modified chips could be stored for at least 30 days with no loss in the sensor sensitivity (Figure 17).

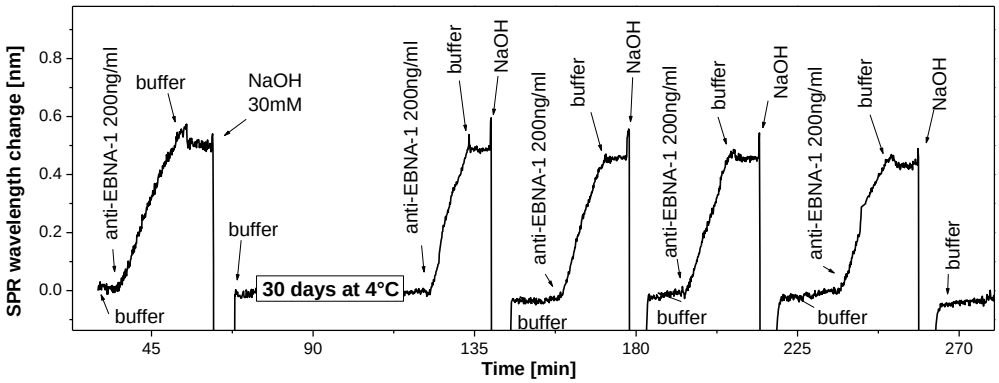

Fig. 17 Sensor responses to anti-EBNA binding on EBNA surface obtained using one sensor chip immediately after functionalization and the same sensor chip after 30 days of storage at 4°C. Before injection of each anti-EBNA solution at concentration of 200 ng/ml, sensor surface was regenerated with NaOH (30 mM).

The demonstrated detection limit was reproduced in a diluted human blood serum. Sensor responses to analyte in human serum and in buffer are compared in Figure 18. Only very low non-specific binding was observed for measurements in 1% human serum. Typical sensorgram obtained during anti-EBNA binding from human serum in measuring (BSA-EBNA) and reference channel, respectively is displayed in Figure 18. The detected concentrations of anti-EBNA corresponded well to clinically relevant values. These results demonstrate the potential of this developed SPR biosensor with synthetic peptide receptor for its use in medical diagnostics.

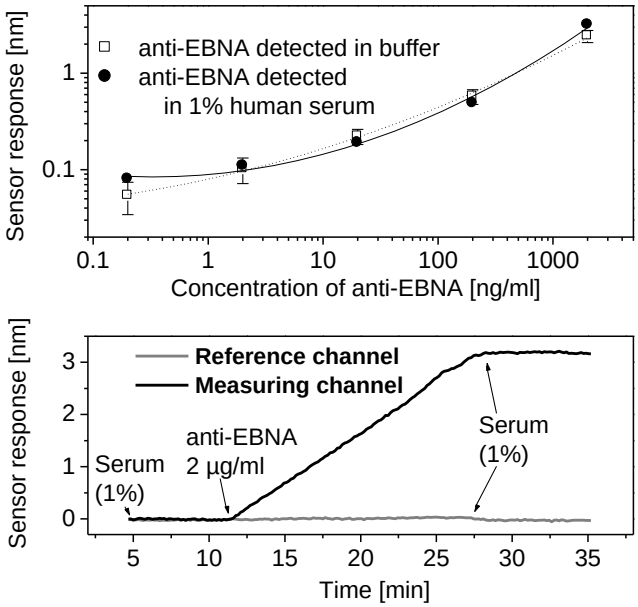

Fig. 18 Detection of anti-EBNA of increasing concentration measured by SPR sensor in buffer and in diluted human serum (upper figure); Lower picture shows sensorgrams corresponding to binding of anti-EBNA at a concentration of 2µg/ml in human serum: specific binding to BSA-EBNA surface (black line) and non-specific binding to reference surface (gray line).

In the **Appendix II** (*Measurement Science and Technology* 2006), a novel sensor design that exploits simultaneous excitation of two different (symmetric and anti-symmetric) surface plasmons in a single sensing spot was presented. Besides the sensor sensitivity and noise, we considered also the cross-sensitivity to background refractive index in the optimization process, which allowed us to evaluate the true sensor resolution. The derived formulae for cross-sensitivity can be directly used for evaluation and optimization of other SPR cross-sensitivity compensating techniques. We have compared the performance of the proposed structure with the two-channel compensated SPR detecting IgE analyte. It was found that the noise of the retrieved surface refractive index change was 11 times worse in the proposed configuration. However, the cross-sensitivity to background refractive index changes was nearly twice as low, which favors the proposed configuration for measurements with relative high background refractive index changes.

A laboratory prototype of the high-throughput SPR sensor based on combination of SPR imaging with polarization contrast and of a spatially patterned multilayer SPR structure with 108 sensing channels was used for detection of human choriogonadotropin (hCG) with antibody against hCG immobilized on the sensor surface. Results showed that this novel SPR sensor was capable of detecting hCG at concentrations lower than 0.5 µg/ml (**Appendix V**,

Biosensors & Bioelectronics 2005). My contribution to the last two publications was in optimization of immobilization procedure for particular biological system and sensor design under study and in the performance of all bioexperiments.

A review of the state of the art of SPR biosensors applications in medical diagnostics, especially a review of the use of SPR biosensors for detection of disease biomarkers (antigens, antibodies or other proteins that are related to diseases such as cancer or heart attack) was reported in the **Appendix IX**, chapter in *Surface Plasmon Resonance Based Sensors, 2006*. It was summarized in this chapter that although majority of the SPR detection experiments have been still performed in pure buffer solutions with minimum or no matrix interferences, clinical samples have also been tackled. It is further expected that advances in SPR sensor instrumentation (reducing size, improving sensitivity, increasing throughput), receptors and methods for their immobilization (increasing sensitivity and specificity) will lead to new systems for rapid detection and identification of disease biomarkers that will extend applicability of SPR biosensor technology in medical diagnostics.

3.3 UV Absorption Study of Oligonucleotide Hybridization

A subject of my diploma thesis was to study hybridization of short synthetic oligonucleotides potentially applicable in antisense therapy by UV absorption spectroscopy. Under supervision of Prof. Josef Štěpánek we developed methodology based on precise measurements of temperature-dependence of whole UV absorption spectra of oligonucleotide mixed solutions. Modified system of temperature monitoring and prepared software for automatic computer control enabled simultaneous measurements of up to six samples. Obtained sets of absorption spectra were analyzed by using statistical data treatment (factor analysis) to determine thermodynamic parameters of oligonucleotide complexes formation [104].

This method, in certain sense complementary to the biosensor approach, was employed in the beginning of my doctoral work to study effect of mismatched base pairs in four nonamer hybrid duplexes formed between the 5'-d(GTGATATGC)-3' complement and its 50-r(GCAUNUCAC)-30 (N=A, C, G, U) counterparts (**Appendix I**, *Biopolymers* 2004). This oligonucleotide set was considered as a molecular model system for future systematic studies of various modifications of internucleotide linkages with respect to their impact on the binding specificity to complementary base sequence. In the paper, UV absorption spectroscopy was used as an additional method to Raman spectroscopy. Determined duplex thermodynamic stabilities obtained from UV absorption analysis showed that the dT•rG mismatch decreased the hybrid duplex stability very weakly while the effect of both

pyrimidine–pyrimidine mismatches was much higher. Results from Raman spectroscopy measurements revealed that the A-like family of torsion angles of the sugar–phosphate backbone of single-stranded RNA oligonucleotides persists in the hybrid duplexes. Since no important increase of B-markers was observed, the A-like local conformation was likely forced to part of the DNA strand as well. The influence of the mismatches on the structure of the hybrid duplexes was significantly weaker than their influence on the structure of analogous DNA-DNA duplexes. In particular it was found, the dT•rG mismatch pair was relatively well incorporated into the double helix structure.

This obtained experience in the field of oligonucleotide hybridization properties was utilized in development and optimization of surface plasmon resonance (SPR) method for monitoring of the oligonucleotide hybridization. Further effort within my doctoral work was concentrated to the surface plasmon resonance biosensor measurements, including methodological development of immobilization chemistries for various analytes and detection and applications of developed methods for different optical platforms of SPR systems.

3.4 Immobilization of Oligonucleotides on the Surface of SPR Sensor

A major part of my doctoral work was focused on oligonucleotide (DNA/RNA) chip development that would be able to direct sensitive detection of oligonucleotide analytes.

Recent trend in development of SPR DNA- or RNA-sensors is to lower the detection limits in order to make the resulting sensor sensitivity comparable with the widely used fluorescent or radioactive-based DNA (micro) arrays. The lowest concentrations of short ON targets that were detected directly and without any additional (enzymatic, electrochemical, fluorescent) amplification by current SPR biosensors, were at a nanomolar level [11, 105, 106]. Nevertheless, a micromolar levels were used in a majority of SPR-based studies of ON hybridization [4, 7, 38, 47, 107].

Another requirement for oligonucleotide chip development is a potential for precise kinetic analysis of oligonucleotide interactions. Because of that, the functionalization method based on “3D” dextran hydrogel matrix that is mostly produced within commercial chips is not suitable since the analyte transport through the gel matrix can influence the resulting kinetics. The immobilization method, which was chosen and optimized for sensitive monitoring of oligonucleotide interactions was based on formation of a “2D” self-assembled monolayer (SAM) followed with covalent attachment of streptavidin and non-covalent binding of biotinylated oligonucleotides (MHA method).

Optimization of this method is in detail described in **Appendix IX**. A streptavidin was covalently attached to NHS-ester-terminated alkanethiolates [83, 85] followed with a coupling of biotinylated oligonucleotide probes. Systematic optimization of parameters influencing the resulting ligand density and activity such as buffers salt composition, pH, reagent concentrations or spacer length was carried out to develop a robust, effective and reproducible DNA chip functionalization method. The final optimized procedure of ON immobilization that is described in the **Appendix IX** was shown to be highly reproducible (≥91% and ≥95% for chip-to-chip and on-chip reproducibility, respectively) with a small ON probe consumption (50nM probe concentration was found to reach the saturation level). Typical sensorgram corresponding to streptavidin and biotinylated ON probe binding is shown in Figure 19.

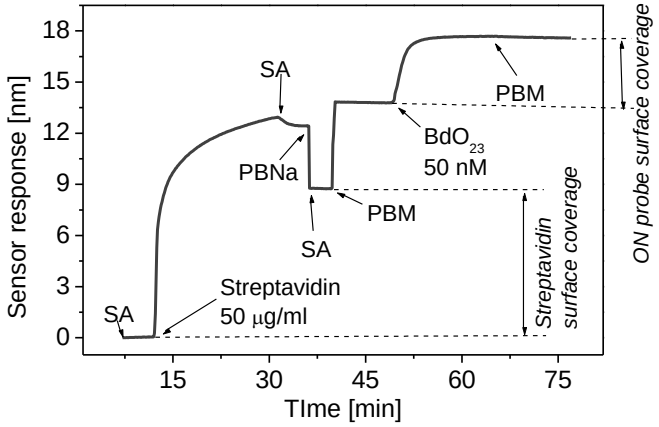

Fig. 19 A typical sensorgram corresponding to DNA chip functionalization with MHA method. The resulting amounts (in sensor response units) of bound streptavidin and ON probe are indicated. Arrows indicate when injections of particular solutions have started.

The MHA method-based sensor characteristics were compared to previously optimized and well established method of streptavidin immobilization to biotin-terminated alkanethiols (BAT method) [72]. By using the approach optimized herein, a significant increase of hybridization efficiency was achieved (86% for MHA method vs. 63% for BAT method in case of maximal available sensor coverage with streptavidin of biotinylated probes). Furthermore, a highly efficient streptavidin immobilization was demonstrated by detected more than three binding sites available for biotinylated probe binding per one immobilized streptavidin molecule.

3.5 Detection of Oligonucleotide Hybridization

Optimized procedure of DNA / RNA chips preparation was employed for detection of oligonucleotide (ON) analytes. It was shown that SPR sensor with optimized MHA method enables a rapid direct detection of short oligonucleotides with high specificity, reproducibility and regenerability over three orders of target concentration (100 pM – 200 nM) (Figures 20-21). The resulting sensor detection limit of 100pM for 23-mer oligonucleotides was one hundred times lower than the typically reported detection limits of SPR-based direct oligonucleotide detections. Detailed characteristics of developed DNA sensor were described in **Appendix VIII** (*Biopolymers* 2006) and **IX**.

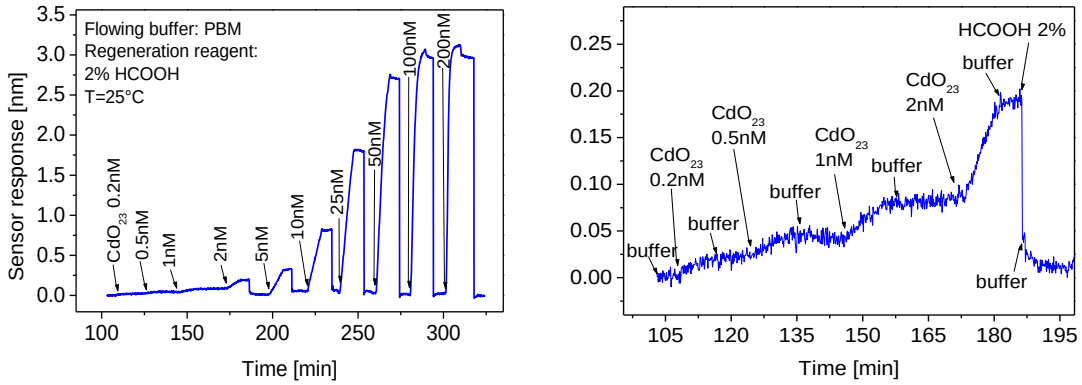

Fig. 20 Detection of oligonucleotide (23-mer) hybridization on sensor chip functionalized with 23-mer biotinylated oligonulucleotide probe (BdO_{23}) using the optimized MHA method. Sensor response to increasing concentration of fully complementary strand CdO_{23} (8 min. incubation time, regeneration performed after injected concentrations higher than 2nM (upper left) with a detail of the concentration range 0.2 nM- 2nM (upper right).

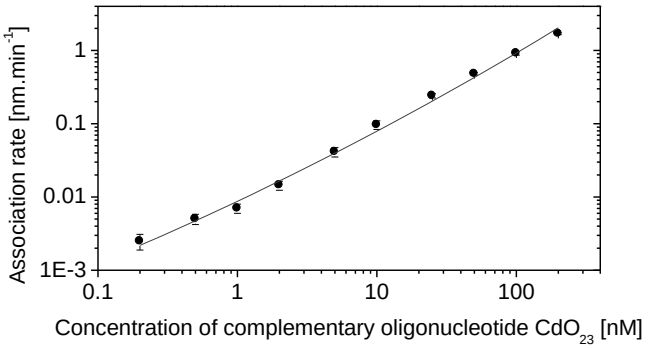

Fig. 21 Calibration curve of ON sensor with optimized MHA method; the calibration curve was derived from association rates for each measured concentration (averaged from four independent sensing channels).

The eight-channel sensor was employed for primary screening of hybridization properties of a set of synthetic modified oligonucleotides with the aim to select potential

candidates for antisense therapy (**Appendix VIII**, *Biopolymers* 2006). The 23-mer ribooligonucleotides (rA_{23}) were immobilized on the sensor surface into all sensing spots via optimized MHA chemistry. Solutions of homothymidine 15-mer deoxyribooligonucleotides (natural and seven synthetic compounds with different internucleotide linkage modification) were injected separately into the functionalized sensing channels. Concentration of each ON was 50 nM and incubation time employed for these experiments was 20 minutes. Real-time observation of hybridization of ON analytes with immobilized RNA complement using the eight-channel SPR system is shown in Figure 22; a scheme of the structural modification is attached to each sensorgram. Different binding kinetics for different modification suggested that the insertion of internucleotide linkage modification caused different interaction mechanisms. It was shown that this rapid screening with very low sample consumption enables primary choice of perspective candidates for antisense therapy. Moreover, if we compared the modified ON sensor response amplitudes to these obtained from ligand (rA_{23}) immobilization and calibrated the values to unified molecular weight, we could conclude that a stoichiometry of formed complexes was in some cases higher than 1:1. This indicated that triplexes were also formed in addition to duplexes for selected modified ONs. Detailed analysis of complex stoichiometry is a subject of our future work.

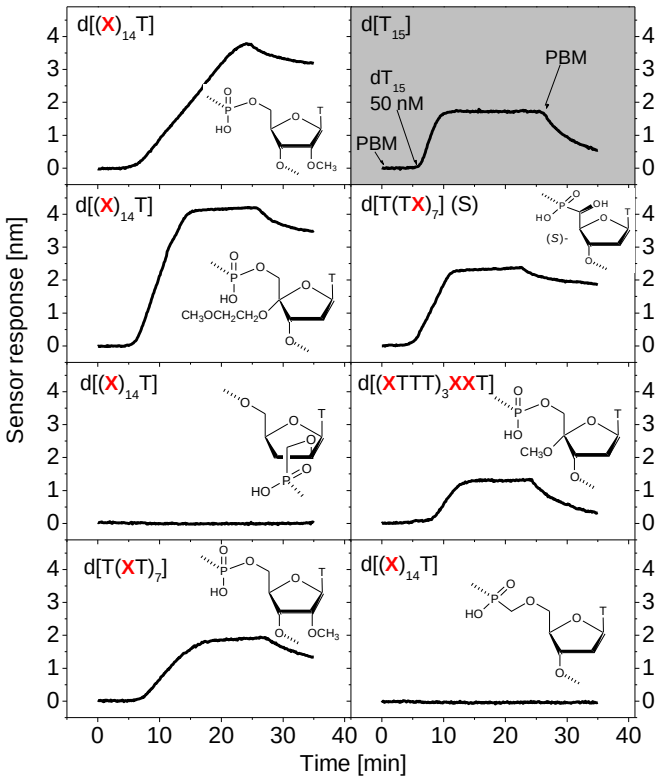

Fig. 22 Screening of synthetic modified oligonucleotide interactions with immobilized natural rA_{23} counterpart in comparison with natural dT_{15} binding; **X** means occurrence of depicted internucleotide linkage modification in 15-mer homothymidine sequence.

Another multi-channel biosensor combining an optical platform based on SPR imaging on special multilayers and polarization contrast with a spatially resolved optimized functionalization was used for detection of oligonucleotides (**Appendix VI**). It was demonstrated that this optical platform offered a considerably higher sensitivity and resolution than the conventional SPR imaging. This sensor could perform 64 independent measurements simultaneously. The spatially resolved functionalization based on microspotting applied to immobilization of short oligonucleotides was shown to provide a surface concentration of oligonucleotide probes higher by 80 percent than the flow-through functionalization method. Sensor response to different concentrations of short oligonucleotides (23-mers) is shown in Figure 23. In these experiments, sensor chips functionalized with dO_{23} probes (sensing channels) and dT_{23} probes (reference channels) were used and samples containing different concentrations of CdO_{23} in PBM buffer were flowed across different flow-chambers of the flow-cell.

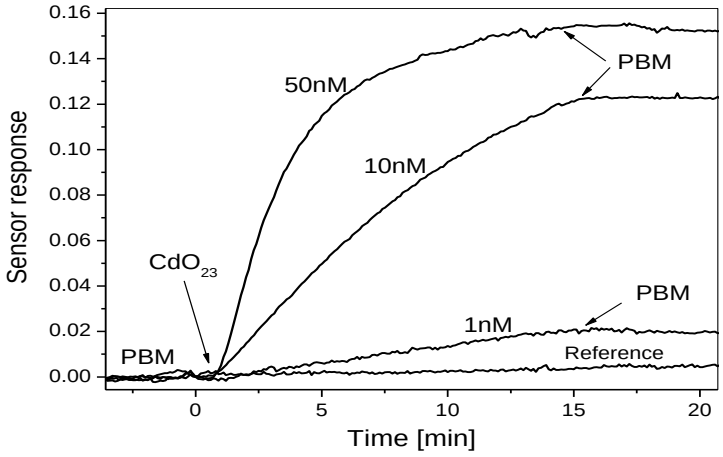

Fig. 23 Detection of oligonucleotides using the multichannel SPR sensor functionalized by the microspotting technique; Temporal sensor response measured for three different concentrations of CdO_{23} oligonucleotide. Response from a reference channel corresponding to CdO_{23} concentration of 50 nM is shown for comparison.

3.6 Kinetics of NA Triplex Formation

A review of molecular interaction models that are mostly used for kinetic analysis of SPR data as well as of hydrodynamic effects discussions is reported in **Appendix XII** (chapter in *Surface Plasmon Resonance Based Sensors* 2006). In this chapter, an interaction model concerning consecutive binding of two analytes ("consecutive binding model") to the receptor binding sites, which was proposed within this doctoral work, is also described. The

advantage of this model is that it can be applied for kinetic analysis of oligonucleotide triplex formation in the case when duplex formation is followed with binding of the third strand to create final triplex. This situation can occur, when an homopurine oligonucleotide is fixed at the sensor surface as a receptor and complementary oligonucleotides consecutively form a triplex. This involves two successive reactions, each occurring at a unique binding site. The corresponding kinetic equations are

$$\mathrm{A} + \mathrm{R} \underset{k_{d1}}{\overset{k_{a1}}{\rightleftharpoons}} \mathrm{AR} \qquad \mathrm{AR} + \mathrm{A} \underset{k_{d2}}{\overset{k_{a2}}{\rightleftharpoons}} \mathrm{ARA} \tag{4}$$

$$\gamma_1 = [\mathrm{AR}] \qquad \gamma_2 = [\mathrm{ARA}]$$

$$\frac{\partial \gamma_2}{\partial t} = k_{a2}\alpha_0\gamma_1 - k_{d2}\gamma_2$$

$$\frac{\partial \gamma_1}{\partial t} = k_{a1}\alpha_0(\beta - \gamma_1 - \gamma_2) - k_{d1}\gamma_1 - \frac{\partial \gamma_2}{\partial t} = k_{a1}\alpha_0(\beta - \gamma_1 - \gamma_2) - k_{d1}\gamma_1 - k_{a2}\alpha_0\gamma_1 + k_{d2}\gamma_2 \tag{5}$$

$$\xi / \xi_S = (\gamma_1 + 2\gamma_2)/\beta$$

where γ_1 is a concentration of the first complex (it can be for instance a duplex in case of describing oligonucleotide triplex kinetics) and γ_2 means the concentration of the consecutive complex (triplex); ξ_S is a standard sensor response (in RU) corresponding to all receptor sites bound to analyte in a 1:1 ratio. Fitting parameters ka_1, kd_1 and ka_2, kd_2 are the investigating kinetic rate constants of the first complex (duplex) formation and consecutive second complex (triplex) formation, respectively.

Figure 24 shows time-dependences of individual participating compound concentrations (free analyte, formed duplex, formed triplex) and a total sensor response for the consecutive binding model. A fit of this model (with incorporated modeled effects of hydrodynamic conditions) to respective SPR data is a subject of our recent work. Based on the fit of the model we would like to determine amounts of the biomolecular complexes with different stoichiometry and the kinetic parameters of each single process with high accuracy.

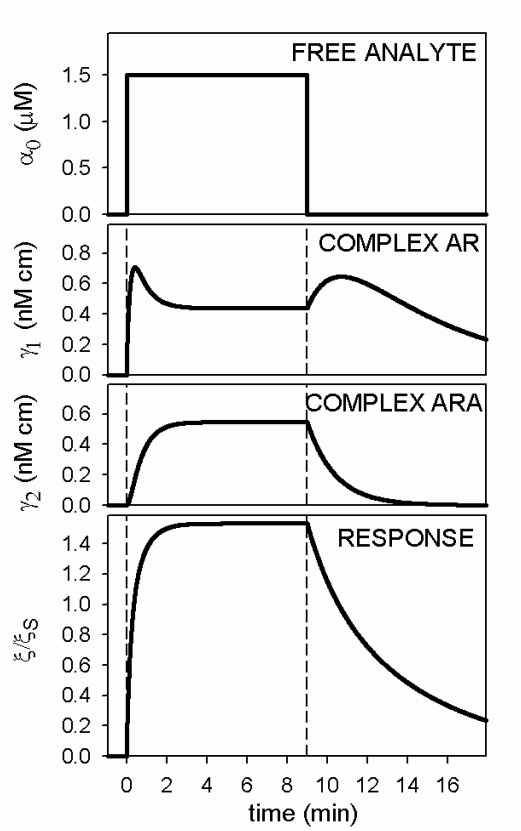

Fig. 24 Kinetics and sensorgram according to the model of two consecutive binding reactions in case of bivalent receptor; Fixed parameters: α_0 = 1.5 μM, β = 1 nM cm, $k_{a1} = 6 \cdot 10^4$ $M^{-1}s^{-1}$, k_{d1} = 0.003 s^{-1}, $k_{a2} = 10^4$ $M^{-1}s^{-1}$, k_{d2} = 0.012 s^{-1}.

3.7 Monitoring of HIV-1 Integrase Activity

The eight-channel SPR sensor with optimized MHA chemistry was employed to study of DNA-enzyme interactions, especially for real-time monitoring of the activity of human immunodeficiency virus (HIV) integrase. HIV-1 integrase (IN) is an enzyme catalyzing integration of a double-stranded DNA copy of the HIV genome into the host genome. It is a crucial step of HIV replication and thus it has become an attractive target for drug design [108]. The catalysis proceeds in two distinct reactions: the 3'-processing reaction, where 5' phosphorylated dimer (pGT) is specifically cleaved from both viral long terminal repeats (LTR) yielding a processed DNA and the strand transfer reaction, in which the exposed 3'-hydroxyl groups of the processed ends are joined to 5' phosphates in the host DNA [109]. The catalytic activity of IN has been demonstrated *in vitro* using oligonucleotide (ON) substrates that mimic the viral DNA ends in the presence of divalent metal cofactor (Mn^{2+} and Mg^{2+}) [110, 111].

It has been demonstrated in **Appendix X** that SPR method can be used for a direct label-free monitoring of the HIV-1 Integrase strand transfer activity. An effect of four different divalent metal cofactors (Mn^{2+}, Mg^{2+}, Ni^{2+} and Co^{2+}) on IN binding to DNA was investigated using model deoxyribooligonucleotides representing viral LTR ends and model triple-helical ONs. Four measuring spots were functionalized with the 23-mer double-stranded ON $(SS')_{23}$ representing viral ends with terminal CA/GT bases. Additional four spots were functionalized with model triple-stranded complexes $(TAT)_{23}$. Model triplexes were used as the reference surfaces with respect to the previously proposed triplex-mediated inhibition of HIV IN activity [108].

Solutions of IN with particular metal cofactor were injected into $(SS')_{23}$ and $(TAT)_{23}$ channels (each type of metal cofactor per one pair of measuring and reference spots was used), Figure 25. It was found that integrase forms stable complexes both with viral DNA substrate $(SS')_{23}$ and with $(TAT)_{23}$ triplexes in the presence of all tested ions. The amount of enzyme that remained bound to ONs after washing the sensor surface with buffer was in average 1.5-times higher for $(TAT)_{23}$ than for $(SS')_{23}$ for all ions.

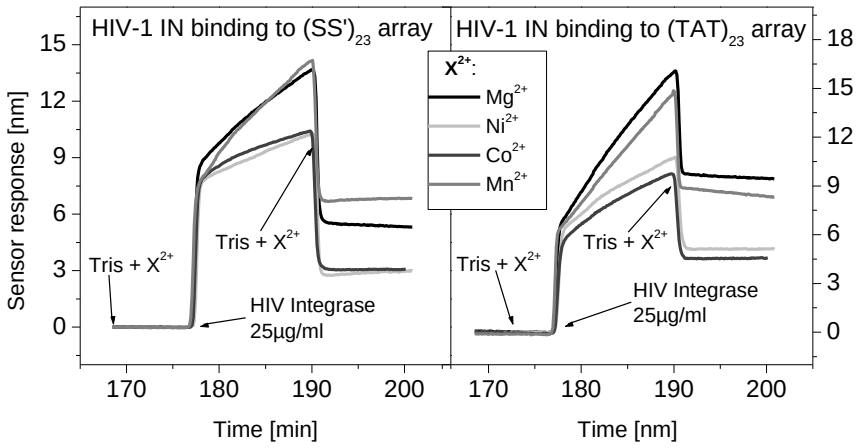

Fig. 25 Sensorgrams corresponding to HIV-1 Integrase binding to $(SS')_{23}$ and $(TAT)_{23}$ arrays in the presence of different divalent metal cofactors. Concentration of each divalent ion in buffer was 8mM; the arrows indicate time point of solution injection containing particular ion (X^{2+}). A) Ni^{2+}, B) Mn^{2+}, C) Co^{2+}, D) Mg^{2+}.

HIV-1 Integrase strand transfer activity and thus integration of viral DNA to target DNA was directly monitored using developed SPR assay. The target DNA was represented by 5´-phosphorylated double-stranded 9-mer ON $(pTS)_{12}$ that was injected into the sensor covered with IN-oligonucleotide complexes. A scheme of this reaction is depicted in Figure 26.

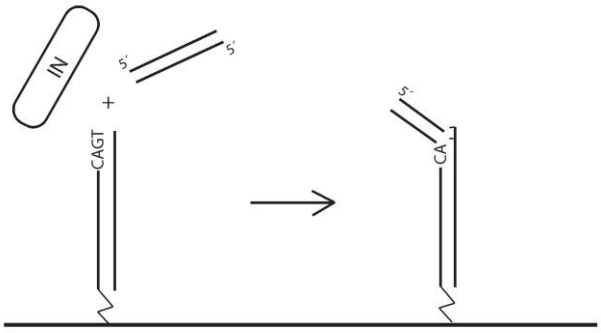

Fig. 26 A scheme of SPR assay for direct monitoring of the HIV-1 integrase strand transfer activity.. The solution of 5'-phophorylated double-stranded 12-mer ON (100nM) representing target DNA is injected into the sensing channel functionalized with ON terminated with viral LTR ends and the strand transfer reaction proceeds resulting in integration of processed target DNA to the simulated viral DNA.

Sensorgram corresponding to the IN-catalyzed strand transfer reaction is shown in Figure 27. It was observed, that the reaction proceeded preferentially in the presence of Mn^{2+}. This is in accordance with the previous reports where *in vitro* reaction was mostly detected in the presence of Mn^{2+}. However, the same reaction *in vivo* proceeds in the presence of Mg^{2+} ions. Using our method, IN reaction in the presence of Mg^{2+} was detected as well; nevertheless the response was relatively weak compared to Mn^{2+}. These results were obtained from two independent experiments using *de novo* functionalized sensor chips.

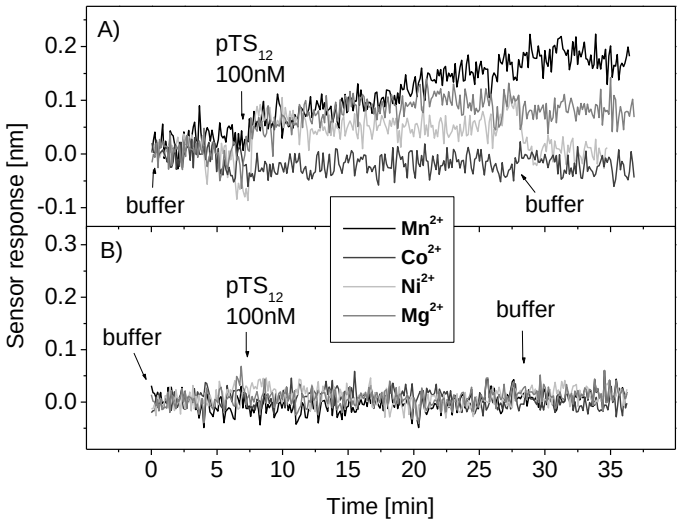

Fig. 27 SPR-sensor based monitoring of IN strand transfer activity: Sensor response to pTS_{12} binding to IN-$(SS')_{23}$ complex (A) and IN-$(TAT)_{23}$ (B) complex in the presence of different divalent metal cofactors; concentration of pTS_{12} was 100nM, incubation time was 25 min.

Our results showed that SPR technique can be used for direct label-free real-time monitoring of DNA-enzyme interactions. Investigation of NA interaction with other enzymes such as ribonuclease H, ribonuclease L is a subject of our future work.

4. Conclusions

Within this doctoral work, a methodology of surface plasmon resonance biosensor measurements was developed and optimized for various biomolecular systems. The methodology was applied for several different platforms of SPR sensors.

The most promising approach to DNA/RNA/protein chips preparation was selected, optimized and set up as a routine procedure. It was shown that the prepared SPR biosensors were capable of detecting oligonucleotides with high sensitivity, specificity and reproducibility compared to previously published results. This demonstrates that it is worth to invest time and effort to optimization of immobilization method because a substantial increase in sensor sensitivity, specificity, and reproducibility can be achieved.

SPR biosensor-based detection of various biomolecules with the sensor chips functionalized with receptors using optimized immobilization chemistries both in pure samples and complex solutions (serum) has been carried out. Results revealed high potential of SPR technique applications in further biomolecular interaction studies as well as in the fields of medical diagnostics.

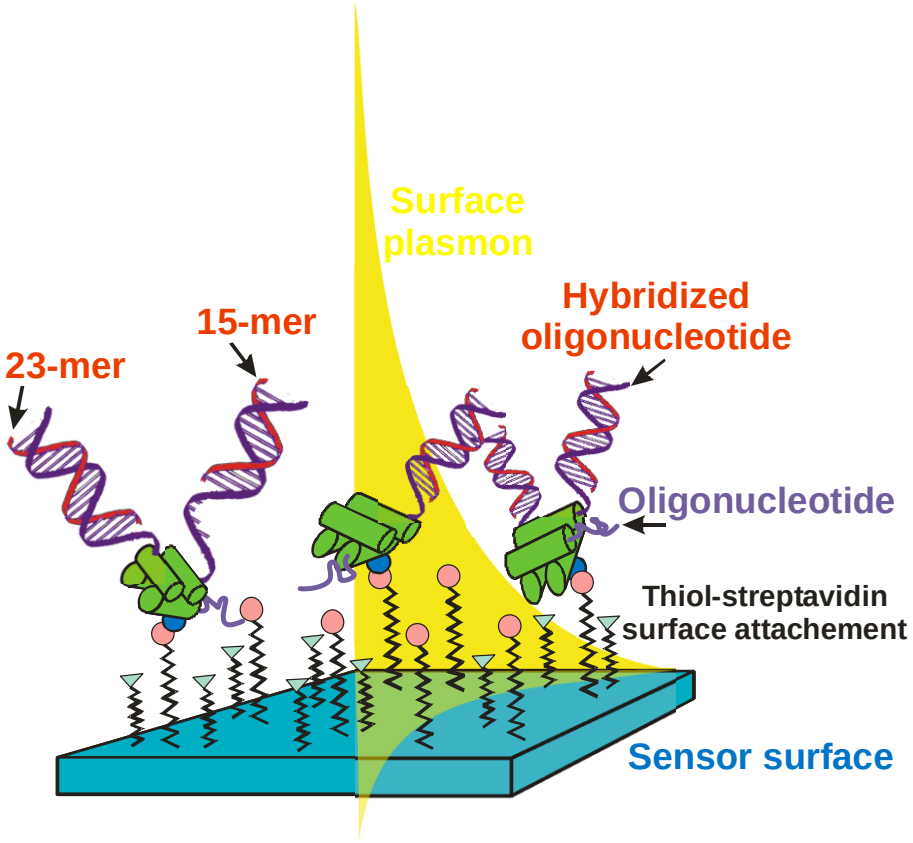

5. References

1. Watson, J.D. and F.H. Crick, *Molecular structure of nucleic acids; a structure for deoxyribose nucleic acid.* Nature, 1953. **171**(4356): p. 737-8.
2. Rajagopal, P. and J. Feigon, *Triple-strand formation in the homopurine:homopyrimidine DNA oligonucleotides d(G-A)4 and d(T-C)4.* Nature, 1989. **339**(6226): p. 637-40.
3. Praseuth, D., A.L. Guieysse, and C. Helene, *Triple helix formation and the antigene strategy for sequence-specific control of gene expression.* Biochim Biophys Acta, 1999. **1489**(1): p. 181-206.
4. Sugimoto, N., et al., *pH and cation effects on the properties of parallel pyrimidine motif DNA triplexes.* Biochemistry, 2001. **40**(31): p. 9396-9405.
5. Mills, M., et al., *Energetics of strand-displacement reactions in triple helices: a spectroscopic study.* J Mol Biol, 1999. **291**(5): p. 1035-54.
6. James, P.L., T. Brown, and K.R. Fox, *Thermodynamic and kinetic stability of intermolecular triple helices containing different proportions of C+*GC and T*AT triplets.* Nucleic Acids Res, 2003. **31**(19): p. 5598-606.
7. Asensio, J.L., et al., *Thermodynamic, kinetic, and conformational properties of a parallel intermolecular DNA triplex containing 5 ' and 3 ' junctions.* Biochemistry, 1998. **37**(43): p. 15188-15198.
8. Hanus, J., et al., *-CH2- lengthening of the internucleotide linkage in the ApA dimer can improve its conformational compatibility with its natural polynucleotide counterpart.* Nucleic Acids Res, 2001. **29**(24): p. 5182-94.
9. Doktycz, M.J., et al., *Optical Melting of 128-Octamer DNA Duplexes - Effects of Base-Pair Location and Nearest Neighbors on Thermal-Stability.* Journal of Biological Chemistry, 1995. **270**(15): p. 8439-8445.
10. Drmanac, R., et al., *DNA-Sequence Determination by Hybridization - a Strategy for Efficient Large-Scale Sequencing.* Science, 1993. **260**(5114): p. 1649-1653.
11. Persson, B., et al., *Analysis of oligonucleotide probe affinities using surface plasmon resonance: A means for mutational scanning.* Analytical Biochemistry, 1997. **246**(1): p. 34-44.
12. Uhlmann, E. and A. Peyman, *Antisense Oligonucleotides - a New Therapeutic Principle.* Chemical Reviews, 1990. **90**(4): p. 543-584.
13. Lofas, S., *Optimizing the hit-to-lead process using SPR analysis.* Assay and Drug Development Technologies, 2004. **2**(4): p. 407-415.
14. Gewirtz, A.M., C.A. Stein, and P.M. Glazer, *Facilitating oligonucleotide delivery: helping antisense deliver on its promise.* Proc Natl Acad Sci U S A, 1996. **93**(8): p. 3161-3.
15. Wang, G., M.M. Seidman, and P.M. Glazer, *Mutagenesis in mammalian cells induced by triple helix formation and transcription-coupled repair.* Science, 1996. **271**(5250): p. 802-5.
16. Uhlenbeck, O.C., *A small catalytic oligoribonucleotide.* Nature, 1987. **328**(6131): p. 596-600.
17. Matteucci, M.D. and R.W. Wagner, *In pursuit of antisense.* Nature, 1996. **384**(6604 Suppl): p. 20-2.
18. Patel, D.J., *Structural analysis of nucleic acid aptamers.* Curr Opin Chem Biol, 1997. **1**(1): p. 32-46.
19. Zamecnik, P.C. and M.L. Stephenson, *Inhibition of Rous sarcoma virus replication and cell transformation by a specific oligodeoxynucleotide.* Proc Natl Acad Sci U S A, 1978. **75**(1): p. 280-4.
20. Galderisi, U., A. Cascino, and A. Giordano, *Antisense oligonucleotides as therapeutic agents.* J Cell Physiol, 1999. **181**(2): p. 251-7.
21. Freier, S.M. and K.H. Altmann, *The ups and downs of nucleic acid duplex stability: structure-stability studies on chemically-modified DNA:RNA duplexes.* Nucleic Acids Res, 1997. **25**(22): p. 4429-43.

22. Furrer, P., et al., *Structural effect of complete [Rp]-phosphorothioate and phosphorodithioate substitutions in the DNA strand of a model antisense inhibitor-target RNA complex.* J Mol Biol, 1999. **285**(4): p. 1609-22.
23. Flanagan, W.M., *Antisense comes of age.* Cancer Metastasis Rev, 1998. **17**(2): p. 169-76.
24. Stein, C.A., *Phosphorothioate antisense oligodeoxynucleotides: questions of specificity.* Trends Biotechnol, 1996. **14**(5): p. 147-9.
25. Stein, C.A. and Y.C. Cheng, *Antisense oligonucleotides as therapeutic agents--is the bullet really magical?* Science, 1993. **261**(5124): p. 1004-12.
26. Agrawal, S., et al., *Mixed-backbone oligonucleotides as second generation antisense oligonucleotides: in vitro and in vivo studies.* Proc Natl Acad Sci U S A, 1997. **94**(6): p. 2620-5.
27. Spiller, D.G., et al., *The influence of target protein half-life on the effectiveness of antisense oligonucleotide analog-mediated biologic responses.* Antisense Nucleic Acid Drug Dev, 1998. **8**(4): p. 281-93.
28. Escude, C., et al., *Stability of triple helices containing RNA and DNA strands: experimental and molecular modeling studies.* Nucleic Acids Res, 1993. **21**(24): p. 5547-53.
29. Ratilainen, T., et al., *Thermodynamics of sequence-specific binding of PNA to DNA.* Biochemistry, 2000. **39**(26): p. 7781-91.
30. Vallone, P.M. and A.S. Benight, *Thermodynamic, spectroscopic, and equilibrium binding studies of DNA sequence context effects in four 40 base pair deoxyoligonucleotides.* Biochemistry, 2000. **39**(26): p. 7835-46.
31. Pollack, J.R., et al., *Genome-wide analysis of DNA copy-number changes using cDNA microarrays.* Nat Genet, 1999. **23**(1): p. 41-6.
32. Pinkel, D., et al., *High resolution analysis of DNA copy number variation using comparative genomic hybridization to microarrays.* Nat Genet, 1998. **20**(2): p. 207-11.
33. Barvik, I., Jr., J. Stepanek, and J. Bok, *Molecular dynamics simulations of nucleic acids: A). Molecular dynamics simulations of the oligonucleotide with the modified phosphate/phosphonate internucleotide linkage.* Gen Physiol Biophys, 1998. **17 Suppl 1**: p. 21-3.
34. Khrapko, K.R., et al., *A method for DNA sequencing by hybridization with oligonucleotide matrix.* DNA Seq, 1991. **1**(6): p. 375-88.
35. Maskos, U. and E.M. Southern, *A study of oligonucleotide reassociation using large arrays of oligonucleotides synthesised on a glass support.* Nucleic Acids Res, 1993. **21**(20): p. 4663-9.
36. Service, R.F., *Microchip arrays put DNA on the spot.* Science, 1998. **282**(5388): p. 396-9.
37. Heller, M.J., *DNA microarray technology: devices, systems, and applications.* Annu Rev Biomed Eng, 2002. **4**: p. 129-53.
38. Bates, P.J., et al., *Biosensor detection of triplex formation by modified oligonucleotides.* Analytical Biochemistry, 2002. **307**(2): p. 235-243.
39. Buckle, M., et al., *Real time measurements of elongation by a reverse transcriptase using surface plasmon resonance.* Proceedings of the National Academy of Sciences of the United States of America, 1996. **93**(2): p. 889-894.
40. Cooper, M.A., *Optical biosensors in drug discovery.* Nature Reviews Drug Discovery, 2002. **1**(7): p. 515-528.
41. Cooper, M.A. and D.H. Williams, *Kinetic analysis of antibody-antigen interactions at a supported lipid monolayer.* Analytical Biochemistry, 1999. **276**(1): p. 36-47.
42. Ghindilis, A.L., et al., *Immunosensors: electrochemical sensing and other engineering approaches.* Biosens Bioelectron, 1998. **13**(1): p. 113-31.
43. Chu, X., et al., *Piezoelectric immunosensor for the detection of immunoglobulin M.* Analyst, 1995. **120**(12): p. 2829-32.
44. Abdel-Hamid, I., et al., *Flow-through immunofiltration assay system for rapid detection of E. coli O157:H7.* Biosens Bioelectron, 1999. **14**(3): p. 309-16.
45. Jung, L.S., et al., *Surface plasmon resonance measurement of binding and dissociation of wild-type and mutant streptavidin on mixed biotin-containing alkylthiolate monolayers.* Sensors and Actuators B-Chemical, 1999. **54**(1-2): p. 137-144.

46. Myszka, D.G., *Survey of the 1998 optical biosensor literature.* Journal of Molecular Recognition, 1999. **12**(6): p. 390-408.
47. Piscevic, D., et al., *Oligonucleotide Hybridization Observed by Surface-Plasmon Optical Techniques.* Applied Surface Science, 1995. **90**(4): p. 425-436.
48. Jordan, C.E., et al., *Surface plasmon resonance imaging measurements of DNA hybridization adsorption and streptavidin/DNA multilayer formation at chemically modified gold surfaces.* Analytical Chemistry, 1997. **69**(24): p. 4939-4947.
49. Homola, J., *Present and future of surface plasmon resonance biosensors.* Analytical and Bioanalytical Chemistry, 2003. **377**(3): p. 528-539.
50. Knoll, W., et al., *Supramolecular architectures for the functionalization of solid surfaces.* Adv Biophys, 1997. **34**: p. 231-51.
51. Rich, R.L. and D.G. Myszka, *Survey of the year 2004 commercial optical biosensor literature.* Journal of Molecular Recognition, 2005. **18**(6): p. 431-478.
52. Karlsson, R., A. Michaelsson, and L. Mattsson, *Kinetic-Analysis of Monoclonal Antibody-Antigen Interactions with a New Biosensor Based Analytical System.* Journal of Immunological Methods, 1991. **145**(1-2): p. 229-240.
53. Myszka, D.G., et al., *Kinetic analysis of a protein antigen-antibody interaction limited by mass transport on an optical biosensor.* Biophysical Chemistry, 1997. **64**(1-3): p. 127-137.
54. Homola, J., S.S. Yee, and D. Myszka, *Surface plasmon biosensors*, in *Optical Biosensors: Present and Future*, F.S. Ligler, Editor. 2002, Elsevier: Amsterdam.
55. Lofas, S., et al., *Bioanalysis with Surface-Plasmon Resonance.* Sensors and Actuators B-Chemical, 1991. **5**(1-4): p. 79-84.
56. Homola, J., et al., *A novel multichannel surface plasmon resonance biosensor.* Sensors and Actuators B-Chemical, 2001. **76**(1-3): p. 403-410.
57. Dostalek, J., H. Vaisocherova, and J. Homola, *Multichannel surface plasmon resonance biosensor with wavelength division multiplexing.* Sensors and Actuators B-Chemical, 2005. **108**(1-2): p. 758-764.
58. Homola, J., et al., *Multi-analyte surface plasmon resonance biosensing.* Methods, 2005. **37**(1): p. 26-36.
59. Nenninger, G.G., M. Piliarik, and J. Homola, *Data analysis for optical sensors based on spectroscopy of surface plasmons.* Measurement Science & Technology, 2002. **13**(12): p. 2038-2046.
60. Hock, B., *Antibodies for immunosensors - A review.* Analytica Chimica Acta, 1997. **347**(1-2): p. 177-186.
61. Wegner, G.J., H.J. Lee, and R.M. Corn, *Characterization and optimization of peptide arrays for the study of epitope-antibody interactions using surface plasmon resonance imaging.* Analytical Chemistry, 2002. **74**(20): p. 5161-5168.
62. Jayasena, S.D., *Aptamers: An emerging class of molecules that rival antibodies in diagnostics.* Clinical Chemistry, 1999. **45**(9): p. 1628-1650.
63. Bamdad, C., *The use of variable density self-assembled monolayers to probe the structure of a target molecule.* Biophysical Journal, 1998. **75**(4): p. 1989-1996.
64. Ansell, R.J., O. Ramstrom, and K. Mosbach, *Towards artificial antibodies prepared by molecular imprinting.* Clinical Chemistry, 1996. **42**(9): p. 1506-1512.
65. Nuzzo, R.G. and D.L. Allara, *Adsorption of Bifunctional Organic Disulfides on Gold Surfaces.* Journal of the American Chemical Society, 1983. **105**(13): p. 4481-4483.
66. Johnsson, B., S. Lofas, and G. Lindquist, *Immobilization of Proteins to a Carboxymethyldextran-Modified Gold Surface for Biospecific Interaction Analysis in Surface-Plasmon Resonance Sensors.* Analytical Biochemistry, 1991. **198**(2): p. 268-277.
67. Oshannessy, D.J., M. Brighamburke, and K. Peck, *Immobilization Chemistries Suitable for Use in the Biacore Surface-Plasmon Resonance Detector.* Analytical Biochemistry, 1992. **205**(1): p. 132-136.
68. Koubova, V., et al., *Detection of foodborne pathogens using surface plasmon resonance biosensors.* Sensors and Actuators B-Chemical, 2001. **74**(1-3): p. 100-105.

69. Busse, S., et al., *Sensitivity studies for specific binding reactions using the biotin/streptavidin system by evanescent optical methods.* Biosens Bioelectron, 2002. **17**(8): p. 704-10.
70. Tombelli, S., M. Mascini, and A.P.F. Turner, *Improved procedures for immobilisation of oligonucleotides on gold-coated piezoelectric quartz crystals.* Biosensors & Bioelectronics, 2002. **17**(11-12): p. 929-936.
71. Anderson, G.P., et al., *Effectiveness of protein A for antibody immobilization for a fiber optic biosensor.* Biosensors & Bioelectronics, 1997. **12**(4): p. 329-336.
72. Ladd, J., et al., *DNA-directed protein immobilization on mixed self-assembled monolayers via a Streptavidin bridge.* Langmuir, 2004. **20**(19): p. 8090-8095.
73. Liedberg, B., C. Nylander, and I. Lundstrom, *Biosensing with surface plasmon resonance--how it all started.* Biosens Bioelectron, 1995. **10**(8): p. i-ix.
74. Homola, J., *Surface Plasmon Resonance Based Sensors*. Springer Series on Chemical Sensors and Biosensors ed. O.S. Wolfbeis. Vol. 4. 2006: Springer-Verlag. 251.
75. Jung, L.S., et al., *Binding and dissociation kinetics of wild-type and mutant streptavidins on mixed biotin-containing alkylthiolate monolayers.* Langmuir, 2000. **16**(24): p. 9421-9432.
76. Smith, R.K., P.A. Lewis, and P.S. Weiss, *Patterning self-assembled monolayers.* Progress in Surface Science, 2004. **75**(1-2): p. 1-68.
77. Peterson, A.W., R.J. Heaton, and R.M. Georgiadis, *The effect of surface probe density on DNA hybridization.* Nucleic Acids Research, 2001. **29**(24): p. 5163-5168.
78. Mannelli, I., et al., *Direct immobilisation of DNA probes for the development of affinity biosensors.* Bioelectrochemistry, 2005. **66**(1-2): p. 129-38.
79. Nelson, K.E., et al., *Surface characterization of mixed self-assembled monolayers designed for streptavidin immobilization.* Langmuir, 2001. **17**(9): p. 2807-2816.
80. Niemeyer, C.M., W. Burger, and R.M.J. Hoedemakers, *Hybridization characteristics of biomolecular adaptors, covalent DNA streptavidin conjugates.* Bioconjugate Chemistry, 1998. **9**(2): p. 168-175.
81. Gonzalez, L., et al., *Synthetic-peptide-based enzyme-linked immunosorbent assay for screening human serum or plasma for antibodies to human immunodeficiency virus type 1 and type 2.* Clinical and Diagnostic Laboratory Immunology, 1997. **4**(5): p. 598-603.
82. Hendrickson, W.A., et al., *Crystal-Structure of Core Streptavidin Determined from Multiwavelength Anomalous Diffraction of Synchrotron Radiation.* Proceedings of the National Academy of Sciences of the United States of America, 1989. **86**(7): p. 2190-2194.
83. Lofas, S., et al., *Methods for Site Controlled Coupling to Carboxymethyldextran Surfaces in Surface-Plasmon Resonance Sensors.* Biosensors & Bioelectronics, 1995. **10**(9-10): p. 813-822.
84. Burgener, M., M. Sanger, and U. Candrian, *Synthesis of a stable and specific surface plasmon resonance biosensor surface employing covalently immobilized peptide nucleic acids.* Bioconjugate Chemistry, 2000. **11**(6): p. 749-754.
85. Lahiri, J., et al., *A strategy for the generation of surfaces presenting ligands for studies of binding based on an active ester as a common reactive intermediate: A surface plasmon resonance study.* Analytical Chemistry, 1999. **71**(4): p. 777-790.
86. Kanayasu-Toyoda, T., et al., *HX531, a retinoid X receptor antagonist, inhibited the 9-cis retinoic acid-induced binding with steroid receptor coactivator-1 as detected by surface plasmon resonance.* Journal of Steroid Biochemistry and Molecular Biology, 2005. **94**(4): p. 303-309.
87. Goldstein, B., et al., *The influence of transport on the kinetics of binding to surface receptors: application to cells and BIAcore.* Journal of Molecular Recognition, 1999. **12**(5): p. 293-299.
88. Sikavitsas, V., J.M. Nitsche, and T.J. Mountziaris, *Transport and kinetic processes underlying biomolecular interactions in the BIACORE optical biosensor.* Biotechnology Progress, 2002. **18**(4): p. 885-897.
89. Witz, J., *Kinetic analysis of analyte binding by optical biosensors: Hydrodynamic penetration of the analyte flow into the polymer matrix reduces the influence of mass transport.* Analytical Biochemistry, 1999. **270**(2): p. 201-206.

90. OShannessy, D.J. and D.J. Winzor, *Interpretation of deviations from pseudo-first-order kinetic behavior in the characterization of ligand binding by biosensor technology.* Analytical Biochemistry, 1996. **236**(2): p. 275-283.
91. Ward, L.D. and D.J. Winzor, *Relative merits of optical biosensors based on flow-cell and cuvette designs.* Analytical Biochemistry, 2000. **285**(2): p. 179-193.
92. de Mol, N.J., et al., *Surface plasmon resonance thermodynamic and kinetic analysis as a strategic tool in drug design. Distinct ways for Phosphopeptides to plug into Src and Grb2 SH2 domain.* Journal of Medicinal Chemistry, 2005. **48**(3): p. 753-763.
93. Schuck, P. and A.P. Minton, *Analysis of mass transport-limited binding kinetics in evanescent wave biosensors.* Analytical Biochemistry, 1996. **240**(2): p. 262-272.
94. Edwards, D.A., B. Goldstein, and D.S. Cohen, *Transport effects on surface-volume biological reactions.* Journal of Mathematical Biology, 1999. **39**(6): p. 533-561.
95. Marrero, J.A. and A.S. Lok, *Newer markers for hepatocellular carcinoma.* Gastroenterology, 2004. **127**(5 Suppl 1): p. S113-9.
96. Breslauer, K.J., et al., *Predicting DNA Duplex Stability from the Base Sequence.* Proceedings of the National Academy of Sciences of the United States of America, 1986. **83**(11): p. 3746-3750.
97. Freier, S.M., et al., *Improved free-energy parameters for predictions of RNA duplex stability.* Proc Natl Acad Sci U S A, 1986. **83**(24): p. 9373-7.
98. Hung, S.H., et al., *Evidence from CD spectra that d(purine).r(pyrimidine) and r(purine).d(pyrimidine) hybrids are in different structural classes.* Nucleic Acids Res, 1994. **22**(20): p. 4326-34.
99. Roberts, R.W. and D.M. Crothers, *Stability and properties of double and triple helices: dramatic effects of RNA or DNA backbone composition.* Science, 1992. **258**(5087): p. 1463-6.
100. Han, H. and P.B. Dervan, *Sequence-specific recognition of double helical RNA and RNA.DNA by triple helix formation.* Proc Natl Acad Sci U S A, 1993. **90**(9): p. 3806-10.
101. Goodrich, T.T., H.J. Lee, and R.M. Corn, *Direct detection of genomic DNA by enzymatically amplified SPR imaging measurements of RNA microarrays.* Journal of the American Chemical Society, 2004. **126**(13): p. 4086-4087.
102. Ladd, J., et al., *DNA-directed protein immobilization on mixed self-assembled monolayers via a streptavidin bridge.* Langmuir, 2004. **20**(19): p. 8090-5.
103. Larsson, C., M. Rodahl, and F. Hook, *Characterization of DNA immobilization and subsequent hybridization on a 2D arrangement of streptavidin on a biotin-modified lipid bilayer supported on SiO2.* Analytical Chemistry, 2003. **75**(19): p. 5080-5087.
104. Malinowski, E.R., *Factor Analysis in Chemistry*. 2002: Wiley. 422.
105. Wang, R.H., et al., *A new approach for the detection of DNA sequences in amplified nucleic acids by a surface plasmon resonance biosensor.* Biosensors & Bioelectronics, 2004. **20**(3): p. 598-605.
106. Su, X., Y.J. Wu, and W. Knoll, *Comparison of surface plasmon resonance spectroscopy and quartz crystal microbalance techniques for studying DNA assembly and hybridization.* Biosens Bioelectron, 2005. **21**(5): p. 719-26.
107. Kukanskis, K., et al., *Detection of DNA hybridization using the TISPR-1 surface plasmon resonance biosensor.* Analytical Biochemistry, 1999. **274**(1): p. 7-17.
108. Cherepanov, P., et al., *HIV-1 integrase forms stable tetramers and associates with LEDGF/p75 protein in human cells.* J Biol Chem, 2003. **278**(1): p. 372-81.
109. Yi, J., E. Asante-Appiah, and A.M. Skalka, *Divalent cations stimulate preferential recognition of a viral DNA end by HIV-1 integrase.* Biochemistry, 1999. **38**(26): p. 8458-68.
110. Esposito, D. and R. Craigie, *Sequence specificity of viral end DNA binding by HIV-1 integrase reveals critical regions for protein-DNA interaction.* Embo J, 1998. **17**(19): p. 5832-43.
111. Sherman, P.A. and J.A. Fyfe, *Human immunodeficiency virus integration protein expressed in Escherichia coli possesses selective DNA cleaving activity.* Proc Natl Acad Sci U S A, 1990. **87**(13): p. 5119-23.

6. Appendices

List of Appendices:

A) JOURNAL PAPERS:

Appendix I

D. Němeček, H. Vaisocherová, J. Štěpánek, and P. – Y. Turpin, Structural features of a central mismatch in oligonucleotide hybrid duplexes visualized via Raman spectroscopy: model system for evaluation of potential "antisense" drugs, *Biopolymers,* **79** (2005), 1 - 8.

Appendix II

R. Slavík, J. Homola and H. Vaisocherová, Advanced biosensing using simultaneous excitation of short and long range surface plasmons, *Measurement Science and Technology*, **17** (2006), 932 – 938.

Appendix III

J. Dostálek, H. Vaisocherová and J. Homola: Multichannel surface plasmon resonance biosensor with wavelength division multiplexing, *Biosensors & Bioelectronics,* **108** (2004), 758 - 764.

Appendix IV

J. Homola, H. Vaisocherová, J. Dostálek and M. Piliarik, Multianalyte surface plasmon resonance biosensor, *Methods*, **37** (2005), 26 - 36.

Appendix V

M. Piliarik, H. Vaisocherová and J. Homola: A new surface plasmon resonance sensor for high-throughput screening applications, *Biosensors & Bioelectronics*, **20** (2005), 2104 – 2110.

Appendix VI

M. Piliarik, H. Vaisocherová and J. Homola: Towards parallelized surface plasmon resonance sensor platform for sensitive detection of oligonucleotides, Submitted to *Sensors & Actuators*, 2006.

Appendix VII

H. Vaisocherová, K. Mrkvová, M. Piliarik, P. Jinoch, M. Šteinbachová and J. Homola, Surface plasmon resonance biosensor for direct detection of antibody against Epstein-Barr virus, *Biosensors & Bioelectronics*, (2006), in press.

Appendix VIII

H. Vaisocherová, A. Zítová, M. Lachmanová, J. Štěpánek, Š. Králíková, R. Liboska, D. Rejman, I. Rosenberg and J. Homola, Investigating oligonucleotide interactions at subnanomolar level by surface plasmon resonance biosensor, *Biopolymers,* **82** (2006), 394-398.

Appendix IX

H. Vaisocherová, I. Rosenberg, K. Mrkvová-Hegnerová, P. Tobiška, J. Štěpánek and J. Homola, Immobilization method immprovement for detection of oligonucleotide hybridization at subnanomolar level by SPR biosensors, manuscript in preparation.

Appendix X

H. Vaisocherová, J. Snášel, I. Rosenberg and J. Homola, Direct monitoring of HIV-1 Integrase strand transfer activity by real-time surface plasmon resonance biosensor, manuscript in preparation.

B) BOOK CHAPTERS:

Appendix XI

H. Vaisocherová and J. Homola, SPR biosensors for medical diagnostics, in Surface Plasmon Resonance Based Sensors, Editor J. Homola, Springer, September 2006.

Appendix XII

J. Štěpánek, H. Vaisocherová and M. Piliarik, Molecular interactions in SPR sensors, in Surface Plasmon Resonance Based Sensors, Editor J. Homola, Springer, September 2006.

Appendix I

D. Němeček, H. Vaisocherová, J. Štěpánek, and P. – Y. Turpin:

Structural features of a central mismatch in oligonucleotide hybrid duplexes visualized via Raman spectroscopy: model system for evaluation of potential "antisense" drugs

Biopolymers, **79** (2005), 1 - 8

Daniel Němeček[1,2*]
Hana Vaisocherová[2]
Josef Štěpánek[2]
Pierre-Yves Turpin[1]
[1] *Université P. et M. Curie, L.P.B.C. (CNRS UMR 7033), 4 place Jussieu, Case 138, F–752 52 Paris Cedex 05, France*

[2] *Institute of Physics, Charles University, Ke Karlovu 5, Praha 2, CZ-121 16, Czech Republic*

Structural Features of a Central Mismatch in Oligonucleotide Hybrid Duplexes Visualized Via Raman Spectroscopy: Model System for Evaluation of Potential "Antisense" Drugs

Received 25 August 2004; revised 15 February 2005; accepted 16 February 2005
Published online 1 April 2005 in Wiley InterScience (www.interscience.wiley.com). DOI 10.1002/bip.20277

Abstract: *Structural features of mismatched base pairs were studied on four nonamer hybrid duplexes formed between the 5′-d(GTGATATGC)-3′ complement and its 5′-r(GCAUNUCAC)-3′ (N = A, C, G, U) counterparts. This oligonucleotide set is considered a model molecular system for future systematic studies of various modifications of internucleotide linkages with respect to their impact on the structure of mismatched base pairs. Raman spectra, measured at 15°C, revealed the prevailing A-like structure of the RNA strand and mixed A-like and B-like characteristics for the DNA strand. All three mismatches disturb only weakly the overall conformation of the hybrid duplex in contrast to analogous mismatched DNA duplexes. In particular, the dT · rG mismatch influences the global hybrid duplex geometry almost negligibly. The dT · rC and dT · rU mismatches induce somewhat more pronounced distortions of the backbone structure and of the thymine position, the latter being expressed by a change of the surrounding methylene group without effect on the carbonyl's vibrations. Structural effects of the mismatches correlate well with the duplex thermodynamic stabilities obtained by ultraviolet (UV) absorption, i.e., the dT · rG mismatch decreases the hybrid duplex stability very weakly while the effect of both pyrimidine–pyrimidine mismatches is considerable.* © 2005 Wiley Periodicals, Inc. Biopolymers 79: 1–8, 2005

This article was originally published online as an accepted preprint. The ''Published Online'' date corresponds to the preprint version. You can request a copy of the preprint by emailing the Biopolymers editorial office at biopolymers@wiley.com

Keywords: *nucleic acid; oligonucleotide; Raman spectroscopy; mismatch; hybrid duplex; antisense*

Correspondence to: Daniel Němeček; e-mail: nemecekd@umkc.edu

**Current address*: UMKC School of Biological Sciences, Division of Cell Biology and Biophysics, 5100 Rockhill Road, Kansas City, MO 64110-2499

Contract grant sponsor: Grant Agency of Charles University (GACU) and Ministry of Education of the Czech Republic (MECR)

Contract grant numbers: 310/2004 (GACU) and MSM 113200001 (MECR)

INTRODUCTION

Several molecular biological techniques require accurate predictions of matched v. mismatched hybridization thermodynamics (e.g., polymerase chain reaction (PCR), sequencing by hybridization, gene diagnostics, antisense strategy). Therefore, thermodynamics and molecular structures of Watson–Crick and mismatch base pairs have been extensively studied by methods of ultraviolet (UV) melting,[1,2] nuclear magnetic resonance (NMR) distance geometry,[3–6] and X-ray diffraction.[7–9]

Single rG · rU or dG · dU mismatches can form stable wobble base pairs[10,11] that are almost as stable as rA : rU or dA : dT Watson–Crick base pairs.[4] dG · dT and dT · dT mismatch base pairs likely form wobble base pairs as well, whereas dC · dT mismatch is rather stabilized by stacking interactions with adjacent purine rings. Structural studies indicate that hydrogen bonds are formed between mismatched nucleotides and that water molecules can be involved in base pairing too.

Stability of hybrid duplexes with a single mismatch is affected by the nature of the mismatch and the adjacent base pairs.[1] It is also different for dN · rN′ and dN′ · rN mismatches. The rG · dT mismatches are the most stable ones, whereas the stability of rU · dT and rC · dT mismatches was found to be weak.[1]

Study of mismatch structures is also important for the development of new synthetic drugs based on a precise recognition of target molecules (i.e., proteins or nucleic acids). They are nowadays intensively searched and investigated in order to improve drug efficiency and to suppress side effects. ''Antisense'' strategy is a concept of novel gene therapy in which the translation of a pathogen gene is inhibited by a short oligonucleotide complementary to the mRNA target sequence. It forms a local double-helical complex that prevents the mRNA to serve as a matrix for deleterious protein synthesis.[12] If the ''antisense'' oligonucleotide is the deoxy type, the effectiveness of the antisense drug can be substantially enhanced by the RNase H enzyme that excises the mRNA strand of the hybrid duplex while the ''antisense'' deoxy strand is left unperturbed. Natural oligonucleotides are unfortunately unsuitable for in vivo applications owing to their lack of resistance against cell nucleases. An intense search is therefore underway to find novel synthetic oligonucleotide analogues that would possess suitable properties, i.e., resistance in a cellular environment, high binding affinity, specificity to the target nucleic acid sequence, and finally elicitation of RNase H activity.

We have investigated thermodynamic properties of new types of internucleotide linkage modifications by Raman spectroscopy, in developing a method that would allow the determination of the stoichiometry, stability, and structure of the complexes formed between a modified oligonucleotide chain and its natural complementary counterpart. This approach, based on precise Raman titration, Raman temperature profile measurements, and special data treatment procedures, has been applied to characterize two families of various isopolar, nonisosteric modifications of internucleotide linkages.[13,14]

Investigation of the binding specificity, i.e., whether the particular internucleotide linkage modification does or not favor ''fake'' base pairing, is a natural continuation of our studies. The first Raman results were obtained for a model system of DNA duplexes[15] based on 5′-d(GTGATATGC)-3′ and 5′-d(GCAT*N*TCAC)-3′ strands, the latter with alternated central nucleobase N = A, C, G, T. We confirmed the sensitivity of Raman spectra to structural deviations of mismatch duplexes and we obtained reference spectral signatures on a complete set of natural deoxyoligonucleotides.

As a next step, this work presents a study of mismatch hybrid duplexes based on the analogous model system of 5′-d(GTGATATGC)-3′ and 5′-r(GCAU-*N*UCAC)-3′ strands, N = A, C, G, U. The emphasis of the study was to determine structural changes in hybrid duplexes due to a mismatched base pair and to obtain their Raman spectral signatures. The structural characteristics were compared with the duplex stabilities determined by UV absorption measurements.

MATERIAL AND METHODS

The deoxyoligonucleotide complement was synthesized in LMFR of Masaryk University in Brno, then high performance liquid chromatography (HPLC) purified and lyophilized. RNA oligonucleotides were purchased from Dharmacon, Inc., in the stable 2′-acetoxyethoxy protected form (for oligonucleotide sequences, see Table I). They were deprotected with enclosed buffer and lyophilized. Stock solutions of the single-stranded oligonucleotides (40 μL) were prepared by dissolution in a Millipore-filtered solution of 4 m*M* Na_2SO_4 and 100 m*M* NaCl. The concentration was 20 m*M* in nucleotides (UV determination). DNA–RNA mixed solutions of 1:1 molar ratio were prepared from the single-strand solutions by weighting. After Raman meas-

Table I Composition of the Studied Oligonucleotides

Oligonucleotide	Sequence
DNA complement	5′-d(GTG ATA TGC)-3′
RNA1	5′-r(GCA UAU CAC)-3′
RNA2	5′-r(GCA UCU CAC)-3′
RNA3	5′-r(GCA UGU CAC)-3′
RNA4	5′-r(GCA UUU CAC)-3′

Table II Thermodynamic Parameters of Nonamer Hybrid Duplexes with Matched or Mismatched Central Base Pair Obtained from UV Absorption[a]

Duplex (Central bp)	ΔS^0 (cal-mol^{-1} · K^{-1})	ΔH^0 (kcal · mol^{-1})	$\Delta G^0_{310\ k}$ (kcal · mol^{-1})	T_m (°C)	
				$C_{tot} = 80\ \mu M$	$C_{tot} = 4\ \mu M$
dT · rA[b]	−210 ± 10	−72 ± 3	−7.08 ± 0.06	38.7 ± 0.2	30.9 ± 0.2
dT · rC[c]	−193 ± 19	−62 ± 6	−2.68 ± 0.28	18.3 ± 0.6	< 5
dT · rG[b]	−187 ± 9	−64 ± 3	−6.15 ± 0.05	34.4 ± 0.2	25.9 ± 0.2
dT · rU[c]	−187 ± 16	−61 ± 5	−3.50 ± 0.17	21.6 ± 0.6	< 5

[a] Confidence limit of 99% probability.
[b] Results of a simultaneous fit on data from 1:1 DNA : RNA mixtures of 4 and 80 μM total nonamer concentrations.
[c] Results obtained just from 80 μM mixtures, because of only part of the melting profile was obtained for 4 μM mixtures ($T_m < 5$°C).

urements, the mixed solutions were lyophilized and then dissolved in 50 m*M* Tris buffer (pH = 7.6) with 100 m*M* NaCl and 1 m*M* EDTA to obtain solutions of 4 and 80 μM total oligonucleotide concentrations for UV measurements. Before both Raman and UV measurement, the 1:1 mixtures were annealed by heating up to 90°C and slow cooling down to the starting temperature.

Raman spectra excited with the 488-nm line of an argon ion laser (power at the sample ~350 mW) were recorded in a 90° scattering geometry on a Jobin Yvon T64000 CCD Raman spectrometer with a 1200 grooves/mm holographic grating. Samples were placed into a 12-μL temperature-stabilized microcell. All measurements were carried out at 15°C; the total exposure time for each spectrum was 180 min. Particular spectrum acquisition was divided into 9 separate accumulations (of 20 min). Before each accumulation, a neon glow lamp spectrum was recorded for precise recalibration of the wavenumber scale. The spectrum of Na_2SO_4 solution was subtracted from the set of Raman spectra by using a homemade code ''Pomlazka.'' Simultaneously, a background adjustment was made by subtraction of trace contributions from the microcell walls. The water signal was used as an internal intensity standard.

UV absorption spectra were recorded with VARIAN Cary 100 Bio spectrophotometer in the 3–58°C temperature range. Sample temperature was measured directly in the absorption cell by using a miniature thermoprobe. Individual acquisitions of UV spectra were performed after 7 min of temperature stabilization at desired temperature.

The melting curves obtained as temperature dependence of the absorbance value at 260 nm (corrected for the experimental offset by subtraction of the absorbance value at 320 nm) were fitted according to the following equation:

$$A_T^{mix} = c_T^{Du}(A_0^{Du} + T \cdot A_1^{Du}) + (c_T^{ssDNA} + c_T^{ssRNA}) \cdot (A_0^{ss} + T \cdot A_1^{ss}), \quad (1)$$

where c_T^{Du}, c_T^{ssDNA}, and c_T^{ssRNA} are concentrations of the duplex, DNA, and RNA single strands at temperature T, mutually related via equilibrium constant of the helix to coil transition given by the van't Hoff equation:

$$\Delta H_0 - T\Delta S_0 = -RT\ln\frac{c_T^{Du}}{c_T^{ssDNA} \cdot c_T^{ssRNA}} \quad (2)$$

A_0^{Du}, A_1^{Du} and A_0^{ss}, A_1^{ss} represent fitted coefficients (normalized to unit concentration) of a linear temperature dependence for both duplex and single strands extinctions.[16,17] Values of enthalpy ΔH_0 and entropy ΔS_0 changes were determined in a least-square sense accordingly to Eqs. (1) and (2), taking into account relations for the total DNA and RNA nonamer concentrations (C^{TotDNA}, C^{TotRNA}). Change of Gibbs energy and the melting temperature were calculated according to

$$\Delta G_T^0 = \Delta H_0 - T\Delta S_0,$$
$$T_m = \frac{\Delta H^0}{\Delta S^0 + R\ln\left(\frac{C^{TotDNA} + C^{TotRNA}}{4}\right)} \quad (3)$$

Monte Carlo simulations of individual temperature profiles within estimated levels of the absorbance value error (±0.001) were performed to determine confidence limits[18] of 99% probability of the thermodynamic parameters. In other words, each absorbance value inside a particular temperature profile was shifted to a random value (within the estimated error interval) and the obtained modified temperature profile was fitted. This procedure was repeated 20 times and the resulting set of thermodynamic parameters (ΔH_0, ΔS_0, ΔG_T^0, and T_m) statistically treated and the confidence intervals of 99% probability were determined.

RESULTS AND DISCUSSION

Thermodynamic parameters determined by fitting UV temperature profiles of 1:1 mixtures of DNA and RNA nonamers are listed in Table II. The confidence intervals of ΔS_0 and ΔH_0 values are substantially

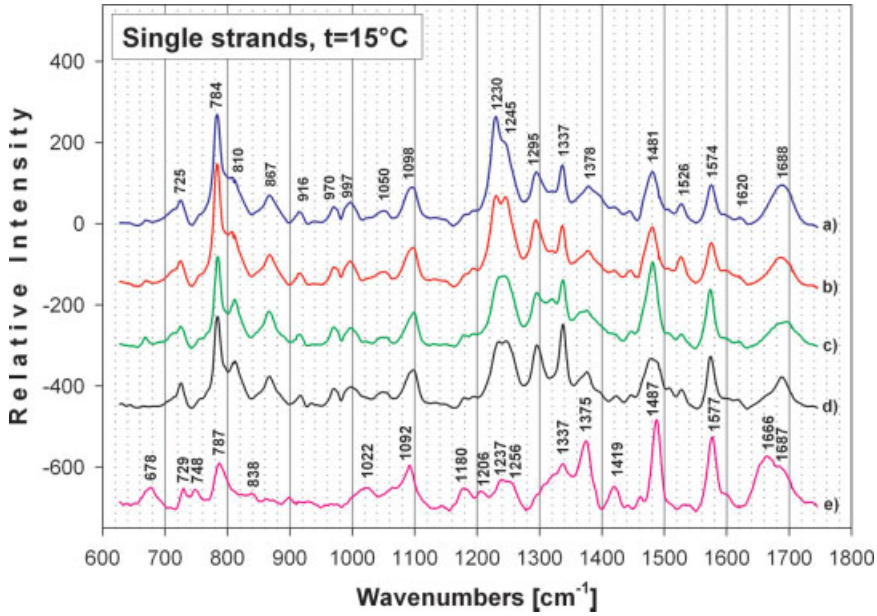

FIGURE 1 Raman spectra of single-strand oligonucleotides: (a) RNA4, (b) RNA2, (c) RNA3, (d) RNA1, and (e) DNA complement.

larger than those of $\Delta G^0_{310\ K}$ and T_m owing to known highly correlated effect of the ΔS_0 and ΔH_0 values on the sum of squared deviations in the fit of the van't Hoff equation.[19] The duplex stability is obviously dependent on the mismatched base-pair composition. While the stability decrease caused by dT · rG mismatch is very weak, dT · rC and dT · rU mismatches reduce the stability considerably. This is in agreement with a previous study of DNA : RNA mismatch duplexes by UV spectroscopy[1] as well as with predictions by SantaLucia and Peyret's database HyTher™ (available at http://ozone2.chem.wayne.edu/), even though the predicted thermodynamic parameters are systematically lower than our results.

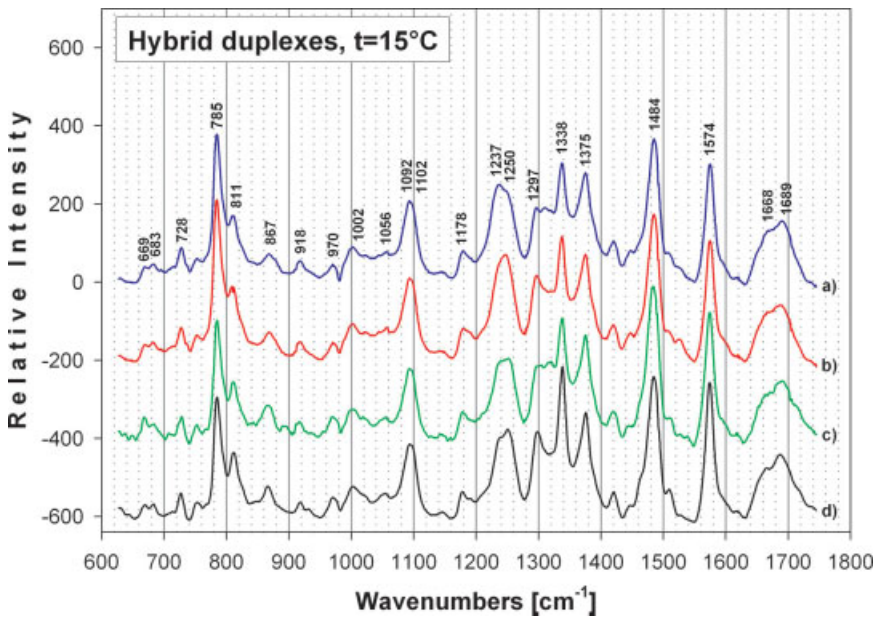

FIGURE 2 Raman spectra of hybrid duplexes with or without a central mismatch: duplex with dT · rU central mismatch (a), with dT · rC central mismatch (b), with dT · rG central mismatch (c), and fully complementary duplex with dT : rA central base pair (d).

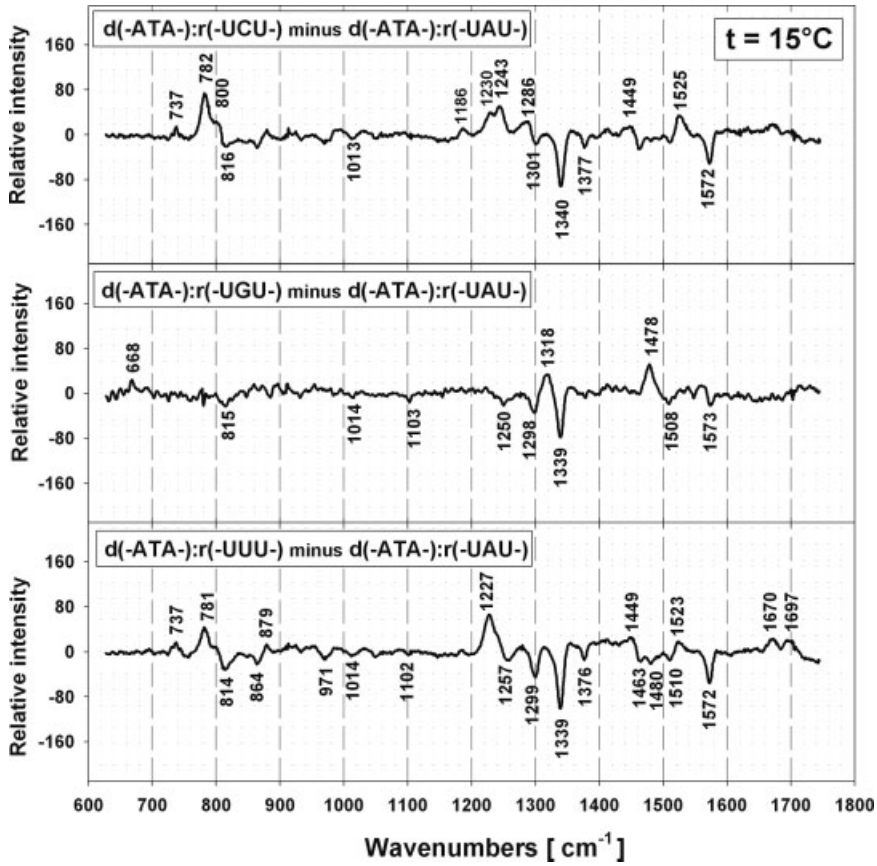

FIGURE 3 Difference Raman spectra between mismatch and match hybrid duplexes.

Spectra of the single-strand oligonucleotides are shown in Figure 1. Different nucleotide compositions cause the main spectral differences between the DNA complement and the various RNA match or mismatch strands. Differences between the RNA strands are due to variation of only one nucleobase among 9 and therefore they are detectable mainly for intense bands, such as 784 (C, U),[20,21] 1230 (U),[22] 1245 (C),[23] 1337 (A),[24,25] 1481 (G),[26] and 1575 cm^{-1} (A, G).[26] Furthermore, there are also remarkable strong markers of A-like conformation of sugar–phosphate backbone (810 cm^{-1}).[24,27] It means that the single-strand RNA oligonucleotides are partly organized into the conformation they adopt in duplexes. On the other hand, the DNA complement spectrum contains only a very weak marker of B-like conformation (838 cm^{-1}).[26,27]

Spectra of hybrid duplexes (shown in Figure 2) are more similar to each other than the single-strand spectra. It confirms that a mismatch does not drastically disturb the overall conformation of the duplexes. Still, the intense bands with major contributions from base vibrations are different from each other, owing to the varied mismatch base. The backbone conformation is reflected by markers of the A-like conformation of the sugar–phosphate backbone, which exceed those of the B-like conformation. The band at about 1094 cm^{-1} assigned to the PO_2^- symmetric vibration is composed of two bands, i.e., 1092 and 1101 cm^{-1}. The former position corresponds to the B-family of backbone torsion angles, the latter to the A-family.[26,27] Nevertheless, difference spectra obtained by subtraction of the relevant single-strand spectra from a given duplex spectrum (not shown) exhibit increased intensities at 1101 cm^{-1} only. On the other hand, the duplex spectra also feature bands assigned to coupled vibrations of bases and sugar moieties in the C2′-*endo*/*anti* puckering, i.e., 669 (dT), 683 (dG), and 728 cm^{-1} (dA).[21,24,26] Hence, the DNA strand bound to its RNA counterpart likely adopts a specific backbone local geometry showing certain structural features of both A-type and B-type double helices.

Structural changes within the mismatch sites in the hybrid duplexes were analyzed at the level of Raman difference spectra between the match and the mismatch duplexes (Figure 3). In the same way as in our previous study of DNA duplexes with a mismatch,[15]

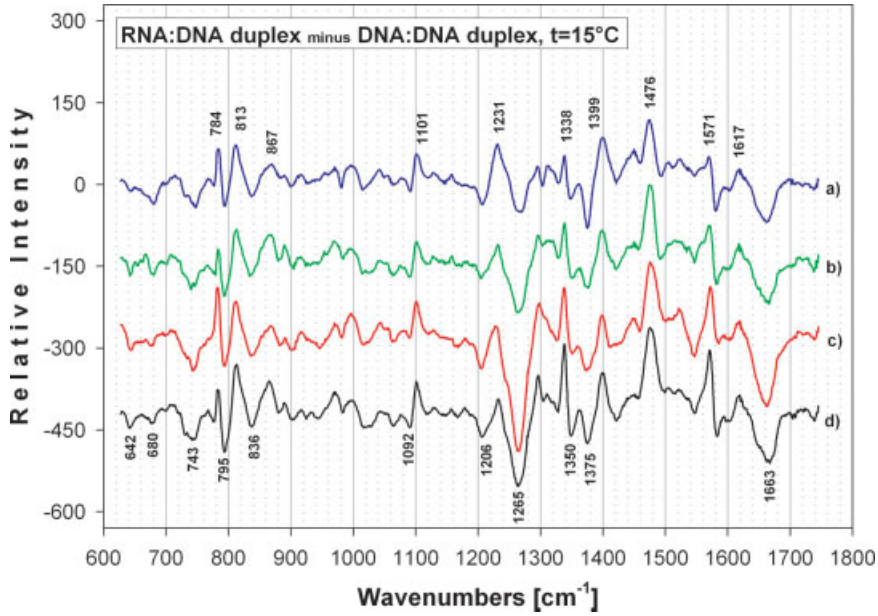

FIGURE 4 Difference spectra between hybrid and DNA duplexes with (a) dT · rU and dT · dT mismatches, (b) dT · rG and dT · dG mismatches, (c) dT · rC and dT · dC mismatches, and (d) with all Watson–Crick base pairs. Positive bands are characteristic for the hybrid duplexes, while the negative ones belong to the DNA duplexes.

the duplex spectra were normalized to unit intensity and the differences obtained with a subtraction factor set to one. These spectra show only the spectral features caused by the substitution of the dT : rA Watson–Crick base pair by the dT · r*N* mismatch one. Many bands simply represent the substitution of the mismatch nucleobase *N*. Missing rA is featured by 1257, 1299, 1339, 1510, and 1572 cm^{-1} negative bands, while replacement by rC, rG, or rU gives rise to 782, 1243, 1286, and 1525 cm^{-1}; 668, 1318, and 1478 cm^{-1}; or 781 and 1227 cm^{-1} positive bands, respectively. The backbone conformation of all mismatch duplexes is weakly altered from the A-like geometry according to the negative peaks at positions of its marker bands,[26,27] i.e., 815 and 1100 cm^{-1}. Nevertheless, the structure of hybrid duplexes is much less disturbed by the mismatched pair occurrence than that of the DNA duplexes.[15] In particular, the difference spectrum of the dT · rG mismatch duplex shows almost no spectral change except the bands of adenosine and guanosine due to the dA → rG substitution.

An interesting spectral feature is the negative band at 1376 cm^{-1}, which is present only in the difference spectra of pyrimidine–pyrimidine mismatches. This band is assigned to a vibration of dT. Intensity decrease of this band was interpreted[26] in terms of a more hydrophilic environment around the thymidine C5—CH_3 methylene group. Because there is no spectral change in the difference spectra of the dT · rG mismatch, it leads to the conclusion that the substitution of adenine with a pyrimidine nucleobase changes stacking of the opposite thymine, whereas the substitution with guanine does not.

Another important finding is very weak or no spectral change in the region of carbonyl vibrations (1600–1700 cm^{-1}). The positive bands at 1670 and 1697 cm^{-1} in the difference spectrum of the dT · rU mismatch only reflect additive carbonyl groups of the substituted uracil. In the case of DNA duplexes with analogous mismatches,[15] this region yielded important spectral differences. Moreover, they were found different for the dT · dC mismatch in comparison to the dT · dG and dT · dT mismatches.

Unique spectral characteristics of the DNA duplexes with respect to the hybrid ones and vice versa are revealed in their difference spectra (Figure 4). Spectrum of the hybrid duplex was subtracted from the DNA duplex spectrum with the corresponding (mis)match base pair by using a subtraction coefficient equal to one, owing to the same normalization of both spectra. Different positions of base pairs within the different double helixes are featured by intensity changes of conformation-sensitive bands[24,25,27] with important contributions from base vibrations such as 1206 (T), 1230 (U), 1265 (C), 1339 (A), 1476 (A), and 1617 cm^{-1} (U) as well as by the spectral shift 1582 → 1571 cm^{-1} (A).

Other spectral changes are similar in all difference spectra. Some bands shift by several wavenumbers (795 → 784 cm^{-1}, 836 → 813, 1092 → 1102 cm^{-1}) showing a change of the backbone geometry from the B-family of backbone torsion angles in the DNA duplexes close to A-family in the hybrid duplexes. A positive band at 867 cm^{-1} is characteristic for RNA oligonucleotides and it is assigned to the base moiety of guanosine.[23] Negative bands at 680 and 743 cm^{-1} reflect C2′-*endo*/*anti* sugar puckering of guanosine and thymidine residues in the DNA duplexes, while a strong band at about 1663 cm^{-1} indicates different interactions of carbonyl groups within the different double helixes.

Comparison of hybrid and DNA duplexes spectra shows significant differences not only in the structure of the duplexes, but also in structural deviations caused by the mismatch. This finding agrees with thermodynamic characteristics of duplexes with a single mismatch.[1,5,28,29] Consequently, only the hybrid and not DNA : DNA duplexes represent a relevant molecular system to study the structural effect of the internucleotide linkage modification on mispaired duplexes possibly formed in ''antisense'' action. The proposed molecular model will consist of four RNA nanomers, 5′-r(GCAU*N*UCAC)-3′ (N = A, C, G, U), and analogs of the DNA complement, 5′-d(GTGATATGC)-3′, with modified internucleotide linkage in the neighborhood of the central base.

CONCLUSIONS

Like in our previous study,[15] the results obtained for hybrid duplexes with or without a central mismatch proved the suitability of Raman spectroscopy to monitor conformational variations within mismatch sites of nucleic acid duplexes. We have found that single-stranded RNA oligonucleotides adopt an A-like family of torsion angles of the sugar–phosphate backbone. This backbone conformation persists in the hybrid duplexes, and since no important increase of B-markers was observed, the A-like local conformation was likely forced to part of the DNA strand as well. The influence of the mismatches on the structure of the hybrid duplexes is significantly weaker than their influence on the structure of analogous DNA duplexes. In particular, the dT · rG mismatch pair is very well incorporated into the double helix structure. The substitution of adenine in the dT : rA pair by pyrimidine causes change of the thymine position that alters the surrounding of its methyl group but does not, in contrast to DNA duplexes, influence interactions of carbonyl oxygens. Overall, magnitudes of obtained changes in Raman structural features correlate well with the duplex stabilities.

This work was partly supported by the Grant Agency of Charles University (project no. 310/2004) and by Ministry of Education of the Czech Republic (MSM 113200001). DN thanks the French government for the support of his stay at LPBC in Paris.

REFERENCES

1. Sugimoto, N.; Nakano, M.; Nakano, S. Biochemistry 2000, 39(37), 11270–11281.
2. Kierzek, R.; Burkard, M. E.; Turner, D. H. Biochemistry 1999, 38(43), 14214–14223.
3. Gervais, V.; Cogner, J. A. H.; Le Bret, M.; Sowers, L. C.; Fazakerley, G. V. Eur J Biochem 1995, 228, 279–290.
4. Allawi, H. T.; SantaLucia, J., Jr. Biochemistry 1997, 36, 10581–10594.
5. Allawi, H. T.; SantaLucia, J., Jr. Nucleic Acid Res 1998, 26(11), 2694–2701.
6. Lane, A. N.; Peck, B. Eur J Biochem 1995, 230, 1073–1087.
7. Hunter, W. N.; Brown, T.; Kneale, G.; et al. J Biol Chem 1987, 262(21), 9962–9970.
8. Kennard, O. J Biomol Struct Dyn 1985, 3, 205–226.
9. Ho, P. S.; Frederic, C. A.; Quigley, G. J.; et al. EMBO J 1985, 4, 3617–3623.
10. Sussman, J. L.; Holbrook, S. R.; Warrant, R. W.; Church, G. M.; Kim, S. H. J Mol Biol 1978, 123(4), 607–630.
11. Brown, T.; Leonard, G. A.; Booth, E. D.; Chamber, J. J Mol Biol 1989, 207(2), 455–457.
12. Kurreck, J.Eur. J.Biochem 2003, 270, 1628–1644.
13. Hanuš, J.; Barvík, I., Jr.; Ruszová-Chmelová, K.; et al. Nucleic Acids Res 2001, 29(24), 5182–5194.
14. Hanuš, J.; Němeček, D.; Štěpánek, J.; Turpin, P.-Y.; Králíková, Š.; Bok, J.; Rosenberg, I. J Raman Spectrosc 2004, 35, 418–425.
15. Němeček, D.; Štěpánek, J.; Turpin, P.-Y.; Rosenberg, I. Biopolymers 2004, 74, 115–119.
16. Petersheim, M.; Turner, D. H. Biochemistry 1983, 22, 256–263.
17. SantaLucia, J., Jr. In Spectrophotometry & Spectrofluorimetry; Gore, M. G., Ed.; Oxford University Press: Oxford, UK, 2000; pp 329–356.
18. Press, W. H.; Teukolsky, S. A.; Vetterling, W. T.; Flannery, B. P. Numerical Recipes in Fortran, 2nd ed.; Cambridge University Press: Cambridge, UK, 1992; pp 684–694.
19. Wu, P.; Nakano, S.; Sugimoto, N. Eur J Biochem 2002, 269, 2821–2830.
20. Thomas, G. J., Jr.; Tsuboi, M. In Advances in Biophysical Chemistry; Bush, C. A., Ed.; JAI Press: Greenwich, CT, 1993; Vol 3, pp 1–70.
21. Benevides, J. M.; Wang, A. H.-J.; van der Marel, G. A.; van Boom, J. H.; Thomas, G. J., Jr. Biochemistry 1989, 28, 304–310.

22. O'Connor, T.; Bina, M. J Biomol Struct Dyn 1984, 2(3), 615–625.
23. Nishimura, Y.; Tsuboi, M. J Mol Struct 1986, 146, 123–153.
24. Thomas, G. J., Jr.; Wang, A. H.-J. In Nucleic Acids and Molecular Biology; Eckstein, F., Lilley, D. M. J., Eds.; Springer-Verlag: Berlin, Heidelberg, Germany, 1988; Vol 2, pp 1–30.
25. Nishimura, Y.; Tsuboi, M. In Advances in Spectroscopy; Clark, R. J. H., Hester, R. E., Eds.; John Wiley & Sons: Chichester, UK, 1986; Vol 13, Chap 4, pp 177–232.
26. Deng, H.; Bloomfield, V. A.; Benevides, J. M.; Thomas, G. J., Jr. Biopolymers 1999, 50, 656–666.
27. Benevides, J. M.; Thomas, G. J., Jr. Biochemistry 1988, 27, 3868–3873.
28. Allawi, H. T.; SantaLucia, J., Jr. Nucleic Acid Res 1998, 26(21), 4925–4934.
29. Peyret, N.; Seneviratne, P. A.; Allawi, H. T.; SantaLucia, J., Jr. Biochemistry 1999, 38, 3468–3477.

Reviewing Editor: Kenneth J. Breslauer

Appendix II

R. Slavík, J. Homola, and H. Vaisocherová:

Advanced biosensing using simultaneous excitation of short and long range surface plasmons

Measurement Science and Technology, **17** (2006), 932 – 938

INSTITUTE OF PHYSICS PUBLISHING MEASUREMENT SCIENCE AND TECHNOLOGY

Meas. Sci. Technol. **17** (2006) 932–938 doi:10.1088/0957-0233/17/4/045

Advanced biosensing using simultaneous excitation of short and long range surface plasmons

Radan Slavík, Jiří Homola and Hana Vaisocherová

Institute of Radio Engineering and Electronics, Academy of Sciences of the Czech Republic, Chaberská 57, 18251 Prague, Czech Republic

Received 9 November 2005, in final form 7 February 2006
Published 23 March 2006
Online at stacks.iop.org/MST/17/932

Abstract
We present a novel optical biosensor which exploits simultaneous excitation of two different surface plasmons in a single sensing spot. It allows compensation of cross-sensitivity to background refractive index change, as a typical surface plasmon resonance sensor is sensitive to both the absorption of a thin film on the surface (sensing event) and the refractive index change of the background (an interfering effect). The structure parameters are optimized to yield low noise and minimum cross-sensitivity. In the performed model experiment, IgE biomolecules at a concentration of 250 ng ml^{-1} are detected during a change in the background refractive index of 10^{-3}.

Keywords: surface plasmon resonance, optical sensor, reference-compensated sensing, biosensor

1. Introduction

The interest in surface plasmon resonance (SPR) for optical biosensing is continuously increasing. Next-generation SPR biosensors, however, require further miniaturization (e.g., using optical waveguides [1, 2]), increase in the resolution (e.g., using advanced detection schemes [3] or advanced data analysis [4]), high throughput (e.g., using SPR imaging [5]) and suppression of cross-sensitivity to background refractive index (e.g., by temperature stabilization [6], using two channels with receptors with different analyte affinity [7], and two-plasmon spectroscopy [8, 9]).

The SPR biosensor cross-sensitivity originates in the fact that the surface plasmon (SP) field penetrates into the background through a thin layer of analyte adsorbed at the sensor surface from a solution (*background*). Thus, both surface-adsorbed analyte (causing *surface refractive index change*) and the background (causing *bulk refractive index change*) are within the SPR sensitive region. The background changes usually have their origin in variations of temperature or composition.

There are several reports on schemes for suppression of the background refractive index cross-sensitivity [6–9]. The temperature stabilization is typically limited to ±0.1 °C [6] and cannot compensate for changes in the background composition. Two-plasmon spectroscopy uses, e.g. [8], a special lightpipe, where light excites two SPs with different penetration depths at two different spots of the sensor surface. Putting a medium under study in contact with both spots and using data analysis, information on surface and background changes are retrieved. Though this method [8, 9] is powerful in its compensation ability, it collects data from two different parts of the sensor surface, at which identical conditions cannot be guaranteed (e.g., temperature and coverage with receptors). Moreover, there is a time delay between the two SPR responses. Using two separate sensor channels covered by receptors with and without affinity to the analyte is another technique (*two-channel-compensated SPR* [7]). Its advantage is compensation ability for both the background and non-specific adsorption. The disadvantages are the need for a higher number of sensing channels and, as for the special lightpipe, the fact that the two signals come from two different sensing spots.

Recently, we suggested another approach to two-plasmon spectroscopy [10]. We demonstrated that in the SPR sensors based on identification of SPR feature spectral position in attenuated total reflection (ATR) configuration (*spectral configuration* [11]), it is possible to excite

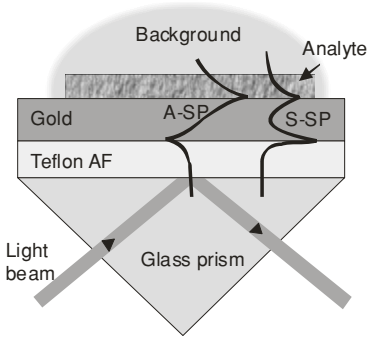

Figure 1. Sensor element configuration for excitation of S/A-SPR.

simultaneously symmetric and anti-symmetric SPs at two different wavelengths at the same (sensing) spot.

In this paper, we expand this idea [10] to develop a new self-referenced biosensor. We optimize the structure in terms of resolution and cross-sensitivity to background refractive index changes. The sensing structures are realized and employed in a model IgE biosensing experiment, where antibodies against human immunoglobulin E (aIgE) are immobilized on the sensor surface. Results are compared with the two-channel-compensated SPR performed on a conventional two-channel SPR instrument.

2. Sensor element structure and principle of operation

Polychromatic light incident from a high-refractive index material (optical prism) can excite two SPs bound to a metal layer, symmetric bound mode (symmetric surface plasmon, S-SP) and anti-symmetric bound mode (anti-symmetric surface plasmon, A-SP) [10], figure 1. However, this is possible only when the metal is surrounded by two dielectric materials of similar refractive indices (background and buffer layer). For a rather thick metal layer, the propagation constant of the S-SP is close to that of the A-SP. Consequently, a polychromatic wave of finite bandwidth can excite both SPs simultaneously. Similarly to two-plasmon spectroscopy [8], the two SPs have different field profiles (and thus also different penetration depths into the medium under study), which enables separation of surface and bulk refractive index changes.

We demonstrated [10] that efficient simultaneous coupling into S/A-SPs, when more than 95% of incident light is coupled into both SPs at the two SPR wavelengths, is possible when Teflon AF is used as the buffer layer in combination with gold as the metal layer. Due to a poor adhesion of gold to Teflon AF, a thin adhesive titanium layer (not shown in figure 1) has to be introduced.

3. Theoretical analysis

In order to compare different sensor designs, we define *surface and bulk refractive index sensitivity* as a change in the SPR wavelength due to a unit change in the thickness of a thin film with refractive index of 1.48 (proteins) adsorbed at the sensor surface and due to a unit change in the background refractive index (RIU), respectively. Further, we define sensor *resolution* as the smallest change of the parameter of interest resolvable by the sensor. The resolution is influenced by the sensitivity, the accuracy with which SPR spectral position is found, and the cross-sensitivity (sensitivity to other than the measured parameter).

As follows from [4], the accuracy with which SPR position is found is linearly proportional to SPR depth and square-root to its width. As there are, to our knowledge, no data for cross-sensitivity analysis for SPR biosensing in the literature, we derive the necessary formulae in the following part, where we adopt the fibre Bragg grating sensors cross-sensitivity analysis published in [12]. There is an important difference between an SPR biosensor and fibre Bragg grating sensor, which allows us to simplify the cross-sensitivity analysis. In an SPR biosensor, a very small change in the parameter of interest (analyte thickness) has to be measured (first simplification—the measured changes are small) and, consequently, the change in the interfering parameter has to be kept reasonably low (e.g., by temperature stabilization), as all compensation techniques are limited in their compensation ability (second simplification—relatively small changes in both the measured and interfering quantities allow for linear analysis).

3.1. Cross-sensitivity analysis

3.1.1. Ideal case. Generally, both SPR spectral positions are sensitive to both bulk and surface refractive index changes. The surface S and bulk B changes are given as follows:

$$\Lambda = K\Omega, \tag{1}$$

where

$$\Lambda = \begin{bmatrix}\lambda_1\\ \lambda_2\end{bmatrix}, \quad \Omega = \begin{bmatrix}S\\ B\end{bmatrix}, \quad K = \begin{bmatrix}K_{1S} & K_{1B}\\ K_{2S} & K_{2B}\end{bmatrix}, \tag{2}$$

where K is the characteristic matrix of the sensor. Provided the determinant of K, $\det(K) = K_{1S}K_{2B} - K_{1B}K_{2S}$, is not equal to zero, the values of interest are found as [12]

$$\Omega = K^{-1}\Lambda = K'\frac{\Lambda}{\det(K)}, \quad K' = \begin{bmatrix}K_{2B} & -K_{1B}\\ -K_{2S} & K_{1S}\end{bmatrix}. \tag{3}$$

Subscripts B and S denote bulk and surface and $\lambda_{1,2}$ are SPR resonance wavelength shifts caused by the sensing event for S-SPR and A-SPR, respectively. K is given by two calibrations (considering the linear regime, as follows from the second simplification), where purely surface (first calibration) and bulk (second calibration) refractive index changes are performed:

$$\begin{bmatrix}\lambda_1^{S=0}\\ \lambda_2^{S=0}\end{bmatrix} = K^{S=0}\begin{bmatrix}0\\ B^{S=0}\end{bmatrix}, \quad \begin{bmatrix}\lambda_1^{B=0}\\ \lambda_2^{B=0}\end{bmatrix} = K^{B=0}\begin{bmatrix}S^{B=0}\\ 0\end{bmatrix}. \tag{4}$$

After some mathematical manipulations we get

$$K = \begin{bmatrix}\lambda_1^{B=0}/S^{B=0} & \lambda_1^{S=0}/B^{S=0}\\ s^S\lambda_1^{B=0}/S^{B=0} & s^B\lambda_1^{S=0}/B^{S=0}\end{bmatrix}, \tag{5}$$

where we considered S/A-SPR sensitivity ratios for surface (s^S) and bulk (s^B):

$$\lambda_2^{B=0} = s^S\lambda_1^{B=0}, \qquad \lambda_2^{S=0} = s^B\lambda_1^{S=0}. \tag{6}$$

From (3) and (5), S and B are then

$$S = S^{B=0}\frac{\lambda_1 s^B - \lambda_2}{\lambda_1^{B=0}(s^B - s^S)}, \quad B = B^{S=0}\frac{-\lambda_1 s^S + \lambda_2}{\lambda_1^{S=0}(s^B - s^S)}. \tag{7}$$

3.1.2. Noise and cross-sensitivity. Considering the linear regime (the second simplification), it can be shown [12] that the sensor output noise is predominantly determined by error (*noise*) in Λ and the sensor cross-sensitivity by error in coefficients of the matrix K. Error in Λ is given by uncertainty of the resonant wavelengths and error in K by inaccuracy of the sensor calibration. For errors in Λ and K we write [12]

$$\Lambda = \Lambda_0 + \Delta\Lambda, \qquad \Delta\Lambda = \begin{bmatrix} \Delta\lambda_1 \\ \Delta\lambda_2 \end{bmatrix}, \tag{8}$$

$$K = K_0 + \Delta K, \qquad \Delta K = \begin{bmatrix} K_{1S}\delta_{1S} & K_{1B}\delta_{1B} \\ K_{2S}\delta_{2S} & K_{2B}\delta_{2B} \end{bmatrix}, \tag{9}$$

where $\delta_{1,2,S,B}$ represents the fractional error in each element of K and $\Delta\lambda_{1,2}$ are absolute errors of $\lambda_{1,2}$. In practice, often only the maximum errors $|\delta|$ and $|\Delta\lambda|$ are known. Supposing the error is cumulative, one can get an estimation of the worst case. Considering that the errors of elements of K are much smaller than the value of these elements, we can approximate the worst case cross-sensitivity (superscript K) [12]:

$$|\Delta S|^K = \{|S|(|K_{1S}K_{2B}\delta_{1S}| + |K_{1B}K_{2S}\delta_{2S}|) + |B||K_{1B}K_{2B}|(|\delta_{1B}| + |\delta_{2B}|)\}/\{|\det(K)|\}, \tag{10}$$

$$|\Delta B|^K = \{|B|(|K_{1B}K_{2S}\delta_{1B}| + |K_{1S}K_{2B}\delta_{2B}|) + |S||K_{1S}K_{2S}|(|\delta_{1S}| + |\delta_{2S}|)\}/\{|\det(K)|\}. \tag{11}$$

The worst case level of noise caused by $\Delta\Lambda$ (superscript Λ) is [12]

$$\Delta S^\Lambda = \frac{|K_{2B}\Delta\lambda_1| + |K_{1B}\Delta\lambda_2|}{|\det(K)|}, \qquad \Delta B^\Lambda = \frac{|K_{2S}\Delta\lambda_1| + |K_{1S}\Delta\lambda_2|}{|\det(K)|}. \tag{12}$$

Considering calibrations (5), (9) is modified to

$$\begin{bmatrix} \delta_{1S} & \delta_{1B} \\ \delta_{2S} & \delta_{2B} \end{bmatrix} = \begin{bmatrix} \frac{\Delta\lambda_1^{B=0}}{\lambda_1^{B=0}} & \frac{\Delta\lambda_1^{S=0}}{\lambda_1^{S=0}} \\ \frac{\Delta\lambda_2^{B=0}}{s^S\lambda_1^{B=0}} & \frac{\Delta\lambda_2^{S=0}}{s^B\lambda_1^{S=0}} \end{bmatrix} = 2\begin{bmatrix} \frac{\Delta\lambda_1}{\lambda_1^{B=0}} & \frac{\Delta\lambda_1}{\lambda_1^{S=0}} \\ \frac{\Delta\lambda_2}{s^S\lambda_1^{B=0}} & \frac{\Delta\lambda_2}{s^B\lambda_1^{S=0}} \end{bmatrix}, \tag{13}$$

where we considered that the calibration errors are caused only by an inaccuracy in determining the resonant wavelengths $\Delta\lambda_{1,2}$ during the calibration:

$$\left|\Delta\lambda_i^{S,B=0}\right| = 2|\Delta\lambda_i|, \qquad i = 1, 2. \tag{14}$$

The expressions for noise ($|\Delta S|^\Lambda$ and $|\Delta B|^\Lambda$) are obtained by substituting K elements given by (5) into (12)

$$|\Delta S|^\Lambda = \left|\frac{S^{B=0}}{\lambda_1^{B=0}}\right| \frac{|s^B\Delta\lambda_1| + |\Delta\lambda_2|}{|s^B - s^S|}, \qquad |\Delta B|^\Lambda = \left|\frac{B^{S-0}}{\lambda_1^{S=0}}\right| \frac{|s^S\Delta\lambda_1| + |\Delta\lambda_2|}{|s^B - s^S|}. \tag{15}$$

The expressions for cross-sensitivity are obtained by substituting K elements given by (5) and δ elements given by (13) into (10) and (11):

$$|\Delta S|^K = |S|\left(2\frac{|s^B\Delta\lambda_1| + |\Delta\lambda_2|}{|\lambda_1^{B=0}||s^B - s^S|}\right) + |B|\left(\left|\frac{2|S^{B=0}|}{|B^{S=0}|}\right| \frac{|s^B\Delta\lambda_1| + |\Delta\lambda_2|}{|\lambda_1^{B=0}||s^B - s^S|}\right), \tag{16}$$

Table 1. Parameters of the sensor.

Gold thickness (nm)	Titanium thickness (nm)	$\lvert s^S - s^B\rvert$	$\lvert\Delta S\rvert^\Lambda$ (pm)	$\lvert\Delta B\rvert^\Lambda$ ($10^{-6}\times$ RIU)	$\lvert\Delta S\rvert^{K,S0}/\lvert B\rvert$ (RIU nm^{-1})
45	1	1.46	9.0	6.9	3.6
	3	0.85	9.6	8.2	3.8
	5	0.59	10.1	9.4	4.0
55	1	0.89	14.3	10.9	5.7
	3	0.42	17.1	14.1	6.8
	5	0.24	19.9	17.4	7.9
65	1	1.05	23.1	17.1	9.2
	3	0.71	16.1	13.6	6.4
	5	0.014	34.5	304	138.6

$$|\Delta B|^K = |B|\left(2\frac{|s^S\Delta\lambda_1| + |\Delta\lambda_2|}{|\lambda_1^{S=0}||s^B - s^S|}\right) + |S|\left(\left|\frac{2B^{S=0}}{S^{B=0}}\right| \frac{|s^B\Delta\lambda_1| + |\Delta\lambda_2|}{|\lambda_1^{S=0}||s^B - s^S|}\right). \tag{17}$$

From (15)–(17) we conclude that all the errors are inversely proportional to $|s^B - s^S|$. This term approaches zero when the two SPs have similar ratios of bulk and surface refractive index sensitivities. The calibration error ((16) and (17)) of B and S is inversely proportional to the calibration-performed change of S $\left(\lambda_1^{B=0}\right)$ and B $\left(\lambda_1^{S=0}\right)$, respectively. Thus, to suppress the cross-sensitivity of B in S, high calibration change in B is desirable (however, we need to stay within the linear regime). Although the cross-sensitivity is a function of both S and B ((16) and (17)), in the following analysis we concentrate on a usual situation in biosensing, where an extremely small change in the surface refractive index is of interest ($S \to 0$) and the bulk change needs to be eliminated (the first simplification). Approximating $S = 0$ in (16) we get

$$|\Delta S|^{K,S_{\text{neglect}}} = |B|\left(\left|\frac{2}{(B^{S=0})^2}\right| \frac{|s^B\Delta\lambda_1| + |\Delta\lambda_2|}{|\lambda_1^{B=0}||s^B - s^S|}\right), \tag{18}$$

where the superscript S_{neglect} means that the surface refractive index change is neglected.

It is worth noting that for a small change in the bulk refractive index B, the noise will dominate over the cross-sensitivity, which is linearly dependent on B and vice versa. For a certain value of B ($B = B_{\text{crit}}$), these two errors are equal ($|\Delta S|^{K,S0} = |\Delta S|^\Lambda$). Using (15) and (18) we get

$$B_{\text{crit}} = B^{S=0}/2. \tag{19}$$

Thus, the relative level of cross-sensitivity is predominantly given by the calibration accuracy and does not depend on the design. However, its absolute value, as well as the noise, is strongly design dependent, as will be shown later (table 1). We can conclude that for $B < B_{\text{crit}} = B^{S=0}/2$, the resolution is given predominantly by the noise $|\Delta S|^\Lambda$, while for $B > B_{\text{crit}} = B^{S=0}/2$ by the cross-sensitivity $|\Delta S|^{K,S_{\text{neglect}}}$.

3.2. Design

Here, we look for optimum parameters of the proposed structure. We consider optical constants shown in figure 2. To analyse propagation of light through the sensor element structure (figure 1), we used a transfer matrix method,

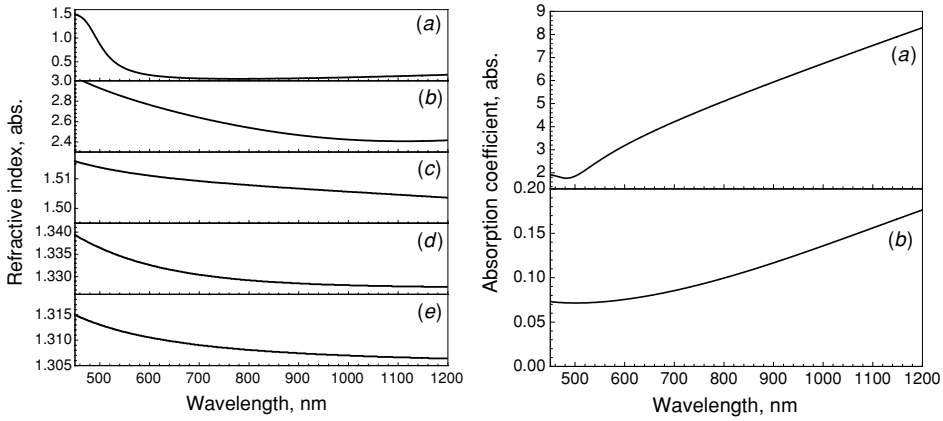

Figure 2. Dispersion relations of the involved materials. On the left is the real part of the refractive index of gold (*a*), Ti (*b*), BK7 glass (*c*), water (*d*) and Teflon AF (*e*). On the right is the imaginary part of the refractive index of gold (*a*) and Ti (*b*), while it is zero for the rest of materials.

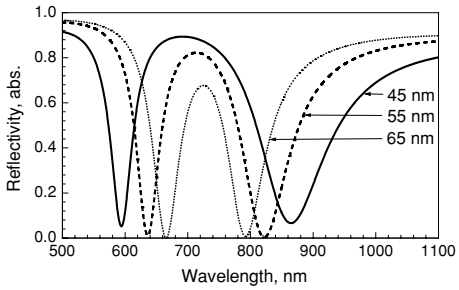

Figure 3. Spectral reflectivity for gold layer thicknesses of 45, 55, and 65 nm; Ti is 3 nm thick. Corresponding Teflon AF thicknesses are 350, 390 and 400 nm.

Fresnel's formulae and multiple-reflection theory, as described, e.g., in [13]. The calibration values $\lambda_1^{S=0,B=0}$ and $s^{S,B}$ are obtained by modifying surface and bulk refractive index and observing shifts in S/A-SPR positions. For the design, we considered realistic calibration changes in S and B of 10 nm and 5×10^{-3}, respectively. For errors $\Delta\lambda_{1,2}$, we considered that they are given as the square-root of SPR resonance widths, as suggested in [4]. Our experimental results showed that $\Delta\lambda_{1,2} \approx 3$ pm for SPR minimum of 100 nm FWHM. Thus, we considered that

$$\Delta\lambda_{1,2} = (3\text{ pm})\sqrt{\frac{\text{FWHM}_{1,2}}{100\text{ nm}}}, \tag{20}$$

where $\text{FWHM}_{1,2}$ are calculated FWHMs for S-SPR and A-SPR, respectively. Further, we varied the thickness of the gold and titanium layers and adjusted the angle of incidence and Teflon AF thickness. The angle of incidence was adjusted to get the two SPRs symmetrically around 730 nm. The Teflon AF thickness was adjusted to get optimum coupling into both SPs. For all considered thicknesses (Ti of 1, 3 and 5 nm, Au of 45, 55 and 65 nm), reflectivity dropped at both SPR wavelengths below 10%. Examples of resulting SPR responses for different gold layer thicknesses are shown in figure 3. The parameters of $|\Delta S|^{\Lambda}$ and $|\Delta B|^{\Lambda}$ (given by (15)), and $|\Delta B|^{K,S0}$ (given by (18)) are summarized in table 1.

In table 1 we see that the term $|s^S - s^B|$ is closer to zero for thicker gold layers. As was already pointed out, this influences also the noise (given by $|\Delta S|^{\Lambda}$ and $|\Delta B|^{\Lambda}$) and cross-sensitivity ($|\Delta S|^{K,S0}/|B|$), which are all higher for thicker gold layers. For a gold layer of 45–55 nm thickness, an increase in the titanium layer results in poorer performance in terms of both noise and cross-sensitivity.

On the basis of the results presented in table 1, we designed the structure in terms of $|\Delta S|^{K,S_{\text{neglect}}}$ and $|\Delta S|^{\Lambda}$ to have the following parameters: gold layer thickness of 45 nm, titanium layer thickness of 1 nm. For this design, the optimum Teflon AF thickness is 355 nm.

4. Experimental details

The set-up is, except for the sensor chip, identical to the single-SPR-based spectral configuration [11]. A 20 W halogen bulb (Avantes Inc., The Netherlands) is TM polarized by a polarizer and delivered to a collimator with 30 mm focal length with nearly diffraction-limited performance (Zeiss Inc., Germany) via a step-index optical fibre of 200 μm core diameter. The transmitted light is captured into two output fibres (400 μm core diameter, step-index) using a pair of 2 mm diameter Selfoc collimating lenses. The dual-channel spectrograph is a 2048-element CCD-based, covering a spectral range of 550–1100 nm (Ocean Optics Inc., USA). To account for spectral characteristics of the used source and the detector, the measured spectra are normalized to system response to TE polarized light. For two-channel-compensated SPR, the sensor chip consists of a glass slide made of glass identical to the prism (BK7, Schott Inc.), a thin titanium adhesion layer and a gold layer. The S/A-SPR sensor chip is similar, but between the glass and the adhesion layer is placed a buffer layer made of Teflon AF 1600 (Dupont Inc.) [10]. The Teflon AF has a refractive index close to that of water and is environmentally stable. The sensor chip is attached to the coupling prism via an index matching liquid. Each of the used materials was first deposited on a bare BK7 glass slide and was characterized using ellipsometry (Sentech Inc., Germany) in the spectral range of 450–1200 nm, figure 2. It is worth noting that the ultra-thin adhesion layer of Ti strongly oxidized during deposition and thus its optical constants are close to those of TiO_2.

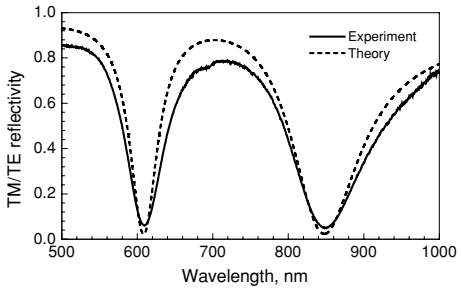

Figure 4. Spectral response of a realized structure together with a theoretical fit, which gave Teflon AF, titanium and gold layers of 360 nm, 2 nm and 49 nm.

The Teflon AF was spin-coated and its thickness was measured to be 350 ± 10 nm using the ellipsometry. The titanium was e-beam vacuum evaporated and the gold was deposited using thermal vacuum evaporation. The temperature of all the vacuum depositions was 150 °C. The layer thicknesses given by a crystal oscillator placed in the vacuum chamber were as follows: Ti: (1–2) nm and Au: (47 ± 2) nm. Subsequently, we characterized the sensor chip, figure 4. The best agreement with the theoretical predictions we got for 360 nm of Teflon AF, 2 nm of titanium and 49 nm of gold (figure 4), which is very close to the expected values.

4.1. Biosensing

The biosensing technique used was described in detail, e.g., in [14]. The reagents used were as follows. The C_{11}-chained and C_{16}-chained alkanethiols (C_{11}-mercapto-1-undecanol and C_{16}-mercaptohexadecanoic acid) and the *N*, *N*, *N*′, *N*′-tetramethyl-*O*-(*N*-succinimidyl)uranium tetrafluoroborate (TSTU), which was used for activation of carboxylic terminal groups on C_{16} alkanethiol were from Sigma-Aldrich, USA. Monoclonal affinity-purified antibodies against human immunoglobulin E (aIgE) and M (aIgM) were from Seva Immuno, CZ and human immunoglobulin E (IgE) from Biodesign, USA. Immune reaction activity of all immune partners was confirmed by the ELISA method. Antibody solutions were prepared in a 10 mM phosphate buffer, pH 7.6 at 20 °C. Antigen solutions were prepared in PBS (10 mM phosphate buffer, 137 mM NaCl, 2.7 mM KCl, pH 7.4 at 20 °C) containing bovine serum albumin (BSA) (Sigma-Aldrich, USA) at a concentration of 100 μg ml^{-1}.

Two sensor chips (with and without a Teflon AF layer, respectively) were UV ozone cleaned for 10 min (UV cleaner 42–220, Jelight Company Inc.), washed with deionized water, and dried with nitrogen stream. A 7:3 mixture of C_{11}-chained and C_{16}-chained alkanethiols was dissolved in degassed absolute ethanol with a total thiol concentration of 1 mM. The C_{16} alkanethiols terminated with a carboxylic head group were used to anchor an antibody; C_{11} alkanethiol chain terminated with a hydroxyl head group was used to form a stable non-fouling background. Sensor chips were immersed in thiol solution and stored in a dark place at room temperature for 24 h. Then, the chips were rinsed with ethanol, dried with nitrogen, rinsed with water and dried with nitrogen again. The carboxylic terminal groups on the sensor surface were activated by TSTU dissolved in dimethylformamide at

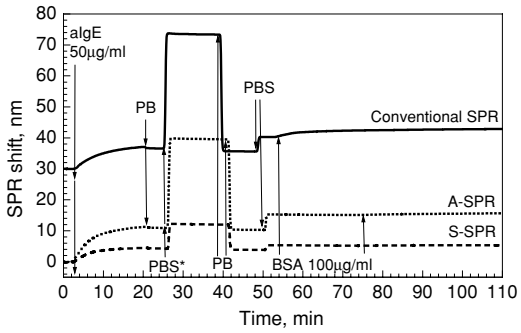

Figure 5. Immobilization of antibodies for the aIgE-covered channel of the two-channel compensated SPR (conventional SPR) and for S/A-SPRs.

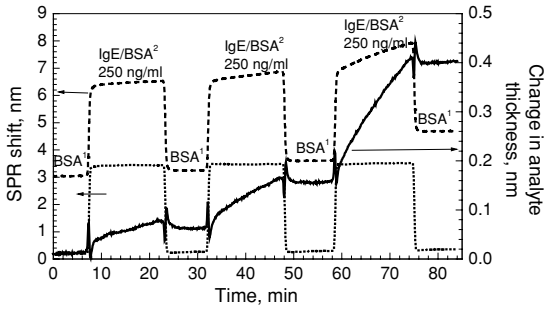

Figure 6. SPR wavelength shifts for two-channel compensated SPR for the sensing (dashed) and reference (dotted) channels. The surface refractive index change *S* is shown as a solid line.

a concentration of 1 mg ml^{-1} for 4 h. After activation, the chips were rinsed with deionized water, dried with nitrogen and immediately mounted into the SPR instrument. The immobilization of antibodies was performed *in situ*, figure 5. First, a phosphate buffer was introduced and flowed through the flow cell until the baseline was achieved. Subsequently, a phosphate buffer solution with 50 μg ml^{-1} of aIgE was injected. For two-channel compensated SPR, 50 μg ml^{-1} of aIgM (receptors not interacting with IgE) was injected into the second sensing channel (not shown in figure 5). It was allowed to flow for 15 min at a flow rate of 20 μl min^{-1}. After the sensor surfaces incubation with a phosphate buffer (PB), the phosphate buffer containing sodium chloride at a concentration of 0.75 M (PBS*) flowed for 15 min to remove all non-covalently bound antibody. The phosphate buffer (PB) was injected again and after a short incubation it was replaced with PBS. Finally, PBS-solution containing BSA at a concentration of 0.5 mg ml^{-1} flowed until a stable baseline was reached.

The SPR wavelength evolution during the sensing events for two-channel compensated SPR and A/S-SPR are shown in figures 6 and 7, respectively. First, buffer solution (marked as BSA^1) flowed through both sensing channels until a stable baseline was achieved (flow rate—20 μl min^{-1}). Antigen solutions were prepared in the BSA/PBS solution of a slightly different refractive index with respect to the BSA^1 (marked as BSA^2). The BSA^2 was prepared from the BSA^1 by adding a small amount of NaCl to the buffer solution. The difference in the refractive indices of BSA^2 and BSA^1 was different for the two experiments being about twice as high for

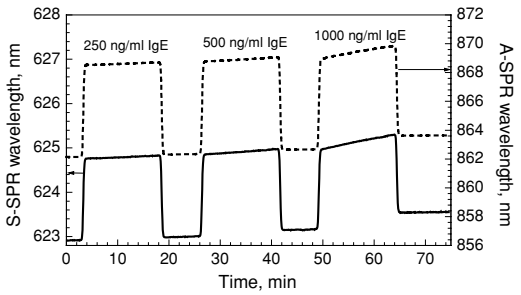

Figure 7. S-SPR (solid) and A-SPR (dashed) wavelengths recorded during the sensing event, when the solution containing increasing concentrations of IgE was introduced.

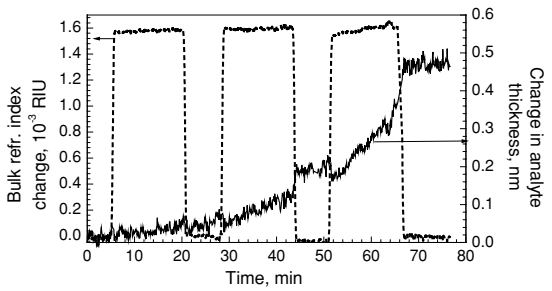

Figure 8. Surface (solid) and bulk (dashed) refractive index change retrieved using (7) from the S/A-SPR wavelengths that are shown in figure 7.

S/A-SPR. After the incubation of the IgE solution for 15 min, it was replaced with BSA[1]. IgE was injected sequentially in concentrations of 250, 500 and 1000 ng ml^{-1}.

4.2. Sensor output

In order to calculate the sensor output using (7), we would need to know the absolute values of surface/bulk refractive index changes during the calibration process, $S^{B=0}$ and $B^{S=0}$. As we do not have these data available, we used the predicted values of the sensor sensitivities: c_B and c_S are surface and bulk refractive index sensitivities of S-SPR and $c_B^{\text{conventional}}$, $c_S^{\text{conventional}}$ are surface and bulk refractive index sensitivities of conventional SPR, respectively. For 360 nm of Teflon AF, 2 nm of titanium and 49 nm of gold (figure 4) we calculated:

$$\begin{aligned} &c_B = 1160 \text{ nm RIU}^{-1}, \qquad c_S = 1.16 \text{ nm nm}^{-1}, \\ &c_S^{\text{conventional}} = 4.6 \text{ nm nm}^{-1}, \quad c_B^{\text{conventional}} = 4500 \text{ nm RIU}^{-1}. \end{aligned} \tag{21}$$

Using these values and data obtained from measurement shown in figure 5 ($\lambda_1^{S=0}$, $\lambda_1^{B=0}$, $\lambda_{\text{conventional}}^{S=0}$, and $\lambda_{\text{conventional}}^{B=0}$) we get the desired values:

$$\begin{aligned} B^{S=0} &= \lambda_1^{S=0}/c_B, \qquad S^{B=0} = \lambda_1^{B=0}/c_S, \\ S_{\text{conventional}}^{B=0} &= \lambda_{\text{conventional}}^{B=0}/c_S^{\text{conventional}}, \\ B_{\text{conventional}}^{S=0} &= \lambda_{\text{conventional}}^{S=0}/c_B^{\text{conventional}}. \end{aligned} \tag{22}$$

The rest of the parameters were retrieved from data shown in figure 5 considering the a-IgE sorption as purely surface change and the PB–PBS difference (around 50 min) as a pure bulk refractive index change:

$$\begin{aligned} &\lambda_1^{S=0} = 1.41 \text{ nm}, \quad \lambda_1^{B=0} = 4.69 \text{ nm}, \quad \lambda_{\text{conventional}}^{S=0} = 6.46, \\ &s_B = 3.47, \qquad s_S = 2.42, \qquad \Delta\lambda_1 = 2.5 \text{ pm}, \\ &\Delta\lambda_2 = 3.7 \text{ pm}, \quad \Delta\lambda_{\text{conventional}} = 3.5 \text{ pm}, \end{aligned} \tag{23}$$

where $\Delta\lambda_{1,2,\text{conventional}}$ are given as standard deviations of baselines, figure 5.

The sensor responses B and S shown in figure 8 are derived using (7), (22) and (23). For two-channel compensated SPR, where $\lambda_{\text{conventional}}$ is given as the difference between the SPR wavelengths of the two channels, the response $S_{\text{conventional}}$ (22) is shown in figure 6.

4.3. Noise and cross-sensitivity analysis

For comparison, we calculated the estimation of the worst case for the realized structure from (15) and (18), where we used the calibrations (23):

$$\begin{aligned} &|\Delta S|^{\Lambda} = 10 \text{ pm}, \qquad |\Delta S|^{K,S0} = 25 \text{ pm}, \\ &|\Delta S|^{K,S0}/B = 16.7 \text{ RIU nm}^{-1}. \end{aligned} \tag{24}$$

The noise (standard deviation) and cross-sensitivity (nearly-instantaneous change detected in S near $S = 0$ caused by a nearly-instantaneous change in B) retrieved from the experimental data (figures 7 and 8) are

$$\begin{aligned} &\Delta S^{\Lambda} = 9 \text{ pm}, \qquad \Delta S^{K} = 20 \text{ pm}, \\ &|\Delta S|^{K,S0}/B = 13.3 \text{ RIU nm}^{-1}, \end{aligned} \tag{25}$$

which are in very good agreement. For two-channel compensated SPR, figure 6, we get

$$\begin{aligned} &\left|\Delta S_{\text{conventional}}^{\Lambda}\right| = 0.8 \text{ pm}, \quad \left|\Delta S_{\text{conventional}}^{K}\right| = 15 \text{ pm}, \\ &\left|\Delta S_{\text{conventional}}^{K}/B\right| = 21 \text{ RIU nm}^{-1}. \end{aligned} \tag{26}$$

5. Discussion

The presented theory provides a good prediction in terms of noise and cross-sensitivity, as shown in (24) and (25). Compared with two-channel compensated SPR, the noise-limited resolution in surface refractive index is about 11 times worse ((25) and (26)), however, the cross-sensitivity given by $|\Delta S|^{K,S0}/B$ and $|\Delta S|_{\text{conventional}}^{K}/B$, respectively, is nearly twice as good in the proposed configuration.

Thus, for lower levels of background refractive index change, where the measurement is limited by the noise, the two-channel compensated SPR has better performance compared to S/A-SPR and vice versa for a measurement limited by the cross-sensitivity. At a certain value of the background refractive index change, B^{lim}, the two configurations are comparable, while above/below this limit S/A-SPR has superior/inferior performance. This limit corresponds to a situation when the noise of S/A-SPR approaches the cross-sensitivity of two-channel compensated SPR:

$$\Delta S^{K,S0}/B^{\text{lim}} = \Delta S_{\text{conventional}}^{\Lambda}, \tag{27}$$

which, for our experiment ((25) and (26)), gives a value of $B^{\text{lim}} = 4.3 \times 10^{-4}$. It is worth noting that this value is about four times lower than that realized experimentally for S/A-SPR, figure 8.

6. Conclusions

We designed a layered structure for two-plasmon-based biosensing using simultaneous excitation of symmetric and anti-symmetric bound surface plasmons. Besides the sensor sensitivity and noise, we considered also the cross-sensitivity to background refractive index in the optimization process, which allowed us to evaluate the true sensor resolution. The derived formulae for cross-sensitivity can be directly used for evaluation and optimization of other SPR cross-sensitivity-compensating techniques.

We have compared the performance of the proposed structure and the two-channel compensated SPR detecting IgE analyte. It was found that the noise of the retrieved surface refractive index change was 11 times worse in the proposed configuration. However, the cross-sensitivity to background refractive index changes was nearly twice as low, which favours the proposed configuration for measurements with relative high background refractive index changes. Besides that, there are other advantages of the proposed method, as only single receptors are used and the number of channels is halved, requiring also half the analyte.

Acknowledgments

This research was supported by the Grant Agency of the Czech Republic under contracts 202/04/P141, 303/03/0249, 203/02/1326 and 102/03/0633 and by the European Commission under contract QLK4-CT-2002-02323.

References

[1] Slavík R, Homola J, Čtyroký J and Brynda E 2001 Novel spectral fiber optic sensor based on surface plasmon resonance *Sensors Actuators* B **74** 106–11

[2] Čtyroký J, Homola J and Skalský M 1997 Tuning of spectral operation range of a waveguide surface plasmon resonance sensor *Electron. Lett.* **33** 1246–8

[3] Wu S Y, Ho H P, Law W C, Lin C and Kong S K 2004 Highly sensitive differential phase-sensitive surface plasmon resonance biosensor based on the Mach–Zehnder configuration *Opt. Lett.* **29** 2378–80

[4] Nenninger G G, Piliarik M and Homola J 2002 Data analysis for optical sensors based on spectroscopy of surface plasmons *Meas. Sci. Technol* **13** 2038–46

[5] Nelson B P, Grimsrud T E, Liles M R, Goodman R M and Corn R M 2001 Surface plasmon resonance imaging measurements of DNA and RNA hybridization adsorption onto DNA microarrays *Anal. Chem.* **73** 1–7

[6] http://www.microvacuum.com/products/biosensor/owlstc.asp

[7] Lofas S, Malmqvist M, Ronnberg I, Stenberg E, Liedberg B and Lundstrom I 1991 Bioanalysis with surface plasmon resonance *Sensors Actuators* B **5** 79–84

[8] Homola J, Dostálek J and Čtyroký J 2001 A novel approach to surface plasmon resonance multichannel sensing *Proc. SPIE: Optical Engineering for Sensing and Nanotechnology (ICOSN 2001, Yokohama, 6–8 June 2001)* vol 4416, ed K Iwata pp 86–9

[9] Dostálek J, Vaisocherová H and Homola J 2005 Multichannel surface plasmon resonance biosensor with wavelength division multiplexing *Sensors Actuators* B **108** 758–64

[10] Slavík R and Homola J 2006 Simultaneous excitation of long and short range surface plasmons in an asymmetric structure *Opt. Commun.* **259** 507–12

[11] Zhang L M and Uttamchandani D 1988 Optical chemical sensing employing surface plasmon resonance *Electron. Lett.* **23** 1469–70

[12] Jin W, Michie W C, Thursby G, Konstantaki M and Culshaw B 1997 Simultaneous measurement of strain and temperature: error analysis *Opt. Eng.* **36** 598–609

[13] Chilwell J and Hodgkinson I 1984 Thin-films field-transfer matrix theory of planar multilayer waveguides and reflection prism-loaded waveguides *J. Opt. Soc. Am.* A **1** 742–53

[14] Homola J, Vaisocherová H, Dostálek J and Piliarik M 2005 Multi-analyte surface plasmon resonance biosensing *Methods* **37** 23–36

Appendix III

J. Dostálek, H. Vaisocherová and J. Homola:

Multichannel surface plasmon resonance biosensor with wavelength division multiplexing

Biosensors & Bioelectronics, **108** (2004), 758 - 764

Available online at www.sciencedirect.com
SCIENCE DIRECT®
Sensors and Actuators B 108 (2005) 758–764
SENSORS AND ACTUATORS B CHEMICAL
www.elsevier.com/locate/snb

Multichannel surface plasmon resonance biosensor with wavelength division multiplexing

Jakub Dostálek, Hana Vaisocherová, Jiří Homola*

Institute of Radio Engineering and Electronics, Academy of Sciences of the Czech Republic, Chaberská 57, 18251 Prague, Czech Republic

Received 14 July 2004; received in revised form 27 November 2004; accepted 11 December 2004
Available online 5 February 2005

Abstract

A novel multichannel surface plasmon resonance (SPR) biosensor with spectral interrogation and wavelength division multiplexing of sensing channels is presented. A special design of SPR prism element is used to enable wavelength division multiplexing of serial sensing channels. In addition to increasing the number of sensing channels, this approach allows discrimination of the sensor response due to analyte–receptor binding from interfering background refractive index fluctuations. A novel eight-channel SPR sensor combining the wavelength division multiplexing of serial sensing channels with the conventional parallel channel architecture is described. Application of this multichannel SPR sensor for simultaneous detection of multiple analytes is described.

Keywords: Surface plasmon resonance; Optical sensor; Biosensor; Multichannel sensor; Wavelength division multiplexing

1. Introduction

Since the end of the last century, surface plasmon resonance (SPR) has been increasingly exploited for development of optical biosensors. SPR biosensors have been applied for analysis of biomolecular interactions (BIA) and detection of chemical and biological analytes [1], where they provide benefits of real-time, sensitive and label-free technology. SPR biosensors have been used for detection of various chemical and biological compounds related to significant areas such as environmental protection (e.g. herbicides [2]), food safety (e.g. protein toxins [3], bacteria [4]) and medical diagnostics (e.g. DNA [5] and hormones [6]). Recent years have witnessed intensive research effort towards increasing the number of sensing channels to introduce benefits of SPR biosensor technology to multianalyte detection and highly parallelized biomolecular interaction analysis. Numerous approaches in multichannel SPR sensor development have been demonstrated to date [7–14]. In these sensors, changes in SPR condition were determined by measuring variations in light intensity (SPR sensors with intensity modulation) or spectrum (SPR sensors based on surface plasmon spectroscopy). The intensity modulation-based SPR imaging devices allow parallel measurements in up to hundreds of sensing channels [9,10] with a typical accuracy in discrimination of SPR changes of 10^{-5} refractive index (RI) units. Sensors based on spectroscopy of surface plasmons are capable of more accurate measurements of SPR changes (up to 3×10^{-7} RIU), however, the number of independent sensing channels usually does not exceed ten [11,12].

Most sensors with surface plasmon spectroscopy rely on the *parallel* architecture and spatial multiplexing of sensing channels [12]. In this approach, light beams exciting surface plasmons in a row of sensing channels are interrogated independently to determine SPR changes in each channel. In SPR biosensors with wavelength modulation, spectral analysis of multiple light beams is performed by multiple spectrographs [3] or by using an optical switch routing light from multiple channels at single spectrograph [13] (time multiplexing). Alternative approach to multiplexing of parallel sensing channels is the wavelength division mul-

* Corresponding author. Tel.: +422 688 1804; fax: +422 688 0222.
E-mail address: homola@ure.cas.cz (J. Homola).

0925-4005/$ – see front matter © 2005 Elsevier B.V. All rights reserved.
doi:10.1016/j.snb.2004.12.096

tiplexing (WDM) by means of a thin dielectric overlayer [14].

In this work we report a novel configuration of multichannel surface plasmon resonance biosensor with *serial* architecture and wavelength division multiplexing (WDM) of sensing channels. We show that this approach makes it possible to discriminate binding of analyte from the interfering effects such as background refractive index fluctuations and thus provide more robust SPR measurements. We present a new eight-channel SPR sensor based on combination of this method with the parallel architecture and describe its application for simultaneous detection of multiple analytes.

2. Theory

2.1. Wavelength division multiplexing of serial SPR sensing channels

Surface plasma wave (SPW) is an electromagnetic wave guided along a metal–dielectric interface. SPW may be optically excited in the Kretschmann geometry of the attenuated total reflection (ATR) method [16]. In this geometry, an optical wave is introduced into a prism, where it undergoes total reflection on the prism base with a thin metal film. The generated evanescent field in the metal film couples to a SPW at outer metal film boundary if their propagation constant components parallel to the metal surface are equal:

$$k_0 n_p \sin(\theta) = k_0 Re\left\{\sqrt{\frac{\varepsilon_1\varepsilon_2}{\varepsilon_1+\varepsilon_2}}\right\}, \quad (1)$$

where k_0 is the wave number of light in vacuum, n_p the prism refractive index, θ the angle of incidence of the optical wave, ε_1 the metal film permittivity and ε_2 the permittivity of the dielectric at the outer interface of the metal film.

In order to achieve the wavelength division multiplexing of serial SPR sensing channels, we use a special design of the ATR prism coupler [15] depicted in Fig. 1a. A collimated polychromatic optical wave launched into this element is made incident on a thin metal film in two distinct regions denoted as A and B. In the first region (region A), it hits the metal film under the angle of incidence α and couples to a SPW at the outer metal surface at the wavelength λ_A. The excitation of SPW produces a sharp absorption dip in the spectrum of the optical wave centered at λ_A. The reflected light is redirected inside the element and made incident on the metal film in the second region (region B) under a different angle of incidence β ($\beta < \alpha$). At this angle of incidence, the optical wave couples to a SPW at a longer wavelength λ_B ($\lambda_B > \lambda_A$) generating a dip in the spectrum of the optical wave centered at λ_B. Consequently, the wavelength spectrum of the transmitted light exhibits two SPR dips corresponding to SPRs in two distinct regions of the metal film, Fig. 1b. Based on the carried out theoretical analysis, materials and parameters of the structure were selected as follows: special prism element, SF14 glass; SPR-active layer, gold; thickness, 55 nm; dielectric, aqueous medium; refractive index, 1.33. For this structure, the angles of incidence $\alpha = 54.6^\circ$ and $\beta = 52.5^\circ$ correspond to SPW excitation at $\lambda_A = 640$ nm and $\lambda_B = 790$ nm, respectively.

2.2. Sensitivity of SPR biosensor with WDM of sensing channels

When the refractive index of the dielectric adjacent to the metal surface is changed, a shift in the SPR wavelength occurs. In principle, there are two types of refractive changes involved in SPR biosensing: (a) bulk refractive index changes within the whole dielectric adjacent to the metal surface and (b) refractive index changes within a thin layer with the thickness much smaller then the SPW penetration depth into the dielectric (typically > 100 nm in the wavelength region 600–1000 nm for the interface between gold and dielectric with RI 1.33). In the approximation of small responses, SPR wavelength shift can be assumed to be a linear function of the bulk refractive index change Δn_B, and surface refractive index change Δn_S:

$$\Delta\lambda_A = S_B(\lambda_A)\Delta n_B + S_S(\lambda_A)\Delta n_S,$$
$$\Delta\lambda_B = S_B(\lambda_B)\Delta n_B + S_S(\lambda_B)\Delta n_S, \quad (2)$$

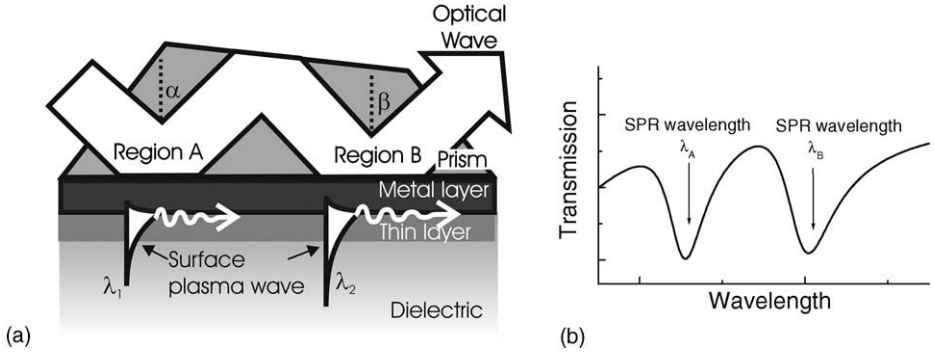

Fig. 1. (a) Special prism coupler for sequential excitation of SPW and wavelength division multiplexing of sensing channels and (b) resulting spectrum of transmitted light.

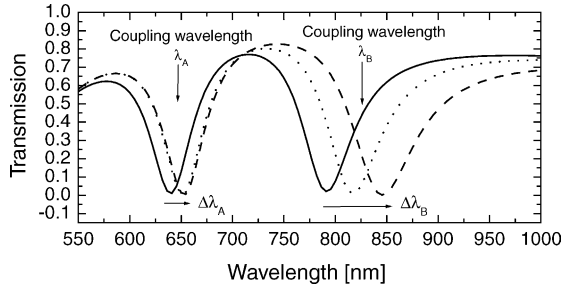

Fig. 2. Transmitted spectrum calculated for (a) bare gold surface with background dielectric medium with a refractive index $n_B = 1.33$, (—) (b) bare gold and a higher refractive index of background dielectric medium $n_B = 1.335$, (– – –) and (c) gold with a thin dielectric layer (thickness $d = 5$ nm, $n_F = 1.43$) and background dielectric medium with a refractive index $n_B = 1.33$, (. . .).

where $\Delta\lambda_i$ is the SPR wavelength change (i = A, B), and S_B and S_S are the bulk and surface RI sensitivities, respectively.

As the penetration depth of SPW increases with the wavelength, SPWs at the wavelengths λ_A and λ_B are unequally sensitive to changes in the refractive index at the surface and in the bulk dielectric. This is illustrated in Fig. 2 which shows a model situation, in which changes in the coupling wavelengths due to the presence of a thin film and the change in bulk refractive index are identical in the short-wavelength channel, while the change due to the bulk refractive index change is more pronounced in the long-wavelength channel. Therefore the Eq. (2) may be inverted and the coupling wavelength shifts can be decomposed into the contributions due to the changes in the refractive index at the surface and in the bulk dielectric:

$$\Delta n_S = \frac{\Delta\lambda_A k_B - \Delta\lambda_B}{(k_B - k_S)S_S(\lambda_A)}, \qquad \Delta n_B = \frac{\Delta\lambda_B - k_S\Delta\lambda_A}{(k_B - k_S)S_B(\lambda_A)}, \tag{3}$$

where $k_B = S_B(\lambda_B)/S_B(\lambda_A)$ and $k_S = S_S(\lambda_B)/S_S(\lambda_A)$ are the bulk and surface RI change calibration constants. By using Fresnel reflectivity model, the sensitivities and calibration constants were calculated to be $S_B(640\,\text{nm}) = 2710\,\text{nm RIU}^{-1}$, $S_B(790\,\text{nm}) = 8500\,\text{nm RIU}^{-1}$, $S_S(640\,\text{nm}) = 21.9\,\text{RIU}^{-1}$, $S_S(790\,\text{nm}) = 41\,\text{RIU}^{-1}$, $k_B = 3.2$, and $k_S = 1.87$.

3. Experimental

3.1. Instrumentation

The special prism element was made of SF14 glass. An SPR chip was attached to the base of the element and optical contact was established using a refractive index matching fluid (from Cargille). The sensor chip consisted of an SF14 glass slide coated by an adhesion promoting chromium layer (thickness, 2 nm) and SPR-active gold layer (thickness, 55 nm) by means of thermal evaporation in vacuum. The optical setup of the eight-channel biosensor instrument is depicted in Fig. 3. Polychromatic light from a halogen lamp (Avalight-Hal from Avantes) was coupled into an optical fiber (FT-400-EMT from Thorlabs) and collimated using two cylindrical lenses. The collimated light beam was polarized by a dichroic polarizer (Polarcor) and coupled in the special SPR prism element, where it was made incident on the SPR-active surface in eight areas denoted as A1–A4 and B1–B4, Fig. 3. Light beams reflected at areas A1–A4 and B1–B4 were collected by four miniature GRIN lenses (NSG America) and coupled in four optical fibers (FT-400-EMT from Thorlabs) connected to four-channel spectrograph (S2000, Ocean Optics). The SPR spectra were measured in TM polarization and normalized with spectra obtained in TE polarization. Measured SPR spectra were averaged in time

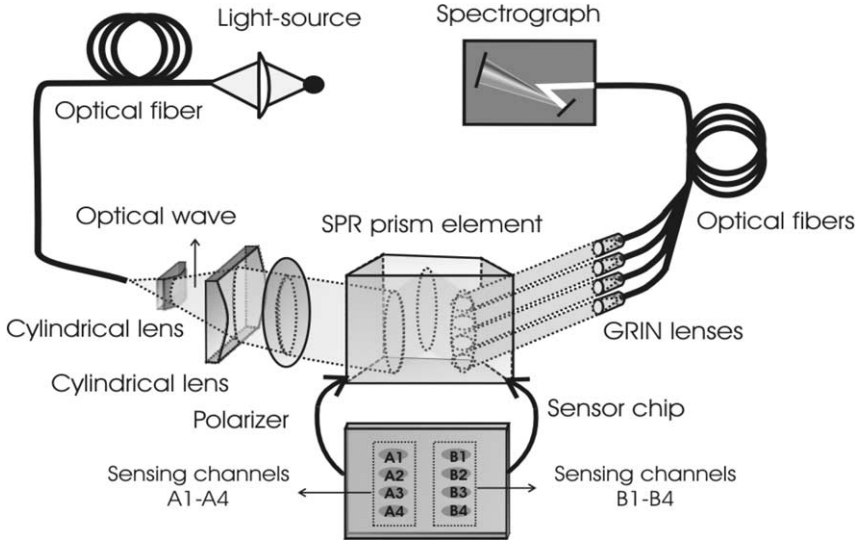

Fig. 3. Scheme of the optical system of eight-channel SPR sensor combining parallel architecture with the wavelength division multiplexing of serially ordered channels.

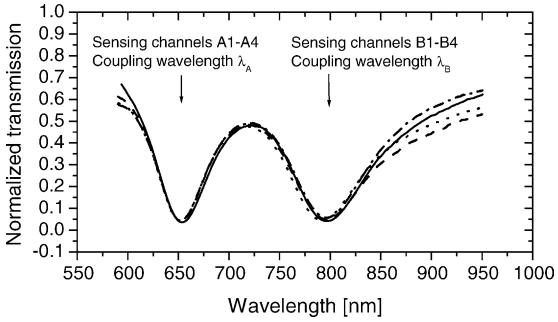

Fig. 4. Transmitted spectra measured from bare gold surface with background dielectric medium refractive index $n_B = 1.33$ in sensing channels A1–A4 and B1–B4.

and polynomial fitting method was applied for determination and tracking of the SPR dip minimum in each sensing channel. Examples of SPR normalized spectra are given in Fig. 4. In comparison with theory (Fig. 2), experimental SPR dips are broader by 30% and observed SPR dips are shifted to longer wavelength by about 13 and 5 nm for short-wavelength and long-wavelength SPW, respectively. This discrepancy is mostly due to an error in the angle of incidence and difference between gold permittivity used in simulations and that of the real layer.

An eight-channel flow-cell was clamped against the SPR chip in order to contain liquid samples during experiments. The flow-cell was made of an acrylic substrate with input and ports interfacing flow-cell chambers for each sensing channel. The flow-cell chambers were cut into a gasket made into a 50 μm thick polyurethane sheet using a CO_2 laser beam (custom made by Micronics, Inc.). The volume of each flow-cell chamber was 2 μl. Input flow-cell ports were connected via tubing (from Upchurch Scientific) with two four-channel peristaltic pumps (Reglo Digital, from Ismatec) to control the flow of liquid samples across the sensor surface. The flow-rate of 50 μl/min was used in the experiments.

3.2. Materials

Bovine serum albumin (BSA), C_{11}-mercapto-1-undecanol acid (C_{11}-chain alkanethiol), C_{16}-mercapto-hexadecanoic acid (C_{16}-chain alkanethiol) and *N*,*N*,*N*′,*N*′-tetramethyl-*O*-(*N*-succinimidyl)uronium tetrafluoroborate (TSTU) were purchased from Sigma–Aldrich, USA. Monoclonal affinity-purified antibodies against human immunoglobulin E (aIgE), human immunoglobulin G (aIgG), human choriogonadotropin (ahCG) and horseradish peroxidase (aPx) were obtained from Seva Immuno, Czech Republic. Human immunoglobulin E (IgE) was purchased from Biodesign, USA, human immunoglobulin G (IgG) was obtained from Laboratory of Anthropology and Human Genetics at Faculty of Sciences, Charles University, Czech Republic, human choriogonadotropin (hCG) was from Calbiochem, USA, and horseradish peroxidase (Px) was from Kem-En-Tec, Denmark. Antibody solutions were prepared in 10 mM phosphate buffer, pH 7.6 at 20 °C. Antigen solutions were prepared in PBS (10 mM phosphate buffer, 137 mM NaCl, 2.7 mM KCl, pH 7.4 at 20 °C) containing bovine serum albumin at the concentration of 100 μg/ml. For the cleaning of the gold surface of the sensor chip we used 1:3 mixture of 30% hydrogen peroxide and 96% sulfuric acid (Piranha solution).

3.3. Sensor chip preparation

The surface of gold was cleaned in Piranha solution for 3 min, rinsed with deionized water and dried in nitrogen stream. Then, the sensor chip surface was immersed in the 7:3 mixture of C_{11}-chain and C_{16}-chain alkanethiols dissolved in degassed ethanol (total thiol concentration, 1 mM) and stored in a dark place at room temperature for 2 days to allow the thiols to form a self-assembled monolayer. Subsequently, the chip was rinsed with ethanol and water and dried in nitrogen stream. C_{16} alkanethiol terminated with a carboxylic head group was used to anchor antibodies, while C_{11} alkanethiol chain terminated with a hydroxyl head group formed a stable non-fouling background. The carboxylic terminal groups on the sensor surface were activated with TSTU dissolved in dimethylformamide at the concentration of 1 mg/ml for 4 h [17]. After the activation, the sensor chip was rinsed with water, dried in nitrogen stream and loaded into the SPR instrument, where in situ immobilization of antibody was performed. Antibodies dissolved in PBS at the concentration of 50 μg/ml were flowed across the sensor surface for 15 min. Different sensing channels were functionalized with different antibodies; specifically, aPx antibody was immobilized in sensing channels A1 and B1, aIgE in A2 and B2, ahCG in A3 and B3, and aIgG in A4 and B4.

3.4. Calibration of the sensor instrument

In order to establish bulk and surface refractive index calibrations of the sensor, the response of sensing channels A1–A4 and B1–B5 to known background medium and surface refractive index changes was measured. Fig. 5a shows SPR wavelength shifts obtained while liquids with different refractive indices were flowed over the sensor surface (the refractive index values are given at the wavelength of 650 nm). These data imply that the average bulk RI sensitivities are $S_B\ (\lambda_A) = 2650\,\text{nm RIU}^{-1}$ and $S_B\ (\lambda_B) = 8800\,\text{nm RIU}^{-1}$. The position of SPR wavelengths in channels A1–A4 and B1–B4 were determined with the standard deviation of 0.0035 and 0.006 nm, respectively. These noise levels correspond to bulk RI changes resolutions of 1.3×10^{-6} RIU in sensing channels A1–A4 and 7×10^{-7} RIU in sensing channels B1–B4. The bulk RI change calibration constant was calculated to lie within the range $k_B = 3.25$–3.32. Within the operating range 3×10^{-3} RIU, no cross sensitivity between sensing channels with SPR encoded in the same wavelength spectrum due to the overlap in their SPR dips was observed. The surface RI change calibration constant was determined

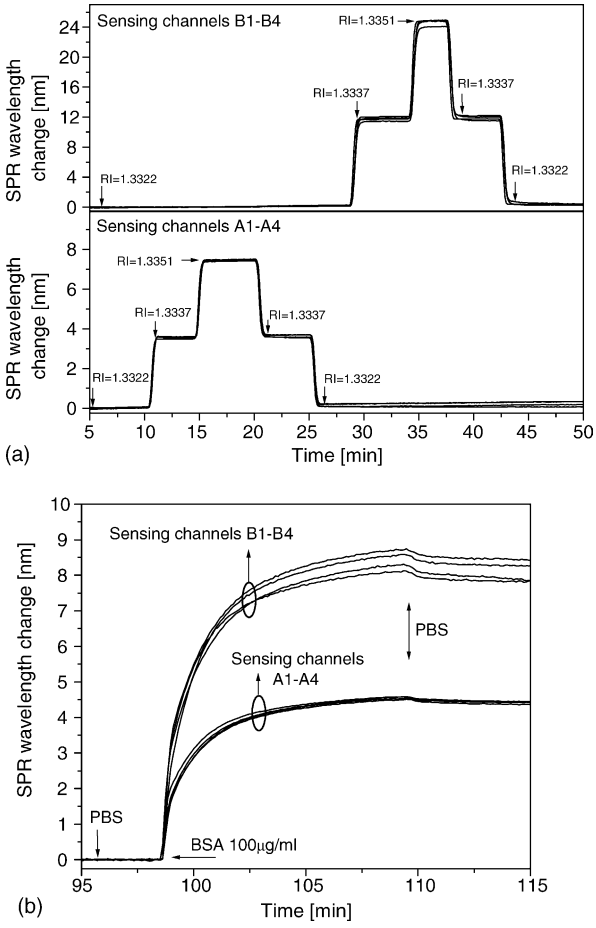

Fig. 5. (a) SPR wavelength shifts due to changes in the refractive index of background dielectric medium, (b) SPR wavelength shifts due to changes in the refractive index at the sensor surface. SPR wavelengths in channels A1–A4 and B1–B4 are offset by 653 and 795 nm, respectively.

from SPR sensor response to formation of BSA layer from PBS (BSA concentration, 100 μg/ml), Fig. 5b. From this experiment, the surface RI calibration constant was determined to lie within k_S = 1.78–1.92. We believe that the observed variations in the calibration constants for different sensing channel pairs are mainly due to inconsistencies in the alignment of the optical beams in the middle of the flow chamber, inhomogeneity of the sensor surface and variations in the sample flow conditions in different sensing channels. Experimental sensor responses shown in this work were calibrated to effective bulk refractive index change at the wavelength λ_B = 795 nm – in channels A1–A4 the SPR wavelength shifts were divided by the factor $S_B(\lambda_B)/k_S$ and in channels B1–B4 the SPR wavelength shifts were divided by the bulk sensitivity $S_B(\lambda_B)$.

4. Results and discussion

4.1. Discrimination of background and surface refractive index changes by WDM SPR

When the same effects occur in complementary sensor chip areas A and B, these effects may be simultaneously monitored at two different wavelengths λ_A and λ_B. As discussed in Section 2.2, by means of measuring SPR dip shift at two different wavelengths, the sensor responses to surface and bulk refractive index changes can be discriminated. This feature is illustrated in the model experiment, in which a thin protein monolayer was grown on a bare gold surface from a liquid the refractive index of which was changing. Initially, liquids with different RI were sequentially injected to the flow-cell of the sensor in the following order – PBS buffer, PBS buffer dissolved in water at the ratio 2:3 (PBS^+) and PBS. Then, a protein layer was grown on a bare gold surface by means of physical sorption from the PBS buffer with BSA at the concentration of 10 μg/ml. While the protein layer was grown, the background dielectric refractive index was continuously changed by means of mixing this solution with a solution containing the same amount of BSA dissolved in PBS^+. Finally, the sensor surface was flushed with the pure PBS buffer until the sensor response became stable. The sensorgram presented in Fig. 6 shows measured SPR wavelength shifts at the wavelength λ_A and λ_B together with the deconvoluted sensor responses associated with the background refractive index change and the growth of the BSA monolayer. The data suggest that the deconvolution was performed with the accuracy better than 97%. The noise in deconvoluted sensor response, however, increased by a factor of 2.5–3.5 compared to that of the individual sensing channels A1–A4, B1–B4. This noise increase can be reduced by increasing the difference between calibration constants for bulk and surface RI changes k_B and k_S, for example, by employing SPWs at more different wavelengths.

4.2. Multianalyte detection by means of WDM SPR biosensor

The antibody-coated SPR biosensor chip was used for multianalyte detection in mixtures comprising proteins Px, IgE, hCG and IgG. Buffer solution was flowed through all the channels until stable baseline in the sensor response was achieved. Then, the solution containing a mixture of antigens Px, IgE, hCG and IgG at concentrations of 0.5, 0.1, 2 and 0.5 μg/ml, respectively, was flowed through sensing channels B1–B4. Simultaneously, four solutions containing only one of the antigens (at an identical concentration) were injected into channels A1–A4 coated with a respective antibody. After the incubation of samples for 15 min, the samples were replaced with pure buffer. The obtained sensorgram presented in Fig. 7 shows the comparison of sensor response to each analyte in pure buffer and mixture of other antigens. The observed higher response to mixture of antigens is probably mainly due to the non-specific binding of other proteins in mixture to antibodies on the sensor surface. After washing the sensor surface with buffer, the sensor response at channels in contact with pure protein and with protein mixture reached almost identical levels suggesting that the non-specific binding was mostly reversible and there were no significant competitive and hindrance effects.

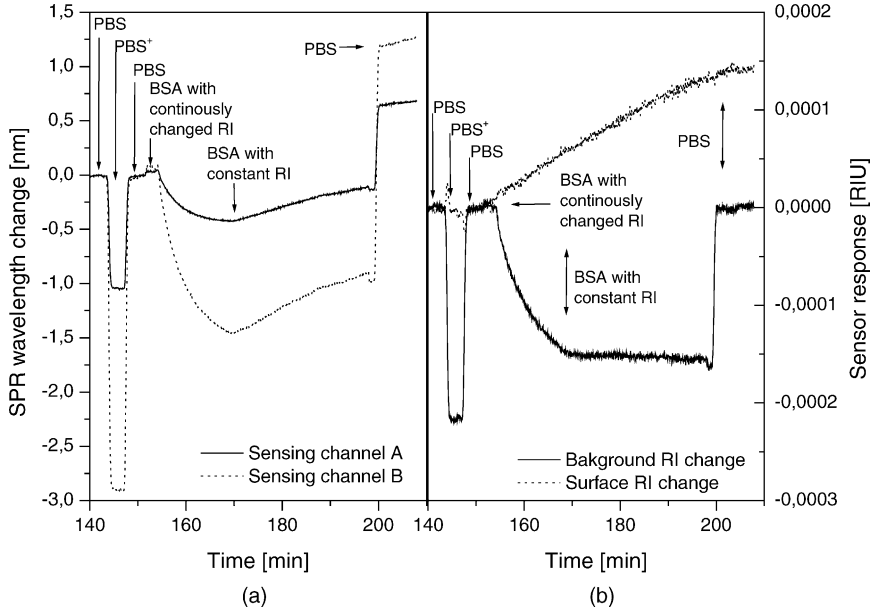

Fig. 6. (a) SPR wavelength change measured at two different wavelengths when BSA monolayer was grown on bare gold surface from the solution refractive index of which was changing, (b) decomposition of the sensor response into the surface and background medium refractive index change contributions.

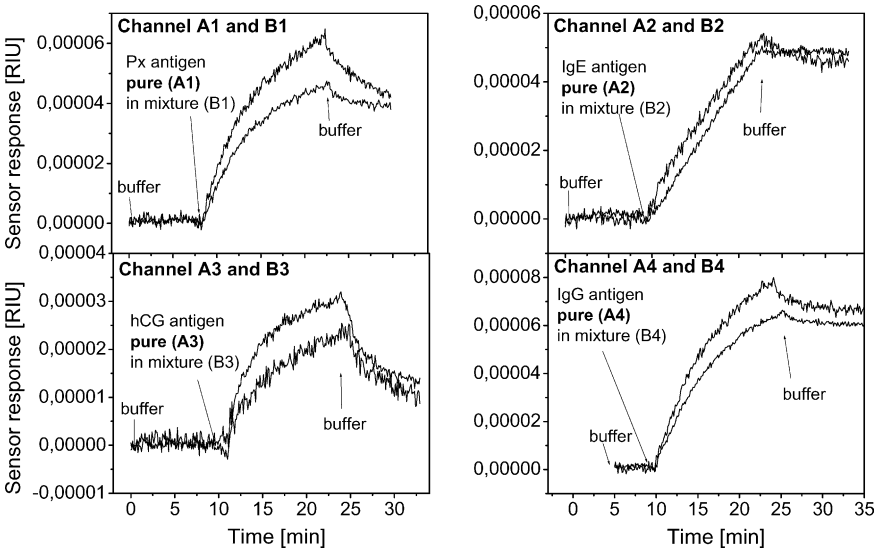

Fig. 7. Sensor response to antigens Px, IgE, hCG and IgG contained in pure buffer and in the mixture of antigens.

5. Conclusions

We have demonstrated a new approach to multichannel SPR sensing based on serial sensing channel architecture and wavelength division multiplexing of sensing channels. This approach was combined with the parallel channel architecture and implemented in a new eight-channel SPR sensor. This multichannel SPR sensor technology offers two modes of operation: (i) all the sensing channels can be functionalized and used for detection of different analytes or (ii) the sensing channels at different wavelengths can be paired for discrimination of specific binding events from interfering background refractive index fluctuations and thus allows more robust biosensing. This feature is expected to be particularly useful for biosensing in complex realistic samples, in which interfering effects pose a major challenge for conventional SPR biosensors.

Acknowledgements

Authors wish to thank Dr. Václav Malina (Institute of Radio Engineering and Electronics, Prague) for deposition of thin films and to Dr. Jiří Škvor (Seva Immuno, Ltd., Prague) for providing antibodies used in this work. This work was done under support of the Academy of Sciences of the

Czech Republic (project K2067107), Grant Agency of the Czech Republic (contracts 303/03/0249, 203/02/1326 and 102/03/0633) and European Commission (contract QLK4-CT-2002-02323).

References

[1] J. Homola, S.G. Yee, Gauglitz: surface plasmon resonance sensors: review, Sens. Actuat. B 54 (1999) 3–15.
[2] C. Mouvet, R.D. Harris, C. Maciag, B.J. Luff, J.S. Wilkinson, J. Piehler, A. Brecht, G. Gauglitz, R. Abuknesha, G. Ismail, Determination of simazine in water samples by waveguide surface plasmon resonance, Anal. Chim. Acta 338 (1997) 109–117.
[3] J. Homola, J. Dostálek, S.F. Chen, A. Rasooly, S. Jiang, S.S. Yee, Spectral surface plasmon resonance biosensor for detection of staphylococcal enterotoxin B in milk, Int. J. Food Microbiol. 75 (2002) 61–69.
[4] V. Koubová, E. Brynda, L. Karasová, J. Škvor, J. Homola, J. Dostálek, P. Tobiška, J. Rošický, Detection of foodborne pathogens using surface plasmon resonance biosensors, Sens. Actuat. B 74 (2001) 100–105.
[5] T.T. Goodrich, H.J. Lee, R.M. Corn, Direct detection of genomic DNA by enzymatically amplified SPR imaging measurements of RNA microarrays, J. Am. Chem. Soc. 126 (2004) 4086–4087.
[6] J. Dostálek, J. Čtyroký, J. Homola, E. Brynda, M. Skalský, P. Nekvindová, J. Špirková, J. Škvor, J. Schröfel, Surface plasmon resonance biosensor based on integrated optical waveguide, Sens. Actuat. B 76 (2001) 8–12.
[7] B. Liedberg, I. Lundstrom, E. Stenberg, Principles of biosensing with an extended coupling matrix and surface plasmon resonance, Sens. Actuat. B 11 (1993) 63–72.
[8] J. Dostálek, J. Homola, M. Miler, Rich information format surface plasmon resonance biosensor based on array of diffraction gratings, Sens. Actuat. B 107 (1) (2005) 154–161.
[9] C.E.H. Berger, T.A.M. Bauer, R.P.H. Kooymann, J. Greve, Surface plasmon resonance multisensing, Anal. Chem. 70 (1998) 703–706.
[10] J.S. Shumaker-Parry, C.T. Campbell, Quantitative methods for spatially resolved adsorption/desorption measurements in real time by surface plasmon resonance microscopy, Anal. Chem. 76 (2004) 918–929.
[11] R. Karlsson, R. Stahlberg, Surface plasmon resonance detection and mutispot sensing for direct monitoring of interactions involving low-molecular-weight analytes for determination of low affinities, Anal. Biochem. 228 (1995) 280–284.
[12] M.J. O'Brien, V.H. Perez-Luna, S.R.J. Brueck, G.P. Lopez, A surface plasmon resonance array biosensor based on spectroscopic imaging, Biosens. Bioelectron. 16 (2001) 97–108.
[13] G.G. Nenninger, J.B. Clendenning, C.E. Furlong, S.S. Yee, Reference-compensated biosensing using a dual-channel surface plasmon resonance sensor system based on a planar lightpipe configuration, Sens. Actuat. B 51 (1998) 38–45.
[14] J. Homola, H.B. Lu, G.G. Nenninger, Jakub Dostálek, S.S. Yee, A novel multichannel surface plasmon resonance biosensor, Sens. Actuat. B 76 (2001) 403–410.
[15] J. Homola, J. Dostálek, J. Čtyroký, Novel approach to surface plasmon resonance multichannel sensing, in: SPIE Proceedings, Yokohama, Japan, June 6–8, Optical Engineering for Sensing and Nanotechnology 4416 (2001) 86–89.
[16] H. Raether, Surface Plasmons on Smooth and Rough Surfaces and on Gratings, vol. 111, Springer-Verlag, Berlin, 1988.
[17] M. Wilchek, K.L. Kundsen, T. Miron, Improved method for preparing *N*-hydroxysuccinimide ester-containing polymers for affinity chromatography, Bioconjugate Chem. 5 (1994) 491–492.

Biographies

Jakub Dostálek (MS 2000) is a doctoral student of the Faculty of Mathematics and Physics in Charles University in Prague (Czech Republic) and carries out his PhD research at the Institute of Radio Engineering and Electronics, Prague (Czech Republic). His research interests are in field of optical sensors and biosensors.

Hana Vaisocherová (MS 2001) is a doctoral student of the Faculty of Mathematics and Physics in Charles University in Prague (Czech Republic) and a research assistant at the Institute of Radio Engineering and Electronics, Prague (Czech Republic). Her research interests are in study of biomolecular interactions by SPR biosensors and in surface chemistry development.

Jiří Homola (MS 1988, PhD 1993) is Head of Photonics Division and Chairman of Department of Optical Sensors at the Institute of Radio Engineering and Electronics, Prague (Czech Republic). He also is Affiliate Associate Professor at the University of Washington, Seattle (USA). His research interests are in photonics and biophotonics with emphasis on optical sensors and biosensors. He is a member of Editorial Boards of Sensors and Actuators B and Biosensors and Bioelectronics and Senior Member of IEEE.

Appendix IV

J. Homola, H. Vaisocherová, J. Dostálek and M. Piliarik:

Multianalyte surface plasmon resonance biosensing

Methods, **37** (2005), 26 - 36

Available online at www.sciencedirect.com
SCIENCE DIRECT®
Methods 37 (2005) 26–36
METHODS
www.elsevier.com/locate/ymeth

Multi-analyte surface plasmon resonance biosensing

Jiří Homola *, Hana Vaisocherová, Jakub Dostálek, Marek Piliarik

Institute of Radio Engineering and Electronics, Academy of Sciences of the Czech Republic, Chaberská 57, 18251 Prague, Czech Republic

Accepted 1 May 2005

Abstract

Surface plasmon resonance (SPR) biosensors are affinity sensing devices exploiting a special mode of electromagnetic field—surface plasmon-polariton—to detect the binding of analyte molecules from a liquid sample to biomolecular recognition elements immobilized on the surface of the sensor. In this paper, we review advances of SPR biosensor technology towards detection systems for the simultaneous detection of multiple analytes (multi-analyte detection). In addition, we report application of a recently developed multichannel SPR sensor based on spectroscopy of surface plasmons and wavelength division multiplexing of sensing channels to multi-analyte detection.

Keywords: Surface plasmon resonance; Biosensor; Multi-analyte detection, Affinity biosensing

1. Introduction

In the last two decades, we have witnessed remarkable progress in the development of biosensors and their applications in the areas such as environmental monitoring, biotechnology, medical diagnostics, drug screening, food safety, and security. Various sensor technologies have been developed (e.g., electrochemical sensors [1], piezoelectric sensors [2], electrical impedance sensors [3], and optical sensors [4]) and applied to detection of chemical and biological analytes [5]. Optical sensors offer several important features—they exhibit high sensitivity, their performance is insensitive to electromagnetic interference, and they do not require electrical signal in a sensing area. Optical methods exploited in affinity biosensors include fluorescence spectroscopy [6], label-free methods such as interferometry [7], spectroscopy of guide modes of dielectric waveguides (grating coupler [8], resonant mirror [9]), and metallic waveguides (surface plasmon resonance [10,11]).

This paper focuses on surface plasmon resonance (SPR) biosensors technology, reviews fundamentals of SPR sensing, and discusses advances of this technology towards multi-analyte detection. A special attention is given to a recently developed multichannel SPR sensor combining the wavelength division multiplexing of serially ordered sensing channels with the conventional parallel channel architecture. Application of this multichannel SPR sensor for simultaneous detection of multiple analytes is described.

2. Principle of operation of SPR biosensors

An affinity optical biosensor consists of an optical transducer and a biological recognition element (BRE) which interacts with an analyte. The SPR transducer incorporates a thin metal film which supports a special mode of electromagnetic field—a surface plasmon-polariton (SPP)—sometimes referred as to a surface plasma wave. The SPP propagates along the surface of the metal film and the intensity of its electromagnetic

* Corresponding author.
E-mail address: homola@ure.cas.cz (J. Homola).

1046-2023/$ - see front matter © 2005 Elsevier Inc. All rights reserved.
doi:10.1016/j.ymeth.2005.05.003

field exponentially decays from the metal surface into the adjacent medium. The most commonly used metal is gold due to its chemical stability. A change in the refractive index due to the binding of analyte molecules to biomolecular recognition elements immobilized on the metal surface results in a change in the propagation constant of the SPP [11]. Surface plasmon resonance biosensors take advantage of this phenomenon and measure changes in the propagation constant of the SPP to determine changes in the amount of bound analyte and subsequently the concentration of analyte in a sample. Changes in the propagation constant of the SPP are determined by measuring one of the characteristics of the light wave that excites the SPP. On the basis of the characteristic of the light wave which is measured, SPR sensors are classified as sensors with angular, wavelength, intensity, phase, and polarization modulations [11].

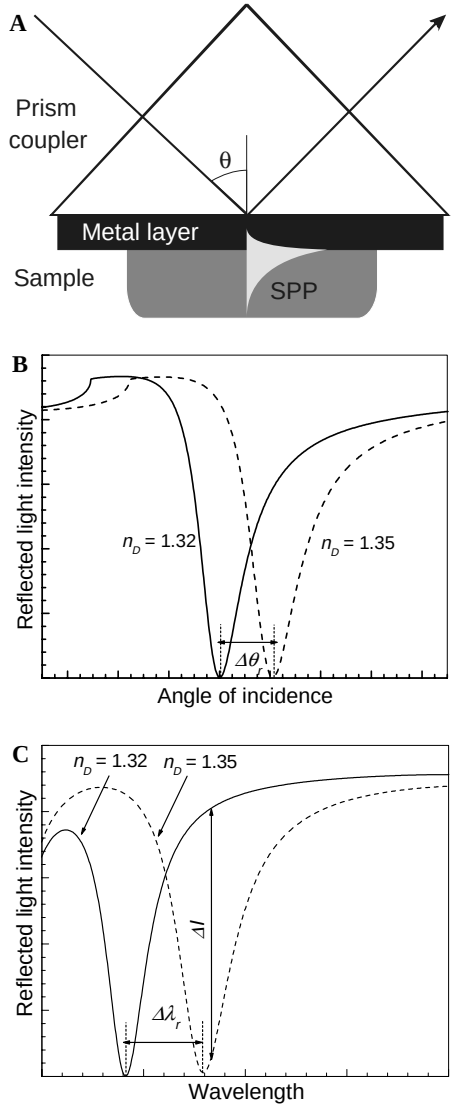

Fig. 1. (A) Excitation of surface plasmons via prism coupler. (B) Intensity of reflected light as a function of angle of incidence for a fixed wavelength and two refractive indices of sample. (C) Intensity of reflected light as a function of wavelength for a fixed angle of incidence and two refractive indices of sample.

The operating principle of the three modulation approaches (angular, wavelength, and intensity) used most frequently in SPR sensors is illustrated in Fig. 1, in which the excitation of surface plasmons is performed by the attenuated total reflection (ATR) in a prism coupler, Fig. 1A [11]. In SPR sensors with angular modulation, a beam of monochromatic light is used to excite an SPP (Fig. 1B). The propagation constant of the SPP and its changes are determined by measuring the intensity of reflected light at multiple angles of incidence and determining the angle of incidence yielding the strongest coupling with an SPP [12,13]. In SPR sensors with wavelength modulation, a beam of polychromatic light incident on the metal film under a fixed angle of incidence is used to excite an SPP (Fig. 1C). The propagation constant of the SPP and its changes are determined by measuring the intensity of reflected light at multiple wavelengths and determining the wavelength at which the strongest coupling with an SPP occurs [14]. In SPR sensors with intensity modulation, a beam of monochromatic light is made incident on the metal film under a fixed angle of incidence near the resonant angle of incidence (Fig. 1C) and changes in the intensity of reflected light are measured [15,16].

3. Advances in development of multi-analyte SPR sensors

3.1. Multichannel SPR sensor platforms

The most straightforward approach to multichannel SPR sensing is SPR imaging. SPR imaging is intensity modulation-based technique in which a collimated beam of monochromatic light passes through a prism coupler and excites SPPs on a thin metal layer. Intensity of the reflected light depends on the strength of the coupling between the light and SPPs which depends on the refractive index at the metal surface. Therefore, spatial distribution of the refractive index at the metal surface can be determined by measuring the distribution of light intensity across the reflected beam by means of a two-dimensional detector array (Fig. 2). This approach to spatially resolved SPR sensing has been applied to characterization of ultrathin films [17] and lipid layers [18,19].

When the metal surface is divided into multiple sensing spots, the SPR imaging device can be used as a multichannel SPR sensor. A multi-analyte biosensor based on SPR imaging was reported by Berger et al., [20], who demonstrated detection of four different analytes in a 16-channel matrix imaging format. SPR imaging was also applied to the observation of DNA hybridization [21], antibody–antigen binding, and

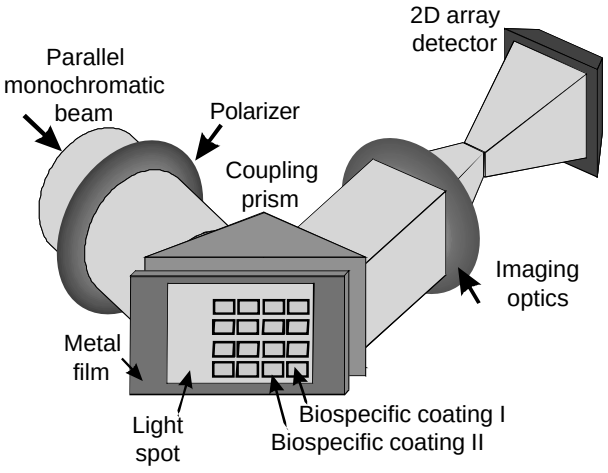

Fig. 2. SPR imaging sensor.

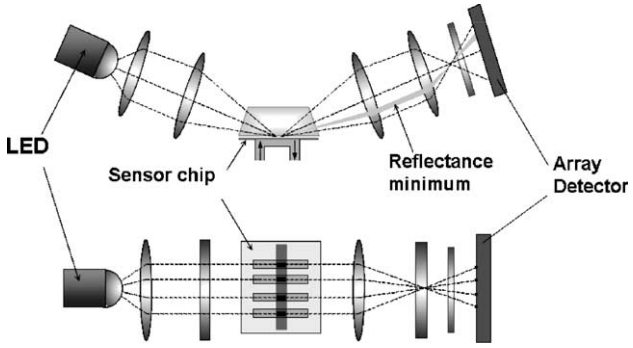

Fig. 3. SPR sensor with four parallel sensing channels (provided by S. Löfås, Biacore AB).

DNA–protein interaction [22], and detection of the sequence-specific binding of transcription regulatory proteins [23]. SPR imaging has also been exploited to study DNA-binding proteins to double-stranded DNA (dsDNA) array immobilized in a 10×12 array proving applicability of this method for monitoring the kinetics of binding of proteins to 120 different dsDNA sequences [24]. The major challenge for application of SPR imaging approach for biosensing is its rather limited resolution. Existing SPR imaging systems are capable of resolving bulk refractive index changes of about $\sim 10^{-5}$ RIU (refractive index units) [25]. To improve resolution of SPR imaging, this method was combined with polarization contrast and a spatially patterned multilayer SPR structure [26]. This approach generates high-contrast SPR images suitable for automated computer analysis, minimizes crosstalk between neighboring sensing channels, and provides compensation for light fluctuations improving the refractive index resolution to 3×10^{-6} RIU. This system was demonstrated to allow simultaneous monitoring of over 100 immunoreactions [26].

In contrast with SPR imaging systems, SPR sensors based on spectroscopy of surface plasmons take advantage of information contained in the whole wavelength or angular spectrum of light and therefore offer a considerably better resolution (up to 3×10^{-7} RIU) [27]. For multiplexing of sensing channels, most SPP spectroscopy-based sensors rely on parallel arrangement of sensing channels in which multiple light beams excite SPPs in different sensing channels and their reflectivity spectra are interrogated independently to determine SPR changes in each channel. Recently, SPR sensors based on serial channel architecture have also been reported. In these sensors, SPR spectra from multiple channels are encoded into a single optical wave [28,29]. Multichannel SPR sensors based on spectroscopy of SPP rely on ATR prism couplers [28–35] and diffraction gratings [36–38]. In ATR-based SPR biosensors with angular modulation and parallel architecture, series of convergent monochromatic beams are focused on a row of sensing channels where they excite SPPs. Light beams reflected from a row of sensing channels are projected on a two-dimensional detector array, Fig. 3. The first multi-channel SPR biosensors with angular modulation of SPR allowed simultaneous measurements in up to four sensing channels [30]; recently, the number of channels was extended to 6 [31], and 10 [32].

Lately, an interesting multichannel SPR sensor with angular interrogation and parallel sensing channels using a special planar sensor chip with diffractive optic coupling elements has been proposed. These elements project monochromatic light on an array of sensing channels and image the angular reflectivity spectra from each sensing channel on a CCD detector array [33]. In ATR-based SPR sensors with wavelength modulation and parallel architecture, series of collimated polychromatic beams are made incident on a row of sensing channels. SPR spectra encoded into the reflected light beams are analyzed by a spectrograph. The spectral analysis of multiple light beams is performed by multiple spectrographs [34] or by using an optical switch routing light from multiple channels to a spectrograph [35]. An alternative approach to multichannel SPR sensing with wavelength modulation is the wavelength division multiplexing (WDM). In the WDMSPR sensors, SPR spectra from multiple channels are encoded in different wavelength regions of a single polychromatic light beam. This is accomplished by changing the angle of incidence of the incident light beam (Fig. 4A) or by a dielectric overlayer deposited over a part of the SPR-active surface (Fig. 4B).

Multichannel sensors based on SPP spectroscopy have been also realized using diffraction grating couplers. These include an SPR compact disk platform employing a rotating sensor chip [36] and an HTS Biosystems SPR sensor in which SPR signal for each channel is determined from an angular reflectivity spectrum acquired by sequential angular scanning of SPR images

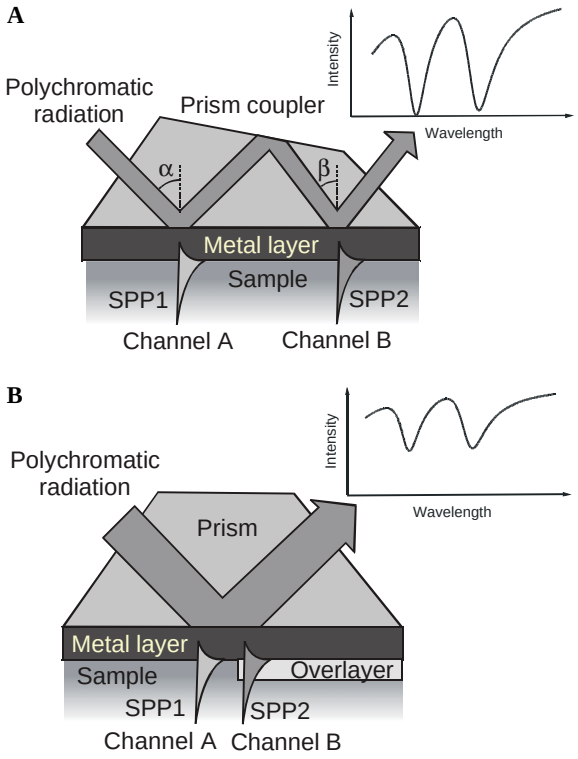

Fig. 4. SPR dual-channel sensors based on wavelength division multiplexing (WDM) of sensing channels. (A) WDM of sensing channels by means of altered angles of incidence [28]. (B) WDM of sensing channels by means of a high refractive index overlayer [29].

[37]. Another approach to multichannel SPR sensing is based on SPP spectroscopy on a two-dimensional array of diffraction gratings, where SPR angular spectra are sequentially scanned from rows of diffraction grating [38]. Mass production of diffraction grating-based SPR chips from plastics by technologies such as hot embossing or injection molding [39] offers potentially low-cost sensing elements [40] Fig. 5.

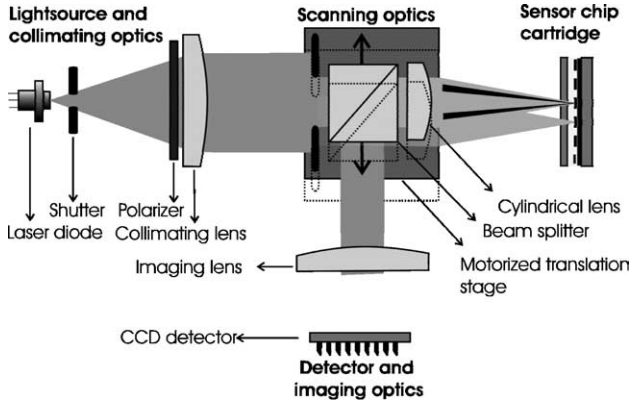

Fig. 5. Multi-channel SPR sensor based on an array of diffraction gratings [38].

3.2. Spatially controlled immobilization for multichannel SPR sensors

Various types of biomolecular recognition elements (antibodies [41], aptamers [42], peptides [43], and molecularly imprinted polymers [44], etc.) have been used in affinity biosensors. To enable multi-analyte detection, multiple biomolecular elements targeted to different analytes need to be immobilized in different sensing channels. This task requires the development of spatially controlled procedures for reproducible attachment of defined concentrations of biomolecular recognition elements on the surface of a sensor chip, Fig. 6. Other important requirements that these immobilization procedures have to fulfill are the conservation of biological activity of immobilized biomolecular recognition elements, non-fouling background of the sensor chip surface and the possibility to regenerate the biomolecular recognition elements (i.e., break their complex with the analyte molecules and make them available for another use).

In general, methods for immobilization of biomolecular recognition elements on gold films exploit physicochemical interactions such as chemisorptions [45], covalent binding [46,47], electrostatic coupling [48], and high-affinity molecular linkers in multilayer systems (e.g., streptavidin–biotin [49,50], proteins A or G [51], and complementary oligonucleotides [52]) and photo-immobilization (e.g., albumin derivatized with aryldiaziridines as a photo-linker [53]). One of the most remarkable techniques in surface chemistry is the spontaneous self-organization of *n*-alkylthiols or disulfides on gold into well-ordered arrays. Self-assembled monolayers (SAMs) have been employed in many immobilization methods for spatially controlled attachment of biomolecular recognition elements to surfaces of sensors [54]. To provide a desired surface concentration of biomolecular recognition elements on gold, mixed SAMs of long-chained ($n = 12$ and higher) *n*-alkylthiols terminated with functional group for further attachment of biomolecular recognition elements and short-chained alkylthiols for a non-fouling background have been developed [55,56].

To deliver molecular recognition elements to different areas of the SPR sensor surface, the immobilization chemistry needs to be spatially controlled. Most of the

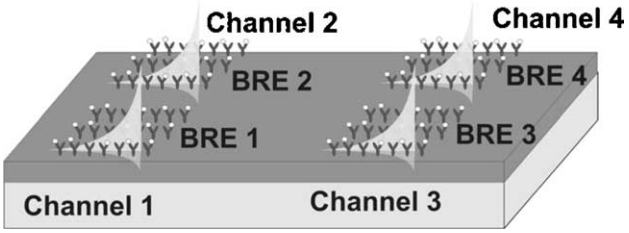

Fig. 6. Concept of multi-channel SPR biosensor.

current technologies of proteins arrays are based on the surfaces and formats that were earlier developed for DNA arrays. However, the chemical aspects of DNA array surfaces could not be easily adopted since proteins are chemically and structurally considerably more complex than nucleic acids and in contrast to DNA, they easily lose their biological activity due to denaturation, dehydration, or oxidation [57]. Most DNA array production techniques were developed for glass supports, but they can be tailored to noble metal surfaces with appropriate immobilization chemistries. Combination of SAMs with covalent coupling of biomolecular recognition elements or non-covalent streptavidin–biotin system as a linker for attachment of biotinylated biomolecular recognition elements are most frequently used approaches to development of protein arrays on gold.

Shumaker-Parry et al. [58] demonstrated microspotting double-stranded DNA on gold for SPR microscopy using two approaches. Both methods use streptavidin and biotinylated oligonucleotides. In the first method, the robotic microspotter was used to deliver nanoliter droplets of dsDNAs onto a uniform layer of streptavidin. In the second method, a streptavidin layer was also microspotted on a mixed-alkylthiol SAM and, subsequently, microspots of dsDNA were added using microspotting. Self-assembly surface chemistry and photopatterning have been combined to develop robust DNA and peptide arrays [59]. In the first step, a monolayer of 11-mercaptoundecylamine (MUAM) was assembled on gold surface. This amine-terminated surface was reacted with 9-fluorenylmethoxycarbonyl (Fmoc). Then, UV light was used to break the gold-thiol bonds and create bare gold pads, which were subsequently filled with MUAM. DNA or peptides were then attached to the MUAM using a covalent multi-step chemistry [59]. Finally, the Fmoc was removed and replaced with a polyethylene derivative to prevent non-specific binding. Another approach to the patterning of DNA or proteins on gold is based on microfluidic networks [60]. First, a set of parallel microchannels from poly(dimethylsiloxane) (PDMS) was created by replication of a silicon master prepared photolithographically. PDMS microchannels were used either to fabricate 1-D arrays consisting of lines of immobilized ligands or to create 2-D arrays in which a second set of PDMS microchannels was placed perpendicular to a 1-D line array. To create 1-D line arrays, the microchannels were attached to a gold surface modified with MUAM and activating reagents were introduced into the microchannels. Then, the DNA or peptides were reacted to the activated functional groups on MUAM. Subsequently, the microchannels were removed and the non-specific background was formed using polyethyleneglycol derivatives. Another approach is based on microcontact printing (μCP) which uses the relief pattern on the surface of an elastomeric PDMS stamp to form patterns on the sensor surface [61]. Various structures have been created on gold using μCP including patterned SAMs [62], proteins [63] or cells [64]. Peptide arrays have been formed using μCP onto reactive SAMs [65].

4. Multichannel SPR sensor with spectral modulation and wavelength division multiplexing

4.1. WDMSPR sensor

In this paper, we demonstrate multi-analyte detection using a recently developed eight-channel WDMSPR sensor [66]. This sensor is based on a special multireflection element in which a collimated beam of polychromatic light is made incident on the SPR sensor surface under two slightly different angles of incidence (Fig. 4A). Upon the first incidence on the surface of the sensor (channel A), light excites an SPP at the outer metal surface at the wavelength λ_A. The excitation of the SPPs produces a sharp absorption dip in the spectrum of optical wave centered at the wavelength λ_A. The reflected light is redirected inside the element and made incident on the metal film in the second region (channel B) under a different angle of incidence β ($\beta < \alpha$). At this angle of incidence, the optical wave couples to an SPP at a longer wavelength λ_B ($\lambda_B > \lambda_A$) generating a dip in the spectrum of the optical wave centered at the wavelength λ_B. Consequently, the wavelength spectrum of the transmitted light exhibits two SPR dips corresponding to SPRs in two distinct areas of the metal film, Fig. 7. These areas form two independent sensing channels. Response of each channel is encoded into a shift in the position of respective SPR dip.

The WDMSPR system reported herein combines the wavelength division multiplexing of pairs of sensing

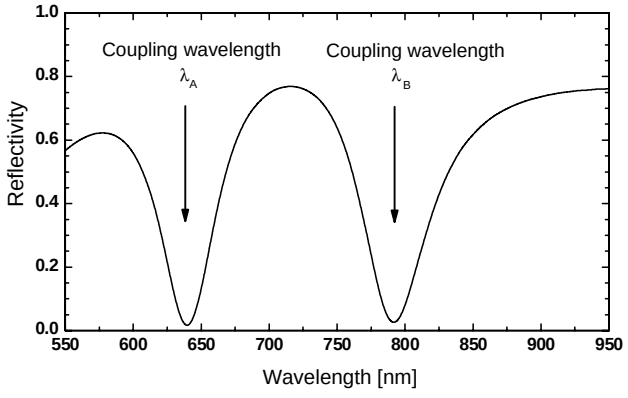

Fig. 7. Reflectivity in the WDMSPR sensing element as a function of wavelength. Sensing element—SF14 glass, metal layer–gold, thickness –55 nm, dielectric–aqueous medium, angles of incidence $\alpha = 54.6°$ and $\beta = 52.5°$.

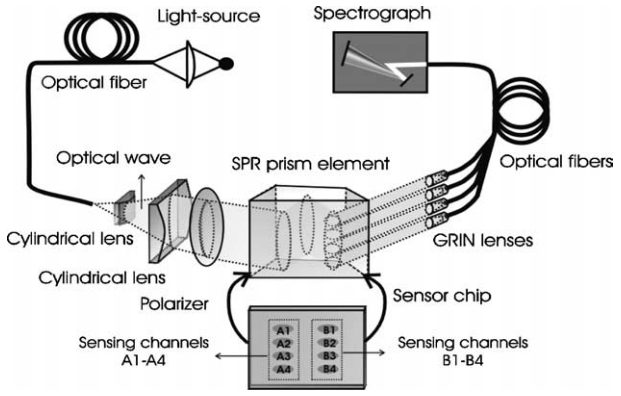

Fig. 8. An eight-channel SPR sensor combining parallel architecture with the wavelength division multiplexing of serially ordered channels.

channel with four parallel light beams to provide the total of eight sensing channels, Fig. 8. In the developed prototype of the sensor, polychromatic light from a halogen lamp (Avalight-Hal from Avantes, Netherlands) was coupled into an optical fiber (FT-400-EMT from Thorlabs, USA) and collimated using two cylindrical lenses. The collimated light beam was polarized by a dichroic polarizer (Polarcor, USA) and coupled in the WDMSPR sensing element to which a sensor chip (SF14 glass slide) coated by an adhesion promoting chromium layer (thickness less than 2 nm) and SPR-active gold layer (thickness 55 nm) was attached. The light was made incident on the SPR-active surface in eight areas denoted as A1–A4 and B1–B4, Fig. 8. Light beams reflected at the sensing areas A1–A4 and B1–B4 were collected by four miniature GRIN lenses (NSG America, USA) and coupled to four optical fibers FT-400-EMT (Thorlabs, USA) connected to a four-channel spectrograph S2000 (Ocean Optics, USA). The SPR spectra were measured in TM polarization and normalized with spectra obtained in TE polarization. Measured SPR spectra were averaged in time and the SPR dip position was determined by the 5th-order polynomial fitting and tracked over time for each sensing channel. An eight-channel flow-cell was clamped against the SPR chip to contain liquid samples during experiments. The flow-cell was made of an acrylic substrate with input and output ports interfacing flow-cell chambers for each sensing channel. The flow-cell chambers were cut into a gasket made of a 50-micrometer thick polyurethane sheet using a CO_2 laser beam (custom made by Micronics, USA). The volume of each flow-cell chamber was 2 μl. Input flow-cell ports were connected via tubings (Upchurch Scientific, USA) with two four-channel peristaltic pumps Reglo Digital (Ismatec, Switzerland) which controlled the flow of liquid samples through the flow-cell. In the reported experiments, the flow rate of 50 μl/min was used.

4.2. Materials

Antibody solutions were prepared in 10 mM phosphate buffer (PB), pH 7.6, at 20 °C. Analyte solutions were prepared in PBS (10 mM phosphate buffer, 137 mM NaCl, and 2.7 mM KCl, pH 7.4, at 20 °C) containing bovine serum albumin at a concentration of 100 μg/ml. Bovine serum albumin (BSA) was purchased from Sigma–Aldrich, USA. The C_{11}-chained and C_{16}-chained alkanethiols (C_{11}-mercapto-1-undecanol and C_{16}-mercaptohexadecanoic acid) and the *N*,*N*,*N*′,*N*′-tetramethyl-*O*-(*N*-succinimidyl)uronium tetrafluoroborate (TSTU) used for activation of carboxylic terminal groups on C_{16} alkanethiol were purchased from Sigma–Aldrich, USA. Monoclonal affinity-purified antibodies against human immunoglobulin E (aIgE), human immunoglobulin G (aIgG), human choriogonadotropin (ahCG), and horseradish peroxidase (aPx) were purchased from Seva Immuno, Czech Republic. Human immunoglobulin E (IgE) was purchased from Biodesign, USA, human immunoglobulin G (IgG) was obtained from the Faculty of Sciences of the Charles University (Laboratory of Anthropology and Human Genetics), Czech Republic, human choriogonadotropin (hCG) was purchased from Calbiochem, USA, and horseradish peroxidase (Px) from Kem-En-Tec, Denmark. Immune reaction activities of all immune partners were confirmed by ELISA method.

4.3. Chip functionalization

The functionalized method used in this work is based on thiol-attachment chemistry and spatially controlled delivery of antibodies using microfluidics. Prior to functionalization, sensor chips were rinsed with Piranha solution (a 1:3 mixture of 30% hydrogen peroxide and 96% sulfuric acid) for 3 min, then washed with deionized water and dried with nitrogen stream. A 7:3 mixture of

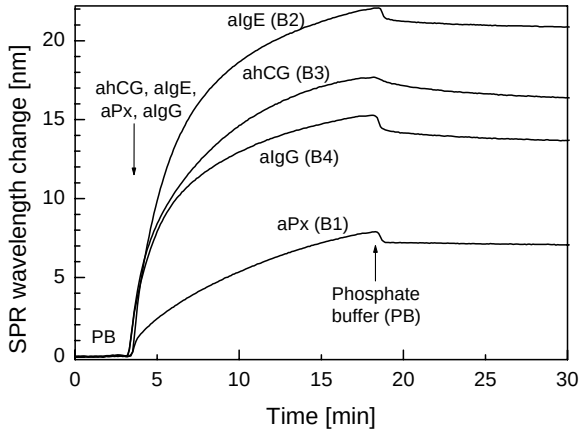

Fig. 9. SPR wavelength change due to the immobilization of aPx, aIgE, ahCG, and aIgG antibodies, antibody concentration—50 μg/ml.

C_{11}-chained and C_{16}-chained alkanethiols was dissolved in degassed absolute ethanol with a total thiol concentration of 1 mM. The C_{16} alkanethiols terminated with a carboxylic head group were used to anchor an antibody; C_{11} alkanethiol chains terminated with a hydroxyl head group were used to form a non-fouling background. Sensor chips were immersed in a thiol solution and stored in a dark place at room temperature for two days.

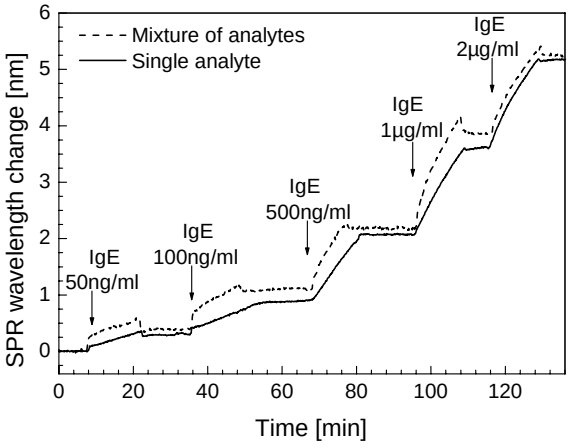

Fig. 10. IgE sensorgrams for solutions containing only IgE (channel B2) and the mixture of analytes (channel A2).

After the formation of a thiol self-assembled monolayer (SAM), the sensor chips were rinsed with ethanol, dried with nitrogen, rinsed with water, and dried with nitrogen again. The carboxylic terminal groups on the sensor surface were activated by TSTU dissolved in dimethylformamide at a concentration of 1 mg/ml for 4 h. After the activation, the sensor chip was rinsed with water, dried with nitrogen, and loaded into the SPR instrument. Antibody attachment was performed in situ by flowing phosphate buffer solution with 50 µg/ml of antibody along a sensing channel surface for 15 min (flow rate 50 µl/min). Specifically, identical solutions containing aPx, aIgE, ahCG, and aIgG were flowed through pairs of sensing channels A1 and B1, A2 and B2, A3 and B3, and A4 and B4, respectively. Then, the antibody solutions were replaced with a phosphate buffer solution containing natrium chloride at a concentration of 1 M, which was flowed through all channels to remove weakly bound antibodies. The immobilization of the aPx, aIgE, ahCG, and aIgG antibodies on the thiol-coated SPR sensing surface was observed using the SPR sensor system described in Section 4.1. Fig. 9 shows the sensor response to the immobilization of antibodies in the sensing channels B1–B4. The sensor response to antibodies ranges from 9 to 23 nm. This difference is believed to be mainly due to different accessibilities of amino groups

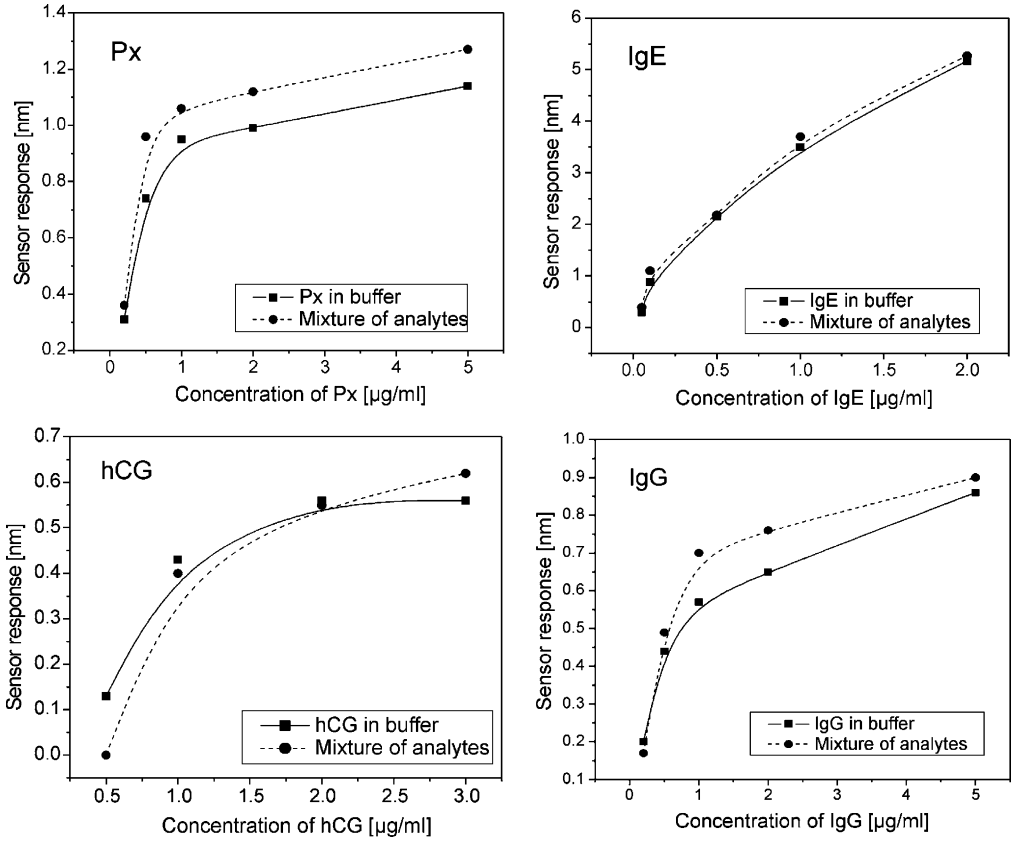

Fig. 11. Sensor response as a function of analyte concentration for Px, IgE, hCG, and IgG measured in pure buffer and mixture of all analytes.

for each type of antibody and electrostatic interaction between the antibody and the surface. Finally, the sensor surface was flushed with BSA dissolved in PBS to interact with the unreacted carboxylic groups.

4.4. Multi-analyte detection

The SPR chip coated with aPx, aIgE, ahCG, and aIgG antibodies was used for simultaneous detection of model analytes—Px, IgE, hCG, and IgG. Detection of these analytes was performed in solutions containing only a single analyte and in mixtures containing Px, IgE, hCG, and IgG. First, buffer (BSA-PBS) was flowed through all eight sensing channels until a stable sensor response was reached. Then, the mixture of Px, IgE, hCG, and IgG was flowed through the sensing channels A1–A4 for 15 min. Simultaneously, four solutions containing only the analyte corresponding to the immobilized antibody at the concentration identical to the one in the mixtures were injected into the sensing channels B1–B4. After the incubation for 15 min, these samples were replaced with buffer. This procedure was performed sequentially with solutions containing Px, hCG, IgG, and IgE at concentrations of 0.2, 0.5, 0.2, and 0.05 μg/ml (MIX 1); 0.5, 1, 0.5, and 0.1 μg/ml (MIX 2); 1, 2, 1, and 0.5 μg/ml (MIX 3); 2, 3, 2, and 1 μg/ml (MIX 4); and 5, 5, 5, and 2 μg/ml (MIX 5), respectively. Typical sensorgrams for samples containing only a single analyte and in mixtures of analytes are shown in Fig. 10.

The sensor response to an increasing concentration of pure analytes and analytes in mixtures was simultaneously measured. The sensor response was determined as a difference in the resonant wavelength in buffer before and after the incubation of the sensor surface with samples. The resulting sensor responses as a function of concentration of analyte are shown in Fig. 11. The reproducibility of the measurements was evaluated in repeated experiments and found to be within ± 10% of the sensor response for Px, hCG, and IgG and ± 5% of the sensor response for IgE. The difference in the sensor response to the same concentration of target analyte in the absence and in the presence of other analytes was found to fall within 18%. Moreover, it was observed that the sensor response to analyte in a mixture was usually higher than that corresponding to a pure sample containing only analyte.

To investigate the specificity of studied biomolecular interactions, the sensor responses to non-target and target analytes were compared. The non-target analytes followed with the target analyte were sequentially flowed

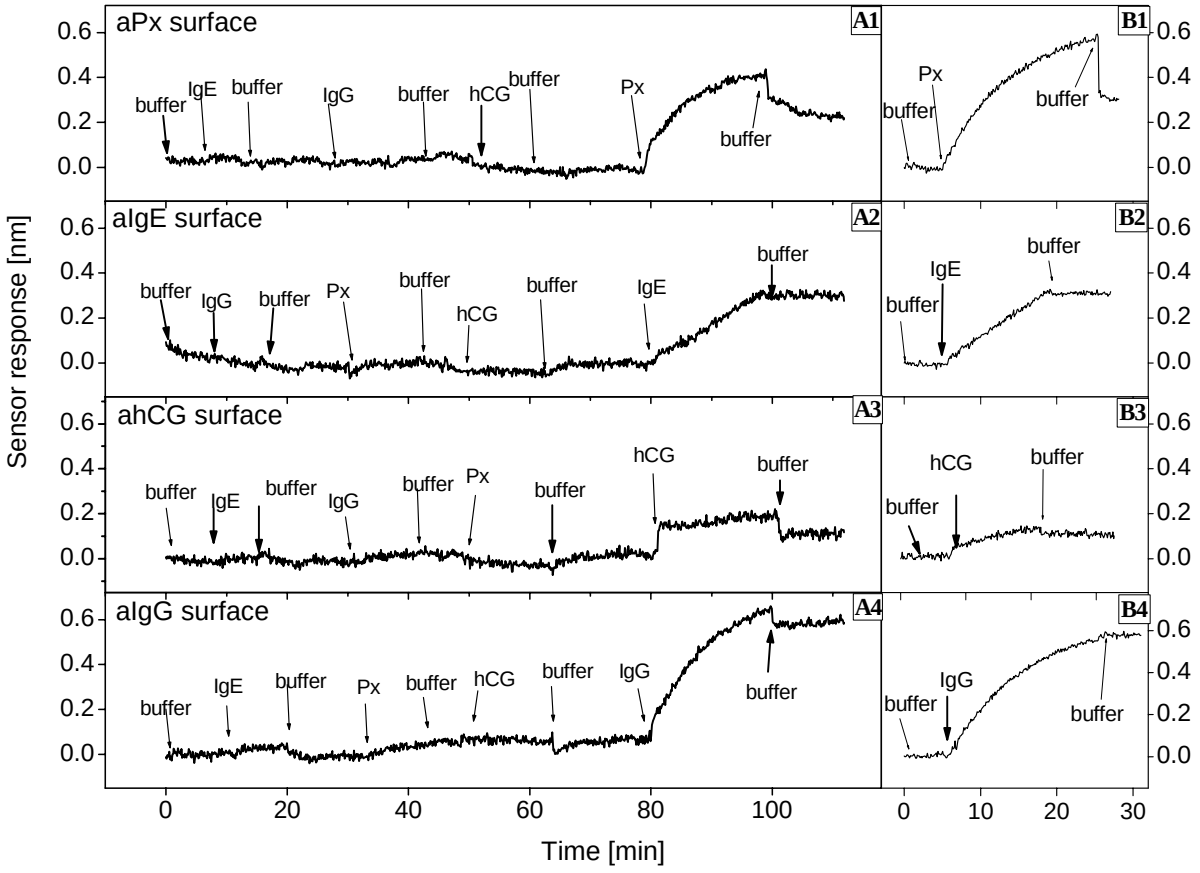

Fig. 12. Sensor response to target analytes injected after a sequence of non-target analytes (A1–A4) and sensor response to specific analytes without the exposure to non-target analytes (channels B1–B4), concentrations of Px, IgE, hCG, and IgG are 0.5, 0.1, 0.5, and 0.5 μg/ml, respectively.

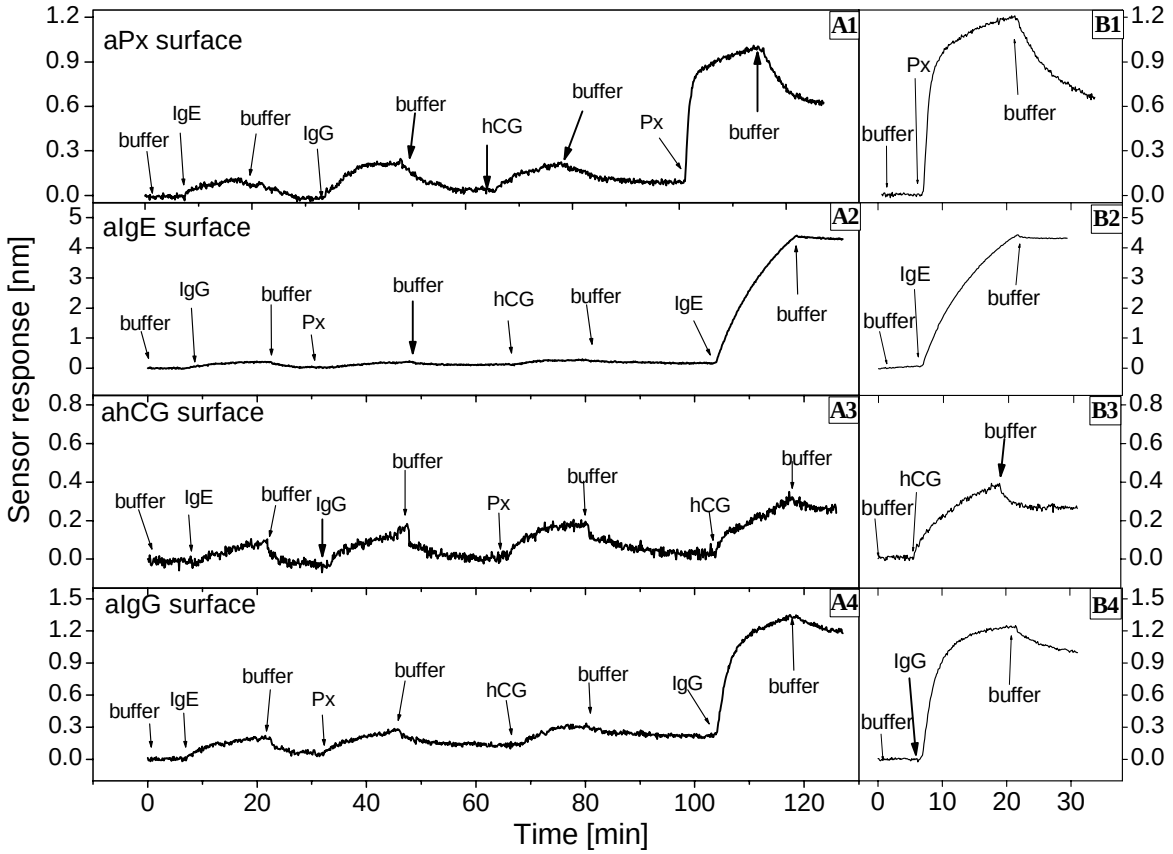

Fig. 13. Sensor response to a target analyte injected after a sequence of non-target analytes (A1–A4) and directly (channels B1–B4), concentrations of Px, IgE, hCG, and IgG are 5, 2, 2, and 5 μg/ml, respectively.

through the sensing channels A1–A4. Simultaneously, solutions with only a specific analyte were flowed through the sensing channels B1–B4. The same experiment was performed for lower and higher concentrations of analyte molecules. Corresponding sensorgrams for low and high concentrations are shown in Figs. 12 and 13, respectively. Concentrations of Px, IgE, hCG and IgG were 0.5, 0.1, 0.5, and 0.5 μg/ml, and 5, 2, 2, and 5 μg/ml for low and high concentrations, respectively.

As follows from Fig. 12, the low concentrations of non-target analytes generated basically no response (less than 0.07 nm) and the subsequent response to the target analytes produced sensor response of 0.25, 0.30, 0.10, and 0.54 nm for Px, IgE, hCG, and IgG, respectively. These values agree well with the sensor responses to samples containing only a target analyte observed in the sensing channels not in contact with the non-target analytes, which were found to be 0.30, 0.30, 0.10, and 0.56 nm for Px, IgE, hCG, and IgG, respectively. High analyte concentrations produced non-specific sensor responses of about 0.1, 0.17, 0.03, and 0.22 nm, on aPx, aIgE, ahCG, and aIgG-coated surfaces, respectively. The subsequent binding of the target analyte produced sensor responses of about 0.62, 4.10, 0.24, and 1.00 nm for Px, IgE, hCG, and IgG, respectively. As follows from the experimental data, majority of the non-specific binding was reversible (Fig. 13) and the observed non-specific response was about 16, 3, 13, and 22% of the specific response to Px, IgE, hCG, and IgG, respectively. Responses to the same concentrations of pure analytes incubated with sensing surfaces unexposed to other analytes were found to be 0.65, 4.3, 0.27, and 1.01 nm for Px, IgE, hCG, and IgG, respectively; Fig. 13.

The ultimate lowest detection limits of the sensor for the model analytes were estimated based on the accuracy of measuring the SPR wavelength that is defined as three standard deviations of sensor response noise and was equal to 0.03 nm for the used WDMSPR sensor system. In pure samples, the ultimate detection limits were 60, 10, 150, and 30 ng/ml for Px, IgE, hCG, and IgG, respectively. Detection of low concentrations of analytes in mixtures was limited by the non-specific binding and determined to be 200, 600, 300, and 200 ng/ml, Px, IgE, hCG, and IgG, respectively.

5. Outlook

A number of surface plasmon resonance (SPR) sensor platforms and attachment/patterning methods suitable

for multi-analyte detection have been proposed over the last decade. So far, the majority of demonstrated SPR multi-sensors have been able to detect simultaneously only a limited number of analytes. However, further advances in development of biomolecular recognition element arrays and microfluidics for both patterning and sample distribution are expected to lead to SPR systems capable of observing and quantifying tens and hundreds of biomolecular interactions in near future. Implementations of such multi-analyte sensors will be driven by the needs of specific applications. The main application areas include pharmaceutical research (high-throughput systems for drug screening), medical diagnostics (high-throughput diagnostic tools), food safety (systems for rapid detection of foodborne pathogens and agents), and security (devices for early detection and identification of biological and chemical warfare agents).

Acknowledgments

The authors thank Václav Malina and Petra Chocholáčová (Institute of Radio Engineering and Electronics, Prague) for deposition of thin films, Jiří Škvor (Seva Immuno, Ltd., Prague) for providing antibodies used in this work, and Markéta Lachmanová for assistance with experiments. This work was supported by the Grant Agency of the Czech Republic under contracts 303/03/0249, 203/02/1326, 102/03/0633, and 202/05/0628 and by European Commission under contract QLK4-CT-2002-02323.

References

[1] A.L. Ghindilis, P. Atanasov, M. Wilkins, E. Wilkins, Biosens. Bioelectron. 13 (1998) 113–131.
[2] X. Chu, Z.H. Lin, G.L. Shen, R.Q. Yu, M. Analyst. 120 (1995) 2829–2832.
[3] P. Pless, K. Futschik, E. Schopf, J. Food Prot. 57 (1994) 369–376.
[4] G. Gauglitz G, Sensor Update Vol. 1, VCH Verlagsgesellschaft, Weinheim 1996.
[5] D. Ivnitski, I. Abdel-Hamid, P. Atanasov, E. Wilkins, Biosens. Bioelectron. 14 (1999) 599–624.
[6] C.A. Rowe-Taitt, J.W. Hazzard, K.E. Hoffman, J.J. Cras, J.P. Golden, F.S. Ligler, Biosens. Bioelectron. 15 (2000) 579–589.
[7] R.G. Heideman, R.P.H. Kooyman, J. Greve, Sens. Act. B 10 (1993) 209–217.
[8] D. Clerc, W. Lukosz, Sens. Act. B 19 (1994) 581–586.
[9] R. Cush, J.M. Cronin, W.J. Stewart, C.H. Maule, J. Molloy, N.J. Goddard, Biosens. Bioelectron. 8 (1993) 347–353.
[10] J. Homola, S. Yee, G. Gauglitz, Sens. Act. B 54 (1999) 3–15.
[11] J. Homola, S.S. Yee, D. Myszka, Surface plasmon biosensors, in: F.S. Ligler (Ed.), Optical Biosensors: Present and Future, Elsevier, Amsterdam, 2002.
[12] K. Matsubara, S. Kawata, S. Minami, Appl. Opt. 27 (1988) 1160–1163.
[13] B. Liedberg, I. Lundstrom, E. Stenberg, Sens. Act. B 11 (1993) 63–72.
[14] L.M. Zhang, D. Uttamchandani, Electron. Lett. 23 (1988) 1469–1470.
[15] C. Nylander, B. Liedberg, T. Lind, Sens. Act. 3 (1982) 79–88.
[16] M.M.B. Vidal, R. Lopez, S. Aleggret, J. Alonso-Chamarro, I. Garces, J. Mateo, Sens. Act. B 11 (1993) 455–459.
[17] B. Rothenhäusler, W. Knoll, Nature 332 (1988) 615–617.
[18] W. Hickel, W. Knoll, Thin Solid Films 187 (1990) 349–356.
[19] R.P.H. Kooyman, U.J. Krull, Langmuir 7 (1991) 1506–1509.
[20] C.E.H. Berger, T.A.M. Beumer, R.P.H. Kooyman, J. Greve, Anal. Chem. 70 (1998) 703–706.
[21] A.J. Thiel, A.G. Frutos, C.E. Jordan, R.M. Corn, L.M. Smith, Anal. Chem. 69 (1997) 4948–4956.
[22] G.J. Wegner, H.L. Lee, G. Marriott, R.M. Corn, Anal. Chem. 75 (2003) 4740–4746.
[23] E.A. Smith, M.G. Erickson, A.T. Ulijasz, B. Weisblum, R.M. Corn, Langmuir 19 (2003) 1486–1492.
[24] J.S. Shumaker-Parry, R. Aebersold, C.T. Campbell, Anal. Chem. 76 (2004) 2071–2082.
[25] E. Fu, T.M. Chinowsky, J. Foley, J. Weinstein, P. Yager, Rev. Sci. Instrum. 75 (2004) 2300–2304.
[26] M. Piliarik, H. Vaisocherová, J. Homola, Biosens. Bioelectron. 20 (2005) 2104–2110.
[27] R. Karlsson, R. Stahlberg, Anal. Biochem. 228 (1995) 280–284.
[28] J. Homola, J. Dostálek, J. Etyroký, Proc. SPIE 4416 (2001) 86–89.
[29] J. Homola, H.B. Lu, G.G. Nenninger, J. Dostálek, S.S. Yee, Sens. Act. B 76 (2001) 403–410.
[30] S. Löfas, M. Malmqvist, I. Rönnberg, E. Stenberg, B. Liedberg, I. Kundström, Sens. Act. B 5 (1991) 79–84.
[31] R. Karlsson, J. Mol. Recogn. 17 (2004) 151–161.
[32] M.J. O'Brien, V.H. Perez-Luna, S.R.J. Brueck, G.P. Lopez, Biosens. Bioelectron. 16 (2001) 97–108.
[33] C. Thirstrup, W. Zong, M. Borre, H. Neff, H.C. Pedersen, G. Holzhueter, Sens. Act. B 100 (2004) 298–308.
[34] J. Homola, J. Dostálek, S.F. Chen, A. Rasooly, S. Jiang, S.S. Yee, Int. J. Food Microbiol. 75 (2002) 61–69.
[35] G.G. Nenninger, J.B. Clendenning, C.E. Furlong, S.S. Yee, Sens. Act. B 51 (1998) 38–45.
[36] W.A. Challener, R.R. Ollman, K.K. Kam, Sens. Act. B 56 (1999) 254–258.
[37] J.M. Brockman, S.M. Fernandez, Am. Lab. 33 (2001) 37–40.
[38] J. Dostálek, J. Homola, M. Miler, Sens. Act. B 108 (2005) 758–764.
[39] M.T. Gale, Microelectron. Eng. 34 (1997) 321–339.
[40] C.R. Lawrence, N.J. Geddes, D.N. Furlong, J.R. Sambles, Biosens. Bioelectron. 11 (1996) 389–400.
[41] B. Hock, Anal. Chem. Acta 347 (1997) 177–186.
[42] S.D. Jayasena, Clin. Chem. 45 (1999) 1628–1650.
[43] G.J. Wegner, H.J. Lee, G.M. Corn, Anal. Chem. 74 (2002) 5161–5168.
[44] R.J. Ansell, O. Ramstrom, K. Mosbach, Clin. Chem. 42 (1996) 1506–1512.
[45] R.C. Nuzzo, D.L. Allaza, J. Am. Chem. Soc. 105 (1983) 4481–4483.
[46] B. Johnsson, S. Lofas, G. Lindquirst, A. Edstrom, R.M. Muller Hillgren, A. Hansson, J. Mol. Recog. 8 (1995) 125–131.
[47] D.J. O'Shanneessy, M. Brigham-Burke, K. Peck, Anal. Biochem. 314 (2001) 1–26.
[48] M. Houska, E. Brynda, K. Bohatá, J. Colloid Interf. Sci. 273 (2004) 140–147.
[49] S. Tombelli, M. Mascini, A.P.F. Turner, Biosens. Bioelectron. 17 (2002) 929–936.
[50] S. Busse, E. Scheumann, B. Menges, S. Mittler, Biosens. Bioelectron. 17 (2002) 704–710.
[51] G.P. Anderson, M.A. Jacoby, F.S. Ligler, K.D. King, Biosens. Bioelectron. 12 (1997) 329–336.
[52] J. Ladd, C. Boozer, Q. Yu, S. Chem, J. Homola, S. Jiang, Langmuir 20 (2004) 8090–8095.
[53] H. Gao, M. Sanger, R. Luginbuhl, H. Sigrist, Biosens. Bioelectron. 10 (1995) 317–328.
[54] W. Knoll, M. Liley, D. Piscevic, J. Spinke, M.J. Tarlov, Adv. Biophys. 34 (1997) 231–251.

[55] L.S. Jung, K.E. Nelson, P.S. Stayton, C.T. Campbell, Langmuir 16 (2000) 9421–9432.
[56] K.E. Nelson, L. Gamble, L.S. Jung, M.S. Boeckl, E. Neemi, S.L. Golledge, T. Sasaki, D.G. Castner, C.T. Campbell, P.S. Stayton, Langmuir 17 (2001) 2807–2816.
[57] M.K. Baller, L.R. Booth, J.F. Burke, R.M. Corn, G. Franklin, J. Fritz, K.A. Hughes, R.J. Kaiser, D. Kambhampati, W. Knoll, H.J. Lee, S. Lofas, in: D. Kambhampati (Ed.), Protein Microarray Technology, Wiley-VCH, Weinheim, 2004.
[58] J.S. Shumaker-Parry, M.H. Zareie, R. Aebersold, C.T. Campbell, Anal. Chem. 76 (2004) 918–929.
[59] J.M. Brockman, A.G. Frutos, R.M. Corn, J. Am. Chem. Soc. 121 (1999) 8044–8051.
[60] R.J. Jackman, D.C. Duffy, E. Ostuni, N.D. Willmore, G.M. Whitesides, Anal. Chem. 70 (1998) 2280–2287.
[61] J. Lahiri, E. Ostuni, G.M. Whitesides, Langmuir 15 (1999) 2053–2060.
[62] R.K. Smith, P.A. Lewis, P.S. Weiss, Progr. Surf. Sci. 75 (2004) 1–68.
[63] H.B. Lu, J. Homola, C.T. Campbell, G.G. Nenninger, S.S. Yee, B.D. Ratner, Sens. Act. B 74 (2001) 91–99.
[64] R.S. Kane, S. Takayama, E. Ostuni, D.E. Ingber, G.M. Whitesides, Biomaterials 20 (1999) 2363–2376.
[65] L. Yan, X-M. Zhao, G.M. Whitesides, J. Am. Chem. Soc. 120 (1998) 6179–6180.
[66] J. Dostálek, H. Vaisocherová, J. Homola, Sens. Act. B 107 (2005) 154–161.

Appendix V

M. Piliarik, H. Vaisocherová and J. Homola:

A new surface plasmon resonance sensor for high-throughput screening applications

Biosensors & Bioelectronics, **20** (2005), 2104 – 2110

Available online at www.sciencedirect.com
SCIENCE DIRECT®
Biosensors and Bioelectronics 20 (2005) 2104–2110
BIOSENSORS & BIOELECTRONICS
www.elsevier.com/locate/bios

A new surface plasmon resonance sensor for high-throughput screening applications

Marek Piliarik, Hana Vaisocherová, Jiří Homola*

Institute of Radio Engineering and Electronics, Academy of Sciences of the Czech Republic, Chaberská 57, 18251 Prague, Czech Republic

Received 7 July 2004; received in revised form 20 September 2004; accepted 29 September 2004
Available online 8 December 2004

Abstract

We report a new high-throughput surface plasmon resonance (SPR) sensor based on combination of SPR imaging with polarization contrast and a spatially patterned multilayer SPR structure. We demonstrate that this approach offers numerous advantageous features including high-contrast SPR images suitable for automated computer analysis, minimum crosstalk between neighboring sensing channels and inherent compensation for light level fluctuations. Applications of a laboratory prototype of the high-throughput SPR sensor with 108 sensing channels for refractometry and biosensing are described. In refractometric experiments, the noise-limited refractive index resolution of the system has been established to be 3×10^{-6} refractive index unit (RIU). Experimental data on detection of human choriogonadotropin (hCG) suggest that in conjunction with monoclonal antibodies against hCG, the reported SPR imaging sensor is capable of detecting hCG at concentrations lower than 500 ng/ml.

Keywords: Surface plasmon resonance; SPR imaging; Biosensor; High-throughput screening

1. Introduction

High-throughput chemical sensor and biosensor technologies are needed in many important areas such as life sciences, drug development, medical diagnostics, food safety and security. Optical sensors based on surface plasmon resonance (SPR) have been demonstrated to be useful for affinity biosensing and biomolecular interaction analysis (Rich and Myszka, 2002; Homola, 2003) and to hold major potential for applications in these areas. However, the majority of existing SPR sensing devices offer only a small number of sensing channels (<10) and thus their throughput is rather limited. Therefore, in recent years we have witnessed growing effort towards development of high-throughput SPR sensing devices.

In traditional multichannel SPR sensors, surface plasmons are excited in multiple areas and spectral (Nenninger et al., 1998) or angular (Löfås et al., 1991) distribution of reflected light is analyzed using separate detectors (Nenninger et al., 1998) or different areas of single detector (Löfås et al., 1991). The number of sensing channels in spectral SPR sensors can be further increased by using the wavelength division multiplexing (WDM) technique in which surface plasmons in different sensing channels are excited at different wavelengths (Homola et al., 1999, 2001). A larger number of sensing channels can be achieved using SPR imaging which is based on analysis of distribution of intensity of light reflected from an SPR surface containing multiple sensing areas. Spatially resolved SPR sensing was introduced by Rothenhäusler and Knoll (1988) who demonstrated SPR microscopy with high contrast for measurements of ultrathin films. Although multichannel sensors based on SPR imaging provide lower resolutions than the systems based on spectroscopy of surface plasmons, the SPR imaging systems have been successfully applied for analysis of polymer networks and monitoring of thin films formation and electropolymerization (Baba and Knoll, 2003). SPR imaging has been also applied to studies of oligonucleotide (Piscevic et al., 1995) and RNA hybridization (Nelson et al., 2001), and DNA interaction with polymer

* Corresponding author. Tel.: +420 266 773 448; fax: +420 284 680 222.
E-mail address: homola@ure.cas.cz (J. Homola).

0956-5663/$ – see front matter © 2004 Elsevier B.V. All rights reserved.
doi:10.1016/j.bios.2004.09.025

functionalized surfaces (Bassil et al., 2003). DNA hybridization signal was amplified by the use of biotinylated oligonucleotides and subsequent binding of streptavidin to biotin to enhance the detection limits with SPR imaging (Jordan et al., 1997). SPR imaging has been also exploited to study protein binding to a DNA array (Shumaker-Parry et al., 2004) and antigen–antibody interactions (Wegner et al., 2003). Detection of small molecules and observation of their interactions still remain beyond capabilities of the SPR imaging systems.

In this paper, we report a new high-throughput SPR sensor based on the combination of SPR imaging with polarization contrast and a spatially patterned multilayer SPR structure. This approach offers several significant advantages over conventional SPR imaging. These include generation of high-contrast SPR images suitable for automated computer analysis, minimization of crosstalk between neighboring sensing channels and compensation for light level fluctuations. Applications of the sensor for refractometry and biosensing are also described.

2. Sensor concept

2.1. SPR imaging

Surface plasmon resonance imaging is an experimental method for spatially resolved measurement of refractive index changes at an SPR-active metal surface. Conventional SPR imaging instruments (Steinerg et al., 1999) utilize the Kretschmann geometry of the attenuated total reflection (ATR) method (Raether, 1988), in which a collimated beam of monochromatic light passes through a prism coupler with a thin SPR-active metal layer on its base. The light evanescently penetrates through the metal film and excites surface plasmons at its outer boundary. Intensity of the reflected light depends on the strength of the coupling of light to a surface plasmon, which depends on the refractive index at the metal surface. Therefore, spatial distribution of the refractive index at the SPR-active surface can be determined by measuring the distribution of light intensity across the reflected beam by means of a two-dimensional detector array. An SPR imaging device can be used as a multichannel SPR sensor if the surface is divided into multiple sensing spots. The smallest spot from which the SPR signal can be read is in principle given by the surface area imaged on an individual pixel of the detector array. However, the spatial resolution is limited by the propagation length of surface plasmons, which is typically of the order of tens of microns (Somekh, 2002) and the resolution of the imaging optics (interferences from neighboring sensing spots).

2.2. SPR imaging using polarization contrast and special SPR multilayer structures

As demonstrated earlier, the surface plasmon resonance phenomenon can be efficiently observed in the polarization

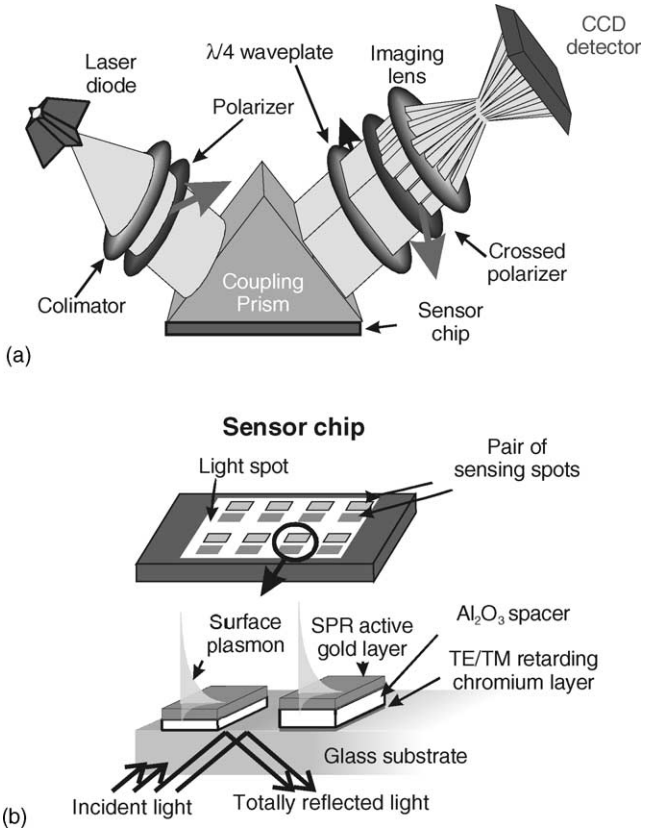

Fig. 1. (a) SPR imaging with polarization contrast and (b) detail of the SPR chip with series of pairs of sensing spots.

contrast (Homola and Yee, 1998; Nikitin et al., 2000). In this geometry, a prism coupler and a chip is placed between two crossed polarizers and a quarter waveplate. In the imaging approach proposed herein, the surface of the sensing chip is not uniformly covered with an SPR-active layer, but with a pattern of distinct SPR sensing spots separated by uncoated areas (bare glass), where the light reflects totally without being influenced by SPR. The first polarizer allocates the same amount of light intensity to both TE and TM polarizations. After the reflection on the sensor chip, the light passes through the quarter waveplate. The polarization of the light reflected from the uncoated surface areas is converted to linear and extinguished by the linear polarizer placed between the waveplate and the CCD camera (Fig. 1). The TM-polarized light component interacting with a surface plasmon on the coated sensor spot undergoes both amplitude and phase change, while the phase and amplitude of the TE-polarization varies only slightly. This effect gives rise to bright sensing spots on a weak background, which are easier to read than images produced by conventional SPR imaging systems. Moreover, it reduces crosstalk between neighboring sensing spots and interference of light not associated with the measured quantity.

In this work, we introduce two different SPR multilayers designed to support surface plasmons and exhibit opposite sensitivities to changes in refractive index at the surface. Both

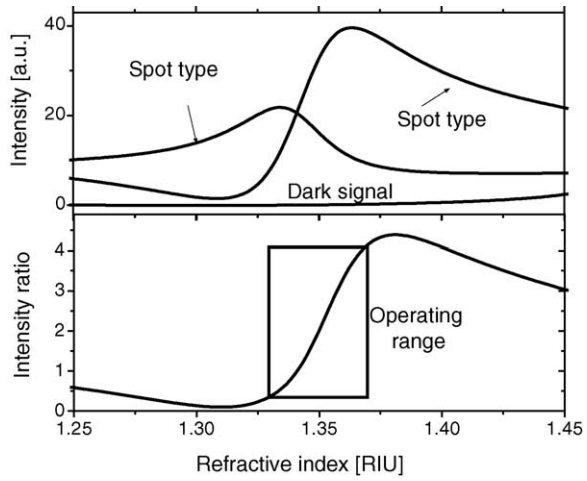

Fig. 2. Dependence of light intensity on the refractive index of sample for the two different sensing spots and their ratio. Intensity at bare surface (dark signal) shown for comparison.

the SPR multilayers are formed on SF2 glass substrate and consist of a chromium layer, an aluminum oxide buffer layer, and an SPR-active gold layer (Fig. 1). Theoretical analysis of light propagation in the multilayer structures in the polarization contrast geometry was performed using the Fresnel equations and Jones matrix calculus (Saleh and Teich, 1991) and parameters of the multilayer structures for the SPR imaging system were selected so that the two multilayers exhibited refractive index sensitivities of opposite signs. The first multilayer (Spot type I) consists of 4 nm chromium layer, 100 nm aluminum oxide buffer layer and 40 nm SPR active gold layer and as follows from Fig. 2, it exhibits dependence of transmitted light on the refractive index typical for conventional SPR structures in polarization contrast (Homola and Yee, 1998); the polarization change is small for refractive indices below the resonance and increases with the refractive index of sample. The second multilayer (Spot type II) consisting of 14 nm chromium layer, 100 nm aluminum oxide buffer layer, and 40 nm SPR-active gold layer employs a thicker chromium layer that acts as a TE–TM phase retarder altering the light polarization and thus increasing intensity of transmitted light in the lower refractive index region. An additional phase shift induced by the SPR decreases the total polarization change and the intensity measured in the polarization contrast system drops. An aluminum oxide buffer layer is used to separate the highly absorbing chromium film from the SPR-active gold layer to reduce the surface plasmon attenuation.

Fig. 2 shows the theoretical dependence of the output light intensity in the polarization contrast mode for the two sensing Spot types I and II as a function of refractive index at the surface. The output light intensity for chip area without any layers is shown for comparison. As follows from Fig. 2, within the expected operating refractive index range of the sensor (1.33–1.37), the intensity of light associated with the Spot type I increases with the refractive index, while the intensity of light associated with the Spot type II decreases with the refractive index. The ratio of these intensities increases with the refractive index and is more sensitive to refractive index than the intensities themselves. In addition, the ratio of light intensities is independent of the intensity of illumination and thus can be used to suppress adverse effects of light source fluctuations on the SPR imaging measurements.

3. Experimental

3.1. Sensor system

A laboratory prototype of the SPR imaging sensor was constructed using a diode laser (SDL-7501-G1, SDL, Inc., USA) emitting at the wavelength of 633 nm, a 1024 × 1024 pixel CCD detector (DV–434, Andor Technology, Ireland), an SF2 glass optical prism and a sensor chip matched to the prism via a refractive index matching fluid. SPR active spots were formed on the SF2 glass chips using vacuum evaporation through a micro-fabricated mask. The mask was cut by a high-power laser into a 200 μm thick stainless steel foil with precision of 20 μm (Micronics Inc., USA). The chips support 216 sensing spots (dimensions: 400 μm × 800 μm) providing a total of 108 sensing channels. The chip was interfaced with a flow-cell consisting of an acrylic manifold and a thin Mylar gasket with holes forming chambers confining liquid samples in 10 columns of sensing channels (the first and last columns contained six pairs of sensing spots each, the eight central columns contained 12 pairs of sensing spots each). The flow-cell can be used repeatedly—used Mylar gaskets are removed, the acrylic manifold is cleaned with sodium hydroxide solution and new Mylar gaskets are attached to the manifold. Each flow-cell chamber was 2.2 mm wide and 12 mm long. The depth of the flow-cell chamber was 70 μm (50 μm thick Mylar sheet plus 20 μm thick adhesive layer). The flow-cell geometry and flow rate were selected based on the theoretical analysis of diffusion limits of molecular binding based on a two-compartment mass transport model (Myszka et al., 1998). For a flow rate of 50 μl/min, the time necessary for the liquid sample to pass one measuring spot is about 0.25 s which together with the diffusion coefficient for the investigated biomolecule (human chorionadotropin, hCG) translated to the transfer coefficient of about 10^{-5} ms^{-1}. Under these conditions, the binding kinetics is reaction-limited unless the association rate constant exceeds 2×10^{-5} M^{-1} s^{-1} which is not the case for the hCG antigen/antibody pair used in this work as a model system. A peristaltic pump Reglo (Ismatec SA., Switzerland) was used for sample injection.

Fig. 3a shows a typical image of the array of sensing spots obtained in the polarization contrast mode. As expected, sensing spots produce a high intensity signal while the uncoated areas produce very weak background signal. Although the observed sensing spots are of approximately the same dimensions and regularly distributed, a permanent mapping of sensing spots on the CCD detector pixels makes the system

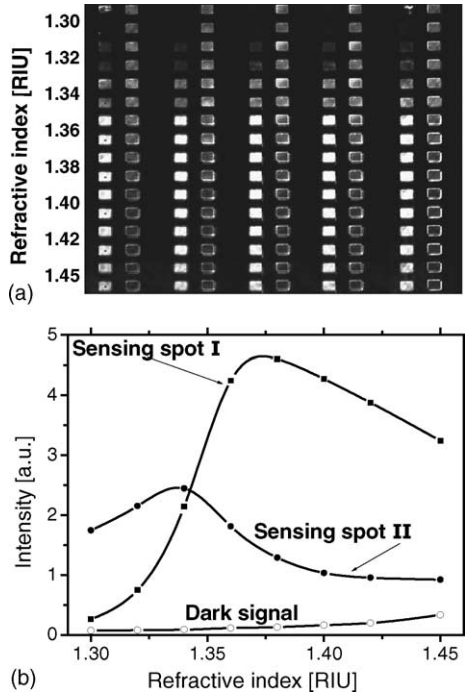

Fig. 3. Dependence of light intensity on the sample refractive index. (a) Image of the SPR sensing chip for rows of sensing spots exposed to different refractive indices; (b) resulting calibration curves for two different types of sensing spots.

rather susceptible to small errors in system alignment and chip to chip variability. Therefore, we developed a computer routine for automatic mapping of the sensing spots. This routine uses one spot with operator-defined borders as a mask and calculates the correlation of this spot with the whole image. The correlation image shows sharp peaks reaching maxima in locations where the mask overlaps precisely with another sensing spot. The coordinates of the CCD pixels of maximum correlation are recorded and the areas of the CCD used for intensity averaging for each sensing spot are defined around these locations. This method allows selecting zones of signal readout identically for all measuring spots, and for measurements on different SPR chips. In the performed experiments, detected light intensity was averaged across the central part of each measuring spot (typically 250 CCD pixels per channel). Transmitted light intensity was normalized in pairs of measuring channels and calibrated using experimental refractometric calibration data. The automated channel mapping based on the auto-correlated image analysis was found to be a fast, reproducible and robust technique independent of illumination fluctuations across different sensing spots. Unlike other object recognition approaches, this approach is also insensitive to parasitic bright features in the image originating from imaging imperfections and chip surface defects.

Control experiments were performed using a dual-channel sensor based on spectroscopy of surface plasmons (Plasmon II) (Homola et al., 2002). In the Plasmon II system, a collimated beam of polychromatic light is used to excite surface plasmons via the attenuated total reflection in a prism coupler. The light reflected from two separate areas of the SPR-active surface is coupled into a dual-channel spectrograph and spectral position of SPR dip in each channel is measured. The Plasmon II instrument provides a refractive index change as low as 10^{-7} RIU. The flow-cell concept used in Plasmon II is the same as that used in the imaging system described in earlier in this Section. It consists of an acrylic manifold and a Mylar gasket forming two flow chambers, each 3 mm wide and 10 mm long. The depth of the flow-cell determined by the thickness of the Mylar gasket was also 70 μm, thereby providing similar hydrodynamic conditions for the interaction between free biomolecules in solution and their biospecific partner immobilized on sensor surface as the flow-cell used in the SPR imaging system.

3.2. Reagents

Solutions were prepared in phosphate-buffered physiological saline (PBS, 10 mM phosphate buffer, 137 mM NaCl, 2.9 mM KCl, pH 7.4 at 20 °C). Bovine serum albumin (BSA) was purchased from Sigma-Aldrich, USA. The C_{11}-mercapto-1-undecanol (C_{11}OH) and C_{16}-mercaptohexadecanoic acid (C_{16}COOH) and the *N*,*N*,*N*′,*N*′-tetramethyl-*O*-(*N*-succinimidyl)uronium tetrafluoroborate (TSTU) used for activation of the COOH groups were purchased from Sigma-Aldrich, USA. Monoclonal affinity-purified antibody against human choriogonadotropin (a-hCG) was purchased from Seva Immuno Ltd., Czech Republic. Human choriogonadotropin was obtained from Calbiochem, USA. Prior SPR biosensing experiments, antibody activity was confirmed by ELISA.

3.3. Preparation of biomolecular coatings

To prepare SPR chips for attachment of antibodies, the chips were soaked in Piranha solution (1:3 mixture of 30% hydrogen peroxide and sulfuric acid) for 3 min, then washed with deionized water and dried with nitrogen stream. A 7:3 mixture of C_{11}OH and C_{16}COOH alkanethiols was dissolved in absolute ethanol with a total thiol concentration of 1 mM. The C_{16}COOH was used to anchor an antibody; C_{11}OH alkanethiol was used to form a stable non-fouling background. Sensor chips were immersed in thiol solution and stored in a dark place at room temperature for 12 h. Then, the chips were rinsed with ethanol, dried with nitrogen, rinsed with water and dried with nitrogen again. The carboxylic terminal groups on the sensor surface were activated by TSTU dissolved in dimethylformamide with concentration of 1 mg/ml for 4 h (Wilchek et al., 1994). After activation, the chips were rinsed with water, dried with nitrogen and mounted into SPR instrument. Immobilization of a-hCG on activated thiols was performed in situ by flowing PBS solution with 100 μg/ml of a-hCG along the sensor surface for 15 min (flow rate—50 μl/min). One of the sensing channels was covered by a BSA layer using similar procedure to form a refer-

ence surface for monitoring non-specific adsorption (BSA concentration—1 mg/ml).

3.4. SPR imaging sensor-based refractometry and biosensing

To quantify the sensor response to bulk refractive index variations, a series of liquid samples with known refractive indices (Cargille Labs, USA) were sequentially injected in the flow-cell and flowed along the sensor surface while the sensor response was recorded. Each solution was flowed through the flow-cell for 5 min at a flow rate of 50 μl/min. SPR-based detection of human choriogonadotropin consisted of three steps. In the first step, the baseline response was established while solution of BSA in PBS was flowed through the flow-cell. Then, known amounts of hCG were added to the BSA-PBS solution to produce solutions with hCG concentrations 0.5, 1.0, 5.0, and 10 μg/ml and these solutions were injected and flowed through different sensing channels for 15 min. Finally, the sample was replaced with buffer. Measurements were performed at a flow rate of 50 μl/min.

The hCG detection was performed using the SPR imaging system and the reference experiment was carried out using the Plasmon II SPR sensor instrument. As the sensitivity of SPR sensors to surface refractive index changes depends on the operating wavelength, which is different for the two SPR sensor systems, the sensor response needs to be calibrated. To account for difference in surface refractive index sensitivity and potentially unequal binding capacities of the bimolecular coatings used in the two sensing systems, the sensor calibration was established by normalizing the sensor response to its response to the attachment of antibodies.

4. Results and discussion

4.1. Refractometry

The sensor response to refractive index changes is illustrated in Fig. 3. Fig. 3a shows the image of SPR active surface where each row of sensing channels is brought into contact with different liquid sample. The image of the reflected light intensity shows that with increasing refractive index, one of the spots becomes darker while the other becomes brighter. The resulting refractive index calibration curves—shown in Fig. 3b exhibit a good agreement with the simulations presented in Fig. 2. Fig. 4a presents calibration curve determined as a ratio of intensities associated with the two different types of sensing spots. Using this calibration curve, the average sensitivity of the ratio of intensities to refractive index was determined to be 65 RIU^{-1}. Fig. 4b shows results of refractometric experiments performed simultaneously in five sensing channels. These data show close agreement between the responses of different channels and suggest that the channel-to-channel response variability is less than 4% of the average sensor response. Analysis of the baseline noise was also performed and it was determined that a typical standard deviation of noise in the intensity ratio is between 2×10^{-4} and 3×10^{-4} which in terms of refractive index resolution translates to about 3–5 $\times 10^{-6}$ RIU. The individual noise of SPR signal for sensing Spot types I and II was divided by the respective experimental sensitivity to refractive index changes yielding the refractive index resolutions 1.2×10^{-5} and 3×10^{-5} RIU for Spot types I and II, respectively. Clearly, the noise of the ratio of the intensities in Spot types I and II is smaller by a factor of 5 than the noise of individual intensities which justifies the proposed pairing of the sensing spots. This observed improvement is mainly due to the fact that besides the photoelectron statistics (shot noise) (Nenninger et al., 2002), major sources of noise in this SPR imaging system are laser emission fluctuations and mechanical vibrations which are highly correlated across the whole image and therefore their contribution can be minimized by the sensing spot pairing. To confirm this assumption, we investigated noise correlation coefficient between sensing Spot types I and II and found about 90% correlation.

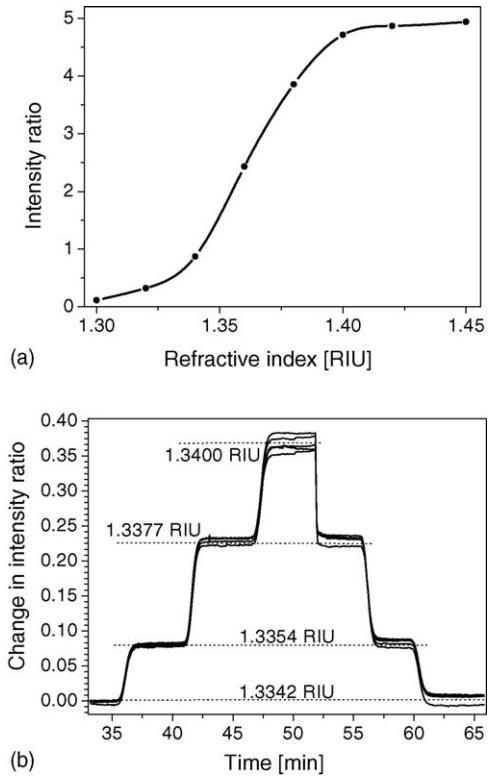

Fig. 4. (a) Calibration curve of SPR imaging refractometric sensor and (b) sensor response to changes in the refractive index observed simultaneously in five sensing channels.

Further noise reduction and resolution improvement could be achieved through reduction of detector noise. This can be achieved by increasing averaging either from a larger surface area (requires lowering the number of sensing channels or using CCD detectors with a larger number of pixels) or by sequential acquisition of several CCD images.

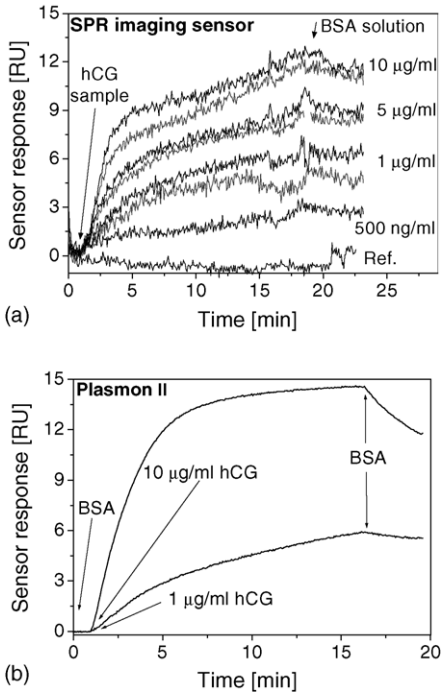

Fig. 5. Detection of different concentrations of hCG using (a) SPR imaging system and (b) dual-channel sensor based on spectroscopy of surface plasmon (Plasmon II).

4.2. Biosensing

The response of the developed SPR imaging sensor to different concentrations of hCG is shown in Fig. 5a. When the hCG solution is injected into the sensor flow-cell, fast increase in the normalized signal occurs. This increase is associated with the specific binding of hCG to a-hCG molecules at the sensor surface. After switching back to the BSA solution, the signal drops slightly and levels off at a lower level. The difference between this new level and initial baseline is associated with the amount of bound hCG. For high hCG concentrations, the initial fast binding is followed with a slower binding. This behavior has been observed with this particular biomolecular pair and may be associated with behavior beyond the pseudo-first order reaction model (e.g. rebinding) or with the non-specific binding of the hCG to an almost saturated surface. However, as the hCG–ahCG pair is only used as a model system illustrating ability of the imaging system to observe biomolecular interactions, a detailed analysis of the observed interaction is beyond the scope of this work. Specific sensor responses observed 15 min after the injection of hCG, were determined to be 3.2, 5.5, 9.1, and 11.2 relative units (RU) for hCG concentrations 500, 1, 5 and 10 μg/ml, respectively. Basically no response was observed in the reference channel, where hCG was flowed at a concentration of 1 μg/ml. The response of the Plasmon II and the SPR imaging sensor were recalibrated to identical relative units by normalizing the hCG antigen response to the sensor response to a-hCG attachment.

The SPR imaging sensor response agrees well with the response of the dual-channel Plasmon II sensor system in which sensor hCG concentrations of 1 and 10 μg/ml were detected; the discrepancy in sensor responses is less than 15% and can be attributed to variations in the surface concentration of antibodies in different sensing channels and differences in flow conditions.

These experimental results indicate that the SPR imaging sensing device is capable of detecting hCG in concentrations lower than 500 ng/ml. In order to assess sensor response channel-to-channel variability for affinity biosensing applications, we applied the same concentration of hCG (10 μg/ml) to 12 sensing channels and compared their responses. All the responses fell within 8% from the average sensor response. This observed reproducibility is worse by a factor of 2 than that observed for the refractometric measurements. It is likely to be due to variations in the surface concentration of antibodies in different sensing channels and differences in flow conditions in different areas across the chip. The ultimate performance is limited by noise in the sensor response. As follows from comparison of data in Fig. 5a and b, the SPR imaging system exhibits noise, which is larger by a factor of 10 than that of its spectroscopic counterpart. This is mainly due to the fact that the Plasmon II system is based on spectroscopy of surface plasmons and therefore exploits 2 orders of magnitude more measurements to calculate sensor response. The wavelength-modulated Plasmon II system typically employs 200 intensity values (determined for different wavelengths) while the SPR imaging system utilizes two light intensities (corresponding to the two spots with different SPR multilayers).

5. Conclusions

We report a novel surface plasmon resonance sensor with over a hundred sensing channels based on the combination of SPR imaging with polarization contrast and a spatially patterned multilayer SPR structure. This approach provides high-contrast SPR images suitable for automated computer analysis, minimum crosstalk between neighboring sensing channels and inherent compensation for light level fluctuations. We evaluated the SPR imaging sensor for refractometry and determined that the sensor provides a refractive index resolution better than 5×10^{-6} RIU, which presents an improvement by a factor of 5 over conventional intensity measurements. Channel-to-channel variability was determined to be less than 4% of sensor response. In conjunction with monoclonal antibodies against human choriogonadotropin, the sensor was applied to detection of hCG and demonstrated to detect hCG levels below 500 ng/ml.

Acknowledgments

Authors wish to thank Dr. Václav Malina (Institute of Radio Engineering and Electronics, Prague) for deposition

of thin films and to Dr. Jiří Škvor (Seva Immuno, Ltd., Prague) for providing antibodies used in this work. This work was done under support of the Academy of Sciences of the Czech Republic (project K2067107), the Grant Agency of the Czech Republic (contracts 303/03/0249, 203/02/1326 and 102/03/0633) and the European Commission (contract QLK4-CT-2002-02323).

References

Baba, A., Knoll, W., 2003. Electrochemical growth of dendritic conducting polymer networks. Adv. Mater. 15, 1015–1019.

Bassil, N., Maillart, E., Canva, M., Levy, Y., Millot, M.C., Pissard, S., Narwa, W., Goossens, M., 2003. One hundred spots parallel monitoring of DNA interactions by SPR imaging of polymer-functionalized surfaces applied to the detection of cystic fibrosis mutations. Sens. Actuators B 94, 313–323.

Homola, J., Yee, S.S., 1998. Novel polarization control scheme for spectral surface plasmon resonance sensors. Sens. Actuators B 51, 331–339.

Homola, J., Lu, H.B., Yee, S.S., 1999. Dual-channel surface plasmon resonance sensor with spectral discrimination of sensing channels using dielectric overlayer. Electron. Lett. 35, 1105–1106.

Homola, J., Lu, H.B., Nenninger, G.G., Dostálek, J., Yee, S.S., 2001. A novel multichannel surface plasmon resonance biosensor. Sens. Actuators B 76, 403–410.

Homola, J., Dostálek, J., Chen, S.F., Rasooly, A., Jiang, S.Y., Yee, S.S., 2002. Spectral surface plasmon resonance biosensor for detection of staphylococcal enterotoxin B in milk. Int. J. Food Microbiol. 75, 61–69.

Homola, J., 2003. Present and future of surface plasmon resonance biosensors. Anal. Bioanal. Chem. 377, 528–539.

Jordan, C.E., Frutos, A.G., Thiel, A.J., Corn, R.M., 1997. Surface plasmon resonance imaging measurements of DNA hybridization adsorption and streptavidin/DNA multilayer formation at chemically modified gold surfaces. Anal. Chem. 69, 4939–4947.

Löfås, S., Malmqvist, M., Rönnberg, I., Stenberg, E., Liedberg, B., Lundström, I., 1991. Bioanalysis with surface-plasmon resonance. Sens. Actuators B 5, 79–84.

Myszka, D.G., He, X., Dembo, M., Morton, T.A., Goldstein, B., 1998. Extending the range of rate constants available from BIACORE: interpreting mass transport-influenced binding data. Biophys. J. 75, 583–594.

Nelson, B.P., Grimsrud, T.E., Liles, M.R., Goodman, R.M., Corn, R.M., 2001. Surface plasmon resonance imaging measurements of DNA and RNA hybridization adsorption onto DNA microarrays. Anal. Chem. 73, 1–7.

Nenninger, G.G., Clendenning, J.B., Furlong, C.E., Yee, S.S., 1998. Reference-compensated biosensing using a dual-channel surface plasmon resonance sensor system based on a planar lightpipe configuration. Sens. Actuators B 51, 38–45.

Nenninger, G.G., Piliarik, M., Homola, J., 2002. Data analysis for optical sensors based on spectroscopy of surface plasmons. Meas. Sci. Technol. 13, 2038–2046.

Nikitin, P.I., Grigorenko, A.N., Beloglazov, A.A., Valeiko, M.V., Savchuk, A.I., Savchuk, O.A., Steiner, G., Kuhne, C., Huebner, A., Salzer, R., 2000. Surface plasmon resonance interferometry for micro-array biosensing. Sens. Actuators A 85, 189–193.

Piscevic, D., Lawall, R., Veith, M., Liley, M., Okahata, Y., Knoll, W., 1995. Oligonucleotide hybridization observed by surface plasmon optical techniques. Appl. Surf. Sci. 90, 425–436.

Rothenhäusler, B., Knoll, W., 1988. Surface plasmon microscopy. Nature 332, 615–617.

Rich, R.L., Myszka, D.G., 2002. Survey of the year 2001 commercial optical biosensor literature. J. Mol. Recognit. 15, 352–376.

Raether, H., 1988. Surface Plasmons on Smooth and Rough Surfaces and on Gratings. Springer-Verlag, Berlin.

Saleh, B.E., Teich, M.C., 1991. Fundamentals of Photonics. Jon Willey & Sons, Inc., New York.

Somekh, M.G., 2002. Surface plasmon fluorescence microscopy: an analysis. J. Microsc. 206, 120–131.

Steinerg, G., Sablinskas, V., Hübner, A., Kuhne, Ch., Salzer, R., 1999. Surface plasmon resonance imaging of microstructured monolayers. J. Mol. Struct. 509, 265–273.

Shumaker-Parry, J.S., Aebersold, R., Campbell, C.T., 2004. Parallel, quantitative measurement of protein binding to a 120-element double-stranded DNA array in real time using surface plasmon resonance microscopy. Anal. Chem. 76, 2071–2082.

Wegner, G.J., Lee, N.J., Marriott, G., Corn, R.M., 2003. Fabrication of histidine-tagged fusion protein arrays for surface plasmon resonance imaging studies of protein–protein and protein–DNA interactions. Anal. Chem. 75, 4740–4746.

Wilchek, M., Kundsen, K.L., Miron, T., 1994. Improved method for preparing *N*-hydroxysuccinimide ester-containing polymers for affinity chromatography. Bioconjug. Chem. 5, 491–492.

Appendix VI

M. Piliarik, H. Vaisocherová and J. Homola:

Towards parallelized surface plasmon resonance sensor platform for sensitive detection of oligonucleotides

Sensors & Actuators, (2006), in press

Available online at www.sciencedirect.com
ScienceDirect
Sensors and Actuators B xxx (2006) xxx–xxx
SENSORS AND ACTUATORS B CHEMICAL
www.elsevier.com/locate/snb

Towards parallelized surface plasmon resonance sensor platform for sensitive detection of oligonucleotides

Marek Piliarik, Hana Vaisocherová, Jiří Homola *

Institute of Radio Engineering and Electronics, Academy of Sciences of the Czech Republic, Chaberská 57, 182 51 Prague, Czech Republic

Abstract

We report a new multichannel biosensor combining an optical platform based on surface plasmon resonance (SPR) imaging on special multilayers and polarization contrast with a spatially-resolved functionalization. We demonstrate that the optical platform offers a considerably higher sensitivity and resolution than the conventional SPR imaging. The spatially-resolved functionalization based on microspotting applied to immobilization of short oligonucleotides is shown to provide a surface concentration of oligonucleotide probes higher by 80% than the flow-through functionalization method. The sensor can perform 64 independent measurements simultaneously and its limit of detection (LOD) for 23-mer oligonucleotides was demonstrated to be as low as 100 pM.

Keywords: Surface plasmon resonance; Biosensors; Oligonucleotide; Hybridization; DNA chip; SPR imaging

1. Introduction

Monitoring of biomolecular interaction in microarray formats has been increasingly applied in molecular biology, medical research and diagnostics, drug development and food safety. A wide range of molecular interactions were utilized in microarrays, including DNA–DNA, protein–protein, protein–DNA, protein–peptide or antigen–antibody interactions. Conventional methods for readout of microarrays typically require fluorescent or other labeling which increases the assay time and costs, and can disturb the binding interaction leading to false negatives [1]. Moreover, fluorescent compounds are invariably hydrophobic, which can produce a background signal leading to false positives [2]. In order to overcome these limitations, label-free measurement technologies have been researched worldwide. Optical biosensors based on surface plasmon resonance (SPR) present an emerging platform for label-free monitoring of biomolecular interactions [3]. In the last decade, several approaches to the development of high-throughput SPR sensors have been proposed. They are based either on SPR imaging [4,5], SPR imaging in the polarization contrast [6] or spectroscopy of surface plasmons on an array of diffraction gratings [7]. The SPR imaging sensors were demonstrated to detect short oligonucleotides in concentrations as low as 10 nM [8].

In this paper, we combine a novel SPR biosensor platform based on highly sensitive SPR imaging on special spatially patterned multilayers and polarization contrast with a spatially-resolved functionalization based on microspotting technique to provide a platform for parallelized detection of oligonucleotides.

2. SPR platform for parallelized measurements

The optical platform used herein is based on the SPR imaging of special multilayers in polarization contrast [6]. In this approach, a light wave is made incident on a dielectric substrate supporting two types of special metal-dielectric multilayers (Spots type I and II) (Fig. 1). A monochromatic light (wavelength, 635 nm) polarized with a plane of polarization, oriented at 45° with respect to the plane of incidence, is made incident through a dielectric substrate on the boundary supporting metal-dielectric multilayers (Fig. 1). The light incident on the bare dielectric-sample interface undergoes total reflection and is reflected as an elliptically polarized wave. The light incident on the multilayers couples with the surface plasmons at the interface between the gold layer and dielectric sample, which alters both the intensity and polarization of the reflected light wave. Polarization of light reflected from the bare surface is turned into linear by means of a quarter-wave plate with the

* Corresponding author. Tel.: +420 2 66773448; fax: +420 2 84680222.
E-mail address: homola@ure.cas.cz (J. Homola).

0925-4005/$ – see front matter © 2006 Elsevier B.V. All rights reserved.
doi:10.1016/j.snb.2006.09.009

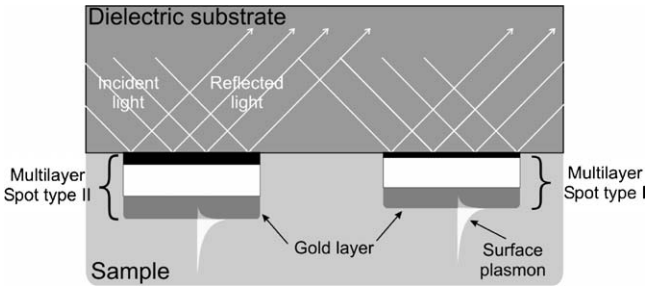

Fig. 1. Scheme of the SPR imaging sensor surface with surface plasmon on two types of metal-dielectric multilayers.

polarization axis oriented at 45° with respect to the plane of incidence and the resulting light wave is extinguished by an output polarizer (polarizer at the angle of 168° with respect to the plane of incidence). The light reflected from the multilayers earns a phase shift from the quarter-wave plate and passes through the output polarizer. The multilayer structures are designed in such a way that the intensity of light associated with the Spot type I increases with the refractive index of sample, while the intensity of light associated with the Spot type II decreases. Therefore, if the sensor response is defined as a ratio of the intensities of light reflected from the Spots type I and II, the sensitivity is higher than the sensitivity for each individual spot. In addition, this approach allows eliminating the effect of light level fluctuations on the sensor output as the ratio of the intensities is insensitive to fluctuations of light occurring in both the areas. The multilayers need to be optimized in terms of sensitivity to refractive index and complexity/feasibility of fabrication. Based on the results of our recent optimization study, we designed a new system of multilayers consisting of 3 nm titanium film, 200 nm aluminum oxide and 40 nm gold layer (Spot type I) and 12 nm titanium film, 200 nm aluminum oxide and 40 nm gold layer (Spot type II). Simulated intensity of transmitted light for both the types of multilayers and the ratio of the two intensities is shown in Fig. 2. The simulations suggest that the dependences of the intensity on the refractive index for the two respective spot types intersect close to their maximum slopes (the maximum slopes occur at 1.338 RIU for Spot Type I and at 1.332 RIU for Spot type II). Therefore, the interval of maximum slopes of individual intensities is associated with the optimum sensor performance and corresponds to the normalized signal close to 1.

The sensor sensitivity to bulk refractive index across the operating range of 1.328–1.34 is depicted in Fig. 3. The sensitivity is compared to the sensitivity of the previously reported design [6] and to the sensitivity of TM reflectivity used in the conventional SPR imaging. Sensitivities of sensors based on the polarization contrast and metal-dielectric multilayers were calculated with the angle of incidence of 61° so that the normalized signal of one (optimum sensor operation) is associated with the refractive index of 1.332 RIU. The sensitivity of the conventional SPR imaging was calculated assuming the angle of incidence of 60.2°, at which the reflectivity equal to 1/3 corresponds to the refractive index of 1.332 RIU. As shown in [9], reflectivity equal to 1/3 yields the maximum slope of reflectivity and subsequently the highest sensitivity (gold layer thickness, 53 nm). As follows from Fig. 3, the sensitivity reported increases with the refractive index. This increase in the sensitivity is approximately proportional to the increase in the normalized signal. For the normalized signal equal to 1, the sensor exhibits sensitivity of 210 RIU^{-1} which exceeds the sensitivity of the previous SPR sensor with polarization contrast [6] by a factor of 2.5 (at 1.332 RIU) and the sensitivity of the conventional SPR imaging by a factor of 6. There are two contributions to the six-fold increase in sensitivity: (i) the use of opposite slopes improve sensitivity of the ratio by a factor of 2 and (ii) the sensitivity scales with the increase of normalized signal by a factor of 3.

In SPR biosensors, the refractive index changes are induced in a very close proximity of the sensor surface. Therefore, the surface sensitivity is typically used to characterize the sensor response to the refractive index or thickness changes within a thin dielectric layer at the sensor surface. The surface sensitivity S_S is defined as a change in the sensor response due to a

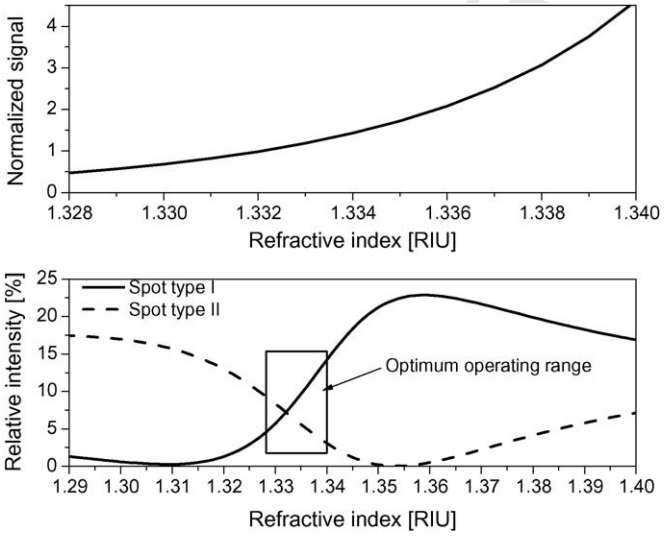

Fig. 2. Dependence of light intensity on the refractive index of sample for two different types of sensing spots (lower plot) and their ratio (upper plot).

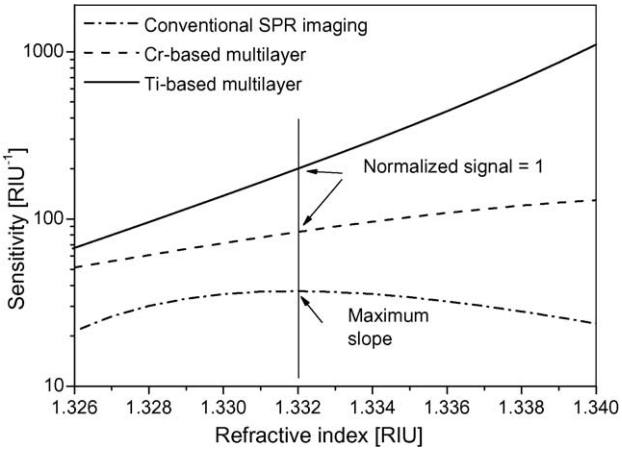

Fig. 3. Sensor sensitivity as a function of refractive index for three SPR sensing platforms: (1) conventional SPR imaging; (2) SPR imaging sensor with polarization contrast and chromium-based multilayers; and (3) optimized SPR imaging sensor with polarization contrast and titanium-based multilayers.

Please cite this article as: Marek Piliarik et al., Towards parallelized surface plasmon resonance sensor platform for sensitive detection of oligonucleotides, Sensors and Actuators B (2006), doi:10.1016/j.snb.2006.09.009

unit change of refractive index within a dielectric layer of a unit thickness. It can be shown that at a fixed wavelength, the surface sensitivity of an SPR sensor is proportional to the bulk refractive index sensitivity [10]. The sensor response to the change of surface refractive index was calculated using the Fresnel equations yielding $S_S = 2.2\,\mathrm{nm}^{-1}\,\mathrm{RIU}^{-1}$ at the normalized signal equal to 1. The change of the sensor response can be translated to the surface coverage of immobilized molecules using the Feijter's formula [11]. For the reported SPR sensor, this formula can be written as

$$\Delta\Gamma = \frac{\Delta R}{S_s(\partial n/\partial c)M_W}, \quad (1)$$

where Γ is the surface coverage expressed in molecules per unit area, ΔR is the change of normalized sensor signal due to the binding, M_W is the molecular weight of adsorbed molecules and the term $\partial n/\partial c$ is the bulk refractive index increment of analyte. In this work, the refractive index increment for streptavidin and oligonucleotides was assumed to be $0.18\,\mathrm{cm}^3/\mathrm{g}$ [12].

The sensor consisted of a light source, SPR coupling optics and two-dimensional detector array. A collimated laser light (wavelength, 635 nm, SDL Inc., USA) passed through polarizer and was totally reflected from the SPR coupling prism made from SF2 glass. The reflected light traveled through a quarter-wave plate and a polarizer and was projected onto a CCD camera (Andor Technology, Ireland) by means of telecentric imaging optics (Fig. 4). A pattern of alternating sensing Spots type I and II was prepared on a glass sensor chip that was optically matched to the coupling prism. Prior to the deposition of thin films using the electron beam evaporation in vacuum, the chips were cleaned in a UV ozone cleaner (Jelight Company Inc., USA). Sensing spots (800 μm × 400 μm) were defined during the evaporation using a mask from a 200 μm thick stainless steel foil (Micronics Inc., USA). Spot type I structure consisted of 3 nm titanium layer, 200 nm aluminum oxide and 40 nm gold layer; Spot type II structure consisted of 12 nm titanium layer, 200 nm aluminum oxide and 40 nm gold layer. The digital image acquired from the CCD camera every 3–6 s displayed regular matrix of bright sensing spots on a dark background. Experimental results reported below were measured simultaneously in 64 sensing channels (normalized signals were calculated from 128 sensing spots). The flow-cell was attached to the sensor surface to contain a liquid sample during the experiments. The sensor surface contained eight separate flow-chambers, each with a volume of 2 μl.

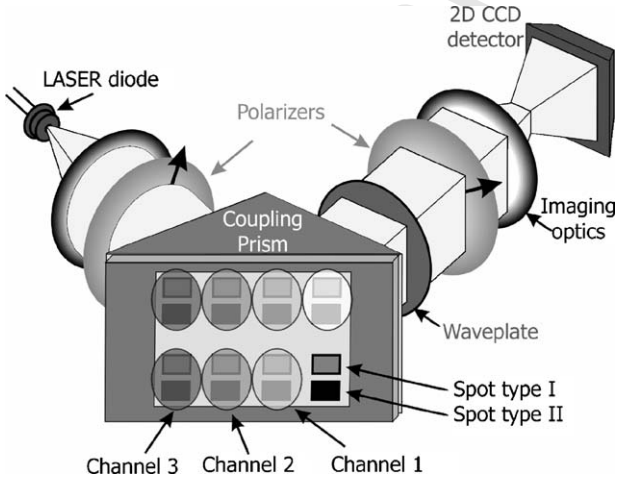

Fig. 4. Scheme of the SPR imaging setup with polarization contrast and special multilayers.

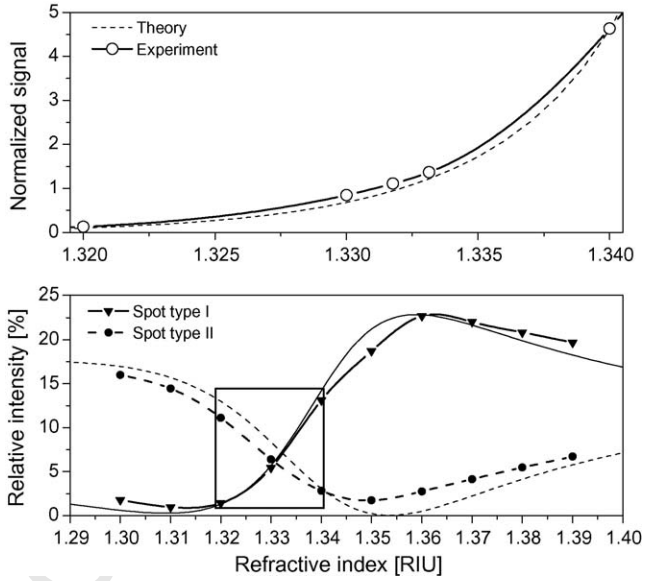

Fig. 5. Sensor refractive index calibration. Relative intensities reflected from Spots type I and II measured for 10 different refractive indices (lower plot) and the normalized signal as their ratio (upper plot). Simulated data shown for comparison.

In order to demonstrate the increased sensitivity of the optimized sensing structure, a model refractometric experiment was performed using liquid samples with different refractive indices (Cargille Labs, USA). Measured intensities from the two types of sensing spots and their ratio are depicted in Fig. 5. The experimentally determined sensitivity of the normalized sensor response to refractive index was found to differ from the theoretical estimate by less 10%. In order to maximize the signal to noise ratio of measured intensities, the utilized CCD detector was operated close to the saturation (the maximum resolvable intensity). Under these conditions, noise of the measured intensity is directly proportional to the square root of the intensity. This assumption allows calculating the standard deviation of the normalized signal (the ratio of intensities of Spots type I and II) that together with the sensor sensitivity determine the sensor resolutions. It can be shown that changes in the normalized signal from 0.5 to 1 and from 1 to 4.5 (within the operating range of the sensor) are accompanied with an increase of noise by a factor of 1.6 and 7.4, respectively. The same changes of normalized signal correspond to an increase in sensitivity by a factor of 2 and 5.5, respectively. Detailed analysis then indicate that the sensor resolution varies across the whole operating range (refractive indices between 1.328 RIU and 1.34 RIU) by less than 25%. This conclusion was confirmed experimentally and an average noise of the sensor response was determined to be $(4.5 \pm 1) \times 10^{-4}$. This value translates to a refractive index resolution of $(2 \pm 0.5) \times 10^{-6}$ RIU.

Please cite this article as: Marek Piliarik et al., Towards parallelized surface plasmon resonance sensor platform for sensitive detection of oligonucleotides, Sensors and Actuators B (2006), doi:10.1016/j.snb.2006.09.009

3. Spatially-resolved functionalization

The spatially-resolved functionalization of SPR chips was performed using the method combining the microspotting technique and the biotin–streptavidin coupling chemistry. In this method, streptavidin was covalently attached to an alkanethiolate self-assembled monolayer and then the biotinylated oligonucleotides were coupled to streptavidin [13,14]. A 3:1 mixture of $C_{11}(EG)_2$ and $C_{16}COOH$ alkanethiols was dissolved in absolute ethanol with a total thiol concentration of 1 mM ($C_{11}(EG)_2$ and $C_{16}COOH$ alkanethiols were from Prochimia, Poland and Sigma–Aldrich, USA, respectively). The $C_{16}COOH$ was used for the attachment of streptavidin, while $C_{11}(EG)_2$ alkanethiols were used to form a stable non-fouling background. Sensor chips were immersed in thiol solution, heated to 40 °C for 15 min and then stored in a dark place at a room temperature for 12 h. Then, the chips were rinsed with ethanol, dried with nitrogen, rinsed with deionized water and dried with nitrogen again. The carboxylic terminal groups on the sensor surface were activated for 2 h in *N*,*N*,*N*′,*N*′-tetramethyl-*O*-(*N*-succinimidyl)uronium tetrafluoroborate (TSTU, purchased from Sigma–Aldrich, USA) dissolved in dimethylformamide with a concentration of 2 mg/ml [15].

The sensing areas of the chips were coated with streptavidin (purchased from Sigma–Aldrich, USA) which was dissolved in 10 mM sodium acetate (SA) buffer (pH 5.0 at 20 °C) and microspotted onto individual sensing channels. Volume of 300 nl was found to form a droplet with diameter of 1.3 ± 0.2 mm on the SPR chip surface and thus cover a pair of neighboring sensing spots. Reproducibility of the volume of the droplets formed using this method was estimated using analytical balance (Mettler-Toledo, USA) to about 92%. The streptavidin was allowed to bind to the alkanethiol monolayer for 60 min and then the SPR chips were functionalized with different oligonucleotide probes in such a way that each pair of measuring spots was coated with one type of probe. The model deoxyribooligonucleotide probes used in this work included (i) biotin-$(TEG)_2$-5′-d(CAG TGT GGA AAA TCT CTA GCA GT)-3′ (=BdO_{23}); (ii) biotin-$(TEG)_2$-5′-T_{23}-3′ (=BdT_{23}); (iii) biotin-$(TEG)_2$-5′-A_{23}-3′ (=BdA_{23}) and their complementary targets with the following sequences (i) 5′-d(ACT GCT AGA GAT TTT CCA CAC TG)-3′ (=CdO_{23}); (ii) 5′-d(A_{23})-3′ (=dA_{23}); and (iii) 5′-d(T_{23})-3′ (=dT_{23}), (deoxyribooligonucleotides were purchased from Masaryk University, Czech Republic). The biotinylated oligonucleotide probes in 10 mM phosphate buffer containing 15 mM $MgCl_2$ (PBM, pH 7.4 at 20 °C) were microspotted on the top of the streptavidin spots and incubated for 120 min. The concentrations of streptavidin and oligonucleotide solutions used in microspotting were calculated in such a way that each droplet of streptavidin solution contained enough streptavidin to form two complete monolayers (0.3 μM) and each droplet of oligonucleotide solution contained 1.5 oligonucleotides per each binding pocket of streptavidin (2 μM) [16]. The surface drying during the microspotting process was carefully avoided as drying of the functionalized surface can result in a loss of streptavidin reactivity. Therefore, the incubation of the microspotted surface took place in a humidity chamber with saturated vapor pressure.

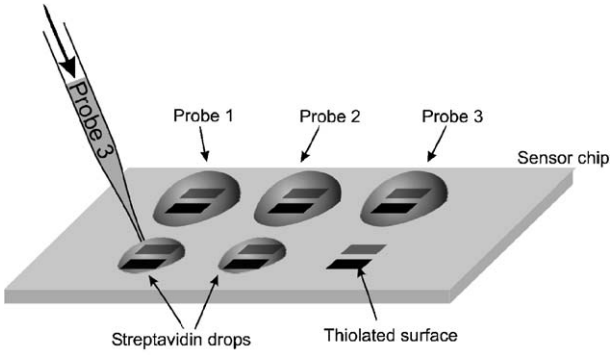

Fig. 6. Concept of functionalization of the multichannel SPR sensor.

After the microspotting, the sensor chips were rinsed with PBM in order to wash off the unreacted probes and streptavidin and then stored in PBM at 4 °C (Fig. 6).

In order to allow for comparison of binding properties of the oligonucleotide chips prepared by microspotting with those prepared by conventional flow-through method [15], a series of reference chips were functionalized using the conventional flow-through procedure. In this procedure, the sensor chips were functionalized directly in the SPR sensor system while the response to binding was monitored in situ. First, SA buffer was flowed across the sensor chip with a self-assembled monolayer of mixed alkanethiols prepared using the procedure described earlier in this section. SA buffer containing 50 μg/ml of streptavidin was flowed across the sensor surface for 12 min and then the solution was replaced with an SA buffer. After a short incubation with 10 mM phosphate buffer containing 0.75 M NaCl (pH 7.4 at 20 °C) to remove non-covalently bound streptavidin and deactivate residual carboxylic groups, the sensor surface was flushed with PBM. Then, a 50 nM solution of biotinylated oligonucleotides was flowed across the sensor surface for 12 min. The sensor surface was divided into measuring and reference groups of channels using separate flow-chambers of the flow-cell. Measuring channels were modified with BdO_{23} probes and reference channels were modified with BdT_{23} or BdA_{23} probes. Finally PBM buffer was flowed along the surface to wash off any unbound probes (Fig. 7).

The surface density of streptavidin layer produced using the flow-through method was calculated using Eq. (1) from the sensor response to the streptavidin monolayer saturation as well as from the sensor response after removal of the unbound streptavidin (see Fig. 7a). The corresponding surface concentrations of streptavidin were determined to be 1.9×10^{12} SA/cm^2 and 1.14×10^{12} SA/cm^2, respectively. While the higher concentration is relevant for the optimization of the microspotting of streptavidin, where the saturation has to be reached from a limited volume of the droplet, the lower number provides an estimate of binding pockets available for biotinylated oligonucleotides at the sensor surface. The surface density of immobilized biotinylated oligonucleotides BdO_{23} (Fig. 7b) was estimated to be about 2.2×10^{12} oligonucleotides per cm^2, which corresponds to about two biotinylated oligonucleotides per a molecule of streptavidin.

Please cite this article as: Marek Piliarik et al., Towards parallelized surface plasmon resonance sensor platform for sensitive detection of oligonucleotides, Sensors and Actuators B (2006), doi:10.1016/j.snb.2006.09.009

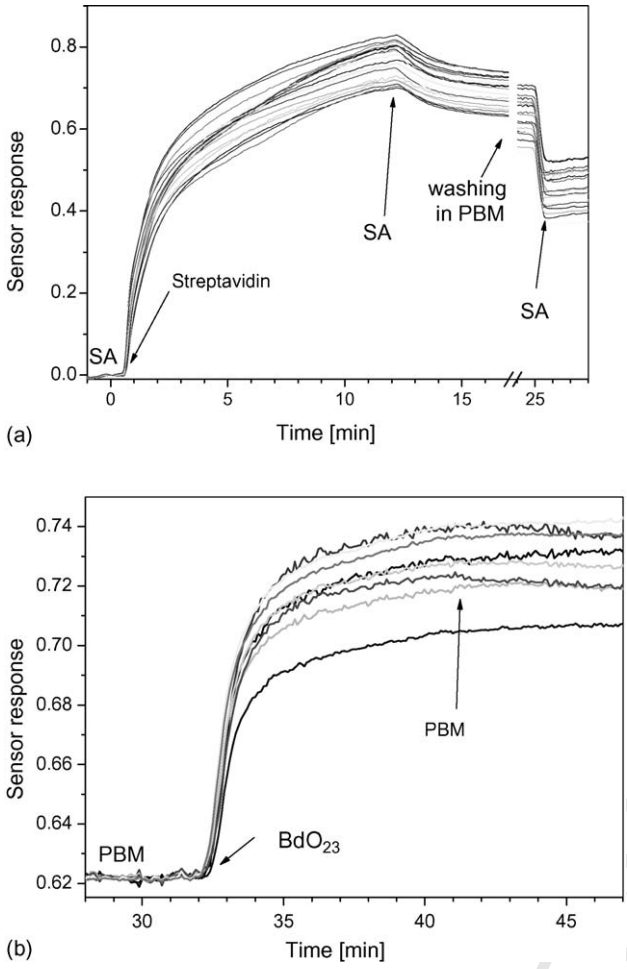

Fig. 7. Typical sensor response to immobilization of (a) streptavidin (measured in 32 channels) and (b) biotinylated oligonucleotides (measured in 8 channels).

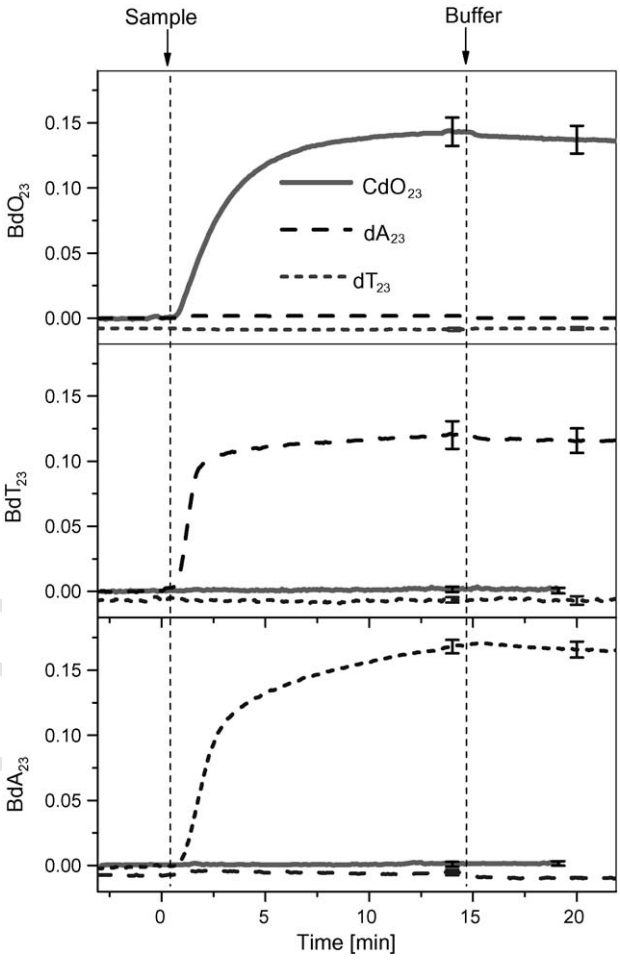

Fig. 8. Detection of three oligonucleotides using an array of complementary probes microspotted on the sensor surface. Probe sequences are given at the vertical axis. Error bars indicate the peak-to-peak variations in the sensor response.

4. Detection of oligonucleotides

In order to determine the cross-talk among the sensing channels and to evaluate potential of the presented approach for parallelized screening of molecular interactions, we performed an experiment in which a solution containing a specific oligonucleotide (concentration, 50 nM) was flowed along the sensor chip with neighboring sensing channels functionalized with complementary oligonucleotides (all present within a single flow-chamber, see Fig. 6). This experiment was carried out using three different solutions; each solution containing only one of oligonucleotides with a sequence complementary to the sequence of one of the immobilized probes. These measurements were performed simultaneously, using different areas of the SPR sensor chip confined in different flow-chambers. Fig. 8 presents response of the sensing channels to different oligonucleotides. Clearly, the sensing channels with probes complementary to the oligonucleotide in solution produced a strong sensor response, while the sensing channels with different oligonucleotides generated no response at all. Each of the hybridization events was measured simultaneously in three or four sensing channels (depending on the layout of sensing spots within each flow-chamber) and the sensor responses were found to fall within ±7% from the average sensor response. This experiment suggests that the presented multichannel SPR platform can be combined with the microspotting functionalization technique to allow for parallelized measurements with no cross-talk among neighboring sensing channels.

In order to assess detection capabilities of the developed sensor platform, detection experiments were performed in which the sensor response to different concentrations of oligonucleotides was measured. In these experiments, sensor chips functionalized with BdO_{23} probes (sensing channels) and BdT_{23} probes (reference channels) were used and samples containing different concentrations of CdO_{23} in PBM buffer were flowed across different flow-chambers of the flow-cell. Typical sensor response to different concentrations of CdO_{23} is shown in Fig. 9. For comparison, the detection experiment was repeated using the SPR sensor chips and functionalized using the flow-through technique (Fig. 10).

As follows from comparison of the sensor responses for the microspotting and flow-through functionalization (Figs. 9 and 10), the equilibrium sensor response at 50 nM concentration obtained using the microspotting functionalization is higher by a factor of about 1.8 than the response obtained on

Please cite this article as: Marek Piliarik et al., Towards parallelized surface plasmon resonance sensor platform for sensitive detection of oligonucleotides, Sensors and Actuators B (2006), doi:10.1016/j.snb.2006.09.009

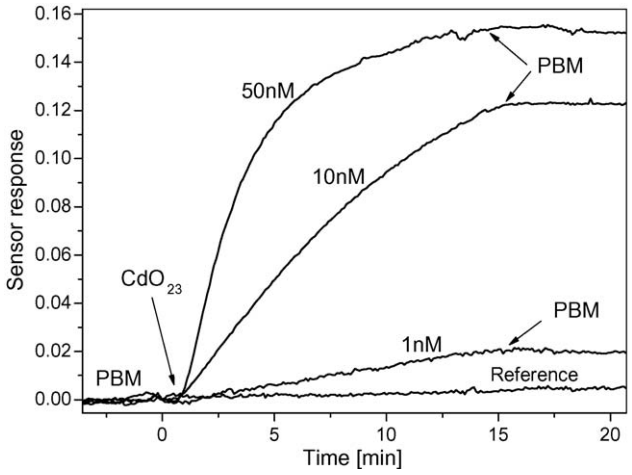

Fig. 9. Detection of oligonucleotides using the multichannel SPR sensor functionalized using the microspotting technique. Temporal sensor response measured for three different concentrations of CdO_{23} oligonucluotide. Response of a reference channel for CdO_{23} concentration of 50 nM shown for comparison.

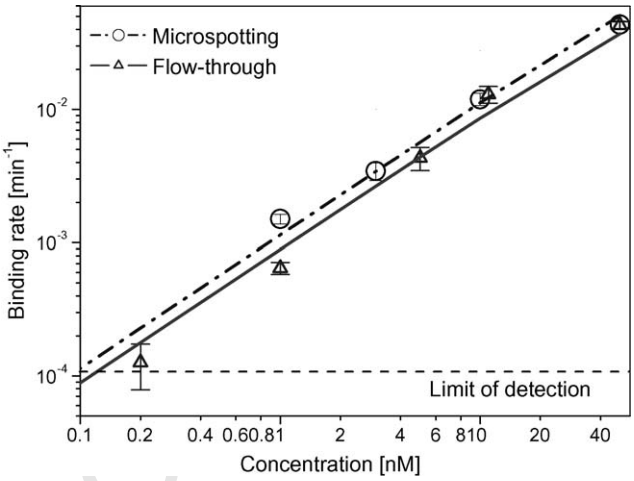

Fig. 11. Calibration curves for the SPR sensor-based detection of CdO_{23} oligonucleotides determined for two method of functionalization (microspotting and flow-through functionalization). Error bars indicate the peak-to-peak interval of measured binding rates.

the sensor chip functionalized using the flow-through technique. This result indicates, that the microspotting procedure yields a surface density of probes higher by 80%, which translates to 4×10^{12} oligonucleotides per cm^2 (this result was calculated using Eq. (1)). The higher surface concentration of probes can be associated with a slower immobilization of probes driven only by the diffusion in the droplet volume and longer incubation times. This result is comparable with the results obtained using SPR chips functionalized under no flow conditions in a cuvette by Su et al. who obtained surface coverage as high as 4.3×10^{12} oligonucleotides per cm^2 [14]. This indicates that when the parameters of the microspotting process are controlled properly, robust functionalization with a high density of probes accessible to target analytes can be achieved. For direct biosensor-based detection of oligonucleotides, it is useful to define the sensor response to analyte as the binding rate of the analyte to the receptors in an initial phase of the binding experiment (see Fig. 9). In this experiment, the binding rates were calculated using a linear regression applied to a portion of the kinetic sensor response fulfilling the criterion that the standard deviation of the fit was smaller than two standard deviations of the baseline noise (for instance, binding rates for 1 nM and 50 nM concentrations were calculated using first 13 min and 1 min of the binding, respectively). The determined binding rates were plotted against the concentration of oligonucleotide (Fig. 11). Clearly, the higher surface concentration of probes was achieved using the microspotting technique results in higher binding rates for all the concentrations of the target oligonucleotides.

As follows from Figs. 9 and 11, the sensor shows a strong response even to oligonucleotide concentrations as low as 1 nM. If we define the limit of detection (LOD) as a concentration of analyte that results in the sensor response equal to three standard deviations of the baseline noise [17], the LOD for this model oligonucleotide system is approximately 100 pM. This detection limit is better by two orders of magnitude than the best detection limits demonstrated using the SPR imaging technology [8] and comparable to best detection limits obtained using high-performance SPR sensors based on spectroscopy of surface plasmons in a small number of sensing channels (<5) [15,18].

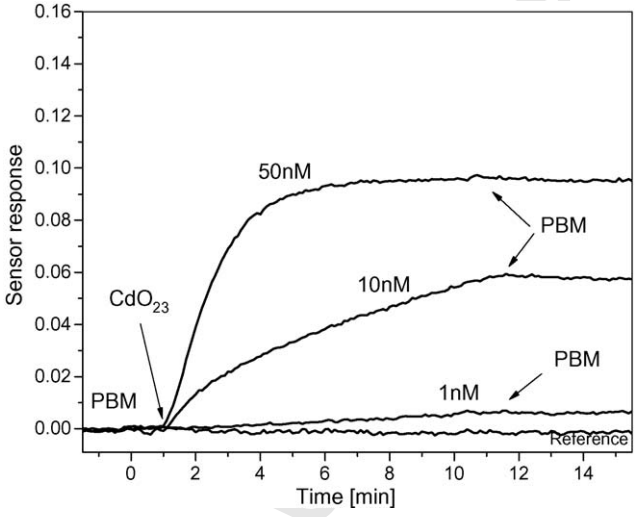

Fig. 10. Detection of oligonucleotides using the multichannel SPR sensor functionalized using the flow-through technique. Temporal sensor response measured for three different concentrations of CdO_{23} oligonucluotide. Response of a reference channel for CdO_{23} concentration of 50 nM shown for comparison.

5. Conclusions

We demonstrate a new multichannel SPR biosensor based on the SPR imaging platform with an array of special multilayers and polarization contrast and the spatially-resolved functionalization based on the microspotting technique. We show that the optical approach presented herein offers considerably higher sensitivity than the competing multichannel SPR sensing platforms such as SPR imaging and allows to measure changes in the refractive index as small as 2×10^{-6} RIU. The optimized microspotting technique employed for the functionalization of the sensor with oligonucleotide probes was found to provide at

Please cite this article as: Marek Piliarik et al., Towards parallelized surface plasmon resonance sensor platform for sensitive detection of oligonucleotides, Sensors and Actuators B (2006), doi:10.1016/j.snb.2006.09.009

least 80% more binding sites than the conventional flow-through functionalization. The limit of detection for model oligonucleotides was demonstrated to be about 100 pM which makes this sensor by far the most sensitive high-throughput SPR platform used for detection of oligonucleotides.

Acknowledgements

This research was supported by Grant Agency of the Czech Republic (202/05/0628) and by the Academy of Sciences of the Czech Republic (AV0Z20670512).

References

[1] J.R. Pollack, C.M. Perou, A.A. Alizadeh, M.B. Eisen, A. Pergamenschikov, C.F. Williams, S.S. Jeffrey, D. Botstein, P.O. Brown, Genome-wide analysis of DNA copy-number changes using cDNA microarrays, Nat. Genet. 23 (1999) 41–46.
[2] M.A. Cooper, Optical biosensors in drug discovery, Nat. Rev. Drug Discov. 1 (2002) 515–528.
[3] J. Homola, Present and future of surface plasmon resonance biosensors, Anal. Bioanal. Chem. 377 (2003) 528–539.
[4] N. Bassil, E. Maillart, M. Canva, Y. Levy, M.C. Millot, S. Pissard, W. Narwa, M. Goossens, One hundred spots parallel monitoring of DNA interactions by SPR imaging of polymer-functionalized surfaces applied to the detection of cystic fibrosis mutations, Sens. Actuators B: Chem. 94 (2003) 313–323.
[5] C.E. Jordan, A.G. Frutos, A.J. Thiel, R.M. Corn, Surface plasmon resonance imaging measurements of DNA hybridization adsorption and streptavidin/DNA multilayer formation at chemically modified gold surfaces, Anal. Chem. 69 (1997) 4939–4947.
[6] M. Piliarik, H. Vaisocherova, J. Homola, A new surface plasmon resonance sensor for high-throughput screening applications, Biosens. Bioelectron. 20 (2005) 2104–2110.
[7] J. Dostalek, J. Homola, M. Miler, Rich information format surface plasmon resonance biosensor based on array of diffraction gratings, Sens. Actuators B: Chem. 107 (2005) 154–161.
[8] B.P. Nelson, T.E. Grimsrud, M.R. Liles, R.M. Goodman, R.M. Corn, Surface plasmon resonance imaging measurements of DNA and RNA hybridization adsorption onto DNA microarrays, Anal. Chem. 73 (2001) 1–7.
[9] E.M. Yeatman, Resolution and sensitivity in surface plasmon microscopy and sensing, Biosens. Bioelectron. 11 (1996) 635–649.
[10] J. Homola, M. Piliarik, in: J. Homola (Ed.), Surface Plasmon Resonance Based Sensors, vol. 4, Springer-Verlag, Berlin, Heidelberg, New York, 2006 (Chapter 2).
[11] J.A. de Feijter, J. Benjamins, F.A. Veer, Ellipsometry as a tool to study the adsorption of synthetic and biopolymers at the air–water interface, Biopolymers 17 (1978) 1759–1772.
[12] T. Tumolo, L. Angnes, M.S. Baptista, Determination of the refractive index increment (d*n*/d*c*) of molecule and macromolecule solutions by surface plasmon resonance, Anal. Biochem. 333 (2004) 273–279.
[13] M. Wilchek, K.L. Knudsen, T. Miron, Improved method for preparing *N*-hydroxysuccinimide ester-containing polymers for affinity-chromatography, Bioconjug. Chem. 5 (1994) 491–492.
[14] X.D. Su, Y.J. Wu, R. Robelek, W. Knoll, Surface plasmon resonance spectroscopy and quartz crystal microbalance study of streptavidin film structure effects on biotinylated DNA assembly and target DNA hybridization, Langmuir 21 (2005) 348–353.
[15] H. Vaisocherova, A. Zitova, M. Lachmanova, J. Stepanek, S. Kralikova, R. Liboska, D. Rejman, I. Rosenberg, J. Homola, Investigating oligonucleotide hybridization at subnanomolar level by surface plasmon resonance biosensor method, Biopolymers 82 (2006) 394–398.
[16] J.S. Shumaker-Parry, C.T. Campbell, Quantitative methods for spatially resolved adsorption/desorption measurements in real time by surface plasmon resonance microscopy, Anal. Chem. 76 (2004) 907–917.
[17] V. Thomsen, D. Schatzlein, D. Mercuro, Limits of detection in spectroscopy, Spectroscopy 18 (2003) 112–114.
[18] B. Persson, K. Stenhag, P. Nilsson, A. Larsson, M. Uhlen, P.A. Nygren, Analysis of oligonucleotide probe affinities using surface plasmon resonance: a means for mutational scanning, Anal. Biochem. 246 (1997) 34–44.

Biographies

Marek Piliarik (MS 2000) is a doctoral student of the Faculty of Mathematics and Physics in Charles University in Prague (Czech Republic) and carries out his PhD research at the Institute of Radio Engineering and Electronics, Prague (Czech Republic). His research interests are in development of optical platforms for biosensors and data processing.

Hana Vaisocherová (MS 2001) is a doctoral student of the Faculty of Mathematics and Physics in Charles University in Prague (Czech Republic) and a research assistant at the Institute of Radio Engineering and Electronics, Prague (Czech Republic). Her research interests are in study of biomolecular interactions by SPR biosensors and in surface chemistry development.

Jiří Homola (MS 1988, PhD 1993) is head of Photonics Division and chairman of Department of Optical Sensors at the Institute of Radio Engineering and Electronics, Prague (Czech Republic) and affiliate associate professor at the University of Washington, Seattle (USA). His research interests are in photonics and biophotonics with emphasis on optical sensors and biosensors. He is a member of Editorial Boards of *Sensors and Actuators B* and *Biosensors and Bioelectronics* and senior member of IEEE.

Please cite this article as: Marek Piliarik et al., Towards parallelized surface plasmon resonance sensor platform for sensitive detection of oligonucleotides, Sensors and Actuators B (2006), doi:10.1016/j.snb.2006.09.009

Appendix VII

H. Vaisocherová, K. Mrkvová, M. Piliarik, P. Jinoch, M. Šteinbachová and J. Homola:

Surface plasmon resonance biosensor for direct detection of antibody against Epstein-Barr virus

Biosensors & Bioelectronics, (2006), in press

Available online at www.sciencedirect.com
SCIENCE DIRECT®
Biosensors and Bioelectronics xxx (2006) xxx–xxx
BIOSENSORS & BIOELECTRONICS
www.elsevier.com/locate/bios

Surface plasmon resonance biosensor for direct detection of antibody against Epstein-Barr virus

Hana Vaisocherová [a,b,1], Kateřina Mrkvová [a], Marek Piliarik [a], Pavel Jinoch [c], Marie Šteinbachová [c], Jiří Homola [a,*]

[a] *Institute of Radio Engineering and Electronics, Academy of Sciences of the Czech Republic, Chaberská 57, 182 51 Prague, Czech Republic*
[b] *Charles University, Faculty of Mathematics and Physics, Ke Karlovu 3, 121 16 Prague, Czech Republic*
[c] *VIDIA Ltd., Nad Safinou II/365, 252 42 Jesenice u Prahy, Czech Republic*

Received 17 August 2005; received in revised form 17 April 2006; accepted 25 April 2006

Abstract

This paper describes the direct label-free detection of antibodies against the Epstein-Barr virus (anti-EBNA) using a surface plasmon resonance (SPR) biosensor. The antibody detection was performed using the immunoreaction between anti-EBNA and a respective synthetic peptide (EBNA-1), which was conjugated with bovine serum albumin (BSA–EBNA) and immobilized on the sensor surface. Three immobilization chemistries for the attachment of BSA–EBNA were investigated to optimize ligand density and minimize loss of EBNA-1 immunoreactivity. The developed SPR biosensor functionalized with the optimal immobilization method was calibrated and characterized in terms of detection limit, reproducibility, regenerability and storability. It was demonstrated that the sensor is capable of detecting concentrations of anti-EBNA as low as 0.2 ng/ml (∼1 pM) both in buffer and 1% human serum and can be stored and regenerated for repeated use.

Keywords: Surface plasmon resonance; Biosensor; Direct detection; Epstein-Barr virus

1. Introduction

The Epstein-Barr virus is one of the most common viruses, which attack the immune system of humans. The infection course varies from asymptomatic infection to various diseases such as infectious mononucleosis in countries with the temperate climate, Burkitt's lymphoma in Africa and nasopharyngeal carcinoma in China. The focus of laboratory testing is to distinguish active illness from past infections and negativity. Currently blood of patients is tested for the presence of non-specific hemaglutinins and hemolysins produced by a human body as a response to the virus as well as for the presence of specific immunoglobulins against the Epstein-Barr virus proteins, i.e. early antigen, viral capsid antigen and nuclear antigen (EBNA), especially EBNA-1. Diagnostic tests for the presence of anti-EBNA in human blood serum are performed using indirect two-step immunoassays with enzymatic, radio or fluorescent labeling (Gomara et al., 2000). The use of labeled secondary ligands contributes to assay time and costs. Antigens required to bind host antibodies are prepared either from infected cells or as recombinant proteins. An attractive alternative are synthetic peptides that mimic specific immunoreactive epitopes and reduce non-specific reactions and cross-reactivity of the assays. Moreover, routine and inexpensive peptide synthesis makes them more affordable than the recombinant proteins (Gonzalez et al., 1997).

Direct, label-free biosensors, such as surface plasmon resonance (SPR) biosensors, present an interesting alternative to conventional methods. SPR biosensors measure refractive index changes produced by the binding of analyte to its biospecific partner immobilized on the sensor surface. In the last decades, several SPR sensor platforms have been developed (Shumaker-Parry and Campbell, 2004; Stabler et al., 2004; Piliarik et al., 2005) and applied to detection of biological and chemical substances and study of molecular interactions (Karlsson and Falt, 1997; Goodrich et al., 2004). Various approaches to the immobilization of molecules on the surface of SPR sensor

* Corresponding author. Tel.: +420 266773448; fax: +420 284680222.
E-mail address: homola@ure.cas.cz (J. Homola).
[1] Tel.: +420 221911472; fax: +420 224922797.

0956-5663/$ – see front matter © 2006 Published by Elsevier B.V.
doi:10.1016/j.bios.2006.04.021

(usually gold) have been also developed. These include procedures based on physicochemical interactions such as chemisorptions (Nuzzo and Allara, 1983), covalent binding (Lofas et al., 1995), hydrophobic and electrostatic coupling (Koubova et al., 2001) and non-covalent high-affinity biomolecular linkers such as streptavidin-biotin (Busse et al., 2002) or complementary oligonucleotides (Ladd et al., 2004).

In this work, we report a novel method of detection of anti-EBNA which utilizes a biosensor platform based on surface plasmon resonance and a special synthetic peptide (EBNA-1) as a receptor. Three different immobilization methods based on covalent coupling (Lahiri et al., 1999), electrostatic (Koubova et al., 2001) and hydrophobic interactions are examined for the immobilization of the peptide on the SPR sensor surface. The resulting anti-EBNA biosensor is characterized in terms of detection limit, reproducibility, regenerability and storability. The performance of the biosensor is compared with that of a conventional peptide-based immuno-analytical assay (ELISA).

2. Experimental

2.1. Reagents

Bovine serum albumin (BSA) was purchased from Sigma–Aldrich, USA. The C_{16}-chained alkanethiol (C_{16}-mercaptohexadecanoic acid) and the *N*,*N*,*N*′,*N*′-tetramethyl-*O*-(*N*-succinimidyl)uronium tetrafluoroborate (TSTU) used for the activation of carboxylic terminal groups on C_{16}-alkanethiol were purchased from Sigma–Aldrich, USA. The C_{11}-chained di(ethylene glycol)-terminated alkanethiol was purchased from Prochimia, Poland. Dextran sulfate (DS), *N*,*N*-dimethylformamid (DMF) and glutaraldehyde 50% (GA) were obtained from Sigma–Aldrich, USA. Absolute ethanol was purchased from Merck, Czech Republic. Mouse monoclonal affinity-purified antibodies against human Epstein-Barr virus (anti-EBNA) and against human Herpes virus (anti-HSV), both IgG2b isotype, were obtained from ExBio, Czech Republic.

Synthetic peptides were synthesized using the Merrifield's method of solid phase peptide synthesis (Fields and Noble, 1990) in VIDIA, Czech Republic. The amino acid sequences of EBNA-1 and reference peptide of human cytomegalovirus (CMV) were: (H)-Ala-Gly-Ala-Gly-Gly-Gly-Ala-Gly-Ala-Gly-Ala-Gly-Gly-Gly-Ala-Gly-Gly-Ala-Gly-(NH2) for EBNA-1 and (H)-Lys-Pro-Thr-Leu-Gly-Gly-Lys-Ala-Val-Val-Gly-Arg-Pro-Pro-Ser-Val-Pro-Val-Ser-Gly-(OH) for CMV. BSA–peptide conjugates were prepared in VIDIA, Czech Republic using the protocol described by Coligan et al. (1995) and glutaraldehyde as a cross-linking agent. Solutions of the conjugates for SPR measurements were prepared (I) in phosphate buffer saline (PBS) consisting of 10 mM phosphate buffer, 137 mM NaCl, 2.9 mM KCl, pH 7.4 at 20 °C or (II) in 0.1 M citrate buffer (CB), pH 4.0 at 20 °C or (III) in 10 mM sodium acetate buffer (SA), pH 5.0 at 20 °C, depending on the immobilization chemistry. Solutions of antibodies were prepared in PBS containing bovine serum albumin at a concentration of 5 mg/ml. For experiments involving human blood serum samples, the solutions were mixed with human blood serum to a resulting serum concentration of 1% (v/v).

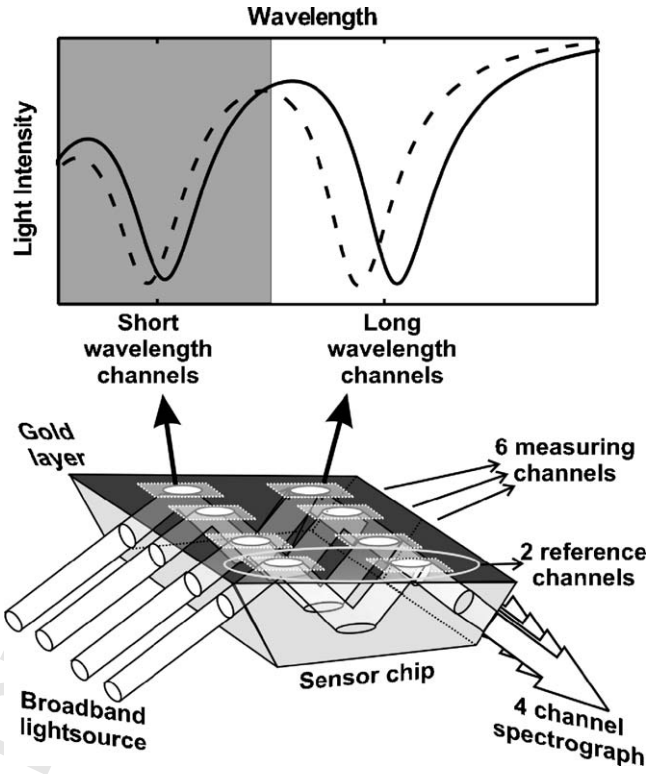

Fig. 1. Scheme of an eight-channel SPR sensor with four parallel light beams and the wavelength division multiplexing of sensing channels (upper picture). Spectrum of transmitted light with two SPR dips before (– – –) and after the binding (—) (lower picture).

Goat-anti-mouse IgG antibodies labeled with horseradish peroxidase were obtained from Southern Biotechnology Associates, USA. A sample of human blood serum was obtained from the University Hospital Motol, Prague; the serum was tested to be negative for anti-EBNA. Polystyrene Nunc-Immuno LockWell™ modules for ELISA tests were purchased from Schoeler-Pharma, Czech Republic.

2.2. SPR sensor

In this research, we used a recently developed SPR sensor platform based on the spectroscopy of surface plasmons (Homola et al., 2001) and wavelength division multiplexing (WDM) (Homola et al., 2002; Dostalek et al., 2005). This sensor combines the wavelength division multiplexing of two serially ordered sensing channels in a special sensing element with four parallel light beams (see Fig. 1) to yield the total of eight sensing channels. Broadband light from a halogen lamp is collimated and polarized, and then introduced into the WDM–SPR sensing element interfaced with a sensor chip made of SF-14 glass coated by an adhesion-promoting titanium film (thickness, 2 nm) and a gold film (thickness, 55 nm). Upon the first incidence on the gold film, each light beam excites a surface plasmon at a certain wavelength (~650 nm). The reflected light is redirected towards the gold film at a different angle of incidence and excites a surface plasmon at a different wavelength (~800 nm). The sequential

excitation of the surface plasmons gives rise to two narrow dips in the spectrum of transmitted light (Fig. 1). The transmitted light is collected into four optical fibers and coupled to a four-channel spectrograph. Acquired spectra are analyzed in real time by a special software that allows tracking the resonant wavelength in each sensing channel (Nenninger et al., 2002). A flow cell with eight separate flow chambers is interfaced with the chip to contain a liquid sample during the experiments. Each flow chamber covers the area, where the surface plasmon is excited—the sensing channel. The flow chambers are designed to provide a laminar flow along the sensor surface. The height of the flow chambers is rather small (50 μm) to facilitate diffusion of the analyte to the surface of the sensor. The volume of each flow chamber is about 1 μl. A peristaltic pump is used to flow liquid samples over each sensing channel at a flow rate of 30 μl/min.

In order to compensate for the non-specific sensor response and thus provide more accurate results, in each binding experiment, two sensing channels (one short-wavelength and one long-wavelength) are coated with a reference peptide (BSA–peptide conjugate). This peptide was derived from CMV and was of the same length and of a similar molecular weight as EBNA-1 and exhibited no immunoreactivity to anti-EBNA. When the analyte (anti-EBNA) is flowed over the sensor surface, the SPR wavelength shift measured in the measuring and reference channels are subtracted to account for temperature fluctuations (causing a drift in the sensor response) and non-specific adsorption of non-target molecules in the sample to sensor surface (see Fig. 1).

The shift in the resonant wavelength shown in Fig. 1 is proportional to the refractive index change at the sensor surface and can be calibrated to the surface concentration of bound molecules. The calibration coefficient interrelating the sensor response and the concentration of analyte is proportional to the molar weight of the molecules (Liedberg et al., 1993) and depends on the resonant wavelength (Dostalek et al., 2005). It was estimated from a theoretical model (Homola, 2006) that a shift in the resonant wavelength of 1 nm corresponds to a change in the surface concentration of BSA of about 10^{-13} mol/cm^2 when measured at the wavelength of 800 nm and 5×10^{-14} mol/cm^2 at the wavelength of 650 nm. All sensorgrams obtained from short-wavelength sensing channels are therefore recalibrated to the operating wavelength of the long-wavelength sensing channels (800 nm).

2.3. Measurement protocols

2.3.1. SPR sensor functionalization

Prior to the functionalization, the sensor chips were cleaned in an UV–ozone cleaner for 15 min, then washed with deionized water and dried with a stream of nitrogen.

2.3.1.1. Peptide immobilization via covalent coupling (CHEM I). A 7:3 mixture of C_{11}-chained and C_{16}-chained alkanethiols was dissolved in degassed absolute ethanol with a total thiol concentration of 1 mM. The C_{16}-alkanethiols terminated with carboxylic head groups were used to anchor BSA–peptide conjugates to the sensor surface via amino coupling; C_{11}-alkanethiols terminated with di(ethylene glycol) groups were used to form a stable non-fouling background. Sensor chips were immersed in a thiol solution at a temperature of 40 °C for 10 min and stored in dark at room temperature for up to 2 days to allow the alkanethiols to form a self-assembled monolayer (SAM). Then, the chips were rinsed with ethanol, dried with nitrogen, rinsed with water and dried with nitrogen again. The carboxylic terminal groups on the sensor surface were transformed into reactive *N*-hydroxysuccinimidyl esters with *N*,*N*,*N*′,*N*′-tetramethyl-*O*-(*N*-succinimidyl)uronium tetrafluoroborate (Knorr et al., 1989; Wester et al., 1996). Sensor chips were immersed in a solution of TSTU in degassed DMF (2 mg/ml), then sonicated for 1 min and shaken for 2 h. The chips were rinsed with water, dried with nitrogen and immediately mounted into the SPR instrument. The attachment of peptide was performed *in situ*. SA buffer was flowed through the flow cell until a stable baseline was established; then SA solution with 25 μg/ml of each BSA–peptide conjugate was brought in contact with the sensor surface for 35 min. Then, the SA buffer was injected again. Finally, the sensor surface was flushed with PBS and BSA to deactivate the residual carboxylic groups.

2.3.1.2. Peptide immobilization via electrostatic coupling (CHEM II). BSA–peptide conjugate or pure BSA assemblies were formed on the gold surface from CB buffer, pH 4.0 via adsorption on a slightly negatively charged gold surface (Koubova et al., 2001). Concentrations of BSA–EBNA and BSA–CMV in the measuring and reference channels were 50 μg/ml; the incubation time was 20 min. After switching to pure CB, dextran sulphate was flowed along the sensor surfaces for 10 min at a concentration of 1 mg/ml. DS is negatively charged in the CB solution of pH 4.0. After repeating injection of CB, BSA–EBNA and BSA–CMV were injected and flowed over the measuring and reference channels for 20 min. Then, CB buffer was injected to remove the loosely bound peptide. Finally, the assemblies were incubated with 0.5 wt.% glutaraldehyde in CB for 20 min to cross-link the BSA–peptide layers. DS and loosely bound ligands were washed out from the cross-linked peptide network with PBS. The uncoated areas of the surface were covered with BSA by incubating the sensor surface with PBS buffer containing 0.5 wt.% BSA. In order to compare the surface density of the immobilized BSA–peptide conjugates with the surface density of a BSA layer and quantify the effect peptide conjugation, a BSA double-layer was formed using the same protocol.

2.3.1.3. Peptide immobilization via hydrophobic interactions (CHEM III). The BSA–peptide conjugate was adsorbed on the gold surface by means of hydrophobic interaction. PBS solution (pH 7.4) containing BSA–peptide conjugates at a concentration of 50 μg/ml was flowed along the sensor surface for 20 min. Then, PBS was injected and flowed along the sensor surface until the stable baseline was reached. The 0.5 wt.% glutaraldehyde was flowed for 20 min to cross-link the assemblies. PBS was injected again to wash off the loosely bound ligands and finally the uncoated areas of the surface were covered with BSA by incubating the sensor surface with PBS buffer containing 0.5 wt.% BSA.

2.3.2. Characterization of anti-EBNA SPR biosensor

To evaluate the used immobilization methods in terms of anti-EBNA binding capacity, measurements of anti-EBNA binding to EBNA-1 in measuring channels and CMV in reference channels was performed. Buffer (0.5 wt.% BSA in PBS) was flowed in the measuring and reference channels until stable baselines were achieved. Then, a solution containing anti-EBNA at a concentration of 0.2 ng/ml was injected and flowed for a period of 15 min. The solution was replaced with buffer which was flowed for 10 min. Then another solution with a higher concentration of anti-EBNA was injected and the whole procedure was repeated. Concentrations of anti-EBNA were 0.2, 2, 20, 200 and 2000 ng/ml. Sensor regenerability was determined using the following procedure. PBS buffer was injected until a stable baseline was established. Then, a solution of anti-EBNA at a concentration of 200 ng/ml was flowed along the sensor surface for 10 min. After a short incubation in PBS, regeneration reagent was injected and flowed for 5 min. Then PBS buffer was flowed over the sensor surface until a stable baseline was reached and then the anti-EBNA solution was injected. Several regeneration reagents, such as hydrochloric acid, glycine, formic acid, etc., with different concentrations or pH values were tested in terms of their ability to disrupt the anti-EBNA/EBNA-1 bond. Sodium hydroxide at a concentration of 30 mM was found to be the most efficient regeneration agent both in terms of reproducibility and maintaining immunoreactivity of the peptide.

To determine reproducibility of the SPR sensor-based detection of anti-EBNA, a series of 6 sensor chips with the total number of 14 measuring channels functionalized with EBNA-1 was used. A series of solutions of anti-EBNA containing an increasing concentration of anti-EBNA (0.2, 2, 20, 200 and 2000 ng/ml) was flowed across the sensor surface for 15 min. The measurement was repeated after the sensor surface regeneration.

Sensor chip storability was investigated by repeating the detection of anti-EBNA at a concentration of 200 ng/ml immediately after the functionalization and after the chip was stored in a container with PBS for 2, 7 and 30 days.

To test ability of the sensor to detect anti-EBNA in complex matrices, the detection of anti-EBNA dissolved in BSA containing 1% (v/v) human serum was performed. These experiments were performed using the same procedure as that used for the determination of sensor reproducibility.

2.3.3. ELISA method

ELISA microwells were coated overnight with BSA–peptide conjugates (measuring surfaces with BSA–EBNA and reference surfaces with BSA–CMV) at a concentration of 10 μg/ml in 0.05 M carbonate–bicarbonate buffer, pH 9.6. The uncoated areas in the wells were blocked with 1% BSA in carbonate–bicarbonate buffer, washed and stored at a temperature of 4 °C. Antibodies were diluted in a special buffer developed by VIDIA, Czech Republic and used in commercial immunoassays to detect anti-EBNA antibodies in patients' sera. This PBS-based buffer containing bovine serum, bovine serum albumin, detergents, preservatives and stabilizers contained anti-EBNA at concentrations ranging from 0.1 to 4000 ng/ml. Experiments with human blood serum samples were performed using solutions of anti-EBNA in the VIDIA dilution buffer containing 1% (v/v) human blood serum. Anti-EBNA solutions were incubated with antigen-coated wells for 1 h at a room temperature. The wells were washed five times with VIDIA wash buffer and the bound anti-EBNA was detected using the Goat-anti-mouse antibody labeled with horseradish peroxidase. The enzymatic reaction was stopped after 10 min. The optical density was measured with an ELISA reader (SLT Spectra) at a wavelength of 450 nm. The specificity of the studied peptide/antibody system was confirmed by measuring the sandwich assay immunoreaction between BSA–CMV and anti-EBNA at a high anti-EBNA concentration (160 ng/ml). No significant signal was observed (data not shown here).

3. Results and discussion

3.1. Comparison of functionalization methods

The functionalization methods employed in this research were based on three different physicochemical principles and a spatially controlled delivery of the peptide to the sensor surface using microfluidics. The sensorgrams illustrating the binding of receptors (BSA–EBNA) and reference ligands (BSA–CMV) are shown in Fig. 2. For CHEM II, the sensor response only to the second layer of BSA–peptide conjugates is shown. The resulting surface coverage of immobilized ligands (BSA–EBNA and BSA–CMV) were calculated from the difference of the sensor response to surface without any ligands (prior to the binding) and ligand-coated surface (after washing off the loosely bound ligand) in the same buffer. The bar graph in Fig. 2 shows the ligand (BSA–EBNA and BSA–CMV) surface coverage obtained for each immobilization method.

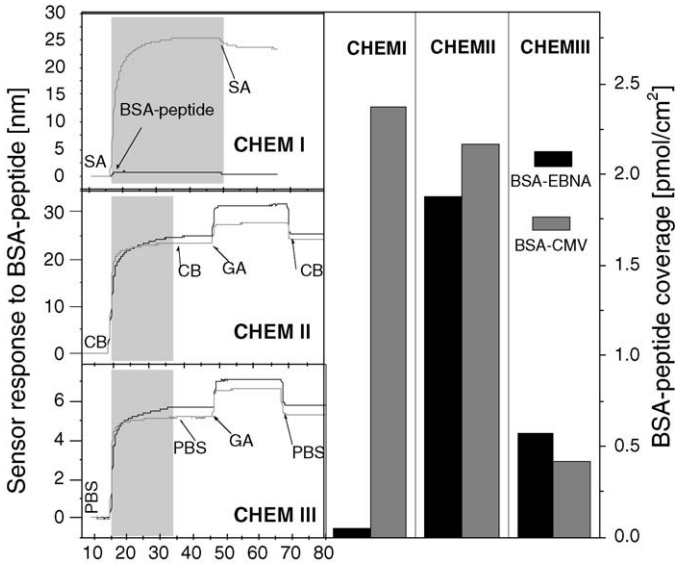

Fig. 2. Surface coverage of BSA–EBNA and BSA–CMV conjugates produced using different immobilization methods. Immobilization of BSA–EBNA (measuring channel; black line) and BSA–CMV (reference channel; gray line) via covalent attachment to the thiol-coated surface (CHEM I), electrostatic coupling (CHEM II) and hydrophobic interactions (CHEM III).

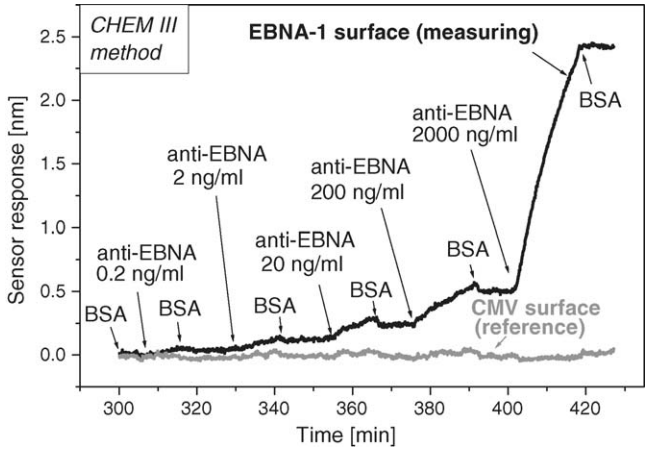

Fig. 3. Sensor response to different concentrations of anti-EBNA for the measuring and reference sensing channels. Sensor surface was functionalized using CHEM III.

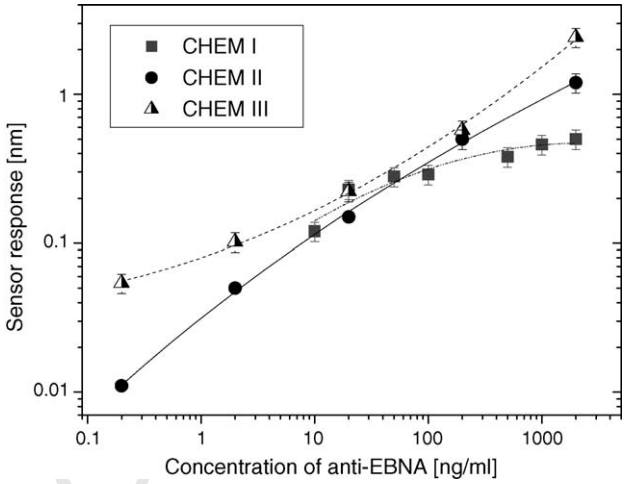

Fig. 4. Sensor response to the binding of anti-EBNA to the EBNA–BSA coatings produced using CHEM I, II and III for different anti-EBNA concentrations.

As follows from Fig. 2, the three immobilization method yield considerably different amounts of immobilized BSA–peptide conjugates, ranging from 5×10^{-14} to 1.9×10^{-12} and 4×10^{-13} to 2.4×10^{-12} mol/cm^2 for BSA–EBNA and BSA–CMV, respectively.

The highest surface density of EBNA-1 was achieved using the electrostatic coupling-based immobilization method. It suggests that pH 4.0 was sufficient for making BSA–peptide conjugates positively charged and physicochemical properties of the peptide did not significantly influence the isoelectric point of BSA. The obtained level of BSA–EBNA agreed well with the coverage observed with bare (non-modified) BSA, when a BSA double-layer was prepared using the same method (data not shown here).

The lowest surface density of EBNA-1 was obtained with the covalent attachment of BSA–EBNA to the SAM (CHEM I), even though the composition of the SAM was optimized to ensure the maximum BSA coverage (Ladd et al., 2004). This result suggests that the non-polarity of the EBNA-1 peptide resulting from its amino acid sequence (alanine and glycine alternation) negatively influences the EBNA-1 binding to the hydrophilic layer of NHS-ester-terminated and di(ethyleneglycol)-terminated groups of alkylthiolates on the sensor surface. The highest coverage of BSA–CMV was achieved using CHEM III. We believe that this is due to the high ratio of polar amino acids in the peptide and due to the presence of lysins in the CMV amino acid sequence, which increases the probability of the amide bond formation with esterificated carboxylic groups. The effect of hydrophobicity of BSA–EBNA is also apparent from the comparison of the amount of BSA–EBNA and BSA–CMV immobilized using CHEM III—a higher surface density was achieved for BSA–EBNA than for BSA–CMV conjugates.

In order to evaluate the immunoreactivity of the immobilized EBNA-1, the detection of anti-EBNA binding to EBNA-1 (and to CMV as reference surface) was carried out for each immobilization method. A typical sensorgram corresponding to the binding of anti-EBNA to EBNA-1 and reference CMV surface prepared using CHEM III is shown in Fig. 3. The interaction between the immobilized EBNA-1 and anti-EBNA was highly specific for all the used immobilization methods (only very low non-specific binding to the BSA–CMV-coated reference surface was observed). This observation was further confirmed by the injection of anti-HSV (antibody of the same isotype IgG2b as the anti-EBNA, but with no immunoreactivity to EBNA-1) at concentrations of 2 μg/ml and 20 μg/ml which generated no sensor response (data not shown here). A reference-compensated sensor response to anti-EBNA calculated as a difference between the sensor response prior to the binding of anti-EBNA and after washing the sensor surface with buffer for 10 min for a series of different antibody concentrations is shown in Fig. 4. The sensor response is proportional to the concentration of anti-EBNA, however, differs for the used immobilization methods. Although the BSA–EBNA coverage was highest for CHEM II, the largest amount of bound antibody was observed, when the peptide was immobilized using CHEM III (Fig. 4). These results suggest that a low pH of the buffer used in CHEM II decreases the peptide immunoreactivity to anti-EBNA. Therefore, CHEM III was used in all the SPR biosensing experiments presented below.

3.2. Sensor regeneration and reusability

Sensor surface with captured anti-EBNA was regenerated using sodium hydroxide at a concentration of 30 mM for 5 min. Repeated detection-regeneration cycles were performed 10 times directly after the functionalization and after storing the sensor chip for 30 days in a controlled environment.

Fig. 5 shows a typical sensor response to anti-EBNA regeneration/measurement cycles before and after the sensor chip storage. The sensor response to the analyte binding was found to reach the same amplitudes on the regenerated surface and after the binding of a lower concentration of anti-EBNA (as in Fig. 3). This is in agreement with simulations which suggest that the binding rate increases linearly with the amount of free receptors. In experiments presented in Fig. 3, about 90% of receptors remain unoccupied (until an anti-EBNA concentration of 2000 ng/ml) and therefore the change in sensor sensitivity is

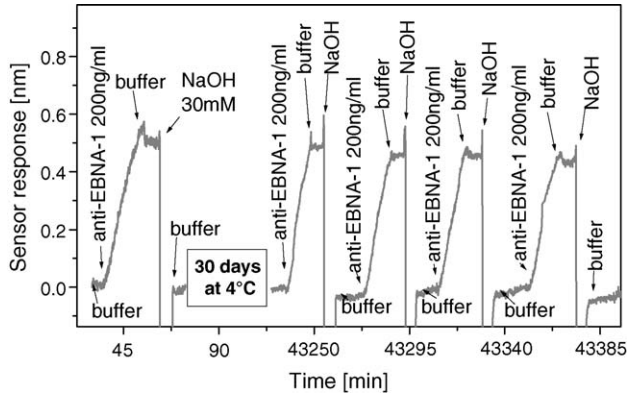

Fig. 5. Detection/regeneration cycles for anti-EBNA obtained immediately after the functionalization and after 30 days of storage. Each cycle consisted of buffer (incubation time ~5–10 min), anti-EBNA binding at a concentration of 0.2 ng/ml (10 min), buffer (5 min), removal of anti-EBNA by 30 mM NaOH (5 min) and buffer (~5–10 min).

insignificant (less than 10%). Clearly, the regeneration resulted in a total removal of the antibody from the sensor surface. No significant loss in the sensor sensitivity was observed for up to 10 regeneration/measurement cycles and the sensor chip did not exhibit any significant decrease in sensitivity after storing the chip up to 30 days.

3.3. Sensor reproducibility

The sensor response to an increasing concentration of anti-EBNA was measured. The sensor response was calibrated to the amount of receptors immobilized on the gold surface. The standard deviation of the sensor response obtained using different sensor chips was found to be in the range of 8–18% (depending on the anti-EBNA concentration), yielding the measurement reproducibility of 82–92%. Reproducibility of the binding experiments on a single chip was better than 90% for concentrations of anti-EBNA from 0.2 to 2000 ng/ml. The calibration curve depicted in Fig. 6A (as squares) shows the dependence of the absolute sensor response to a 15 min incubation of the sensor with anti-EBNA solutions. The error bars indicate the standard deviation for the set of measurements on different chips.

The results of the SPR measurements were compared with the results obtained with ELISA. ELISA measurements of the optical density (OD) (indirect detection) were performed 32 times (eight times using one titration plate, totally repeated four times) for each concentration of anti-EBNA. OD obtained from blank sample produced by BSA–CMV peptide was subtracted. Experimental error was calculated as a standard deviation of OD variability obtained from 32 experiments. To determine standard deviation of OD variability (instrumental error), each OD was measured 10 times. The standard deviation of the OD was found to fall between 5% (at high concentrations) and 20% (at low concentrations).

3.4. Detection limit

The limit of detection (LOD) is defined as the concentration of analyte that induces the smallest resolvable change in the sensor response, usually assumed as three standard deviations of the baseline noise (Thomsen et al., 2003). For the reported SPR biosensor, the LOD was estimated to be 0.1 ng/ml. Detection of anti-EBNA at this level was not performed in our experiments, however, the concentration of 0.2 ng/ml (~1 pM) was clearly detectable both in the buffer and 1% human blood serum. The limit of detection for ELISA was determined to be 1 ng/ml.

3.5. Detection of anti-EBNA in human serum

All antibody concentrations in the range 0.2–2000 ng/ml were detected also in 1% human blood serum. Sensor responses to analyte in serum and in buffer are compared in Fig. 6A. Only very low non-specific binding was observed for measurements in serum. A typical sensorgram obtained during the anti-EBNA binding from human serum in measuring (BSA–EBNA) and reference (BSA–CMV) channels is displayed in Fig. 6B. This demonstrates the potential of the developed sensor for the detection of anti-EBNA in even more concentrated human blood serum samples.

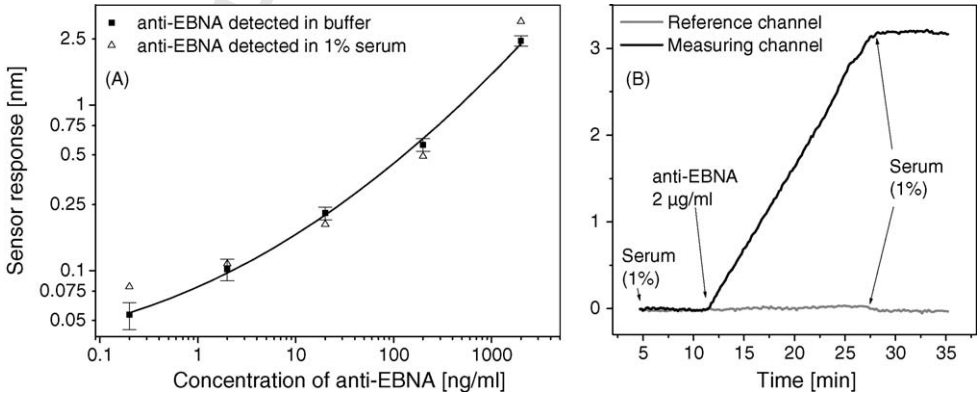

Fig. 6. (A) Sensor response to different concentrations of anti-EBNA in buffer (the error bars indicate the chip to chip reproducibility). Sensor responses to the same concentrations of anti-EBNA in 1% human serum shown for comparison. (B) Temporal sensor response to the binding of anti-EBNA at a concentration of 2 µg/ml in human blood serum: specific binding to BSA–EBNA surface (black line) and non-specific binding to BSA–CMV surface (gray line).

4. Conclusions

An SPR sensor for detection of anti-EBNA utilizing synthetic peptide EBNA-1 as a recognition element was developed. Three different methods were investigated for the immobilization of EBNA-1 conjugated with BSA on the sensor surface to obtain the highest sensitivity of the sensor to anti-EBNA. Non-polar amino acid composition of the EBNA-1 peptide was found to significantly influence the amount of immobilized BSA–EBNA conjugate. Although the highest amount of immobilized receptors was obtained using the electrostatic coupling-based immobilization method, the highest immunoreactivity of EBNA-1 was achieved with the immobilization method based on the physical adsorption of BSA–EBNA conjugates to the gold surface in physiological conditions. Thus, the hydrophobic interactions as the principle of ligand immobilization for CHEM III was best compatible with the non-polar structure of EBNA.

Sensor response to anti-EBNA exhibited a high degree of reproducibility (standard deviation < 18%). The limit of detection for the direct detection of anti-EBNA was estimated to be 0.1 ng/ml, which is lower by an order of magnitude than the limit of detection of ELISA. The minimum experimentally observed concentration of anti-EBNA was 0.2 ng/ml. The procedure for the regeneration of SPR sensor chips was developed and only a minor loss in sensor sensitivity was observed after 10 regeneration/measurement cycles. It was demonstrated that the developed peptide-coated sensor chips can be stored for at least 30 days with no loss in the sensor sensitivity. The demonstrated detection limit was reproduced in a diluted human blood serum. The ability of the developed SPR biosensor to directly detect anti-EBNA at clinically relevant levels illustrates the potential of this technology for medical diagnostics.

Acknowledgements

Authors would like to thank Markéta Lachmanová and Soňa Voslářová for their help in carrying out the experiments and Dr. Eduard Brynda for helpful discussions concerning surface chemistries. This project was supported by the Grant Agency of the Czech Republic (contracts 303/03/0249 and 102/03/0633) and the European Commission (contract QLK4-CT-2002-02323).

References

Busse, S., Scheumann, V., Menges, B., Mittler, S., 2002. Biosens. Bioelectron. 17, 704–710.
Coligan, J.E., Kruisbeek, A.M., Margulies, D.H., Shevach, E.M., Strober, W., 1995. Current Protocols in Immunology. John Wiley & Sons.
Dostalek, J., Vaisocherova, H., Homola, J., 2005. Sens. Actuators B-Chem. 108, 758–764.
Fields, G.B., Noble, R.L., 1990. Int. J. Pept. Protein Res. 35, 161–214.
Gomara, M.J., Ercilla, G., Alsina, M.A., Haro, I., 2000. J. Immunol. Methods 246, 13–24.
Gonzalez, L., Boyle, R.W., Zhang, M.L., Castillo, J., Whittier, S., DellaLatta, P., Clarke, L.M., George, J.R., Fang, X.D., Wang, J.G., Hosein, B., Wang, C.Y., 1997. Clin. Diagn. Lab. Immunol. 4, 598–603.
Goodrich, T.T., Lee, H.J., Corn, R.M., 2004. J. Am. Chem. Soc. 126, 4086–4087.
Homola, J., Lu, H.B.B., Nenninger, G.G., Dostalek, J., Yee, S.S., 2001. Sens. Actuators B-Chem. 76, 403–410.
Homola, J., Dostalek, J., Chen, S.F., Rasooly, A., Jiang, S.Y., Yee, S.S., 2002. Int. J. Food Microbiol. 75, 61–69.
Homola, J., 2006. Surface Plasmon Resonance. Springer-Verlag, Berlin, Heidelberg, New York.
Karlsson, R., Falt, A., 1997. J. Immunol. Methods 200, 121–133.
Knorr, R., Trzeciak, A., Bannwarth, W., Gillessen, D., 1989. Tetrahedron Lett. 30, 1927–1930.
Koubova, V., Brynda, E., Karasova, L., Skvor, J., Homola, J., Dostalek, J., Tobiska, P., Rosicky, J., 2001. Sens. Actuators B-Chem. 74, 100–105.
Ladd, J., Boozer, C., Yu, Q., Chen, S., Homola, J., Jiang, S., 2004. Langmuir 20, 8090–8095.
Lahiri, J., Isaacs, L., Tien, J., Whitesides, G.M., 1999. Anal. Chem. 71, 777–790.
Liedberg, B., Lundstrom, I., Stenberg, E., 1993. Sens. Actuators B-Chem. 11, 63–72.
Lofas, S., Johnsson, B., Edstrom, A., Hansson, A., Lindquist, G., Hillgren, R.M.M., Stigh, L., 1995. Biosens. Bioelectron. 10, 813–822.
Nenninger, G.G., Piliarik, M., Homola, J., 2002. Meas. Sci. Technol. 13, 2038–2046.
Nuzzo, R.G., Allara, D.L., 1983. J. Am. Chem. Soc. 105, 4481–4483.
Piliarik, M., Vaisocherova, H., Homola, J., 2005. Biosens. Bioelectron. 20, 2104–2110.
Shumaker-Parry, J.S., Campbell, C.T., 2004. Anal. Chem. 76, 907–917.
Stabler, G., Somekh, M.G., See, C.W., 2004. J. Microsc. Oxford 214, 328–333.
Thomsen, V., Schatzlein, D., Mercuro, D., 2003. Spectroscopy 18, 112–114.
Wester, H.J., Hamacher, K., Stocklin, G., 1996. Nucl. Med. Biol. 23, 365–372.

Appendix VIII

H. Vaisocherová, A. Zítová, M. Lachmanová, J. Štěpánek, Š. Králíková, R. Liboska, D. Rejman, I. Rosenberg and J. Homola:

Investigating oligonucleotide interactions at subnanomolar level by surface plasmon resonance biosensor

Biopolymers, **82** (2006), 394-398

Hana Vaisocherová[1,2]
Alice Zítová[1]
Markéta Lachmanová[1]
Josef Štěpánek[2]
Šárka Králíková[3]
Radek Liboska[3]
Dominik Rejman[3]
Ivan Rosenberg[3]
Jiří Homola[1]

[1] *Institute of Radio Engineering and Electronics, Academy of Sciences of the Czech Republic, Chaberská 57, 182 51 Prague, Czech Republic*

[2] *Charles University, Faculty of Mathematics and Physics, Ke Karlovu 3, 121 16 Prague, Czech Republic*

[3] *Institute of Organic Chemistry and Biochemistry, Academy of Sciences of the Czech Republic, Flemingovo n. 2, 166 10 Prague, Czech Republic*

Investigating Oligonucleotide Hybridization at Subnanomolar Level by Surface Plasmon Resonance Biosensor Method

Received 12 October 2005; revised 7 December 2005; accepted 8 December 2005
Published online 19 December 2005 in Wiley InterScience (www.interscience.wiley.com). DOI 10.1002/bip.20433

Abstract: *We have optimized surface plasmon resonance (SPR) biosensor technology for a rapid, direct, and low-consumption label-free multianalyte screening of synthetic oligonucleotides (ONs) with modified internucleotide linkages potentially applicable in antisense therapy. Monitoring of the ONs hybridization is based on the formation of complex between the natural oligonucleotide probe immobilized on the sensor surface and the ON in solution in contact with the sensor surface. An immobilization chemistry utilizing the streptavidin–biotin interaction was employed to obtain desired ligand density and high hybridization efficiency. It was demonstrated that the sensor is capable of detecting complementary 23-mer ONs in concentrations as low as 0.1 n*M *with high specificity and reproducibility.* © 2005 Wiley Periodicals, Inc. Biopolymers 82: 394–398, 2006

This article was originally published online as an accepted preprint. The ''Published Online'' date corresponds to the preprint version. You can request a copy of the preprint by emailing the Biopolymers editorial office at biopolymers@wiley.com

Correspondence to: H. Vaisocherová; e-mail: vaisocherova@ure.cas.cz

Keywords: *oligonucleotide interactions; hybridization; surface plasmon resonance biosensor*

INTRODUCTION

A great deal of research has been recently focused on development of strategies for gene therapy based on specific oligonucleotides (ONs). The antisense concept consists in binding of the ON to its complementary target sequence in a specific mRNA blocking translation of a deleterious gene. Due to the instability of DNA ONs in living cells, their synthetic analogs are employed.[1,2] The search for novel types of ON modifications can benefit from methods allowing real-time observation and quantification of NA hybridization with high specificity and good signal-to-noise ratio.

Direct, label-free biosensors, such as surface plasmon resonance (SPR) biosensors, present an interesting alternative to conventional NA-hybridization screening that requires enzymatic amplification and/or radio- or fluorescent labeling. SPR biosensors detect refractive index changes produced by the analyte binding to its biospecific partner immobilized on the sensor surface.[3–5]

Typical concentrations of short ON targets used in NA hybridization studies using SPR biosensors were at a micromolar level,[6,7] however, some experiments involving lower concentrations, i.e., 10−100 n*M*, have been carried out.[5,8–10] Hybridization efficiencies (percentage of immobilized ligands present in complexes with interacting partner) as high as 60–80% have been reported.[8]

In this work, we describe application of a recently developed multichannel SPR biosensor for parallelized monitoring of ON hybridization.

EXPERIMENTAL

Reagents

The C_{16}-chained alkanethiol (C_{16}-mercaptohexadecanoic acid) and streptavidin from *Streptomycea avidinii* were purchased from Sigma–Aldrich, St. Louis, MO, USA. The C_{11}-chained di(ethylene glycol)-terminated alkanethiol was purchased from Prochimia, Sopot, Poland. Biotinylated deoxyribooligonucleotide probes (23-mers) with sequence of biotin-$(TEG)_2$-5′-d(CAG TGT GGA AAA TCT CTA GCA GT)-3′ (BdO_{23}), biotin-$(TEG)_2$-5′-(dA_{23})-3′ (BdA_{23}), and their complementary targets 5′-d(ACT GCT AGA GAT TTT CCA CAC TG)-3′ (CdO23), dT_{23}, and dT_{15} were purchased from LMFR of Masaryk University in Brno, Czech Republic. Biotinylated ribunucleotide probes biotin-$(TEG)_2$-5′-(rA_{23})-3′ (BrA_{23}) were purchased from Dharmacon, Lafayette, CO, USA. Synthetic homothymidine oligonucleotides (15-mers) with chemically modified sugar-phosphate backbones were prepared as described elsewhere.[11]

SPR Sensor

The SPR sensor platform used in this work is based on the spectroscopy of surface plasmons[12] and wavelength division multiplexing (WDM).[13] This sensor combines wavelength division multiplexing of two serially ordered sensing channels with four parallel light beams (see Figure 1) to yield the total of eight sensing channels. Broadband light from a halogen lamp is collimated, polarized, and then directed into the WDM-SPR sensing element interfaced with a chip made of SF-14 glass coated by an adhesion-promoting titanium film (2 nm thickness) and a gold film (55 nm). Upon the first incidence on the gold film, the light beam excites a surface plasmon at a wavelength ~650 nm. The reflected light is redirected again toward the gold film at larger angle of incidence and excites a surface plasmon at longer wavelength (~800 nm). This arrangement generates two narrow dips in the spectrum of the light leaving the sensing element (Figure 1). The output light is coupled to a four-channel spectrograph connected to a computer running a data acquisition and real-time data processing.[14] A flow-cell with eight separate flow chambers (each with a volume of 1 μL) aligned to the eight measuring spots is interfaced with the chip. A peristaltic pump is used to flow liquid samples along the sensor surface; a flow rate of 30 μL/min was used.

In each binding experiment one sensing spot was coated by an ON of noncomplementary sequence to form a reference channel. The SPR wavelength shift measured at the measuring channel and that obtained at the reference one were subtracted to account for a nonspecific adsorption and for temperature fluctuations.

Immobilization of Oligonucleotide Probe

The method of ON probes immobilization on the gold surface employed herein is based on the coupling of biotinylated probes to the streptavidin assemblies via a noncovalent, high-affinity, and stable streptavidin–biotin bond.[8,15,16] Streptavidin is a tetrameric molecule with dyad symmetry, therefore each streptavidin contains four equivalent binding pockets for biotin.[17] Streptavidin is fixed via the covalent attachment to an alkanethiolate self-assembled monolayer[18] and the delivery of probes to the sensor surface is spatially controlled using microfluidics. A 7:3 mixture of C_{11}-chained and C_{16}-chained alkanethiols was dissolved in degassed absolute ethanol with a total thiol concentration of 1 m*M*. Sensor chips were immersed in the solution at temperature of 40°C and stored in a dark place at room temperature for up to 2 days. The alkanethiols self-organize on a clean gold surface forming a self-assembled monolayer. The C_{16} alkanethiols terminated with a carboxylic head group were used to anchor streptavidin by amino coupling; C_{11} alkanethiols terminated with a di(ethylene glycol) group formed a stable nonfouling background. The carboxylic terminal groups on the sensor surface were activated by TSTU and then replaced with reactive *N*-hydroxysuccinimidyl-esters. The chips were rinsed with water,

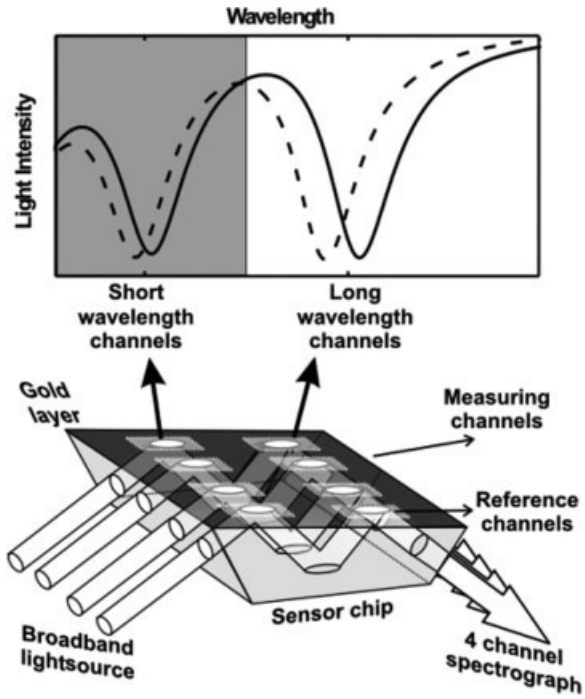

FIGURE 1 Scheme of the eight-channel SPR WDM sensor (bottom) and typical detected normalized dual spectrum (top) before (dashed line) and after (solid line) the analyte binding.

dried, and immediately mounted into the SPR instrument. Streptavidin attachment was performed in situ at 20°C. First, 10 m*M* sodium acetate (SA) buffer (pH 5.0) was flowed along the sensor surface until the baseline was achieved, then, SA solution with 50 μg/mL of streptavidin was brought into contact with the sensor surface for 20 min and the SA buffer was injected again. After a short period of incubation with 10 m*M* phosphate buffer containing 0.75 *M* NaCl (pH 7.4) to remove noncovalently bound ligands and deactivate residual carboxylic groups, the sensor surface was flushed with 10 m*M* phosphate buffer containing 15 m*M* $MgCl_2$ (PBM). A 50 n*M* solution of biotinylated ONs was then flowed along the sensor surface for 15 min followed by PBM injection.

Because SPR response is proportional to the mass of the adsorbed/captured molecules, it is possible to determine binding stoichiometry of biotinylated ONs to streptavidin as a ratio between sensor responses to ON and streptavidin. The stoichiometry was determined from the total of 30 sensing channels (4 different sensor chips) as 2.9 ± 0.4 ON molecules per 1 streptavidin. This result suggests that the streptavidin is favorably oriented and maintains its binding activity upon immobilization.

Measurement Protocols

All detection experiments were carried out at a temperature of 25°C. To determine reproducibility of the SPR sensor response to DNA hybridization, a series of seven sensor chips functionalized with BdA_{23} was used. The dT_{23} detection was performed as follows: PBM buffer was flowed along the sensor surface until a stable baseline was achieved. Solution of dT_{23} at a concentration of 100 n*M* then was flowed along the functionalized sensor surface for 20 min followed by PBM buffer.

To characterize the sensor in terms of detection limit, binding of CdO_{23} to BdO_{23} was performed using the following procedure: after stable baselines were achieved with flowed PBM buffer, CdO_{23} solution of the lowest concentration was flowed for a period of 10 min and replaced with the buffer for next 10 min. Another solution with a higher concentration of CdO_{23} then was injected and the whole procedure was repeated.

Measurements on synthetic modified ONs were performed on the BrA_{23} surface created on one 8-channel sensor chip using an experimental procedure similar to the one described above for the dT_{23} detection. Concentrations of all the targets were 50 n*M* and the incubation time employed for this experiment was 20 min.

RESULTS AND DISCUSSION

Sensor response to dT_{23} binding to BdA_{23} immobilized on the sensor surface obtained from seven individual

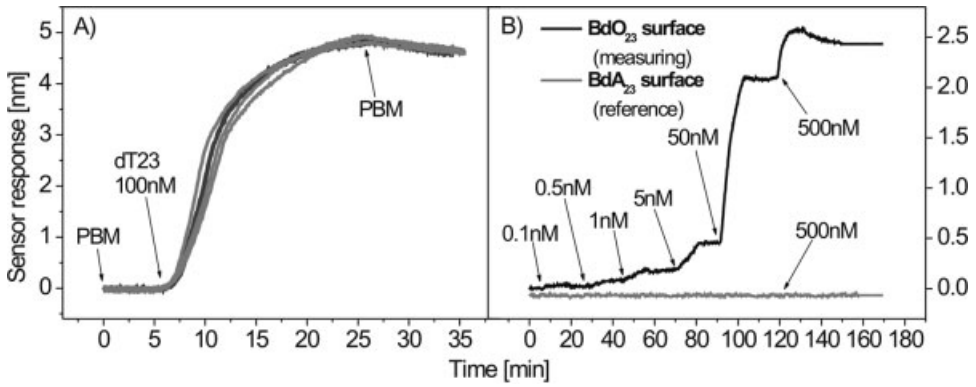

FIGURE 2 Sensor response to dT_{23} binding to BdA_{23} immobilized on the sensor surface obtained from 7 individual sensor chips (A). Sensor response to CdO_{23} binding to BdO_{23} and BdA_{23} surface, respectively, with increasing target concentration (B).

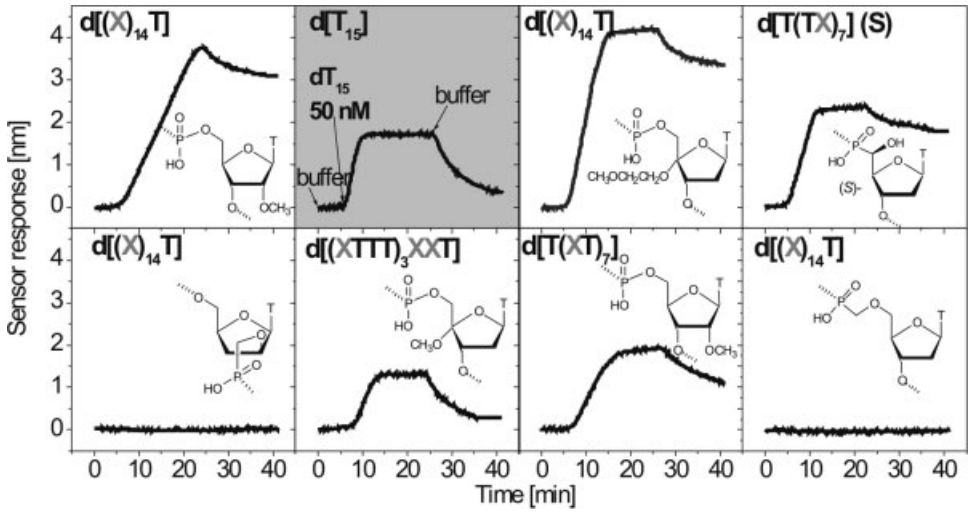

FIGURE 3 Multianalyte screening of synthetic modified oligonucleotide interactions with BrA23 in comparison with natural dT15; *X*, presence of depicted internucleotide linkage modification (*X*) in 15-mer homothymidine sequence.

sensor chips is shown in Figure 2A. Sensor response was calibrated to the amount of receptors (BdA_{23}) immobilized on the sensor surface. Relative standard deviation of amplitudes of sensor responses obtained for different sensor chips was determined to be 5%.

Sensor response to increasing concentrations of CdO_{23} binding to BdO_{23} surface (fully complementary sequence) and BdA_{23} surface (reference) is shown in Figure 2B. Clearly, the detection of DNA hybridization using the developed SPR biosensor is highly specific (see gray line in Figure 2B). The noise-limited detection limit of the SPR sensor was calculated as a triple of baseline noise standard deviations and was determined to be 0.1 n*M*. This value is better by two orders of magnitude in comparison with the detection limits achieved by other SPR biosensors previously reported.[5–10] The hybridization efficiency was found to be more than 85% for system BdO_{23}–CdO_{23}.

Real-time observation of hybridization of synthetic modified and natural dT_{15} with immobilized rON complement using the eight-channel SPR system is shown in Figure 3; a scheme of the internucleotide linkage modification is attached to each sensorgram. Different binding kinetics suggest different interaction mechanisms associated with the insertion of internucleotide linkage modification. This primary screening with very low sample and time consumption enables primary choice of prospective candidates for antisense therapy. Moreover, if we compare the modified ON sensor response amplitudes to those obtained from ligand (BrA_{23}) immobilization and calibrate the values to unified molecular weight, we can conclude that a stoichiometry of formed complexes was higher than 1:1, which indicates that triplexes were also formed in addition to duplexes for selected modified ONs (Figure 3). Triplex formation was also observed in case of the natural BdA_{23}–dT_{23} system. Detailed analysis of complex stoichiometry is in progress.

CONCLUSION

A surface plasmon resonance biosensor for sensitive and real-time observation of NA hybridization has been reported. Biotinylated oligonucleotide probes were immobilized on the streptavidin surface, which was created via an optimized version of amine coupling chemistry. The resulting SPR sensor was characterized in terms of detection limit and reproducibility. This sensor enables rapid DNA/RNA oligonucleotide screening with high chip-to-chip reproducibility (>95%), specificity, and hybridization efficiency (>85%). The detection limit for detection of 23-mer hybridization as low as 0.1 n*M* ($\sim$ 0.7 ng/mL) was achieved. This sensor can be applied to primary screening and stoichiometry prediction of synthetic modified oligonucleotides.

The authors thank Kateřina Mrkvová, Praskovia Boltovets, and Soňa Voslářová (IREE, Prague, Czech Republic) for kind help in carrying out the reported experiments. This project was supported by the Grant Agency of the Czech Republic (contracts 303/03/0249, 102/03/0633, and 202/05/0628).

REFERENCES

1. Uhlmann, E.; Peyman, A. Chem Rev 1990, 90, 543–584.
2. Nordgren, S.; Slagter-Jager, J. G.; Wagner, E. G. H. J Mol Biol 2001, 310, 1125–1134.
3. Shumaker-Parry, J. S.; Campbell, C. T. Anal Chem 2004, 76, 907–917.
4. Piliarik, M.; Vaisocherová, H.; Homola J. Biosens Bioelectron 2005, 20, 2104–2110.
5. Kambhampati, D.; Nielsen, P. E.; Knoll, W. Biosens Bioelectron 2001, 16, 1109–1118.
6. Asensio, J. L.; Dosanjh, H. S.; Jenkins, T. C.; Lane, A. N. Biochemistry 1998, 37, 15188–15198.
7. Kukanskis, K.; Elkind, J.; Melendez, J.; Murphy, T.; Miller, G.; Garner, H. Anal Biochem 1999, 274, 7–17.
8. Su, X. D.; Wu, Y. J.; Robelek, R.; Knoll, W. Langmuir 2005, 21, 348–353.
9. Persson, B.; Stenhag, K.; Nilsson, P.; Larsson, A.; Uhlen, M.; Nygren, P. A. Anal Biochem 1997, 246, 34–44.
10. Nair, T. M.; Myszka, D. G.; Davis, D. R. Nucleic Acids Res 2000, 28, 1935–1940.
11. Rejman, D.; Masojidkova, M.; Rosenberg, I. Nucleosides, Nucleotides & Nucleic Acids 2004, 23, 1683–1705.
12. Homola, J.; Dostálek, J.; Chen, S. F.; Rasooly, A.; Jiang, S. Y.; Yee, S. S. Int J Food Microbiol 2002, 75, 61–69.
13. Dostálek, J.; Vaisocherová, H.; Homola, J. Sens Actuators B 2005, 108, 758–764.
14. Nenninger, G. G.; Piliarik, M.; Homola, J. Meas Sci Technol 2002, 13, 2038–2046.
15. Tombelli, S.; Mascini, M.; Turner, A. P. F. Biosens Bioelectron 2002, 17, 929–936.
16. Jung, L. S.; Nelson, K. E.; Campbell, C. T.; Stayton, P. S.; Yee, S. S.; Perez-Luna, V.; Lopez, G. P. Sens Actuators B 1999, 54, 137–144.
17. Hendrickson, W. A.; Pahler, A.; Smith, J. L.; Satow, Y.; Merritt, E. A.; Phizackerley, R. P. Proc Natl Acad Sci U S A 1989, 86, 2190–2194.
18. Lahiri, J.; Isaacs, L.; Tien, J.; Whitesides, G. M. Anal Chem 1999, 71, 777–790.

Reviewing Editor: Friedrich Siebert

Appendix IX

H. Vaisocherová, I. Rosenberg, K. Mrkvová-Hegnerová, P. Tobiška, J. Štěpánek and J. Homola:

Immobilization method improvement for detection of oligonucleotide hybridization at subnanomolar level by surface plasmon resonance biosensor

Manuscript in preparation

Immobilization Method Improvement for Detection of Oligonucleotide Hybridization at Subnanomolar Level by SPR Biosensor

Authors: Hana Vaisocherová[1,2], Ivan Rosenberg[3], Kateřina Mrkvová-Hegnerová[1], Petr Tobiška[1], Josef Štěpánek[2], Jiří Homola[1]

[1]Institute of Radio Engineering and Electronics, Academy of Sciences of the Czech Republic, Chaberská 57, 182 51 Prague, Czech Republic

[2]Charles University, Faculty of Mathematics and Physics, Ke Karlovu 3, 121 16 Prague, Czech Republic

[3]Institute of Organic Chemistry and Biochemistry, Academy of Sciences of the Czech Republic, Flemingovo n. 2, 166 10 Prague, Czech Republic

Abstract:

In this work, an oligonucleotide chip functionalization method based on formation of mixed carboxylic group-terminated and oligo(ethylene glycol)-terminated alkanethiols, amide bond formation between streptavidin and activated carboxylic group and biotinylated oligonucleotide probe binding to streptavidin was modified to reach a high streptavidin and oligonucleotide probe density and accessibility to target molecules. A systematic investigation of immobilization parameters such as streptavidin binding buffer pH or salt concentration, probe spacer length, and concentration of reagents was carried out. The DNA-sensor with optimized immobilization method was capable to direct detection of short ON hybridization at subnanomolar level with high reproducibility, specificity, efficiency and regenerability. The resulting sensor immobilization and detection characteristics were compared with well established method of immobilization utilizing self-assembled monolayer (SAM) composed of mixture of biotin-terminated and di(ethylene glycol) terminated alkanethiols (BAT method).

List of abbreviations:

SPR	surface plasmon resonance
ON	oligonucleotide
ELISA	enzyme-linked immunosorbent assay
NA	nucleic acid
DNA	deoxyribonucleic acid
PCR	polymerase chain reaction
TSTU	*N,N,N',N'*-Tetramethyl-O-(*N*-succinimidyl)uronium tetrafluoroborate
SAM	self-assembled monolayer
DMF	*N, N*-dimethylformamide

NHS	*N*-hydroxysuccinimide
NHS-ester	*N*-hydroxysuccinimidyl ester
EDC	*N*-ethyl-*N'*-(3-diethylaminopropyl) carbodiimide
MHA	C_{16}-mercaptohexadecanoic acid
OEG	C_{11}-chained alkanethiol terminated with di(ethylene glycol)
BAT	C15-chained biotin-terminated alkanethiol
TEG	Tri(ethyleneglycol)
HE%	hybridization efficiency [%]
PB	phosphate buffer
PBS	phosphate buffer saline
PBM	phosphate buffer with addition of magnesium ions
PBNa	phosphate buffer with addition of natrium ions
SA	sodium acetate buffer

Keywords: surface plasmon resonance biosensor, oligonucleotide detection, hybridization, oligonucleotide immobilization

1. INTRODUCTION

Detection and characterization of nucleic acids (NAs) allow the identification of biological samples and are of great interest in molecular bioligy. The analysis relies on sensitive and specific detection of hybridization between short oligonucleotide (ON) probes and target nucleic acid sequence. Molecular biology techniques such as polymerase chain reaction (PCR), blotting techniques, DNA-based gene sequencing, reactions based on reverse transcription, DNA-based ELISAs, *etc.* routinely utilize hybridization reaction [1, 2]). Basically DNA hybridization can be detected in bulk [3-5] or using ON probe immobilized on the sensor surface (surface-based hybridization) [6-9]. Currently, there is an explosive interest regarding the use of surface-based hybridization due to potential of DNA chips development enabling simultaneous screening of hundreds of DNA or RNA samples in array format [10-13].

Using common hybridization-based instruments, the actual hybridization process can not be monitored and typically only the final NA complex is detected. The lack of information about hybridization process still hampers the full exploitation of hybridization-based techniques. Moreover, the read-out system typically requires labeling of the oligonucleotide probes with radioactive isotopes, chemiluminiscent or fluorescent molecules [14].

Surface plasmon resonance (SPR) biosensors allow direct and label-free detection of hybridization reaction [7, 15-18]. Kinetic properties of ON interactions can be determined due to the ability of the SPR sensors to monitor the binding of target ON to surface-immobilized probe in real time [7, 19-21]. These characteristics together with potential array platform of SPR sensors development [22, 23] make SPR biosensors excellent candidates for further DNA or RNA chip applications. Recently, the trend inn SPR genosensors development is to lower the detection limits of hybridization detection to make SPR sensors

comparable with the common and well established fluorescence or radioactive-based DNA microarrays.

The lowest concentrations of short ON targets that were detected directly and without any additional (enzymatic, electrochemical, fluorescent) amplification by current SPR biosensors, were at a nanomolar level [15, 24, 25], moreover in many SPR-based studies, ON hybridization at a micromolar level was exploited [21, 26-29],

A method of probe immobilization influences significantly the sensitivity and efficiency of the sensor and thus it is a fundamental step during SPR biosensor development [30-32]. A common goal of surface chemists is to develop a robust procedure for immobilization of probes on the sensor chip with high stability, reproducibility, sensitivity and efficiency with minimal impact on probe hybridization activity.

Various immobilization procedures for attachment of ON probes on gold SPR sensor surface have been reported. Two most common strategies are as follows: (1) assembly of thiol-terminated oligonucleotide probes on gold [32-34], and (2) coupling of biotinylated probes to the streptavidin assemblies via a non-covalent highly affinitive streptavidin-biotin interaction [30, 35, 36]. Streptavidin is a tetrameric protein with dyad symmetry and with extremely high affinity to biotin (K_d~10^{-15} M) [37]. Each streptavidin contains with four equivalent binding pockets for biotin [38].

In commercially available SPR biosensors, streptavidin coating is prepared using “amine coupling chemistry” based on covalent attachment of streptavidin by primary amines to activated carboxylate groups in carboxymethyl groups-terminated dextran matrix. The transformation of carboxymethyl groups into the reactive *N*-hydroxysuccinimidyl esters (process of activation) is performed using *N*-hydroxysuccinimide (NHS) and *N*-ethyl-*N’*-(3-diethylaminopropyl) carbodiimide (EDC) reagents [39, 40]. This method (if you start from clean gold) is rather laborious, and problems with stability [2], non-specific binding [41] and reproducibility [30] were reported.

In this work, a more robust method of covalent attachment of streptavidin to NHS-ester-terminated alkanethiolates [39, 41] followed with coupling of biotinylated probes was used to achieve high DNA-sensor sensitivity, reproducibility, efficiency and specificity. This procedure (assembly of mixed alkanethiols, activation of carboxylic groups, streptavidin and probes attachment) was optimized in terms of reagent concentrations, buffer salt composition, pH, and probe spacer length. As it was reported in our previous work, the resulting SPR sensor is capable to detect concentrations of ON probes as low as 0.1nM with high reproducibility and specificity [18], In this work, the achieved high hybridization efficiency, streptavidin binding accessibility and sensor regenerability are further compared with a well established protocol of another functionalization strategy where streptavidin is non-covalently attached to the biotin-terminated SAM (“BAT” method) [36, 42-44]).

2. EXPERIMENTAL

2.1 Reagents

The C_{16}-chained alkanethiol (C_{16}-mercaptohexadecanoic acid), and streptavidin from *Streptomycea Avidinii* were purchased from Sigma-Aldrich, USA. The C_{11}-chained di(ethylene glycol)- terminated alkanethiol was purchased from Prochimia, Poland. The C_{15}-chained alkanethiol linked to a biotin headgroup by three ethylene glycol groups was obtained from the University of Washington, USA. The *N,N,N',N'*-Tetramethyl-*O*-(*N*-succinimidyl)uronium tetrafluoroborate (TSTU) (pure, ≥98%) was purchased from Sigma-Aldrich, USA. Absolute ethanol was purchased from MERCK, Czech Republic. The anhydrous *N, N*-dimethylformamide (DMF) (≥99.8%) was from Sigma-Aldrich, USA. Formic acid and bovine serum albumin were purchased from Sigma-Aldrich, USA.

Biotinylated deoxyribooligonucleotide probes (23-mers, HPLC-purified) with sequence of biotin-$(TEG)_2$-5'-d(CAG TGT GGA AAA TCT CTA GCA GT)-3' (= BdO_{23}), biotin-$(TEG)_2$-5'-(dA_{23})-3' (= BdA_{23}) and the target oligonucleotide 5'-d(ACT GCT AGA GAT TTT CCA CAC TG)-3' (= CdO23) with a complementary sequence to BdO_{23} were purchased from LMFR of Masaryk University in Brno, Czech Republic.

The buffer solutions used for streptavidin or oligonucleotide binding were of compositions as follows: **PB** (1.4 mM KH_2PO_4, 8 mM $Na_2HPO_4.12H_2O$, 2.7 mM KCl, pH 7.4 at 20°C); **PBS** (1.4 mM KH_2PO_4, 8 mM $Na_2HPO_4.12H_2O$, 137 mM NaCl, 2.7 mM KCl, pH 7.4 at 20°C), **PBM** (1.4 mM KH_2PO_4, 8 mM $Na_2HPO_4.12H_2O$, 15 mM $MgCl_2$, pH 7.4 at 20°C); **PBNa** (1.4 mM KH_2PO_4, 8 mM $Na_2HPO_4.12H_2O$, 0.75 M NaCl, 2.7 mM KCl, pH 7.4 at 20°C); and **SA** (1 mM sodium acetate, pH 5.0 at 20°C).

2.2 SPR sensor

In this research, we used a recently developed SPR sensor platform based on the spectroscopy of surface plasmons [45] and wavelength division multiplexing (WDM) [46]. This sensor combines the wavelength division multiplexing of two serially ordered sensing channels in a special sensing element with four parallel light beams (see Figure 1) to yield the total of eight sensing channels. Broadband light from a halogen lamp is collimated and polarized, and then introduced into the WDM-SPR sensing element interfaced with a sensor chip made of SF-14 glass coated by an adhesion-promoting titanium film (thickness - 2 nm) and a gold film (thickness - 55 nm). Upon the first incidence on the gold film, each light beam excites a surface plasmon at a certain wavelength (~ 650 nm). The reflected light is redirected towards the gold film at a different angle of incidence and excites a surface plasmon at a different wavelength (~ 800 nm). The sequential excitation of the surface plasmons gives rise to two narrow dips in the spectrum of transmitted light (Figure 1). The transmitted light is collected into four optical fibers and coupled to a four-channel spectrograph. Acquired spectra are analyzed in real time by a special software

that allows tracking the resonant wavelength in each sensing channel [47]. A flow-cell with eight separate flow chambers is interfaced with the chip to contain the sample during the experiments. Each flow chamber covers the area, where the surface plasmon is excited – the sensing channel. The flow chambers are designed to provide laminar flow along the sensor surface. The height of the flow chambers is rather small (50 µm) to facilitate the diffusion of the analyte to the surface of the sensor. The volume of each flow chamber is about 1 µl. A peristaltic pump is used to flow liquid samples over each sensing channel at a flow rate of 30 µl/min.

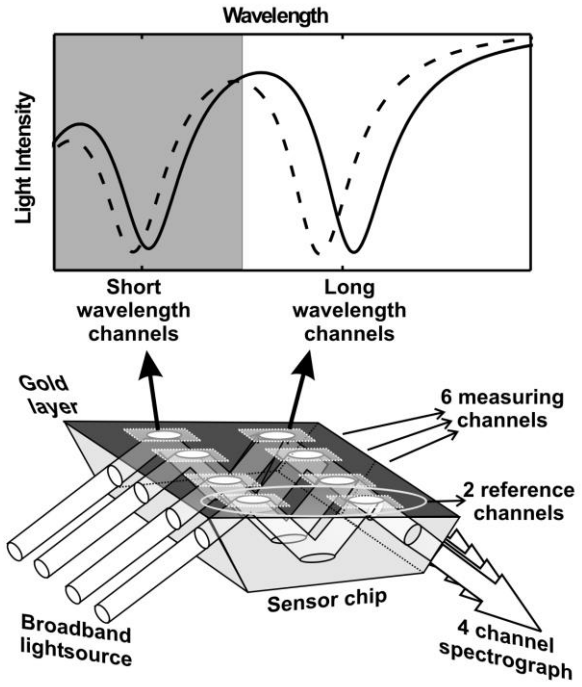

Figure 1 Scheme of an eight-channel SPR sensor with four parallel light beams and the wavelength division multiplexing (WDM) of sensing channels (lower picture). Spectrum of transmitted light with two SPR dips before (------) and after the binding (_____) (upper picture).

In order to compensate for the non-specific sensor response and thus provide more accurate results, typically in reported experiments one sensing channel was coated with a reference ligand, especially with bovine serum albumin (BSA) for monitoring of potential non-specific binding of biotinylated probes, or with ON (BdA_{23}) with fully non-complementary base sequence to target molecule(CdO_{23}). When the analytes were flowed over the sensor surface, the SPR wavelength shift measured in the measuring and reference channels are subtracted to account for temperature fluctuations (causing a drift in the sensor response).

The shift in the resonant wavelength shown in Figure 1 is proportional to the refractive index change at the sensor surface. A typical SPR-sensorgram as the nanometers over time obtained from the analyte binding to receptor immobilized on the sensor surface is shown in the Figure 2. Three phases of measurement can be distinguished: washing the sensor surface with buffer till the stable baseline is achieved (Fig. 2, I.), flowing with the solution of analyte over the

sensor surface - complex formation with immobilized biomolecular partner is monitored (Fig. 2, II.), washing the sensor surface with the same buffer as before the analyte injection – dissociation of complexes can be measured (Fig 2, III.). The level of bound analyte to the sensor surface is determined as the difference in sensor response nanometers of the buffer equilibrium level after washing the bound surface and baseline level obtained from flowing with the same buffer before injection of the analyte solution.

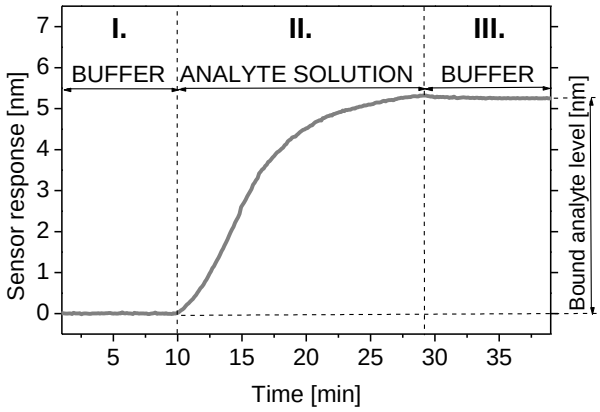

Figure 2 The typical SPR sensorgram corresponding to real-time measurement of analyte binding; In the first phase, the functionalized sensor surface is washed with buffer (I.), then the solution of analyte is injected and biomolecular complex formation can be occurred (II.), washing the solution with the same buffer as in the phase I. to monitor a potential dissociation and to achieve a level of not-removed analytes.

The sensor response can be calibrated to the surface concentration of bound molecules. The calibration coefficient interrelating the sensor response and the concentration of analyte is proportional to the molar weight of the molecules [48] and depends on the resonant wavelength. It was estimated from a theoretical model that a shift in the resonant wavelength of 1 nm corresponds to a change in the surface concentration of streptavidin of about 1.8×10^{11} molecules/cm^2 when measured at the wavelength of 750 nm. It can be shown, that the sensor response per unit mass coverage is comparable for most proteins and single-stranded or double-stranded oligonucleotides [49]. Therefore the probe/streptavidin binding ratio and target/probe hybridization efficiency can be calculated from the ratio of sensor responses when different molecular weigths of these ligands are taken into account. To allow comparable sensor response quntification all sensorgrams were recalibrated to the sensitivity at operating wavelength of 750 nm.

SPR sensor chips, SF14 glass chips 32mmx18mmx1.5mm (Schott, USA), were coated with 2 nm of Ti and 55 nm of Au by electron beam evaporation. These chips were exhaustively rinsed with absolute ethanol and water and dried with nitrogen stream. These substrates were then cleaned in UV ozone cleaner

for 15 minutes, washed with water and dried with nitrogen stream. The cleaned sensor chips were stored in desiccator before use.

2.3 Functionalization of the sensor chips

To save the purity of the SPR chips, the majority of manipulations with the chips was performed in the flow box (Schoeller-Pharma, Czech Republic).

MHA method

Functionalization method that was systematically investigated herein “MHA method” utilized covalent attachment of streptavidin to ω-carboxyalkylthiol- (MHA) and self-assembled monolayer via amide bond forming chemistry followed with biotinylated oligonucleotide target coupling [41]. The di(ethylene glycol)alkylthiols (OEG) were also present in the SAM to form a non-fouling background.

A typical MHA-functionalization procedure was as follows:

A molar 7:3 mixture of C_{11}-chained (OEG) and C_{16}-chained (MHA) alkanethiols was dissolved in degassed absolute ethanol with a total thiol concentration of 1 mM. Sensor chips were immersed in thiol solution at temperature of 40°C and stored in a dark place at room temperature for up to 2 days. Then, the chips were rinsed with ethanol, dried with nitrogen, rinsed with water and dried with nitrogen again. The carboxylic terminal groups on the sensor surface were transformed into reactive *N*-hydroxysuccinimidyl esters with N,N,N',N'-Tetramethyl-O-(N-succinimidyl)uronium tetrafluoroborate (TSTU) in this way: A sensor chip was immersed in solution of TSTU in argon (≥99.999%)-bubbled DMF (1 mg/ml), and slightly shaked at a temperature of 20°C for 1 h. The sensor chip was rinsed with water, dried with nitrogen and immediately mounted into the SPR instrument.

Streptavidin attachment was performed *in situ* (Figure 3) by flowing sodium acetate (SA) buffer until the baseline was achieved, then SA solution with 50 µg/ml of streptavidin was brought into the contact with the sensor surface for 15 minutes. Then the SA buffer was injected again. After short chip incubation with 10 mM phosphate buffer containing sodium chloride at concentration of 0.75 M, pH 7,4 at 20°C (PBNa) to remove all non-covalently bound ligands from the surface, the sensor surface was flushed with SA again. Phosphate buffer with addition of magnesium ions (PBM) was injected. Solutions of biotinylated oligonucleotide targets (BdO_{23} and BdA_{23}, respectively) were flowed along the sensor surface for 15 minutes at concentration of 50nM followed with PBM injection.

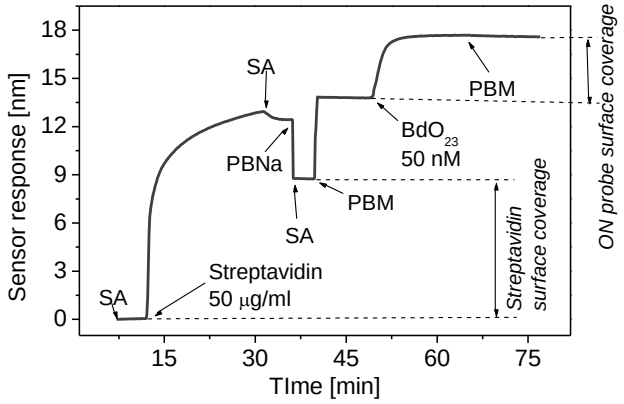

Figure 3 A typical sensorgram corresponding to DNA chip functionalization with MHA method; The resulting streptavidin and ON probe surface densities are indicated. Arrows indicate time of injection of solution of particular analyte or buffer.

As you can see from figure 3, streptavidin and oligonucleotide probe surface densities can be determined from measured sensorgrams. These values in dependence of various factors, such as molar fraction of MHA, concentration of TSTU, use of inert argon atmosphere during activation process, buffer salt composition, pH, and ON probe spacer length were monitored.

BAT method

A 4:1 molar mixture of C_{11}-chained di(ethylene glycol) alkanethiol (OEG) and biotinylated alkanethiol (BAT) was dissolved in absolute ethanol with a total thiol concentration of 100nM [50, 51]. The C_{15}-chained alkanethiol chain linked to a biotin head group by three ethylene glycol groups, was used as the specific binding element. The clean sensor chips were immersed in BAT/OEG thiol solution as it was described above and stored for up to 2 days at room temperature. After cleaning the sensor surface with ethanol and water, the sensor chips were mounted into SPR instrument. Streptavidin solution (50 µg/ml) in PB buffer was flowed along the sensor surface for 15 minutes. After short-time switching to PB buffer, PBM buffer was injected. Fifteen-minutes incubation of probes BdO_{23} and BdA_{23}, respectively, both at concentration of 50 nM was followed.

2.4 Detection of DNA hybridization on surface prepared using both MHA and BAT method

Detection of ON hybridization: Hybridization buffer (PB or PBS buffer with addition of magnesium and/or natrium ions in concentration range 0-20mM) was flowed over the functionalized sensor surface (measuring and reference) until the stable baseline was achieved. ON target CdO23 in hybridization buffer was injected at concentration of 100nM and incubated for 15 minutes. Hybridization buffer was then injected again.

Regeneration of the sensor surface: Regeneration of the sensor chips was performed using the following procedure: after binding of the target (CdO_{23}) to immobilized probe BdO_{23} in PBM buffer at concentration of 100 nM, the solution was replaced with PBM buffer for a short time. Then, the sensor surface was incubated with the regeneration reagent (2% HCOOH) for 3 minutes and switched to PBM buffer until a stable baseline was achieved. After that, the same solution of target was injected again and the whole procedure was repeated.

Calibration curve measurements: After reaching a baseline with PBM buffer, the ON target CdO_{23} was sequentially injected for 8 minutes over the functionalized sensor surface at concentration of 0.2, 0.5, 1, 2, 5, 10, 25, 100 and 200 nM. PBM buffer was injected again. Between individual injections of CdO23 the sensor surface was regenerated using regeneration procedure described above except for concentrations of CdO_{23} lower than 2 nM for which the regeneration was not carried out (the amount of complexes formed from ONs injected at such low concentrations was much smaller in comparison with the total sensor binding capacity).

2.5 Ellipsometry

Ellipsometric measurements in this study were performed using spectral ellipsometer with a rotating analyzer (SE850, Sentech, Germany). The sensor chips for ellipsometric experiments were functionalized with SAM using the same procedure as it was used for SPR measurements. The cleaned gold chips were used as a reference. The gold permittivity was modeled by a Drude model with three Lorentz oscilators, the thickness of the layer was fixed to 55nm. To achieve a reliable fit, each sensor chip was measured at angles of incidence 50, 60 and 70 degrees in the range from 400 to 1600nm. The measured molar ratios of C16COOH were 0, 0.1, 0.3, 0.6 and 1. Measurements at angles of incidence 50, 60 and 70 degrees in the range from 400 to 800nm was performed in a set of spots on the chip surface to ensure a homogeneity and to estimate an error in the thickness.

3. RESULTS AND DISCUSSION

3.1 Optimizing a self-assembled monolayer formation

To validate the assembly of the alkanethiols and homogeneity of the formed self-assembled monolayer (SAM) on the surface, the thickness of the SAM versus χ(MHA) was measured by optical ellipsometry in a set of spots from different positions of each sensor chip. Refractive index of thiolate layer was supposed to be 1.45. The increasing thickness with the increasing molar fraction of MHA in the mixture of alkanethiols was measured (Figure 4). Especially for the χ(MHA) of 0.3, the averaged thickness of the SAM of (1.8±0.1) nm was obtained.

The standard deviation error of 12% shows a good homogeneity of the SAM formed in the whole area of the sensor surface.

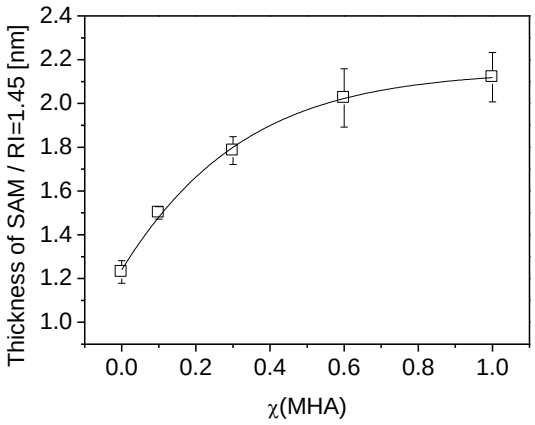

Figure 4 A thickness of alkanethiolate monolayer formed on gold sensor surface in dependence on the MHA molar fraction in solution of MHA/OEG alkanethiols prepared before chip incubation.

To find an optimal molar fraction of MHA in MHA/OEG solution that was prepared for formation of SAM on the clean gold sensor surface, a set of sensor chips covered with SAM of different MHA fraction was prepared. A total concentration of alkanethiols in SAM solution was hold constant (1 mM) and the molar fraction of MHA was varied from 0 - 1. Streptavidin binding was then monitored in four different sensing channels on each individually prepared sensor chip under the same binding conditions. The resulting surface density vs. molar fraction of MHA is shown in the Figure 5. It was found that **χ(MHA) of 0.3** was sufficient value that reaches the maximal streptavidin coverage.),

In the study of Lahiri et al. [41], the same value (0.3) of longer chained alkanethiol fraction present in a mixed formed SAM was observed to reach the maximal sensor coverage with other proteins , i. e. cytochrome c (MW of 12.4 kDa) and lysosyme (MW of 14.4 kDa. Compared to streptavidin (MW of 60 kDa) these proteins are much smaller and thus of higher diffusivity coeficient. This result suggests that streptavidin diffusion through the flow cell to the sensor surface under the measuring conditions (streptavidin concentration of 50µg/ml, flow rate 30µl/min, flow cell dimensinons) did not influence the binding reaction (amide bond formation) A specificity of streptavidin binding was confirmed using sensor chip pretreated only with OEG (χ(MHA)=0.0). No significant sensor response to streptavidin binding to the SAM composed of OEG was found (Figure 5).

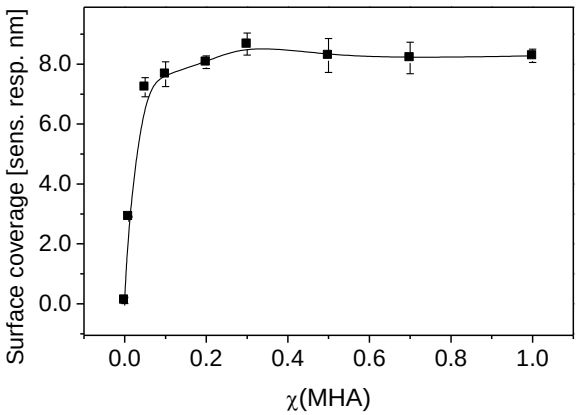

Figure 5 Streptavidin surface coverage on activated SAM in dependence of molar fraction of MHA. Total thiol concentration was 1 mM, streptavidin was injected in SA buffer for 15 minutes at concentration of 50µg/ml. Non-covalently bound ligands were removed from the surface by short-time washing the surface with PBNa buffer. The final streptavidin level was determined as a wavelength shift between the sensor response obtained after 10 minutes washing of the streptavidin surface with PB buffer (injected after incubation with PBNa buffer) and the level of the PB before injection of streptavidin.

3.2 Optimizing activation of carboxylic groups

After washing the sensor chip in ethanol and water, each sensor chip was immersed in activation solution to create the reactive NHS-esters. The *N,N,N',N'*-Tetramethyl-*O*-(*N*-succinimidyl)uronium tetrafluoroborate (TSTU) dissolved in DMF as the activation reagent was used [52, 53]. A significant positive effect of inert (argon-degassed) conditions during the activation process was observed (data not shown). Air humidity interfered with formation of NHS-esters and thus could lower the yield of the required reaction.

A strong dependence of percentage of activated carboxylic groups monitored by streptavidin binding on sensor chip activated by TSTU in DMF in argon-degassed conditions on concentration of TSTU in DMF (see Figure 6) was observed. The activation time of 2 hours with slight shaking under argon atmosphere was constant across the performed experiments. This time was previously found to be long enough for activation of maximal amount of carboxylic groups (data not shown). It was found that DMF-solution containing **TSTU at concentration of 2 mg/ml** almost activated the maximal streptavidin-accessible amount of carboxylic groups and thus this concentration was used for all further experiments.

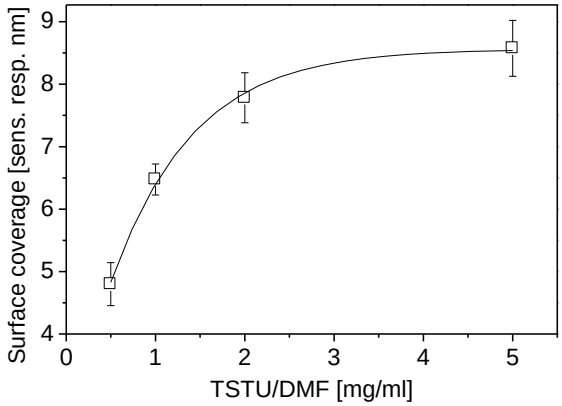

Figure 6 Effect of TSTU concentration on activation efficiency monitored by level of immobilized streptavidin (time of activation: 2 hours, streptavidin was injected over the activated SAM in PB buffer at a concentration of 50µg/ml for 20 minutes at flow rate 30µl/min).

3.3 Optimizing streptavidin binding

Streptavidin binding buffer composition was investigated. MHA molar ratio (0.3), activation process (1 hr under inert atmosphere with TSTU concentration of 2 mg/ml), streptavidin concentration (50 µg/ml), and streptavidin incubation time (20 minutes) were hold constant, A strong dependence of streptavidin coverage on pH and salt concentration of sodium acetate buffer (SA) was observed (Figure 7A). Buffer pH of 5.0 that is by 1 lower than is the value of streptavidin isoelectric point (~6) was found to be optimal to reach the maximal streptavidin coverage. This result is a good agreement with that obtained for other proteins in the study of Lahiri et al. [41]. It was further found that addition of salt (natrium chloride) into streptavidin binding solution significantly decreased the streptavidin coverage. This effect is probably caused by the fact that added ions can decrease the electrostatic attraction between the positively charged streptavidin and slightly negatively charged sensor surface of mixed alkanethiolates.

To confirm the streptavidin binding activity after immobilization at particular conditions displayed in the Figure 4A, biotinylated probe coupling to free streptavidin layer was monitored. The concentration of ON probes (100nM), binding buffer (PB) and incubation time were constant. The resulting ON probe surface coverage levels are shown in the Figure 7B. It was found that maximal streptavidin coverage yields also maximal sensor coverage with ON probes suggesting that there are not any steric hindrances or repulsions in probe binding process due to the high streptavidin density.

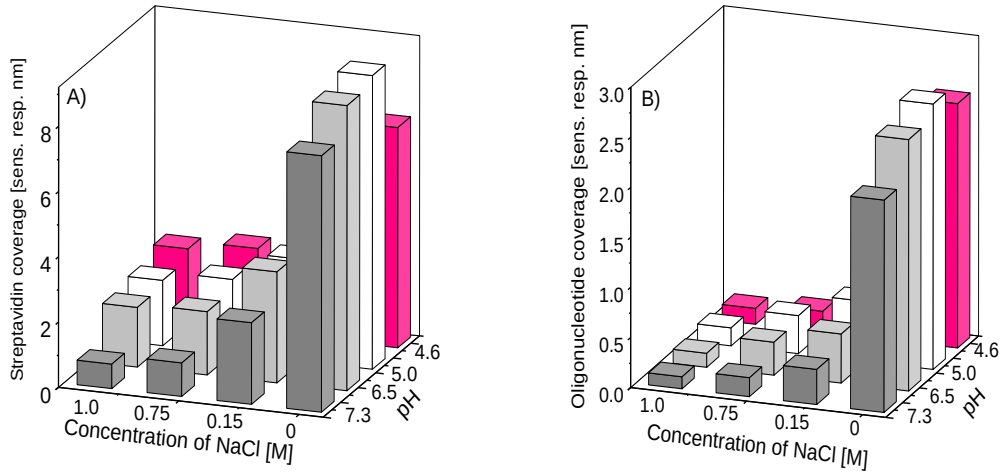

Figure 7 Streptavidin binding buffer optimization: A) Effect of salt concentration and pH on streptavidin binding carried out in 1 mM sodium acetate buffer, B) Immobilized levels of oligonucleotide probes BdO_{23} that were injected at concentration of 100nM in PB buffer over streptavidin layer prepared in SA buffer by the particular conditions displayed in the Figure 6A; (The values of NaCl concentrations and pH displayed in Figure 4B are referred to streptavidin binding buffer)

Effect of streptavidin concentration in injected SA buffer solution (incubation time was 20 minutes) was investigated. Figure 8 shows the final streptavidin coverage levels (that were averaged from four independent experiments) in dependence on streptavidin concentration in injected solution. From that we concluded that concentration of **50 µg/ml** was a good compromise between sample consumption and immobilized ligand density, so we used this concentration in all other experiments.

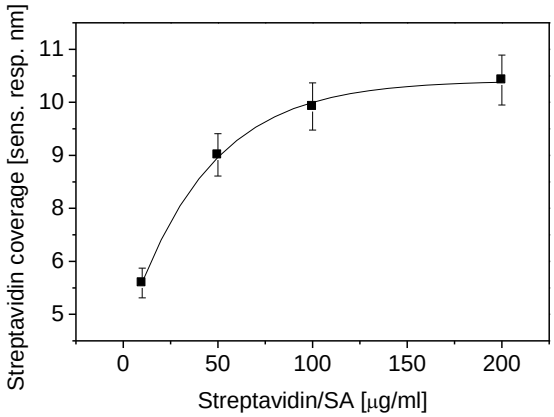

Figure 8 Surface coverage with streptavidin (in sensor units) in dependence on streptavidin concentration in SA buffer (interaction time 20 minutes, flow rate 30 µl/min). Streptavidin solutions were injected with concentrations of 10, 50, 100 and 200µg/ml, respectively, were injected into

individual sensing channels over the activated sensor surface. The final levels were averaged from four individual sensor chips.

3.4 Optimizing biotinylated probe binding

Oligonucleotide probes used in this study were modified with biotin at their 5'-end through the inserted spacer. The probe binding buffer was PB, concentration of probe (BdO_{23}) was 50 nM, and incubation time was 15 minutes. Tri(ethyleneglycol) (TEG) was chosen as a spacer due to its slightly hydrophilic properties, which makes this spacer well compatible with the proteins and NAs. This spacer length was optimized herein. The obtained probe coverage levels for spacer lengths (TEG), 2x(TEG), and 3x(TEG) were 2.2 nm, 3.7 nm and 3.6 nm, respectively, after conversion to unique molecular weight of probes, showing a a surprisingly high effect of spacer length on probe binding to streptavidin pockets. The highest probe coverage was obtained for a probe containing a spacer with length of 2x(TEG) (=hexa(ethyleneglycol))). This longer spacer probably increased the mobility of the bound ONs that increased the accessibility of unbound streptavidin binding sites and thus the probability of binding of another probe molecule to free streptavidin pocket was higher. Further increase of probe coverage with increasing of spacer length was not observed, thus the hexa(ethyleneglycol spacer was the chosen as the optimal length.

The concentration-dependent sensor response to binding of BdO_{23} probe containing hexa(ethyleneglycol spacer is shown in the Figure 9. It was found that under experimental conditions the **probe concentration** in PB buffer solution **of 50nM** is sufficient enough to reach the saturation level of accessible streptavidin binding sites. The specificity of the biotinylated probe-streptavidin binding was confirmed with the flowing of BdO_{23} at concentration of 1 µM for 20 minutes along the surface functionalized with bovine serum albumin. No response was observed (data not shown).

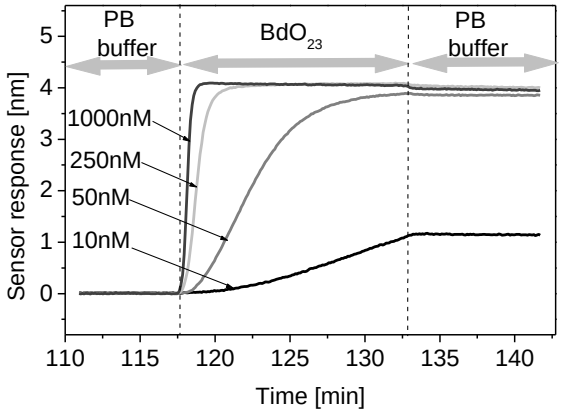

Figure 9 Sensor response to biotinylated probe (BdO_{23}) binding with different concentration to streptavidin layer; binding buffer was PB, incubation time was 15 minutes.

3.5 Optimizing target binding

As it was shown in the part 3.4, concentration of 23-mer probe of 50 nM is sufficient to reach the saturation level on streptavidin surface under the experimental conditions and similarly the target concentration of 100nM was found to reach the probe saturation level (Figure 12A). Using these oligonucleotide concentrations and using previously optimized parameters, an hybridization efficiency (=percentage of immobilized probes present in complexes with complementary oligonucleotide target) was investigated.

To increase the hybridization efficiency (HE%), effect of $MgCl_2$ concentration in hybridizing buffers (PB and PBS) was studied. Hybridization efficiency was than calculated as a HE% = saturation level of bound CdO_{23} [nm] / saturation level of BdO_{23} [nm] x 1.1. Coefficient 1.1 was a conversion factor to different molecular weights of BdO_{23} (7.9 kDa) and CdO_{23} (7.0 kDa). A strong dependence of HE% on concentration and types of present ions was observed (Figure 10). The best hybridization conditions were measured in the presence of high concentration of magnesium ions (concentration of $MgCl_2$ in PB was higher than 15mM). That shows a stabilizing effect of magnesium divalent ions on surface-based DNA hybridization of short oligonucleotides. Addition of magnesium ions into the buffer containing NaCl at concentration of 137 mM (PBS) had not such positive effect on HE% as it was observed for PB buffer. This suggests that high concentration both of monovalent and divalent ions in hybridizing buffer has a negative effect on HE%. Presence of monovalent and divalent ions in hybridizing solution can increase the probe-target repulsion and thus to reduce the oligonucleotide complex fomration Buffer of composition of 10 mM phosphate buffer, 15 mM $MgCl_2$, pH 7.4 at 20°C (=PBM) was used in all other experiments for binding of oligonucleotides (probes and targets).

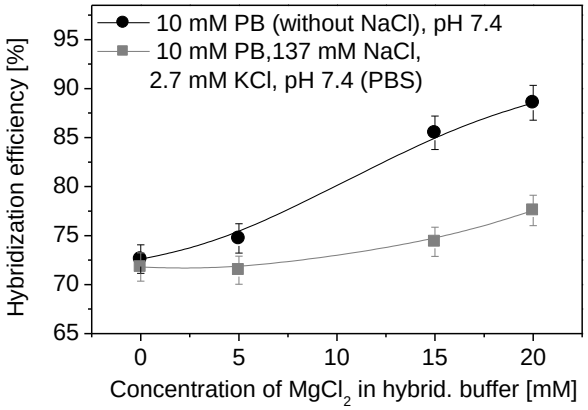

Figure 10 Effect of concentration of addition of NaCl and $MgCl_2$ into the hybridizing buffer on hybridization efficiency. Targets with complementary sequence were injected over the streptavidin/probe layer in hybridization phosphate buffer at concentration of 100 nM for 15 minutes.

It was observed by other SPR groups, that HE% of surface-hybridization is strongly dependent on density of immobilized probes, and the decreasing HE% with increasing probe density was reported [32, 49]. Hybridization efficiencies as high as 60% have been reported for amine coupling chemistry in case of maximal density of immobilized probes on the sensor surface [49]. Using MHA method with optimized parameters reported herein the HE% of ≥85% was achieved in case of a maximal available probe density.

3.6 MHA functionalization procedure with optimized parameters

The procedure of functionalization of the DNA-chip via MHA method with the optimized parameters was summarized as follows:

Clean the sensor surface (gold) in UV ozone cleaner for 15 minutes, exhaustively wash it with water (milliQ) and dry with nitrogen stream. Immerse the clean sensor chip into alkanethiolate OEG and MHA ethanol solution at a total thiol concentration of 1 mM with a MHA molar fraction of 0.3 at temperature of 40°C. After 10 minutes incubation at 40°C store the chip in this solution in a dark place at room temperature for up to 2 days. Rinse the chip with ethanol, dry with nitrogen stream, rinse with water and dry with nitrogen again. Immerse the sensor chip in solution of TSTU in argon degassed DMF (2 mg/ml), and slightly shake it for 1 h under inert atmosphere. Then rinse the sensor chip with water, dry with nitrogen and immediately mount it into the SPR instrument.

After short-time incubation of the sensor surface with SA buffer, inject streptavidin in SA buffer at concentration of 50 µg/ml for 15 minutes at room temperature with flow rate 30 µl/min. Switch to SA buffer again. Flow with PBNa buffer along the streptavidin coated surface for 5 minutes to remove all non-covalently bound ligands. Flush the sensor surface again with SA to monitor the final streptavidin immobilization level. Switch to PBM buffer. Inject a solution of biotinylated oligonucleotide targets at concentration of 50 nM until the plateau is achieved (typically for 15 minutes using flow rate 30 µl/min). Switch to PBM buffer again. When the stable baseline is reached, the sensor is ready for ON targets detection.

The reproducibility of DNA and RNA chips preparation was calculated from the ON probe coverage values obtained from 7 individually prepared sensor chips and 3 channels per one sensor chip. The chip-to-chip reproducibility was 91%, on-chip reproducibility was 96% (in terms of standard deviation calculations). Figure 11 shows the sensor response to BdO_{23} binding to streptavidin obtained from 3 individual sensing channels.

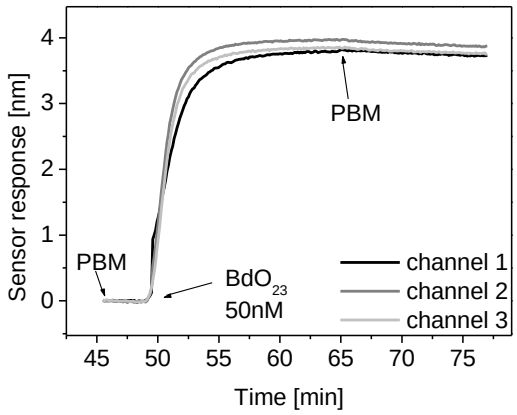

Figure 11 Sensorgrams corresponding to BdO23 probe binding to streptavidin obtained from three individual sensing channels; concentration of BdO23 was 50nM, sensor chip was prepared using optimized MHA method

3.7 Detection of DNA hybridization using an SPR sensor functionalized by optimized MHA method

A high specificity and chip-to-chip reproducibility (≥95%) of ON hybridization detection via the optimized-MHA-method functionalization was reported in our previous study [18].

The regeneration procedure to remove target molecules from immobilized probes without lost of probe hybridization activity was applied using 2% freshly prepared solution of formic acid and incubation time of 3 minutes. It was confirmed from the experiments including repeated injection of CdO_{23} at concentration of 100 nM followed with the regeneration procedure, the sensor did not significantly lose its sensitivity to ON hybridization detection for minimally 10 measurement/regeneration cycles (data not shown here).

Sensor response to ON hybridization detection represented by increasing concentration of CdO_{23} in the range 0.2nM – 200nM on MHA-method functionalized sensor chip is displayed in Figure 12A. A detail of detection of ON hybridization for low target concentrations is shown in the Figure 12B. After measurement with CdO_{23} at concentration of ≥2nM the sensor surface was regenerated using the protocol that was described above. The theoretical noise-limited detection limit of the SPR sensor was calculated as the analyte concentration that generates the sensor response of the triple of baseline noise standard deviations and was determined to be 100 pM (see Figure 12B). The lowest concentration of 23-mer ON target that was detected with reported reproducibility (>95%) [18] was 200 pM (Fig. 12B).

The calibration curve of developed ON-sensor was determined as the binding rate of ON target binding curve injected at particular concentration versus that concentration. This approach was previously shown to be suitable for rapid biosensor data analysis [54]. The resulting calibration curve is displayed in Figure

12C. The linearity of the measured calibration curves is in a good agreement with the theoretical Langmuir isotherm of concentration-dependent target binding profile.

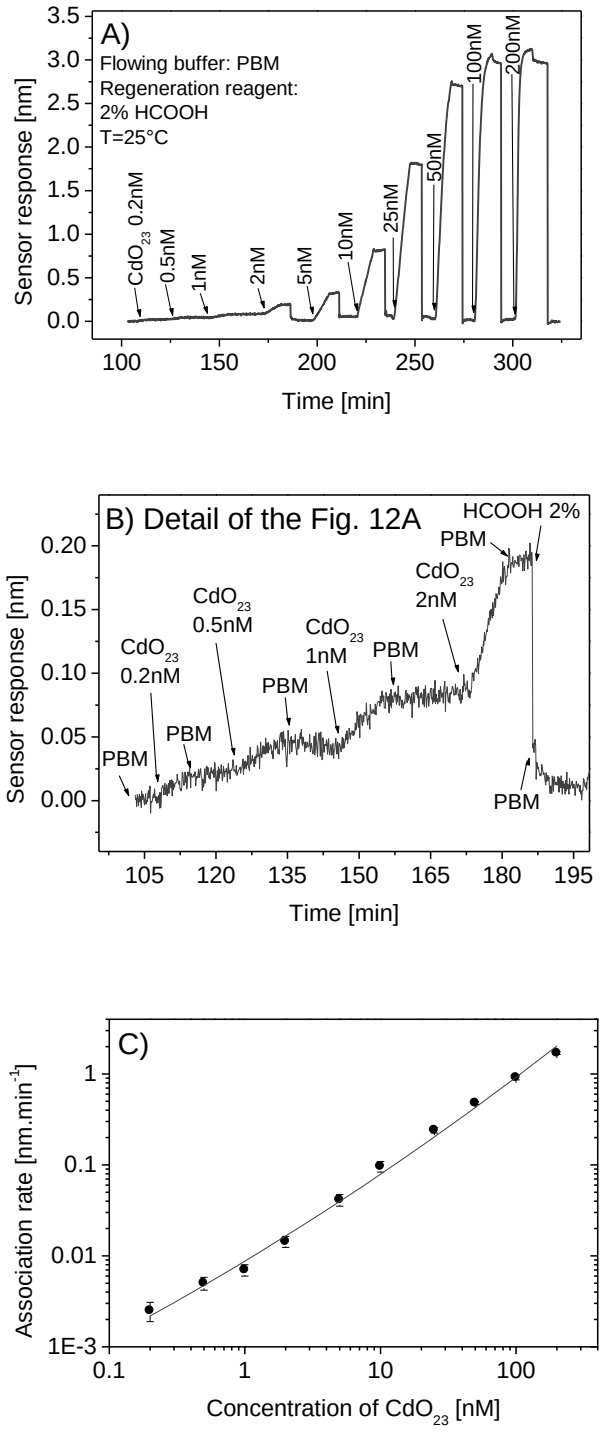

Figure 12 Detection of ON (23-mer) hybridization on sensor chip functionalized with BdO_{23} probe using the optimized MHA method; A) Sensor response to increasing concentration of CdO_{23} target (incubation time 8 minutes, regeneration of the sensor surface was performed using 2%

HCOOH in 3 minutes long flowing) B) a detail of the ON hybridization detection for the target concentration range 0.2 nM- 2nM. C) a resulting sensor calibration curve ;the measuring metrics were switched off during incubation of sensor surface with HCOOH due to its high resonant shift that was not under our study.

3.8 A comparison of MHA and BAT functionalization methods

Detection of ON hybridization was carried using the sensor chips prepared via both MHA (with optimized parameters) and BAT methods. The summary of results is shown in the Table 1. A high probe/streptavidin binding ratio (~3.2) for optimized MHA method suggests a very good accessibility of streptavidin to ON probes binding and thus very good streptavidin binding efficiency (at average only one binding pocket became to be inaccessible for biotinylated probe after streptavidin immobilization). The achieved probe/streptavidin ratio is more than two times higher in comparison with the value of ~1.2 that was determined for maximal sensor coverage with the streptavidin and probes in the work of Su et al. [55] for amine coupling chemistry without optimizing parameters. This difference is probably due to better accessibility of NHS-esters followed with higher mobility of streptavidin in the SAM in our approach, because longer chained (C_{16}) reactive alkanethiols were present in the SAM compared to C_{11} chained alkanethiols in reference study. Our results suggest that by the optimizing functinalization conditions the streptavidin can be attached to the sensor surface with high density as well as without significant disruption of its biological activity.

The streptavidin/probe binding ratio for BAT method (~1.7) was comparable with that obtained in the reference study (~1.5) [49]. This value is still lower than expected value of 2 when assuming that two binding sites were not occupied after streptavidin binding to biotin-terminated alkanethiols. The reason for that is maybe in steric hindrances due to tight arrangement of streptavidin molecules on the sensor surface. By varying the BAT/OEG ratio and other immobilization parameters we could probably get closer to the expected value of 2.

The hybridization efficiency (86%) of MHA method achieved on the sensor surface with maximized probe coverage was much higher than the HE% obtained for BAT method (64%). This result suggest a very good availability of by MHA-method immobilized probes for ON target detection showing a great potential of this method for highly sensitive ON hybridization detection.

Table 1 A comparison of optimized MHA method and BAT method in terms of ligands coverage levels, biotinylated probe/streptavidin ratio and hybridization efficiency

Step	MHA method with optimized parameters	BAT method
Streptavidin	(8.9 ± 0.7) nm	(13.0 ± 0.7) nm
Biotinylated probe	(3.8 ± 0.3) nm	(2.9 ± 0.1) nm
Target	(2.9 ± 0.3) nm	(1.7 ± 0.1) nm
Biotinylated probe/streptavidin ratio	3.2	1.7
Hybridization efficiency	86%	64%

4. CONCLUSIONS

A method of DNA chip functionalization (MHA method) based on formation of self-assembled monolayer followed with covalent attachment of streptavidin and non-covalent biotinylated oligonucleotide binding was investigated using an home-made multi-channel SPR biosensor and optical ellipsometry herein. A systematic optimization of parameters influencing the ligand density and activity such as buffers salt composition, pH, reagent concentrations, spacer length, etc. was carried out to develop a robust, effective and reproducible DNA chip functionalization method. The resulting procedure of oligonucleotide immobilization was shown to be highly reproducible (≥91% and ≥95% for chip-to-chip and on-chip reproducibility, respectively) with the small ON probe consumption (concentration of probe of 50nM was found to reach the saturation level of the streptavidin layer). The high efficiency of streptavidin immobilization was shown because more than three binding sites per one immobilized streptavidin molecule were available for biotinylated probe binding. It was further shown that SPR sensor with this optimized immobilization method enables a rapid direct detection of short oligonucleotides with high specificity, reproducibility and regenerability over the three orders of magnitude of target concentration (100 pM – 200 nM). The resulting sensor detection limit of 100pM for 23-mer oligonucleotides was one hundred times lower than typically reported detection limits of SPR-based direct ON detections.

The resulting sensor performance was compared to previously optimized and well establish method of streptavidin immobilization to biotin-terminated alkanethiols (BAT method). Using approach optimized in this work, a significant increase of hybridization efficiency was achieved (86% for MHA method vs. 63% for BAT method in case of maximal available sensor coverage with streptavidin of biotinylated probes).

The results show a great potential of application of optimized protocol of MHA method in further SPR microarray technology.

5. REFERENCES

1. Drmanac R, Drmanac S, Strezoska Z, Paunesku T, Labat I, Zeremski M, Snoddy J, Funkhouser WK, Koop B, Hood L, Crkvenjakov R (1993) Science 260: 1649
2. Burgener M, Sanger M, Candrian U (2000) Bioconjugate Chemistry 11: 749
3. Breslauer KJ, Frank R, Blocker H, Marky LA (1986) Proceedings of the National Academy of Sciences of the United States of America 83: 3746
4. Doktycz MJ, Morris MD, Dormady SJ, Beattie KL (1995) Journal of Biological Chemistry 270: 8439
5. Hanus J, Barvik I, Ruszova-Chmelova K, Stepanek J, Turpin PY, Bok J, Rosenberg I, Petrova-Endova M (2001) Nucleic Acids Res 29: 5182
6. Hianik T, Gajdos V, Krivanek R, Oretskaya T, Metelev V, Volkov E, Vadgama P (2001) Bioelectrochemistry 53: 199
7. Nair TM, Myszka DG, Davis DR (2000) Nucleic Acids Research 28: 1935
8. Nilsson P, Persson B, Uhlen M, Nygren PA (1995) Analytical Biochemistry 224: 400
9. Wang L, Carrasco C, Kumar A, Stephens CE, Bailly C, Boykin DW, Wilson WD (2001) Biochemistry 40: 2511
10. Goodrich TT, Lee HJ, Corn RM (2004) J Am Chem Soc 126: 4086
11. Heller MJ (2002) Annu Rev Biomed Eng 4: 129
12. Pinkel D, Segraves R, Sudar D, Clark S, Poole I, Kowbel D, Collins C, Kuo WL, Chen C, Zhai Y, Dairkee SH, Ljung BM, Gray JW, Albertson DG (1998) Nat Genet 20: 207
13. Pollack JR, Perou CM, Alizadeh AA, Eisen MB, Pergamenschikov A, Williams CF, Jeffrey SS, Botstein D, Brown PO (1999) Nat Genet 23: 41
14. Peter C, Meusel M, Grawe F, Katerkamp A, Cammann K, Borchers T (2001) Fresenius J Anal Chem 371: 120
15. Persson B, Stenhag K, Nilsson P, Larsson A, Uhlen M, Nygren PA (1997) Analytical Biochemistry 246: 34
16. Nilsson P, Persson B, Larsson A, Uhlen M, Nygren PA (1997) Journal of Molecular Recognition 10: 7
17. Rich RL, Myszka DG (2005) Journal of Molecular Recognition 18: 431
18. Vaisocherová H, Zítová A, Lachmanová M, Štěpának J, Rosenberg I, Králíková Š, Liboska R, Rejman D, Homola J (2006) Biopolymers
19. Schuck P (1997) Annual Review of Biophysics and Biomolecular Structure 26: 541
20. Zhao Y, Kan ZY, Zeng ZX, Hao YH, Chen H, Tan Z (2004) Journal of the American Chemical Society 126: 13255
21. Sugimoto N, Wu P, Hara H, Kawamoto Y (2001) Biochemistry 40: 9396
22. Piliarik M, Vaisocherova H, Homola J (2005) Biosensors & Bioelectronics 20: 2104
23. Shumaker-Parry JS, Aebersold R, Campbell CT (2004) Analytical Chemistry 76: 2071
24. Wang RH, Minunni M, Tombelli S, Mascini M (2004) Biosensors & Bioelectronics 20: 598
25. Su X, Wu YJ, Knoll W (2005) Biosens Bioelectron 21: 719
26. Asensio JL, Dosanjh HS, Jenkins TC, Lane AN (1998) Biochemistry 37: 15188
27. Kukanskis K, Elkind J, Melendez J, Murphy T, Miller G, Garner H (1999) Analytical Biochemistry 274: 7
28. Bates PJ, Reddoch JF, Hansakul P, Arrow A, Dale R, Miller DM (2002) Analytical Biochemistry 307: 235
29. Piscevic D, Lawall R, Veith M, Liley M, Okahata Y, Knoll W (1995) Applied Surface Science 90: 425
30. Shankaran D, Gobi K, Sakai T, Matsumoto K, Toko K, Miura N (2005) Biosensors and Bioelectronics 20: 1750
31. Johnsson B, Lofas S, Lindquist G (1991) Analytical Biochemistry 198: 268
32. Peterson AW, Heaton RJ, Georgiadis RM (2001) Nucleic Acids Research 29: 5163

33. Bamdad C (1998) Biophysical Journal 75: 1989
34. Mannelli I, Minunni M, Tombelli S, Wang R, Michela Spiriti M, Mascini M (2005) Bioelectrochemistry 66: 129
35. Tombelli S, Mascini M, Turner APF (2002) Biosensors & Bioelectronics 17: 929
36. Chinowsky TM, Jung LS, Yee SS (1999) Sensors and Actuators B-Chemical 54: 89
37. Gonzalez L, Boyle RW, Zhang ML, Castillo J, Whittier S, DellaLatta P, Clarke LM, George JR, Fang XD, Wang JG, Hosein B, Wang CY (1997) Clinical and Diagnostic Laboratory Immunology 4: 598
38. Hendrickson WA, Pahler A, Smith JL, Satow Y, Merritt EA, Phizackerley RP (1989) Proceedings of the National Academy of Sciences of the United States of America 86: 2190
39. Lofas S, Johnsson B, Edstrom A, Hansson A, Lindquist G, Hillgren RMM, Stigh L (1995) Biosensors & Bioelectronics 10: 813
40. Oshannessy DJ, Brighamburke M, Peck K (1992) Analytical Biochemistry 205: 132
41. Lahiri J, Isaacs L, Tien J, Whitesides GM (1999) Analytical Chemistry 71: 777
42. Ohlson S, Jungar C, Strandh M, Mandenius CF (2000) Trends in Biotechnology 18: 49
43. Knoll W, Zizlsperger M, Liebermann T, Arnold S, Badia A, Liley M, Piscevic D, Schmitt FJ, Spinke J (2000) Colloids and Surfaces a-Physicochemical and Engineering Aspects 161: 115
44. Busse S, Scheumann V, Menges B, Mittler S (2002) Biosens Bioelectron 17: 704
45. Homola J, Lu HBB, Nenninger GG, Dostalek J, Yee SS (2001) Sensors and Actuators B-Chemical 76: 403
46. Dostalek J, Vaisocherova H, Homola J (2005) Sensors and Actuators B-Chemical 108: 758
47. Nenninger GG, Piliarik M, Homola J (2002) Measurement Science & Technology 13: 2038
48. Liedberg B, Lundstrom I, Stenberg E (1993) Sensors and Actuators B-Chemical 11: 63
49. Su XD, Wu YJ, Robelek R, Knoll W (2005) Langmuir 21: 348
50. Jung LS, Nelson KE, Stayton PS, Campbell CT (2000) Langmuir 16: 9421
51. Ladd J, Boozer C, Yu Q, Chen S, Homola J, Jiang S (2004) Langmuir 20: 8090
52. Knorr R, Trzeciak A, Bannwarth W, Gillessen D (1989) Tetrahedron Letters 30: 1927
53. Wester HJ, Hamacher K, Stocklin G (1996) Nuclear Medicine and Biology 23: 365
54. Edwards PR, Leatherbarrow RJ (1997) Analytical Biochemistry 246: 1
55. Larsson C, Rodahl M, Hook F (2003) Analytical Chemistry 75: 5080

Appendix X

H. Vaisocherová, J. Snášel, I. Rosenberg, and J. Homola:

Direct monitoring of HIV-1 Integrase strand transfer activity by surface plasmon resonance biosensor

Manuscript in preparation

Direct Monitoring of HIV-1 Integrase Strand Transfer Activity by Surface Plasmon Resonance Biosensor

Authors: Hana Vaisocherová[1,2*], Jan Snášel[3]* Ivan Rosenberg[3], Praskovia Boltovets[1], Josef Štěpánek[2], Jiří Homola[1*]

[1]Institute of Radio Engineering and Electronics, Academy of Sciences of the Czech Republic, Chaberská 57, 182 51 Prague, Czech Republic
Tel: +420 266773563, Fax: +420 284681534
E-mail: homola@ure.cas.cz

[2]Charles University, Faculty of Mathematics and Physics, Ke Karlovu 3, 121 16 Prague, Czech Republic

[3]Institute of Organic Chemistry and Biochemistry, Academy of Sciences of the Czech Republic, Flemingovo n. 2, 166 10 Prague, Czech Republic

* equally corresponding authors

Keywords: surface plasmon resonance biosensor, HIV-1 Integrase, strand transfer reaction

Integration of a double-stranded DNA copy of the human immunodeficiency virus (HIV) genome into the host cell chromosome is a crucial step in HIV replication and therefore presents an attractive target for drug development. The process of integration is catalyzed by retroviral integrase (IN). The catalysis proceeds in two reactions: 3'-processing reaction, where 5' phosphorylated dimer (pGT) is specifically cleaved from both ends of viral long terminal repeats (LTR) yielding a processed DNA and strand transfer reaction, in which the exposed 3'-hydroxyl groups of the processed ends are joined to 5' phosphates in the host DNA [1]. The catalytical activity of IN has been demonstrated *in vitro* using oligonucleotide (ON) substrates that mimic the viral LTR ends [2, 3] and techniques such as polyacrylamide gel electrophoresis (PAGE) [4], fluorescence resonance energy transfer (FRET) [5] or microtiter plate assays [6, 7]. However, these methods yielded different DNA-binding specificity or activity [2, 8]. Moreover, these techniques are rather laborious and require fluorescent or radioactive labeling thus increasing the complexity of the assay.

In this work, we demonstrate label-free monitoring of IN strand transfer activity using a surface plasmon resonance (SPR) biosensor. In addition, the effect of four different divalent metal cofactors (Mn^{2+}, Mg^{2+}, Ni^{2+} and Co^{2+}) on IN binding ability to LTR mimic as well as to triplex ON was also examined. The results obtained using the SPR method were compared with those obtained from PAGE.

SPR biosensors are based on measuring refractive index changes in the proximity of a metal (gold) surface which are produced by the binding of analyte to its biospecific partner immobilized on the metal surface [9]. In this work, we employ a recently developed eight-channel SPR sensor based on spectroscopy of surface

plasmons and wavelength division multiplexing [10]. Each sensing channel of a sensor chip coated with self-assembled monolayer of alkanethiols with covalently immobilized streptavidin, was functionalized with biotinylated ONs[11]. For monitoring of the IN-catalysed strand transfer, four sensing channels were modified with the un-processed ds-LTR mimic (23-mer) (SS'_{23}) with terminal ...CAGT-3' sequence and four channels with triplex T_{23}*A_{23}*T_{23} used as a reference. .

Solutions of IN with particular metal cofactor were injected into the appropriate channels (each type of metal cofactor per one pair of measuring and reference channels was used), Figure 1. It was found that IN forms stable complexes with both ds-LTR mimic and triplex in the presence of all examined ions. The amount of enzyme that remained bound to ONs after washing the sensor surface with buffer was in average 1.5-times higher for triplex than for ds-LTR mimic. The amount of bound enzyme to both ds-LTR mimic and triplex in the presence of Mg^{2+} and Mn^{2+} cofactors was up to two times higher than in the presence of Co^{2+} and Ni^{2+}. This suggests that Mg^{2+} and Mn^{2+} cofactors stabilize the IN-DNA complex much better than remaining cations. While Mn^{2+} exhibits the highest stabilizing effect on the binding of IN to ds-LTR mimic , the Mg^{2+} is generally known to stabilize the triplex DNA [12] as well as better binding of IN to triplex. As demonstrated previously, IN forms stable complexes with both DNAs in the presence of metal ions[1]. The ds-LTR mimic binds preferentially to the catalytic site of IN but also in some extent to other sites in the IN multimer, thus also serving as a target DNA. In contrast, triplex occupies mostly target site within the IN multimer. The existence of the strong metal dependent interaction between IN and DNA triplex and its possible connection with some IN function is subject of further study. Similarly, the strong binding of IN to „Y" intermediate has been previously reported and was supposed to be connected with its disintegration activity [13].

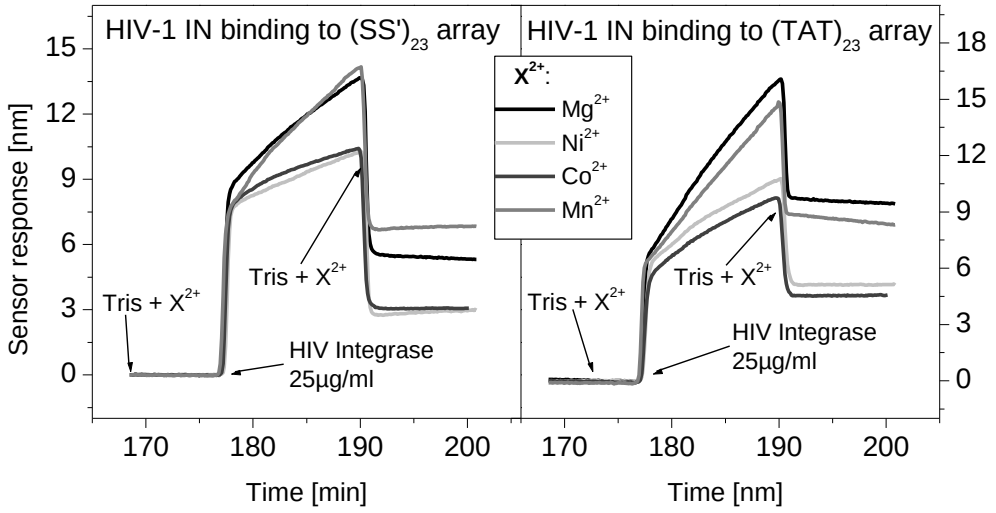

Figure 1 Sensorgrams corresponding to HIV-1 Integrase binding to $(SS')_{23}$ and $(TAT)_{23}$ oligonucleotides in the presence of different metal ions. Concentration of each ion in buffer was 8mM; the arrows indicate the time point of solution injection containing particular ion (X^{2+}). A) Ni^{2+}, B) Mn^{2+}, C) Co^{2+}, D) Mg^{2+}.

To detect the strand transfer reaction, 5´-phosphorylated self-complementary 12-mer ON (pTS_{12}) serving as a target DNA was passed over the surface of the sensing channels with IN-DNA complexes. The arrangement of the strand transfer reaction is schematically shown in Figure 2.

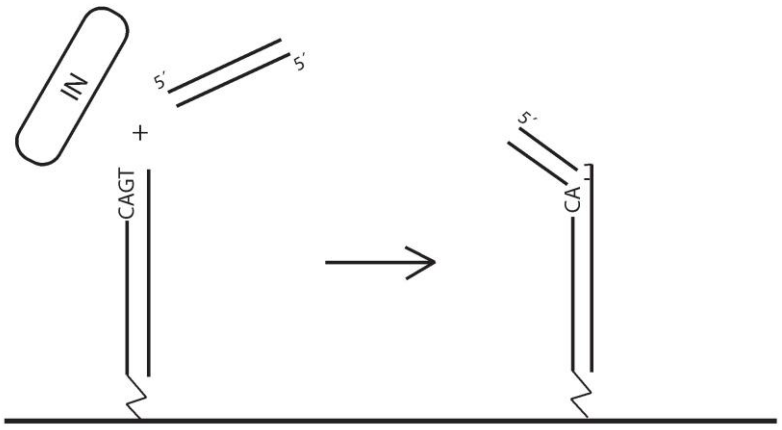

Figure 2 Scheme of the strand transfer reaction monitored using SPR biosensor. In the first step, the ON representing viral LTR end was immobilized on the sensor surface. Then HIV IN was added and shortly incubated with the sensor surface. Finally, the solution of 5'-phophorylated self-complementary 12-mer ON pTS_{12} representing target DNA was injected to the sensing channel. The strand transfer reaction proceeded for 30 min resulting in integration of the immobilized processed viral DNA to the target DNA.

Sensorgram of the strand transfer reaction (Figure 3) shows that the reaction was mostly detected in the presence of Mn^{2+} and moderately detected in the presence of Mg^{2+} ions. This is in agreement with previous reports where *in vitro* strand transfer reaction was preferentially detected in the presence of Mn^{2+} [14] . The fact that pTS_{12} was covalently bound to the SS'_{23} in the presence of Mn^{2+} and Mg^{2+} was confirmed by exhaustive washing of the surface with aqueous 2% formic acid to remove all non-covalently bound ligands. The final increase in sensor response in measuring channels corresponded well to the level obtained from pTS_{12} binding to SS'_{23} (data not shown). These results were reproduced in several independent experiments using *de novo* functionalized chips.

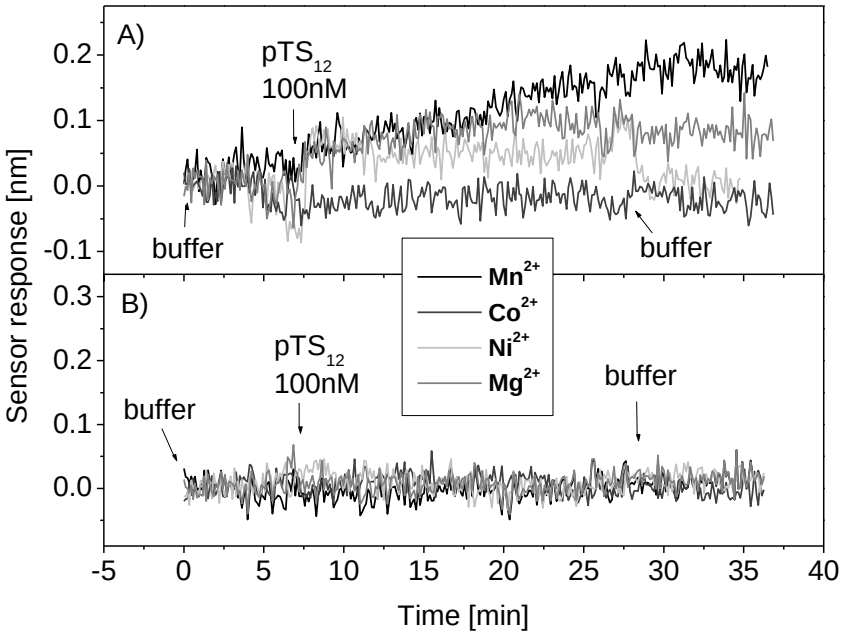

Figure 3 SPR-sensor based monitoring of IN strand transfer activity: Sensor response corresponding to pTS_{12} joining to IN-$(SS')_{23}$ complex (A) and IN-$(TAT)_{23}$ complex in the presence of different metal ions; concentration of pTS_{12} was 100nM, incubation time was 25 min.

To confirm the SPR results, a similar system (the same IN and ONs except for the length of the SS'_{23} that was 21-mer SS'_{21}) employed using radiolabeled ONs and separation of products by PAGE. The product of the strand transfer reaction was observed in the presence of Mn^{2+}. Nevertheless, the actual process of integration could not be monitored using this method.

In conclusion, we demonstrated that the SPR technique allows sensitive label-free real-time observation of strand transfer reaction in the presence of metal cofactors. We anticipate that further advances in SPR sensor instrumentation and functionalization chemistries will allow screening large libraries of compounds as possible inhibitors of the HIV-1 IN activity as well as improving sensitivity of monitoring of strand transfer reaction.

EXPERIMENTAL

Oligonucleotides: Biotinylated 23-mer ON probe representing a viral DNA substrate (S_{23}) was of the sequence biotin-$(TEG)_2$-5'-d(CAG TGT GGA AAA TCT CTA GCA GT)-3'. The homopurine reference probe was of the sequence biotin-$(TEG)_2$-5'-$d(A)_{23}$-3'. S'_{23} (5'-d(ACT GCT AGA GAT TTT CCA CAC TG)-3') and dT_{23} were of complementary base sequences to S_{23} and dA_{23}, respectively. Self-complementary 12-mer serving as the DNA target substrate was of a sequence 5'-d(ACC GAC GTC GGT)-3' (pTS_{12}). The ONs used in PAGE as donor substrates $(OO')_{21}$ were fully complementary; O_{21} was of 5'-d(GTG TGG AAA ATC TCT AGC AGT)-3' sequence.

HIV-1 IN binding (SPR): Chips coated with duplexes (SS'_{23}) (spots 2, 4, 6, 8) and triplexes (TAT_{23}, spots 1, 3, 5, 7) were prepared for detection of IN binding. All the SPR experiments were carried out at room temperature in Tris (20mM Tris, 50mM

NaCl, pH7.4 at 20°C) containing 0.05% BSA with addition of particular divalent ion (Ni^{2+}, Mn^{2+}, Co^{2+} and Mg^{2+}, respectively) at a concentration of 8mM. The solutions were first flowed through the eight channels until the baselines were achieved; solution containing a particular cofactor was flowed along one measuring and one reference surface. Then, in the same order, solutions of HIV-1 integrase with an IN concentration of 25µg/ml in Tris buffer containing particular cofactor were injected. After 15 minutes incubation, buffers were injected again.

Strand transfer reaction (SPR): To study IN strand-transfer activity, buffer solutions with particular divalent ions containing 12-mer ON (pTS_{12}, 100nM) were passed over the surface of the sensing channels after the injection of the HIV IN. The individual reactions proceeded in 25 minutes. Then the particular starting buffers were injected.

ACKNOWLEDGEMENTS

This research was supported by the Czech National Science Foundation (202/05/0628) and the Academy of Sciences of the Czech Republic (AV0Z20670512) and grant No.203/05/P557.

References

[1] J. Yi, E. Asante-Appiah, A. M. Skalka, *Biochemistry* **1999**, *38*, 8458.
[2] D. Esposito, R. Craigie, *Embo J* **1998**, *17*, 5832.
[3] P. A. Sherman, J. A. Fyfe, *Proc Natl Acad Sci U S A* **1990**, *87*, 5119.
[4] R. Craigie, K. Mizuuchi, F. D. Bushman, A. Engelman, *Nucleic Acids Res* **1991**, *19*, 2729.
[5] S. P. Lee, M. L. Censullo, H. G. Kim, J. R. Knutson, M. K. Han, *Anal Biochem* **1995**, *227*, 295.
[6] C. Vink, M. Banks, R. Bethell, R. H. Plasterk, *Nucleic Acids Res* **1994**, *22*, 2176.
[7] D. J. Hazuda, J. C. Hastings, A. L. Wolfe, E. A. Emini, *Nucleic Acids Res* **1994**, *22*, 1121.
[8] K. Hiom, M. Gellert, *Cell* **1997**, *88*, 65.
[9] J. Homola, *Analytical and Bioanalytical Chemistry* **2003**, *377*, 528.
[10] J. Dostalek, H. Vaisocherova, J. Homola, *Sensors and Actuators B-Chemical* **2005**, *108*, 758.
[11] H. Vaisocherová, A. Zítová, M. Lachmanová, J. Štěpának, I. Rosenberg, Š. Králíková, R. Liboska, D. Rejman, J. Homola, *Biopolymers* **2006**.
[12] D. Coman, I. M. Russu, *Nucleic Acids Res* **2004**, *32*, 878.
[13] A. Mazumder, A. Engelman, R. Craigie, M. Fesen, Y. Pommier, *Nucleic Acids Res* **1994**, *22*, 1037.
[14] A. L. Wolfe, P. J. Felock, J. C. Hastings, C. U. Blau, D. J. Hazuda, *J Virol* **1996**, *70*, 1424.

Appendix XI

H. Vaisocherová and J. Homola:

SPR biosensors for medical diagnostics

In Surface Plasmon Resonance Based Sensors, Editor J. Homola,
Springer, September 2006

Springer Ser Chem Sens Biosens (2006) 4: 1–x
DOI 10.1007/5346_022

Published online: ■ May 2006

SPR Biosensors for Medical Diagnostics

Hana Vaisocherová · Jiří Homola (✉)

Institute of Radio Engineering and Electronics, Prague, Czech Republic
homola@ure.cas.cz

Keywords Biosensor · Cancer markers · Detection of antibodies · Detection of disease biomarkers · Detection of hormones · Disease diagnostics · Heart attack markers · Monitoring drug levels · Sensor · Surface plasmon resonance

1 Introduction

Advances in the life sciences (e.g., genomics, proteomics, molecular engineering) have improved the treatment of a wide range of diseases, resulting in an improved public health and a longer life expectancy. In developed countries, lifestyle diseases such as cardiovascular disease have become a major public health concern and one of the leading causes of mortality. Modern health care increasingly involves diagnostic methods based on the monitoring of disease biomarkers in bodily fluids, as some of these markers allow for identification of a disease at its very early stage even before its symptoms can be found. In addition, the monitoring of concentrations of biological markers in bodily fluids can help determine predispositions for the disease and disease progression. Furthermore, the detection of biological markers can help redefine the diseases and their therapies by shifting the emphasis of traditional practices of depending on symptoms and morphology to a more rational objective molecular basis. While biomarkers for certain diseases are established and already in clinical use (e.g., prostate-specific antigen for prostate cancer), the search for reliable diagnostic biomarkers for other diseases continues [1].

Currently, most methods for the determination of biomarkers in bodily fluids are carried out in hospitals or specialized laboratories. These include enzyme-linked immunosorbent assay (ELISA), chemiluminescent, immunofluorescent, radiological, and microscopic assays. The immunoassays utilize antibodies as biomolecular recognition elements and, due to the advances in antibody engineering and synthesis of humanized antibodies [2], present one of the fastest growing diagnostic technologies. However, these methods are rather laborious and time-consuming and offer limited automation and integration of the various operational steps [3]. Detection formats typically require labeling and the use of additional reagents to report binding of the analyte to the receptor [4]. The labeling prolongs assay time, increases costs, and can disturb receptor binding sites leading to false negatives. Moreover, fluorescent compounds are invariably hydrophobic, and in many screening methods, background is a significant problem potentially leading to false positives. Furthermore, at present there are no accepted immunoassay tests for certain serious diseases (e.g., cancer) that are sufficiently specific, sensitive, fast, and economically sustainable.

An ideal screening platform should be rapid, sensitive, specific, robust, simple-to-use, and have sufficient throughput to be widely applicable in medical diagnostics. In addition, the determination of an analyte should preferably be carried out directly in tested samples (e.g., blood, plasma, urine, saliva, cerebrospinal fluid) with limited or no sample preparation. Diagnostic instruments allowing continuous monitoring of analyte concentration, which is not possible using conventional homogeneous and heterogeneous immunoassays, are also desirable. Biosensors present a promising alternative to established diagnostic technologies and can potentially meet many of these requirements. Surface plasmon resonance (SPR) biosensors offer a label-free direct measurement platform for rapid screening of medically relevant analytes. Recent advances in SPR sensor hardware, biorecognition elements and their immobilization, and sensor data analysis have made SPR biosensors a strong candidate for development of new analytical systems for medical diagnostics.

In the following section, we review the state of the art in applications of SPR biosensor technology for detection of disease biomarkers such as antigens and antibodies related to cancer, heart attack, and other diseases. Review of SPR applications in the field of hormone detection and monitoring of drug serum levels is also reported.

2
Cancer Markers

Early diagnosis is the key to successful treatment for most types of cancer. Conventional diagnostic methods such as X-ray imaging, computer tomog-

raphy, or ultrasound are not appropriate for early stage cancer diagnostics because they detect already formed tumors. Detection of biological markers of cancer that are produced as the cancer grows is a helpful tool in cancer diagnostics and monitoring. For example, the prostate-specific antigen (PSA) – a biomarker of prostate cancer – can be detected in blood even before the cancer can be diagnosed by the conventional methods [5]. Diagnostic tests based on detection of biomarkers are non-invasive and less expensive than conventional methods such as biopsy of tissues (liver, kidneys, and testicles) and examinations involving mammography, ultrasonography, X-ray imaging instruments, or radiological and cytological devices. This makes cancer biomarker tests more applicable to large scale population screening, or repetitive screening of an individual [6].

There is a vast effort in research laboratories worldwide to identify new cancer biomarkers present in the circulatory system [7] and gene markers present in the human genome [8]. In the past two decades, hundreds of thousands of substances have been investigated as potential biomarkers for cancer diagnosis, but only about 50 serological tumor markers are currently available [9] and only 12 cancer biomarkers are recognized by the US Food and Drug Administration (FDA) [10]. Biomarkers of malignancy already in clinical use include PSA as the marker of prostate cancer [11, 12], carcinoembryonic antigen (CEA) marker (colorectal, breast cancer) [13, 14], cancer antigen (CA) marker CA 15-3 (breast cancer) [15], CA 125 (ovarian cancer) [16] carbohydrate antigen CA 19-9 (pancreas, colon, stomach cancer) [17], and alpha fetoprotein (AFP) marker (liver, testicular cancer) [18]. Many other potential cancer markers such as beta hCG (testicular cancer), calcitonin marker (thyroid cancer), and thyroglobulin marker (thyroid cancer) are under evaluation [8, 19, 20].

PSA is one of the most widely used cancer biomarkers. It is a chymotrypsin-like serine protease that is produced by epithelial cells of the prostate gland and secreted into the prostatic fluid. Prostate-cancer invasion disrupts the epithelial membrane barrier leading to elevated serum levels of PSA. Detection of PSA in blood can therefore be useful in the diagnosis of prostate abnormalities and for evaluation of prostate cancer therapy efficacy [21]. Two different forms of PSA are immunologically detectable: the free form (MW 34 kDa) and a complex with α-1-antichymotrypsin (MW 96 kDa). Diagnostic assays developed for detection of PSA (e.g., enzyme-linked immunosorbent assays) detect total PSA concentrations down to 0.1 ng mL^{-1} [22, 23].

An immunoassay for the detection of PSA in PBS buffer based on a dual-channel SPR instrument with angular modulation (IBIS II) has been reported [24]. This work compared direct and sandwich detection of PSA on planar- and hydrogel-type sensor surfaces. Amplification with colloidal gold and latex microspheres, respectively, was employed in the sandwich assay. Sensor chips with carboxylated matrices of different thicknesses were used. Mouse monoclonal antibodies against PSA were immobilized on the both

types of chip surfaces via amine coupling chemistry. The first amplification step consisted of incubation with rabbit anti-PSA polyclonal antibodies. In experiments employing latex amplification, incubation with biotinylated goat anti-rabbit IgG was followed with streptavidin-coated latex microspheres. In experiments with gold microspheres, detection continued with immersion in a solution containing goat anti-rabbit IgG-coated colloidal gold. The chip with a thinner dextran matrix was found to lead to a higher sensor sensitivity for both the direct and sandwich detection formats. Specifically, detection limits of 0.15 ng mL^{-1} and 2.4 ng mL^{-1} were determined for the detections

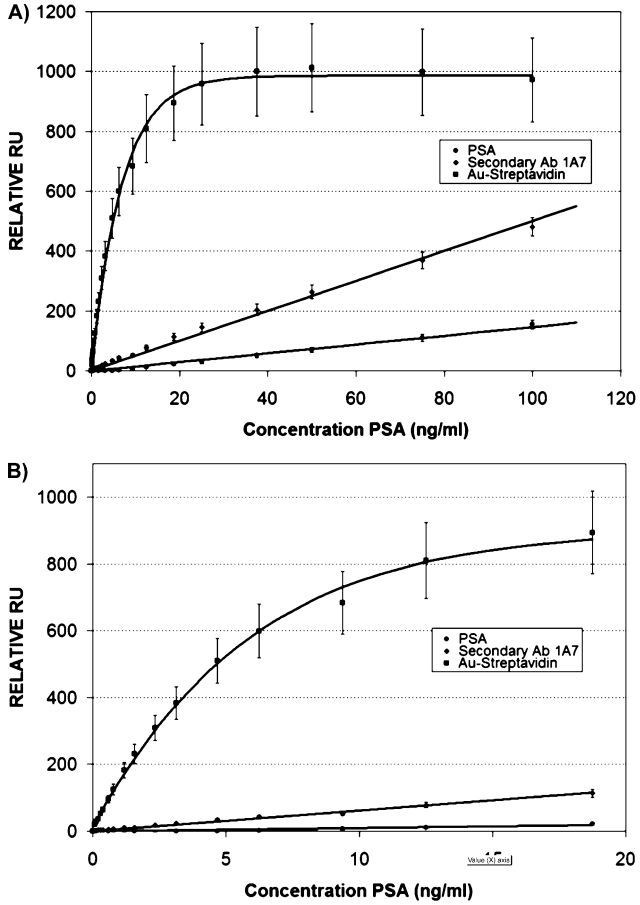

Fig. 1 Detection of PSA in buffer directly and using sandwich assay format. The signals generated upon binding of the different partners [PSA (● *bottom*), biotinylated secondary antibody (▲ *middle*) and 20 nm gold nanoparticles modified with streptavidin (■ *top*)] are shown for: **a** PSA concentrations varying between 73 pg mL^{-1} and 100 ng mL^{-1}; **b** PSA concentrations between 73 pg mL^{-1} and 20 ng mL^{-1} [25]

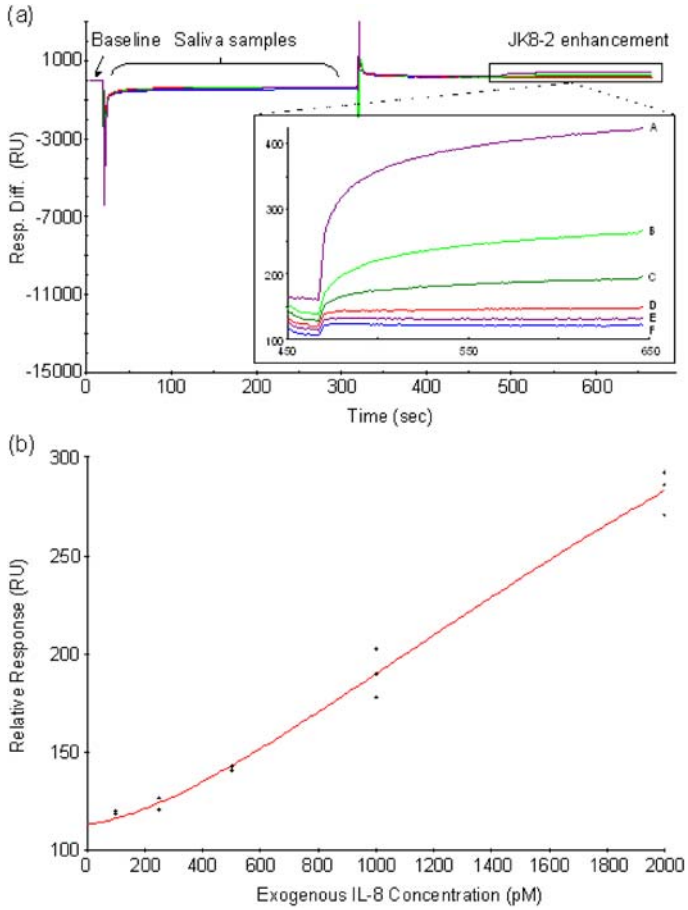

Fig. 2 Sensorgrams and calibration curve for different IL-8 concentrations in saliva supernatant premixed with 10 mg mL^{-1} of CM dextran sodium salt. **a** Sensorgrams corresponding to enhanced detection by secondary antibody for different IL-8 concentrations (5 nM, 2 nM, 1 nM, 500 pM, 250 pM, and 0 pM labeled as *A*, *B*, *C*, *D*, *E*, and *F*, respectively). **b** Calibration curve covering the IL-8 concentration range from 0 to 2 nM [26]

employing gold particle enhancement on planar-type and gel-type sensor surfaces, respectively.

Huang et al. investigated detection of PSA using direct and sandwich immunoassay formats using an SPR sensor Biacore 2000 [25]. PSA-receptor molecules consisting of a single domain antigen-binding fragment were covalently immobilized on the sensor surface via a mixed alkanethiol self-assembled monolayer (SAM). PSA concentrations as low as 10 ng mL^{-1} were detected in buffer. It was demonstrated that a sandwich assay involving a bi-

otinylated secondary antibody and streptavidin-modified gold nanoparticles lowered the limit of detection for PSA below 1 ng mL^{-1}. Signal levels corresponding to direct and amplified PSA detections in buffer are displayed in Fig. 1.

Yang et al. [26] measured levels of interleukin-8 (IL-8) protein in the saliva of healthy individuals and patients with oropharyngeal squamous cell carcinoma using a Biacore X instrument. A sandwich assay using two monoclonal antibodies, which recognize different epitopes on the IL-8, was used. Monoclonal antibody against IL-8 was immobilized onto a dextran surface via amine coupling chemistry. Saliva samples were first centrifuged to clarify the supernatants. The supernatants were then aspirated and separated from the cellular pellet. The detection limit for IL-8 was determined to be 2.5 pM ($\sim$ 0.02 ng mL^{-1}) for detection in buffer and 184 pM ($\sim$ 1.5 ng mL^{-1}) for detection in saliva samples. Sensorgrams corresponding to IL-8 binding at different concentrations and a calibration curve for secondary antibody-enhanced detection of IL-8 (sandwich assay) are displayed in Fig. 2.

Nayeri et al. [27] presented an SPR (Biacore 2000)-based direct qualitative detection of hepatocyte growth factor (HGF), which is an angiogenic growth factor related to breast cancer, in reconstituted fecal samples from patients with infectious gastroenteritis ($n = 20$) and normal controls ($n = 10$) (dissolved in distilled water at a dilution rate of 1 : 6). Mouse anti-human HGF monoclonal antibodies and recombinant human HGF receptor were immobilized on a dextran surface. The proportion of antibody-positive patient samples detected by SPR correlated well with results obtained using ELISA.

3 Heart Attack Markers

Diagnosis of cardiac muscle injury relies on the detection of biomarkers such as troponin I (TnI), troponin C (TnC), myoglobin, fatty acid binding protein (FABP), glycogen phosporylase isoenzyeme BB (GPBB), C-reactive protein (CP), urinary albumin, creatine kinase myocardial band (CK-MB), and brain (B-type) natriuretic peptide in blood and urine [28–30].

Troponin complex is a heteromeric protein which plays an important role in the regulation of skeletal and cardiac muscle contraction. It consists of three subunits, troponin I (TnI), troponin T (TnT), and troponin C (TnC). Each subunit is responsible for part of troponin complex function. For more than a decade, the cardiac form of Tn I (cTn I) has been known as a reliable marker of cardiac tissue injury. The greatest advantage of detection of cTn I is its cardio-specificity [31].

Detection of human cTn I (29 kDa) in serum, utilizing direct and sandwich immunoassay formats, was carried out by an SPR sensor with wavelength modulation [32]. Biotinylated antibodies against cTn I were immobilized on

an avidin layer created using amine coupling chemistry on an activated SAM. Sensor responses to cTn I binding to immobilized antibody in serum samples were compared with standard solutions containing known concentrations of cTn I. Two detection modes for cTn I were demonstrated: (1) direct detection of cTn I with a detection range of 2.5–40 ng mL^{-1}, and (2) a sandwich assay with a detection limit of 0.25 ng mL^{-1} and detection range of 0.5–20 ng mL^{-1}.

Detection of myoglobin and cTn I markers was carried out using a home-made two-channel multimode SPR fiber-optic sensor [33]. The two respective biomolecular recognition elements, human anti-myoglobin and human anti-cardiac troponin I, were immobilized on a dextran surfaces via amine coupling chemistry. Both myoglobin and cTnI were detected in buffer at concentrations lower than 3 ng mL^{-1}.

4 Antibodies

Antibodies are soluble proteins (immunoglobulins) secreted by B-lymphocytes in response to exogenous and endogenous antigens. Antibodies specifically bind to antigens to form antigen–antibody complexes. Antigens in this complex are typically inactive and thus interaction of antigen with other host molecules is blocked. These antibodies are referred to as neutralizing or inhibiting antibodies. In contrast, there are antibodies with a stimulating effect, i.e., they activate bound molecules. An example of disease caused by activating antibody is Grave's disease when antibodies function as ligands to cell receptors. Presence of specific antibodies in the circulatory system can thus serve as a biomarker of various diseases such as microbial infection, virus infection, allergy, autoimmune disease, or tissue injury.

Direct detection of antibodies against Epstein–Barr virus (anti-EBNA) in 1% human serum was carried out using a wavelength-modulated SPR biosensor (sensor setup description in [34, 35]). Synthetic peptides were used as receptors and immobilized on the sensor surface in the form of BSA–peptide conjugates via hydrophobic and electrostatic interactions [36]. A sensor calibration curve was established for an anti-EBNA concentration range of 0.2–2000 ng mL^{-1} (Fig. 3). The sensor response showed reproducibility better than 82% for all concentrations and multiple chips and over 90% for measurements performed on a single chip. The lowest detection limit for the direct detection of anti-EBNA was found to be 0.2 ng mL^{-1}. A procedure for regeneration of the sensor was developed and was demonstrated to allow at least 10 repeated anti-EBNA detection experiments without a significant loss in sensor sensitivity. In addition, it was demonstrated that the sensor chips can be stored for 30 days without deterioration in performance (Fig. 4).

The presence of antibodies against human respiratory syncytial virus (RSV) in 26 patient sera was detected using an SPR biosensor (Biacore 2000)

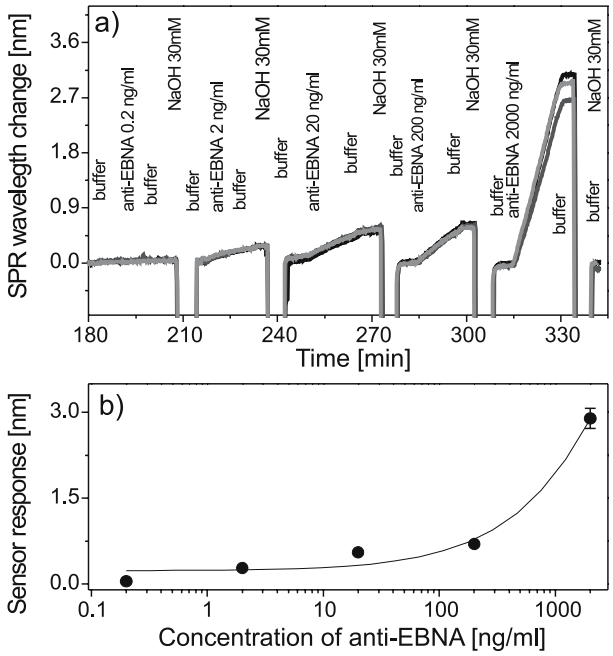

Fig. 3 **a** Sensor response to anti-EBNA detection obtained from three individual sensing channels on regenerated surface. **b** Sensor calibration curve

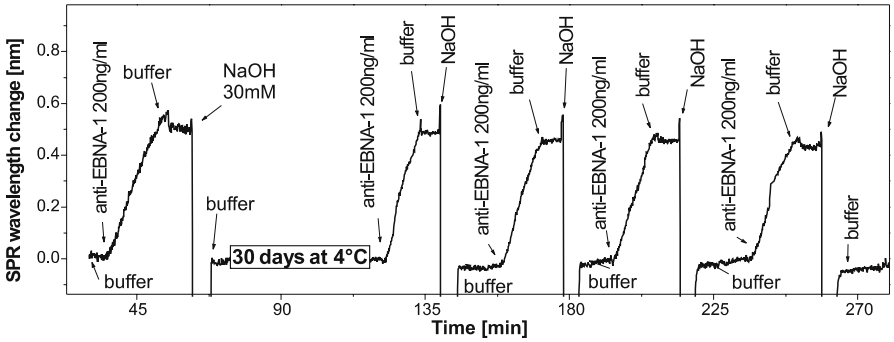

Fig. 4 Sensor responses to anti-EBNA binding obtained using one sensor chip immediately after functionalization and after 30 days of storage

by McGill et al. [37]. Monoclonal antibodies against the virus glycoproteins (F- and G-glycoproteins) were covalently attached to a dextran matrix via amine coupling chemistry and then used to immobilize the respective virus glycoproteins. Serum samples isolated from patient respiratory tracts were diluted in HBS buffer (1 : 10), filtered (0.22 μm filter), and injected into the

sensor surfaces. It was shown that, in contrast to an immunofluorescence assay, the SPR biosensor was capable of recognizing the antigenic differences between the two different contemporary genotypes of the virus (G- and F- virus glycoproteins). In order to confirm that the material binding to virus antigen was immunoglobulin, monoclonal mouse anti-human IgG was injected after each serum sample. In all SPR measurements the detection of antibodies was genotype specific.

Isotype-specific anti-adenoviral antibodies in patients dosed with adenoviral-based gene therapy vectors were detected using a Biacore 3000 by Abad et al. [38]. In this assay, whole intact virus was immobilized on the sensor surface (dextran matrix) using amine coupling. The binding of antibodies from patient blood sera (1 : 10 diluted) was measured by SPR sensor and ELISA. The results obtained by the SPR biosensor were consistent with those obtained using ELISA.

Direct qualitative detection of antibodies against hepatitis G virus from patient sera was presented by group the of Rojo [39]. A Biacore 1000 immunoassay utilized synthetic peptides, which were immobilized on dextran surface via amine coupling chemistry. Sera from 38 chronic hepatitis C patients, 36 hemodialyzed patients and 110 control healthy patients (1 : 100 dilution) were tested for the presence of specific antibodies. The results were in good agreement with those obtained using ELISA.

The detection of antibodies against herpes simplex virus type 1 and type 2 (HSV-1, HSV-2) in 1 : 100 diluted human sera with HBS buffer using the Biacore X instrument is reported in the work of Wittekindt et al. [40]. Peptides, used as a biorecognition element, were biotinylated and immobilized on the streptavidin-coated sensor chip. Two peptides from a series of eight peptides selected from segments of HSV-1 and HSV-2 gB, respectively were identified as immunogenic. Employing both peptides, a good agreement between the SPR biosensor and immunoblotting (reference method) was obtained (correlation 83% and 86% for antibodies against HSV-1 and HSV-2, respectively).

An angular modulation-based SPR biosensor for syphilis screening has been reported by Severs et al. [41]. Antibodies against the causative organism *Treponema pallidum* were detected in serum (1 : 20 diluted in Tris buffer) using sensor chips coated with recombinant *Treponema pallidum* membrane protein A (TmpA) and blocked with 0.1% gelatin. Direct and sandwich assay formats were used for detection. It was shown that the direct detection of antibodies in serum was not sufficiently reproducible, most likely due to non-uniformity of patient serum samples. In contrast, the results obtained with the SPR sandwich assay for ten blind-coded sera corresponded well with conventional syphilis tests (*Trepanema pallidum* haemagglutination assay, fluorescent treponemal antibody-absorbed test, venereal diseases research laboratory flocculation test, and TmpA-based ELISA test).

Monitoring plasma levels of anti-protein S antibodies following Varicella–Zolter virus infection has been reported by Regnault et al. [42], who used

an SPR sensor (Biacore X) to detect the presence of antibodies to protein S in infected patients [43]. Immobilization of protein S and IgG, respectively on dextran surfaces was carried out using amine coupling chemistry. Direct qualitative detection of antibodies was performed in diluted plasma (1 : 5) of patient sera samples each day during a 45-day infection. Twelve plasma samples from healthy patients were used as a control for potential non-specific binding.

Direct and sandwich format detection of antibodies against glucose 6-phosphate isomerase (GPI) in synovial fluids of rheumatoid arthritis and osteoarthritis patients (diluted 1 : 100 in HEPES) using a Biacore 2000 is presented in the work of Kim et al. [44]. Recombinant human GPI proteins produced from *E. coli* were immobilized on the dextran sensor surface via amine coupling chemistry. The synovial fluid samples from rheumatoid arthritis patients showed a significantly higher level of antibodies binding to the recombinant GPI proteins than samples from osteoarthritis patients.

Wilkop et al. reported the use of an SPR imaging sensor and a microcontact printed array for parallelized detection of antibodies against cholera toxin (CT) [45]. Immobilization of the toxin was performed by combining the microprinting method with the covalent linkage of the protein to NHS-activated terminal groups on a self-assembled monolayer of thiols. Detection of anti-cholera toxin IgG (anti-CT IgG) was demonstrated for antibody concentrations ranging from 10 to 100 $\mu g\,mL^{-1}$, Fig. 5.

An assay for diagnosing type I diabetes mellitus based on the detection of anti-glutamic acid decarboxylase (GAD) antibodies in buffer by a Biacore 2000, is presented in [46, 47]. Biotinylated GAD was immobilized on a streptavidin-coated surface. The effect of mixed SAM composition (differing in ratios of hydroxyl- and carboxyl-terminated alkanethiols) on the sensitivity of the sensor was investigated. On SPR sensor chips prepared with the optimized SAM composition (10 : 1 ratio of 3-mercaptopropanol to 11-mercaptoundecanoic acid), a concentration of anti-GAD as low as $0.75\,\mu g\,mL^{-1}$ was detected.

An SPR sensor-based detection of antibodies against granulocyte macrophage colony stimulating factor (GM-CSF) was performed in the work of Rini et al. [1]. GM-CSF is cytokine that is involved in human immunotherapy protocols for various cancers including prostate cancer [48]. Antibodies against GM-CSF were induced in prostate cancer patients by repeated administration of GM-CSF and their presence in patient sera was monitored using a Biacore 2000 (sera diluted 1 : 5) and ELISA (sera diluted 1 : 20). The GM-CSF antigen used as a biomolecular recognition element was immobilized on the carboxymethylated dextran on the surface of the SPR sensor via amine coupling chemistry. The measurements performed using the SPR biosensor revealed that all 15 prostate cancer patients treated with GM-CSF produced GM-CSF reactive antibodies, which was in agreement with reference ELISA measurements.

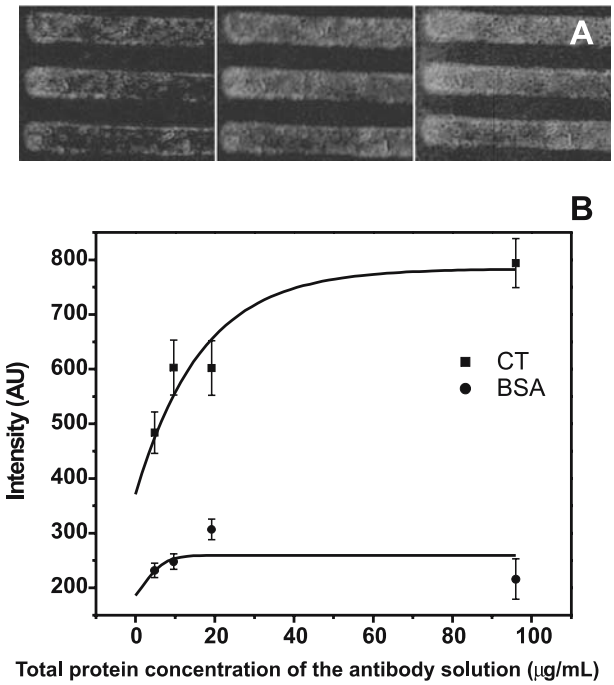

Fig. 5 Detection of anti-CT antibodies with printed CT proteins. **a** Images of printed CT patterns before and after incubation with increasing amount of anti-CT antibodies (background corrected). From *left* to *right*: sensor surface before incubation with anti-CT; after exposure to anti-CT (0.001 mg mL^{-1}); and after exposure to anti-CT (0.002 mg mL^{-1}) **b** Concentration-dependent response to anti-CT binding to CT (measuring surface) and BSA (reference surface), respectively [45]

Direct detection of antibody against insulin in patient sera using an SPR sensor Biacore 2000 is presented in [49]. Purified human insulin was used as a biorecognition element and immobilized on the sensor surface via amine coupling chemistry. Test sera samples were pretreated to remove insulin and filtered before SPR measurements. Insulin antibodies were detected in eight selected patient sera samples and fell in the range 2.91–16.3 μg mL^{-1}.

5 Hormones

Monitoring concentrations of female hormones is important for female disease diagnostics as well as for fetal health monitoring. The most important female cycle biomarkers, which are typically measured in clinical laboratory tests or commercial test strips, include follicle stimulating hormone (FSH) as a marker of non-pregnancy, luteinizing hormone (LH) as a marker of ovu-

lation, and human chorionic gonadotropin hormone (hCG) as a marker of pregnancy.

Direct detection of hCG in buffer in the concentration range 0.05–1 $\mu g\,mL^{-1}$ was demonstrated using a wavelength modulation-based SPR sensor, Fig. 6. A regeneration protocol was developed that allowed repeated use of the sensor with measurement reproducibility over 90%. The same group used an SPR imaging instrument with antibodies against hCG covalently immobilized to a mixed SAM to detect hCG at concentrations lower than 500 $ng\,mL^{-1}$ [50].

Ladd et al. reported SPR sensor-based detection of hCG [51], exploiting a DNA-directed antibody immobilization method. The immobilization consisted of non-covalent attachment of streptavidin to a biotinylated SAM followed by binding of biotinylated oligonucleotides to available streptavidin binding sites. Antibodies chemically modified with oligonucleotides with a complementary sequence were finally attached to this surface via DNA hybridization. The detection limit for direct detection of hCG in buffer by a dual-channel SPR sensor with wavelength modulation was determined to be 0.5 $ng\,mL^{-1}$.

Detection of estrone and estradiol in buffer using SPR sensors Biacore 2000 and Biacore 1000 was carried out by Coille et al. [52]. Analyte–BSA conjugates and BSA were immobilized in the sensing and reference channels of a sensor chip, respectively, using NHS-esters. Analyte concentrations detected using inhibition format in this work were in the range 0.01–3000 $ng\,mL^{-1}$.

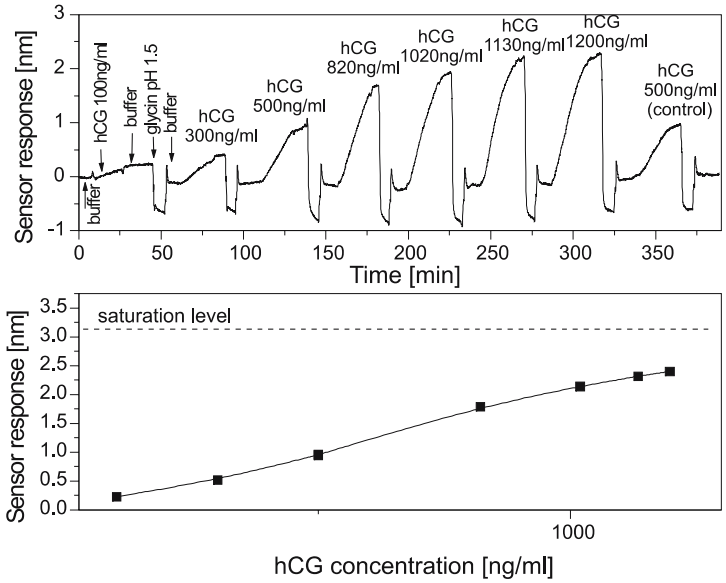

Fig. 6 Sensorgrams corresponding to binding of hCG at various concentration on anti-hCG immobilized on the sensor surface and hCG-sensor calibration curve

Miyashita et al. [53] present an SPR Biacore X-based immunoassay for the detection of 17β-estradiol in buffer. The assay was performed in an inhibition format, in which 17β-estradiol BSA conjugates were immobilized on the sensor surface and the binding of antibody to 17β-estradiol conjugates on the surface was measured. The 17β-estradiol was detected in the concentration range 0.47–21.4 nM ($\sim$ 0.14–6.4 ng mL^{-1}).

6 Drugs

Therapeutic drug monitoring is very important for treatment of many serious diseases (e.g., HIV [54], heart failure [55], Parkinson's, malaria, cystic fibrosis, diabetes mellitus [56], etc.) and for treatment of pregnant women, children, and patients with special conditions (e.g., pre-existing liver damage) where routine recommended dosing is not always appropriate.

An inhibition assay for the detection of anticoagulatory coumarin derivative 7-hydroxycoumarin (7-OHC) using a Biacore SPR sensor and competitive assay was presented by Keating et al. [57]. A 7-OHC conjugated with BSA was immobilized on a carboxymethylated dextran sensor chip via amine coupling chemistry. Serum samples (diluted with buffer) were premixed with a polyclonal anti-7-OHC antibody and injected over the sensor surface. The binding of excess antibodies to the immobilized conjugate generated a sensor response inversely proportional to the 7-OHC concentration. The assay had a measuring range of 0.5–80 μg mL^{-1}. This immunoassay exhibited reproducibility and sensitivity comparable to established methods of analysis.

Fitzpatrick et al. detected oral anticoagulant warfarin using a Biacore 3000 SPR sensor and an inhibition assay [58]. 4′-Aminowarfarin or 4′-azowarfarin–BSA was immobilized on a dextran matrix via amine coupling chemistry. Detection of warfarin was performed in plasma ultrafiltrate (diluted 1 : 100) in a concentration range of 4–250 ng mL^{-1}. The observed calibration curve and residual plot are shown in Fig. 7. A procedure for regeneration of the sensor chips was established, allowing for more than 70 binding cycles.

Direct detection of a cytokine protein, recombinant human interferon-γ, using an IBIS SPR sensor is presented in [59]. Several types of sensor chip coatings, including self-assembled monolayers and hydrogel-derivatized SAMs, were characterized in terms of their ability to resist non-specific adsorption from plasma. The best results with respect to plasma adsorption and surface regenerability were obtained with antibodies immobilized on the dextran-modified 11-mercaptoundecanoic acid SAM. The detection limit for detection of human interferon-γ in 1 : 100 diluted plasma was established at 250 ng mL^{-1}.

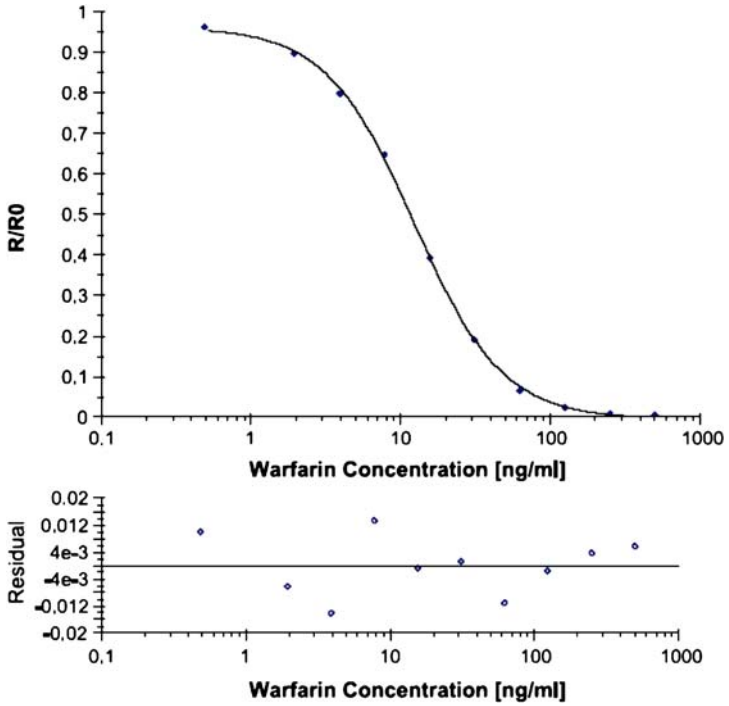

Fig. 7 Calibration and residual plot for the inhibition assay-based detection of warfarin in plasma ultrafiltrate ($n = 3$). The mean normalized response value (RAG/R0) at each analyte concentration from three independent assays was used to calculate the calibration curve and to determine the assay variation [58]

Detection of low molecular weight heparin oligosaccharide (Fragmin), which is an antithrombotic agent, was demonstrated using purified monoclonal antibodies immobilized via amine coupling chemistry onto the surface of a Biacore 3000 [60]. Monoclonal antibodies were immobilized on a sensor surface prefunctionalized with Fragmin–HSA conjugates. The detection limit for Fragmin in PBS buffer was determined to be 125 nM (~ 625 ng mL^{-1}).

The Sakai group [61] developed an SPR sensor-based inhibition immunoassay for detection of morphine in buffer and in 1% human urine. They used an SPR sensor SPR-20 and immobilized morphine–BSA conjugates on the gold surface via physical adsorption. The addition of morphine to the anti-morphine antibody solution was found to reduce the SPR signal because of the inhibition effect of morphine. The detection limit of morphine in 1% urine was established at 2 ng mL^{-1}.

A Biacore 1000 inhibition assay for the detection of morphine-3-glucuronide (M3G), the main metabolite of heroin and morphine, was demonstrated in buffer and diluted urine by Dillon et al. [62]. M3G–ovalbumin conjugate was

Table 1 Overview of biomarkers related to medical diagnostics detected with SPR biosensors

Biomarker	Disease	Normal level	Detection limit [ng mL^{-1}]	BRE, detection format	Sample	Refs.
Cancer biomarkers:						
PSA	Prostate cancer	0–4 ng mL^{-1}	0.15	Antibody, enhanced detection by gold nanoparticles conjugated with antibody	Buffer containing 3% BSA	[24]
PSA	Prostate cancer	0–4 ng mL^{-1}	10	PSA-specific receptor, direct	Buffer	[25]
PSA	Prostate cancer	0–4 ng mL^{-1}	< 1	PSA-specific receptor, sandwich detection enhanced with gold nanoparticles	Buffer	[25]
Interleukin-8	Oropharyngeal cancer		0.02	Antibody, sandwich	Buffer	[26]
Interleukin-8	Oropharyngeal cancer		1.5	Antibody, sandwich	Saliva (diluted)	[26]
Heart attack markers:						
Troponin I	Cardiac tissue injury	0–0.1 ng mL^{-1}	2.5	Antibody, direct	Serum	[32]
Troponin I	Cardiac tissue injury	0–0.1 ng mL^{-1}	0.25	Antibody, sandwich	Serum	[32]
Troponin I	Cardiac tissue injury	0–0.1 ng mL^{-1}	< 3	Antibody, direct	Buffer	[33]
Myoglobin	Cardiac tissue injury	0–85 ng mL^{-1}	< 3	Antibody, direct	Buffer	[33]
Antibodies:						
Antibody against Epstein–Barr virus	Mononucleosis		0.2	BSA–peptide conjugate, direct	Serum (1%)	
Antibody against cholera toxin			10 000	Antigen, direct (SPR imaging)	Buffer	[45]
Antibody against GM-CSF	Prostate cancer			GM-CSF antigen, direct	Serum (diluted 1 : 5 with buffer)	[1]
Antibody against insulin	Diabetes mellitus		2910	Antigen, direct	Serum (pretreated to remove insulin)	[49]

Table 1 (continued)

Biomarker	Disease	Normal level	Detection limit [ng mL^{-1}]	BRE, detection format	Sample	Refs.
Hormones:						
hCG	Female hormonal diseases/ pregnancy marker	Normal: 0–10 U/L Pregnancy: > 500 U/L	50	Antibody, direct	Buffer	
hCG	Female hormonal diseases/ pregnancy marker	Normal: 0–10 U/L Pregnancy: > 500 U/L	500	Antibody, direct	Buffer	[50]
hCG	Female hormonal diseases/ pregnancy marker	Normal: 0–10 U/L Pregnancy: > 500 U/L	0.5	Antibody, sandwich	Buffer	[51]
17β-Estradiol	Hormonal diseases	M: 0.02–0.05 F (0–55 years): 0.01–0.5 F (55–110 years): 0–0.04	0.14	Antibody, inhibition	buffer	[53]
Drugs:						
Warfarin			4	Antibody, inhibition	Plasma ultrafiltrate (diluted 1 : 100)	[58]
interferon-γ			250	Antibody, direct	Spiked plasma (1 : 100)	[59]
Fragmin			625	Antibody, direct	Buffer	[60]
Morphine-3-glucuronide			0.7	Antibody, inhibition	Urine (1 : 250 diluted)	[62]
Morphine			2	Antibody, inhibition	Urine (1%)	[61]

SPR Surface plasmon resonance, *BRE* biorecognition elements, *PSA* prostate-specific antigen, *BSA* bovine serum albumin, *GM-CSF* granulocyte macrophage colony stimulating factor, *hCG* human chorionic gonadotropin

immobilized on a dextran matrix via amine coupling chemistry. Two polyclonal antibodies were produced, purified, and tested for M3G detection. The range of detection of M3G in buffer and in urine (diluted 1 : 250) was found to be 0.7 and 24.4 ng mL^{-1}, respectively.

7 Summary

Recently, we have witnessed an increasing effort to exploit SPR biosensor technology for medical diagnostics. Detection of a variety of disease biomarkers, hormones, and drugs at clinically relevant levels has been demonstrated. Although many of these detection experiments were performed in pure model samples with minimal or no matrix interferences, clinical samples have also been tackled, Table 1.

It is expected that advances in SPR sensor instrumentation (reducing size, improving sensitivity, increasing throughput), biorecognition elements and methods for their immobilization (increasing sensitivity and specificity) will lead to new systems for rapid detection and identification of disease biomarkers. These will further extend the applicability of SPR biosensor technology in medical diagnostics.

References

1. Rini B, Wadhwa M, Bird C, Small E, Gaines-Das R, Thorpe R (2005) Cytokine 29:56
2. Luppa PB, Sokoll LJ, Chan DW (2001) Clin Chim Acta 314:1
3. McGlennen RC (2001) Clin Chem 47:393
4. Peter C, Meusel M, Grawe F, Katerkamp A, Cammann K, Borchers T (2001) Fresenius J Anal Chem 371:120
5. Landman J, Chang Y, Kavaler E, Droller MJ, Liu BC (1998) Urology 52:398
6. Hlawatsch A, Teifke A, Schmidt M, Thelen M (2002) Am J Roentgenol 179:1493
7. Canto EI, Shariat SF, Slawin KM (2004) Curr Urol Rep 5:203
8. Yasui W, Oue N, Ito R, Kuraoka K, Nakayama H (2004) Cancer Sci 95:385
9. Wu J (2001) Diagnosis and management of cancer using serologic tumor markers. Saunders, Philadelphia
10. Anderson NL, Anderson NG (2002) Mol Cell Proteomics 1:845
11. Schmid HP, Riesen W, Prikler L (2004) Crit Rev Oncol Hematol 50:71
12. Caplan A, Kratz A (2002) Am J Clin Pathol 117:S104
13. Goldstein MJ, Mitchell EP (2005) Cancer Invest 23:338
14. Duffy MJ (2001) Clin Chem 47:624
15. Duffy MJ, Duggan C, Keane R, Hill AD, McDermott E, Crown J, O'Higgins N (2004) Clin Chem 50:559
16. Fehm T, Heller F, Kramer S, Jager W, Gebauer G (2005) Anticancer Res 25:1551
17. Micke O, Bruns F, Schafer U, Kurowski R, Horst E, Willich N (2003) Anticancer Res 23:835

18. Daniele B, Bencivenga A, Megna AS, Tinessa V (2004) Gastroenterology 127:S108
19. Diamandis EP (2004) Clin Chem 50:793
20. Marrero JA, Lok AS (2004) Gastroenterology 127:S113
21. Polascik TJ, Oesterling JE, Partin AW (1999) J Urol 162:293
22. Kuriyama M, Wang MC, Papsidero LD, Killian CS, Shimano T, Valenzuela L, Nishiura T, Murphy GP, Chu TM (1980) Cancer Res 40:4568
23. Acevedo B, Perera Y, Ruiz M, Rojas G, Benitez J, Ayala M, Gavilondo J (2002) Clin Chim Acta 317:55
24. Besselink GA, Kooyman RP, van Os PJ, Engbers GH, Schasfoort RB (2004) Anal Biochem 333:165
25. Huang L, Reekmans G, Saerens D, Friedt JM, Frederix F, Francis L, Muyldermans S, Campitelli A, Hoof CV (2005) Biosens Bioelectron 21:483
26. Yang CY, Brooks E, Li Y, Denny P, Ho CM, Qi FX, Shi WY, Wolinsky L, Wu B, Wong DTW, Montemagno CD (2005) Lab on a Chip 5:1017
27. Nayeri F, Aili D, Nayeri T, Xu JY, Almer S, Lundstrom I, Akerlind B, Liedberg B (2005) BMC Gastroenterol 5:13
28. McDonough JL, Van Eyk JE (2004) Prog Cardiovasc Dis 47:207
29. Thielmann M, Massoudy P, Marggraf G, Knipp S, Schmermund A, Piotrowski J, Erbel R, Jakob H (2004) Eur J Cardiothorac Surg 26:102
30. Matveeva EG, Gryczynski Z, Lakowicz JR (2005) J Immunol Methods 302:26
31. Bodor GS, Porterfield D, Voss EM, Smith S, Apple FS (1995) Clin Chem 41:1710
32. Wei J, Mu Y, Song D, Fang X, Liu X, Bu L, Zhang H, Zhang G, Ding J, Wang W, Jin Q, Luo G (2003) Anal Biochem 321:209
33. Masson JF, Obando L, Beaudoin S, Booksh K (2004) Talanta 62:865
34. Dostalek J, Vaisocherova H, Homola J (2005) Sensor Actuator B Chem 108:758
35. Homola J, Vaisocherova H, Dostalek J, Piliarik M (2005) Methods 37:26
36. Houska M, Brynda E, Bohata K (2004) J Colloid Interface Sci 273:140
37. McGill A, Greensill J, Marsh R, Craft AW, Toms GL (2004) J Med Virol 74:492
38. Abad LW, Neumann M, Tobias L, Obenauer-Kutner L, Jacobs S, Cullen C (2002) Anal Biochem 310:107
39. Rojo N, Ercilla G, Haro I (2003) Curr Protein Pept Sci 4:291
40. Wittekindt C, Fleckenstein B, Wiesmuller K, Eing BR, Kuhn JE (2000) J Virol Methods 87:133
41. Severs AH, Schasfoort RBM, Salden MHL (1993) Biosens Bioelectron 8:185
42. Regnault V, Boehlen F, Ozsahin H, Wahl D, de Groot PG, Lecompte T, de Moerloose P (2005) J Thromb Haemost 3:1243
43. Levin M, Eley BS, Louis J, Cohen H, Young L, Heyderman RS (1995) J Pediatr 127:355
44. Kim JY, Lee MH, Jung KI, Na HY, Cha HS, Ko EM, Kim TJ (2003) Exp Mol Med 35:310
45. Wilkop T, Wang Z, Cheng Q (2004) Langmuir 20:11141
46. Choi SH, Lee JW, Sim SJ (2005) Biosens Bioelectron 21:378
47. Lee JW, Sim SJ, Cho SM, Lee J (2005) Biosens Bioelectron 20:1422
48. Mellstedt H, Fagerberg J, Frodin JE, Henriksson L, Hjelm-Skoog AL, Liljefors M, Ragnhammar P, Shetye J, Osterborg A (1999) Curr Opin Hematol 6:169
49. Kure M, Katsura Y, Kosano H, Noritake M, Watanabe T, Iwaki Y, Nishigori H, Matsuoka T (2005) Intern Med 44:100
50. Piliarik M, Vaisocherova H, Homola J (2005) Biosens Bioelectron 20:2104
51. Ladd J, Boozer C, Yu Q, Chen S, Homola J, Jiang S (2004) Langmuir 20:8090
52. Coille I, Gauglitz G, Hoebeke J (2002) Anal Bioanal Chem 372:293
53. Miyashita M, Shimada T, Miyagawa H, Akamatsu M (2005) Anal Bioanal Chem 381:667

54. Cooley LA, Lewin SR (2003) J Clin Virol 26:121
55. Dunselman PHJM, Scaf AHJ, Kuntze CEE, Lie KI, Wesseling H (1988) Eur J Clin Pharmacol 35:461
56. Lin EHB, Katon W, Von Korff M, Rutter C, Simon GE, Oliver M, Ciechanowski P, Ludman EJ, Bush T, Young B (2004) Diabetes Care 27:2154
57. Keating GJ, Quinn JG, O'Kennedy R (1999) Anal Lett 32:2163
58. Fitzpatrick B, O'Kennedy R (2004) J Immunol Methods 291:11
59. Stigter EC, Jong GJ, van Bennekom WP (2005) Biosens Bioelectron 21:474
60. Liljeblad M, Lundblad A, Ohlson S, Pahlsson P (1998) J Mol Recognit 11:191
61. Sakai G, Ogata K, Uda T, Miura N, Yamazoe N (1998) Sensor Actuator B Chem 49:5
62. Dillon PP, Daly SJ, Manning BM, O'Kennedy R (2003) Biosens Bioelectron 18:217

Appendix XI

J. Štěpánek, H. Vaisocherová and M. Piliarik:

Molecular interactions in SPR sensors

In Surface Plasmon Resonance Based Sensors, Editor J. Homola,
Springer, September 2006

Springer Ser Chem Sens Biosens (2006) 4: 1–x
DOI 10.1007/5346_015

Published online: ■ May 2006

Molecular Interactions in SPR Sensors

Josef Štěpánek[1] (✉) · Hana Vaisocherová[2] · Marek Piliarik[2]

[1]Faculty of Mathematics and Physics, Charles University, Prague, Czech Republic
stepjos@karlov.mff.cuni.cz

[2]Institute of Radio Engineering and Electronics, Prague, Czech Republic

Keywords Association · Diffusion · Dissociation · Equilibrium constant · Flow cell · Mass transport · Rate constants · Reaction kinetics · Sensor · Surface plasmon resonance

Abbreviations

A Analyte (free reagent in solution)
B Complex of analyte and receptor
D Diffusion coefficient (coefficient of translational diffusion)
Da Damköhler number
h Flow cell height
k_a Association rate constant
k_d Dissociation rate constant
K Equilibrium association constant (binding affinity)
l Flow cell length
N_A Avogadro's number
PDE Fundamental equation of analyte transport inside flow cell (partial differential equation)
Pe Peclét number
R Receptor (binding target for the analyte immobilized at the sensor surface)
RU Units of the SPR sensor response (resonance units)
Re Reynolds number
w Flow cell width
[X] Molar concentration of X
x Space coordinate in direction of the analyte flow

y Space coordinate in direction perpendicular to the sensor surface
α Free analyte concentration ($\equiv [A]$)
α_0 Injected analyte concentration
β Surface concentration of receptor (moles per square area)
γ Surface concentration of complex (indexed for various types of complexes when necessary)
ξ Sensor response (in RU)
ξ_S Standard sensor response (in RU) corresponding to all receptor sites bound to analyte in 1 : 1 ratio

1 Introduction

Binding and/or unbinding of biomolecules at the active surface of an SPR biosensor is controlled by various mechanisms that result in variety of temporal profiles of the SPR biosensor response and in dependence on microenvironmental conditions. The determination of binding kinetics provides important new information about interacting molecules. This is commonly considered one of the greatest advantages of the SPR biosensor technique. Although in ideal cases an appropriate kinetic model of molecular interaction is able to completely describe the SPR biosensor response, in reality the influence of hydrodynamic conditions often has to be taken into account [1]. This chapter is devoted to molecular interaction models that correspond to the processes most frequently encountered at SPR biosensor surfaces. It also deals with hydrodynamic effects and their exact or approximate mathematical description.

2 Interaction Models

To quantitatively analyze the sensor response to interactions between the studied biomolecule (analyte) and the surface bound receptors, it is necessary to employ a relevant mathematical model. The core part of the model is a kinetic equation that describes how the temporal amounts of formed/dissociated complexes depend on the momentary local concentrations of the free analyte and the free binding sites of the receptors.

SPR biosensor experiments measure only relative changes in the molecular mass attached to the sensor surface from the beginning of the interaction being studied. The response ξ is then directly proportional to the concentration of the bound analyte (conditions that guarantee a linear sensor response are assumed throughout the chapter). In the case of a single type of analyte binding to the receptors in a 1 : 1 stoichiometric ratio, the response is proportional

to the concentration of the formed complexes:

$$\xi = \text{const}\, M_A \gamma \,, \tag{1}$$

where M_A is the mass of the analyte molecule and γ is the surface concentration of the formed complexes. It can be shown that for sufficiently high analyte concentrations, the sensor response will eventually reach its maximum value, which corresponds to all of the receptors being occupied. This response does not change measurably with further increases in the analyte concentration. Considering that the maximum possible response for the 1 : 1 stoichiometry is given by:

$$\xi_S = \text{const}\, M_A \beta \,, \tag{2}$$

where β is the surface concentration of receptors, it is widely useful to characterize the sensor response by its normalized value:

$$\xi/\xi_S = \gamma/\beta \,. \tag{3}$$

2.1 Pseudo First-Order Kinetics

Whenever we deal with analyte binding to receptors fixed at a sensor surface, the second order reaction model represents the basis of its description. This model concerns the situation when two partners, A and R, form a single complex AR. This can be, for instance, binding of an antigen to an antibody, docking of a substrate to an enzyme with a single binding pocket, or duplex formation by two complementary chains of nucleic acid. In the case of interactions at the sensor surface, we have to distinguish between the immobilized receptor R and the analyte A present in the solution. Two processes are considered by the model: (1) the association process whereby A and R bind to each other and create the immobilized complex AR and (2) the dissociation process whereby the complex AR dissociate into two parts, A and R. These processes are symbolized by:

$$\mathrm{A} + \mathrm{R} \rightarrow \mathrm{AR} \quad \text{and} \quad \mathrm{AR} \rightarrow \mathrm{A} + \mathrm{R} \,. \tag{4}$$

For the association, it is essential that A and R are in close proximity, i.e., their distance must be shorter than a critical radius. If this condition is satisfied, there is a certain probability that within a unit time interval A and R will form a complex. For a set of given environmental conditions (temperature, pressure, solvent properties) this probability is the same for all neighboring pairs of A and R, provided we do not consider microscopic conditions such as their mutual orientation or their instantaneous speeds of translation and rotation. For a given receptor the probability that any molecule of analyte appears within the critical distance is proportional to the concentration of A. The total number of associations per time interval in a particular region is proportional

to the total number of receptors involved, because they all can create a complex with the same probability. As a result, we obtain a relationship between the amount of the complexes γ formed per unit time, the instantaneous concentrations of the free analyte $[A] = \alpha$, and the concentration of free receptors $\beta - \gamma$:

$$\frac{\mathrm{d}\gamma_\mathrm{a}}{\mathrm{d}t} = k_\mathrm{a}\alpha\left(\beta - \gamma\right) , \tag{5}$$

where k_a is a constant that characterizes the chemical reaction in the sense that it is independent of time and of the reactants concentrations. It is called the association or forward rate constant.

On the other hand, for each complex there is certain probability that within a unit time interval it will dissociate into A and R separated by a distance larger than the critical radius. This probability is the same for all complexes at the given conditions. The dissociation leads to a decrease of the complex concentration proportional to its instantaneous value:

$$\frac{\mathrm{d}\gamma_\mathrm{d}}{\mathrm{d}t} = - k_\mathrm{d}\gamma , \tag{6}$$

where k_d is called the dissociation or reverse rate constant. In a real system, both the association and dissociation processes occur simultaneously. It can be symbolically expressed as:

$$\mathrm{A} + \mathrm{R} \underset{k_\mathrm{d}}{\overset{k_\mathrm{a}}{\rightleftharpoons}} \mathrm{AR} . \tag{7}$$

The time dependence of the total complex concentration is then described by the summed effects of both processes:

$$\frac{\mathrm{d}\gamma}{\mathrm{d}t} = \frac{\mathrm{d}\gamma_\mathrm{a}}{\mathrm{d}t} + \frac{\mathrm{d}\gamma_\mathrm{d}}{\mathrm{d}t} = k_\mathrm{a}\alpha\left(\beta - \gamma\right) - k_\mathrm{d}\gamma . \tag{8}$$

Both quantities β and γ must be expressed in the same kind of local density. In the case of a solution phase reaction, we would understand them as molar concentrations, i.e., number of moles per unit volume. For receptors fixed on the sensor surface it is more straightforward to define them as surface concentrations, i.e., number of moles per unit area.

The solution of Eq. 8 depends strongly on how the concentration of the free analyte α is controlled. In the case of an active sensor surface surrounded by a solvent occupying certain closed volume V, the analyte can be injected as a highly concentrated solution [1, 2]. In the ideal case of a perfectly mixed solution, the effect of the injection can be described as an immediate jump in the analyte concentration from zero to a certain starting value α_0. During the consequent process the free analyte will be consumed by association with the receptor, while the sum of the free and bound analyte will be kept constant:

$$\alpha V + \gamma S = \alpha_0 V = \mathrm{const} , \tag{9}$$

where S is the sensor area. The temporary change in the complex concentration is then proportional to a quadratic polynomial of its instantaneous value (Fig. 1):

$$\frac{\mathrm{d}\gamma}{\mathrm{d}t} = k_\mathrm{a}\left(\alpha_0 - \frac{S}{V}\gamma\right)\left(\beta - \gamma\right) - k_\mathrm{d}\gamma\,. \tag{10}$$

At longer times, the solution of Eq. 10 converges to an equilibrium state $\left(\frac{\mathrm{d}\gamma}{\mathrm{d}t} = 0\right)$, which is characterized by the well-known equation:

$$K = \frac{k_\mathrm{a}}{k_\mathrm{d}} = \frac{\gamma_\mathrm{eq}}{\left(\alpha_0 - \gamma_\mathrm{eq}S/V\right)\left(\beta - \gamma_\mathrm{eq}\right)}\,, \tag{11}$$

where K is the equilibrium (association) constant. Sometimes it is also referred to as the binding affinity. A sense of Eq. 11 is demonstrated in Fig. 1: changes in the association rate influence how fast both the concentration of the complexes and that of the free analyte come to equilibrium. Note that their equilibrium values are not changed, because the equilibrium constant is fixed.

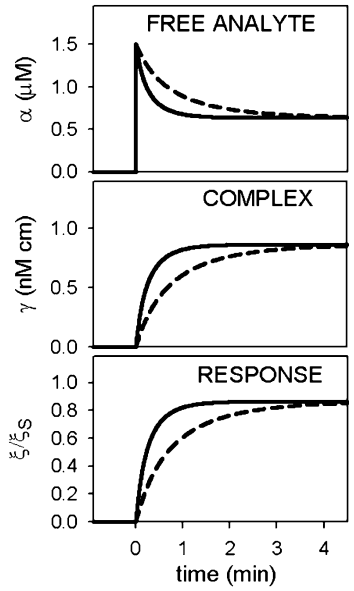

Fig. 1 Analyte-to-receptor binding after the analyte injection, according to the model of the second order reaction in closed volume (Eq. 10). Parameters: $\alpha_0 = 1.5\,\mu\mathrm{M}$, $\beta = 10^{-9}\,\mathrm{M\,cm}$, $S = 1\,\mathrm{cm}^2$, $V = 1\,\mu\mathrm{L}$, $K = 10^7\,\mathrm{M}^{-1}$. *Solid line* $k_\mathrm{a} = 4.5 \times 10^4\,\mathrm{M}^{-1}\,\mathrm{s}^{-1}$, *dashed line* $k_\mathrm{a} = 1.5 \times 10^4\,\mathrm{M}^{-1}\,\mathrm{s}^{-1}$

Very often the number of molecules of analyte in volume V is much higher than the amount of the receptors at the surface S. In this case, the term $\gamma S/V$ in Eq. 10 can be neglected and we obtain:

$$\frac{\mathrm{d}\gamma}{\mathrm{d}t} = k_\mathrm{a}\alpha_0\left(\beta - \gamma\right) - k_\mathrm{d}\gamma\,. \tag{12}$$

Equation 12, originally derived by Langmuir for interactions at a surface in contact with reactants in solution, is formally identical with the equation describing a first-order reaction in solution. It is therefore usually referred to as pseudo first-order kinetics. Its solution is a single exponential function with an asymptote corresponding to the equilibrium fulfilling equation:

$$K = \frac{k_\mathrm{a}}{k_\mathrm{d}} = \frac{\gamma_\mathrm{eq}}{\alpha_0\left(\beta - \gamma_\mathrm{eq}\right)}\,. \tag{13}$$

Pseudo first-order kinetics is also typical for sensors that employ flow cells, where the free analyte concentration is primarily controlled by flowing a solution through the cell. In this case, the free analyte concentration can be either increased stepwise or decreased stepwise. As a result, an SPR sensorgram usually consists of two stages: an association stage that begins with the stepwise increase of the free analyte concentration to a constant value α_0, followed by a dissociation stage where the free analyte concentration is stepped down to zero. An ideal SPR response corresponding to this experiment (pseudo first-order kinetics) is shown in Fig. 2.

After a sufficiently long time, the association and the dissociation rates become practically equal and a dynamic equilibrium state is achieved. The

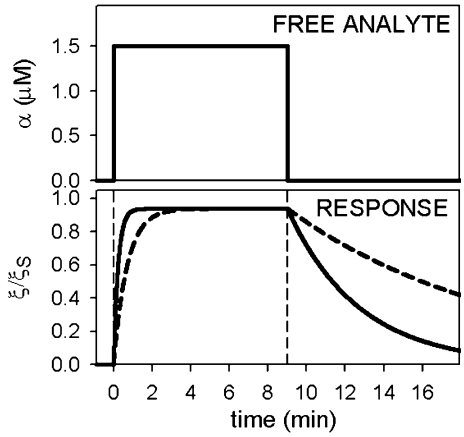

Fig. 2 Ideal flow-cell sensorgram according to the model of pseudo first-order reaction (Eq. 12). Parameters: $\alpha_0 = 1.5\,\mu\mathrm{M}$, $\beta = 1\,\mathrm{nM\,cm}$, $K = 10^7\,\mathrm{M}^{-1}$. *Solid line* $k_\mathrm{a} = 4.5 \times 10^4\,\mathrm{M}^{-1}\,\mathrm{s}^{-1}$, *dashed line* $k_\mathrm{a} = 1.5 \times 10^4\,\mathrm{M}^{-1}\,\mathrm{s}^{-1}$. *Vertical dashed lines* indicate beginning of the association and the dissociation stage

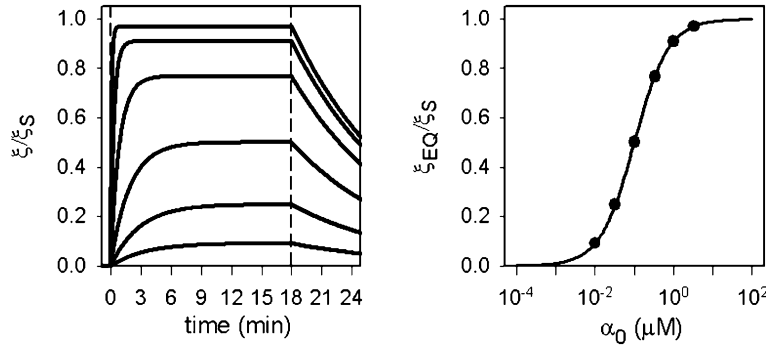

Fig. 3 Set of sensorgrams (model) suitable for equilibrium analysis (*left*) and binding isotherm with indicated equilibrium sensorgram results (*right*). Model of pseudo first-order reaction. Parameters: $\beta = 1$ nM cm, $K = 10^7$ M^{-1}, $k_a = 4.5 \times 10^4$ M^{-1} s^{-1}

equilibrium association constant K [3–7] can be determined by measuring the dependence of the sensor's equilibrium response on the injected analyte concentration (binding isotherm). For pseudo first-order kinetics the binding isotherm (Fig. 3) is given by:

$$\frac{\xi_{EQ}}{\xi_S} = \frac{K\alpha_0}{(1 + K\alpha_0)} . \tag{14}$$

An advantage of equilibrium analysis is that, in contrast to the other parts of the sensorgram, the equilibrium phase of the association curve is not affected by mass transport (see below).

2.2 Other Kinetic Models

In reality, the processes in the active sensor layer may be more complicated and the sensor response will be a superposition of several parallel or consecutive reactions. We will present some kinetic models that correspond to more complex molecular interactions at the sensor surface.

Zero order reactions following the initial binding are usually interpreted as conformational changes of the AR complex. Once the conformation is changed, the complex cannot dissociate unless it transforms back into its original state. This additional reaction can slow down the kinetics. The model, first presented in [8], has been applied in a few studies of complex biomolecular systems where the analyte binding may substantially change the physicochemical properties of the receptor, such as the interaction of angiotensin II with a receptor at a lipid membrane [9] or the interactions of sulfated polysaccharides with immobilized enzyme targets [10]. The reaction scheme of this

two-state model is:

$$\mathrm{A} + \mathrm{R} \underset{k_{\mathrm{d1}}}{\overset{k_{\mathrm{a1}}}{\rightleftharpoons}} \mathrm{AR} \underset{k_{\mathrm{d2}}}{\overset{k_{\mathrm{a2}}}{\rightleftharpoons}} \mathrm{AR}^{*} \,. \tag{15}$$

Assigning γ_1 and γ_2 to the concentrations of the complex in particular states:

$$\gamma_1 = [\mathrm{AR}] \;, \quad \gamma_2 = \left[\mathrm{AR}^{*}\right] \;, \tag{16}$$

the corresponding kinetic equations that account for the relationships between both types of complexes and the free receptor sites can be written as:

$$\begin{aligned} \frac{\partial \gamma_2}{\partial t} &= k_{\mathrm{a2}}\gamma_1 - k_{\mathrm{d2}}\gamma_2 \\ \frac{\partial \gamma_1}{\partial t} &= k_{\mathrm{a1}}\alpha_0 \left(\beta - \gamma_1 - \gamma_2\right) - \frac{\partial \gamma_2}{\partial t} \\ &= k_{\mathrm{a1}}\alpha_0 \left(\beta - \gamma_1 - \gamma_2\right) - k_{\mathrm{d1}}\gamma_1 - k_{\mathrm{a2}}\gamma_1 + k_{\mathrm{d2}}\gamma_2 \,. \end{aligned} \tag{17}$$

As the conformational change does not influence the mass of the complex, the sensor response will be:

$$\xi/\xi_{\mathrm{S}} = \left(\gamma_1 + \gamma_2\right)/\beta \,. \tag{18}$$

Models of parallel pseudo first-order reactions consider the case when two interactions with different rate constants proceed simultaneously. Such situations can be attributed to different kinds of receptor sites or to different states of the analyte [8, 11]. In the first case the model can describe heterogeneity of the sensor surface; the second may concern a macromolecular analyte that can be present in various conformations, protonation states, etc. Besides two sets of rate constants, the models also require specification of proportion p between the two fractions of the receptor or analyte. For the model considering two kinds of receptors, the following equations are obtained:

$$\mathrm{A} + \mathrm{R}_1 \underset{k_{\mathrm{d1}}}{\overset{k_{\mathrm{a1}}}{\rightleftharpoons}} \mathrm{AR}_1 \quad \mathrm{A} + \mathrm{R}_2 \underset{k_{\mathrm{d2}}}{\overset{k_{\mathrm{a2}}}{\rightleftharpoons}} \mathrm{AR}_2 \tag{19}$$

$$\beta_1 = [\mathrm{R}_1] = p\beta \quad \beta_2 = [\mathrm{R}_2] = \left(1 - p\right)\beta \quad \gamma_1 = [\mathrm{AR}_1] \quad \gamma_2 = [\mathrm{AR}_2]$$

$$\frac{\mathrm{d}\gamma_1}{\mathrm{d}t} = k_{\mathrm{a1}}\alpha_0 \left(\beta_1 - \gamma_1\right) - k_{\mathrm{d1}}\gamma_1 \quad \frac{\mathrm{d}\gamma_2}{\mathrm{d}t} = k_{\mathrm{a2}}\alpha_0 \left(\beta_2 - \gamma_2\right) - k_{\mathrm{d2}}\gamma_2 \tag{20}$$

$$\xi/\xi_{\mathrm{S}} = \left(\gamma_1 + \gamma_2\right)/\beta \,.$$

Results of this model are illustrated in Fig. 4. For the case with two states of the analyte, the equations are analogous to the previous ones except that the

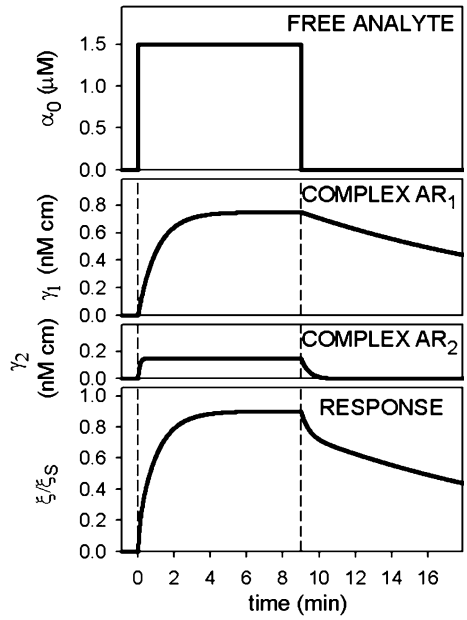

Fig. 4 Kinetics and sensorgram according to the model of two parallel pseudo first-order reactions attributed to two kinds of receptors (Eq. 19). Parameters: $\alpha_0 = 1.5\ \mu M$, $\beta = 1\ nM\ cm$, $p = 0.8$, $k_{a1} = 10^4\ M^{-1}\ s^{-1}$, $k_{d1} = 0.001\ s^{-1}$, $k_{a2} = 8 \times 10^4\ M^{-1}\ s^{-1}$, $k_{d2} = 0.04\ s^{-1}$

effect of competition for the receptor sites must be included:

$$A_1 + R \underset{k_{d1}}{\overset{k_{a1}}{\rightleftharpoons}} A_1R \quad A_2 + R \underset{k_{d2}}{\overset{k_{a2}}{\rightleftharpoons}} A_2R \tag{21}$$

$$\alpha_1 = [A_1] = p\alpha_0 \quad \alpha_2 = [A_2] = (1-p)\,\alpha_0 \quad \gamma_1 = [A_1R] \quad \gamma_2 = [A_2R]$$

$$\frac{d\gamma_1}{dt} = k_{a1}\alpha_1\left(\beta - \gamma_1 - \gamma_2\right) - k_{d1}\gamma_1 \quad \frac{d\gamma_2}{dt} = k_{a2}\alpha_2\left(\beta - \gamma_1 - \gamma_2\right) - k_{d2}\gamma_2 \tag{22}$$

$$\xi/\xi_S = \left(\gamma_1 + \gamma_2\right)/\beta\,.$$

Equations 22 can also be employed in the case of two different analytes, although the last relationship for calculating the sensor response must be modified to account for the different masses of the analytes.

Multivalent receptor binding is a case when a single receptor molecule can bind more than one molecule of analyte. Multivalent binding capacity is a frequent feature of many biomolecular systems, for instance antibodies. Another example is the formation of triplexes by oligonucleotides. If a purine oligonucleotide is fixed at the sensor surface as a receptor, a complementary oligonucleotide can bind to it and to create a duplex. In special cases, another oligonucleotide molecule may bind to the duplex and form a triplex.

This situation involves two successive reactions, each occurring at a unique binding site. The corresponding kinetic equations are:

$$\mathrm{A} + \mathrm{R} \underset{k_{\mathrm{d1}}}{\overset{k_{\mathrm{a1}}}{\rightleftharpoons}} \mathrm{AR} \quad \mathrm{AR} + \mathrm{A} \underset{k_{\mathrm{d2}}}{\overset{k_{\mathrm{a2}}}{\rightleftharpoons}} \mathrm{ARA} \tag{23}$$

$$\gamma_1 = [\mathrm{AR}] \quad \gamma_2 = [\mathrm{ARA}]$$

$$\frac{\partial \gamma_2}{\partial t} = k_{\mathrm{a2}} \alpha_0 \gamma_1 - k_{\mathrm{d2}} \gamma_2 \tag{24}$$

$$\begin{aligned} \frac{\partial \gamma_1}{\partial t} &= k_{\mathrm{a1}} \alpha_0 \left(\beta - \gamma_1 - \gamma_2\right) - k_{\mathrm{d1}} \gamma_1 - \frac{\partial \gamma_2}{\partial t} \\ &= k_{\mathrm{a1}} \alpha_0 \left(\beta - \gamma_1 - \gamma_2\right) - k_{\mathrm{d1}} \gamma_1 - k_{\mathrm{a2}} \alpha_0 \gamma_1 + k_{\mathrm{d2}} \gamma_2 \end{aligned}$$

$$\xi / \xi_{\mathrm{S}} = \left(\gamma_1 + 2\gamma_2\right) / \beta \, .$$

Here the standard sensor response is assumed to be the case when all receptors are bound in 1 : 1 complexes (duplexes). That is why the relative response can exceed 1, as is seen in Fig. 5.

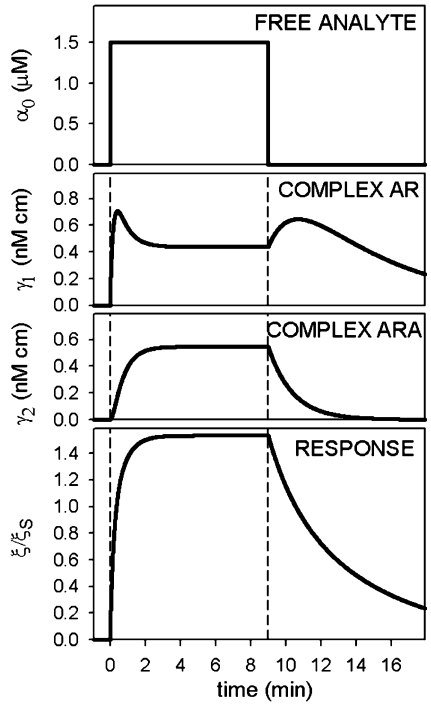

Fig. 5 Kinetics and sensorgram according to the model of consecutive two binding reactions in case of bivalent receptor (Eq. 23). Parameters: $\alpha_0 = 1.5$ μM, $\beta = 1$ nM cm, $k_{\mathrm{a1}} = 6 \times 10^4$ M^{-1} s^{-1}, $k_{\mathrm{d1}} = 0.003$ s^{-1}, $k_{\mathrm{a2}} = 10^4$ M^{-1} s^{-1}, $k_{\mathrm{d2}} = 0.012$ s^{-1}

Binding of a multivalent analyte occurs when a single analyte molecule can simultaneously occupy more than one receptor molecule. This case does not mirror the previous one, because the resulting analyte/receptor interaction strongly depends on the receptor distribution on the sensor surface. For sufficiently sparse receptor spacing, only a single binding mode is available despite the number of analyte binding sites – once the analyte is caught by a receptor, it is isolated from other distant receptors. Increasing the receptor density increases the probability of forming a receptor pattern that allows an analyte to bind multiple receptors. In [12] the authors introduced the concept of dividing the active sensor layer into spheres with a radius equal to the functional distance between the two binding sites of the analyte. Using Poisson statistics they estimated the portion p of those receptors (R_C) that were at least by two inside one sphere. Remaining receptors (R_S) were expected to be single within a sphere. The kinetic model considered simple 1 : 1 binding on R_S receptors and consecutive binding on R_C receptors:

$$\mathrm{A} + \mathrm{R_S} \underset{k_d}{\overset{k_a}{\rightleftharpoons}} \mathrm{AR_S} \quad \mathrm{A} + \mathrm{R_C} \underset{k_d}{\overset{k_a}{\rightleftharpoons}} \mathrm{AR_C} \quad \mathrm{AR_C} + \mathrm{R_C} \underset{k_d}{\overset{k_a}{\rightleftharpoons}} \mathrm{AR_CR_C}\,. \tag{25}$$

Assuming the same rate constants for both binding sites on the analyte, the following set of equations is obtained:

$$\begin{aligned}
&\beta_1 = [\mathrm{R_S}] = (1-p)\,\beta \quad \beta_2 = [\mathrm{R_C}] = p\beta \\
&\gamma_1 = [\mathrm{AR_S}] \quad \gamma_2 = [\mathrm{AR_C}] \quad \gamma_3 = [\mathrm{AR_CR_C}] \\
&\frac{\partial \gamma_1}{\partial t} = 2k_a\alpha_0\left(\beta_1 - \gamma_1\right) - k_d\gamma_1 \quad \frac{\partial \gamma_2}{\partial t} = 2k_a\alpha_0\left(\beta_2 - \gamma_2 - 2\gamma_3\right) - k_d\gamma_2 - \frac{\partial \gamma_3}{\partial t} \\
&\frac{\partial \gamma_3}{\partial t} = k_a\gamma_2\frac{\beta_2 - \gamma_2 - 2\gamma_3}{\beta_2}\frac{1}{V_{sp}N_A} - 2k_d\gamma_3 \\
&\xi/\xi_S = \left(\gamma_1 + \gamma_2 + 2\gamma_3\right)/\beta\,.
\end{aligned} \tag{26}$$

Note that a factor of 2 appears in the kinetic equations to account for the doubled probability because of two binding sites on the analyte. In the equation for $\frac{\partial \gamma_3}{\partial t}$, the fraction $\frac{\beta_2-\gamma_2-2\gamma_3}{\beta_2}$ is the probability that there is a free receptor inside the sphere where the AR_C complex occurs. The second fraction, $\frac{1}{V_{sp}N_A}$, where V_{sp} is the sphere volume and N_A is Avogadro's number, represents the concentration of the available analyte – one molecule in the V_{sp} sphere. It has been demonstrated in [12] that this model fits experimental data substantially better than a solvent kinetic model of multiple binding, which does not respect the fixed positions of the receptors.

At the end of this section it is worth mentioning that besides SPR studies where the analyte binding to the receptor is the only running interaction, competitive SPR biosensor experiments with two concurrent interactions,

i.e., analyte-immobilized receptor and analyte-another ligand in solution, can also be performed. Proper kinetic models for competitive SPR studies should be developed based on the appropriate kinetic equations for the particular interactions, using an approach analogous to the aforementioned cases.

2.3 Thermodynamic Context of Equilibrium and Kinetic Constants

The equilibrium association constant K is directly related to the change of the molar Gibbs energy attributed to complex formation ΔG^0:

$$\Delta G^0 = -RT \ln \left(K_a C^0\right) , \tag{27}$$

where R is the universal gas constant, T is the absolute temperature, and C^0 is a standard concentration – as a rule its value is taken as 1 M. The basic temperature dependence of ΔG is given by the van't Hoff equation:

$$\Delta G = \Delta H - T\Delta S , \tag{28}$$

where ΔH and ΔS are the changes of enthalpy and of entropy. If they are both temperature independent, a plot of $\ln \left(K_a C^0\right)$ versus $1/T$ (van't Hoff plot) should be linear. The ΔH and ΔS values can be determined directly from the graph; more precise is a least square fit of Eqs. 27 and 28.

The simple van't Hoff equation (Eq. 28) is not completely correct if the complex formation results in a change of the specific heat capacity ΔC_p, in which case neither ΔH nor ΔS are exactly independent of temperature. A more precise form of the van't Hoff equation is [13]:

$$\Delta G\left(T\right) = \Delta H_{To} - T\Delta S_{To} + \Delta C_p \left(T - T_0\right) + \Delta C_p T \ln \left(\frac{T}{T_0}\right) , \tag{29}$$

where T_0 is a reference temperature. To obtain reliable values of ΔH_{To}, ΔS_{To}, and ΔC_p (T_0 is defined, usually $T_0 = 298.15$ K, i.e., 25 °C), precise data over a wider range of temperatures are necessary for the fit. Estimation of any of the thermodynamic parameters from another experiment is very helpful.

The temperature dependence of k_a and k_d is usually characterized by means of activation energy (E_a^{act} and E_d^{act}) according to the Arrhenius equation:

$$\ln k = \ln P - \frac{E^{act}}{RT} , \tag{30}$$

where P is a constant known as the pre-exponential factor. The activation energy is assumed to be a measure of the amount of thermal energy required for binding or dissociation. Because E_a^{act} and E_d^{act} can be considered as activation enthalpies, the reaction enthalpy can be calculated from the relationship:

$$\Delta H = E_a^{act} - E_d^{act} . \tag{31}$$

An unusually high E^{act} value indicates that binding and/or dissociation requires the surmounting of high potential energy barriers, suggesting that conformational rearrangements are required.

When possible, the kinetic rate constants determined using SPR sensors have been compared to those obtained in bulk solution using other methods. Good agreement was obtained only in some cases. For instance, it has been reported [14] that when a study of the interactions between small inhibitor molecules and immobilized proteins was carefully designed, performed, and analyzed, very good agreement with the bulk data was achieved.

The basic formula for the association rate constant is given by Debye–Smoluchowski theory:

$$k_a = 4\pi\varphi\varepsilon r \left(D_A + D_R\right) N_A/1000 \,, \tag{32}$$

where φ is a steric interaction factor, ε is an electrostatic interaction factor, r is an interaction radius. D_A and D_R are translation diffusion coefficients of the analyte and the receptor molecule.

Let us consider the term of the translation diffusion. The diffusion coefficient D expresses the ability of a molecule to change its position in solution due to chaotic translation motion. Basic evaluation of the diffusion coefficient can be obtained from the Stokes formula for a sphere in a fluid:

$$D = \frac{k_B T}{6\pi a \eta} \,, \tag{33}$$

where k_B is the Boltzmann constant, T is the absolute temperature, η is the viscosity of the fluid and a is the radius of the sphere approximating the molecule size. Therefore, the diffusion coefficient decreases strongly with increasing size of the molecule. In contrast to the case of both interaction partners in solution, the translation diffusion of the receptor is limited when it is immobilized at the sensor surface. The value inside the parentheses in Eq. 32 may then be reduced and approximated as close to the D_A term alone. The final effect of immobilization on the translation diffusion term would depend on the ratio between D_A and D_R. If the receptor is a large molecule like protein and the analyte is a small molecule like the inhibitors used in the experiments reported in [14], then $D_A \approx (D_A + D_R)$ and the association and dissociation rate constants may be very close for both the SPR biosensor and for reactions in the bulk. On the other hand, a small receptor interacting with a large analyte may be characterized by rate constants significantly different from those measured in the bulk.

To conclude this section we summarize that, in general, the kinetic rate constants obtained from SPR sensors may not agree with those obtained in solution. The SPR technique seems to be better suited to performing comparative studies of molecules according their affinity and other interaction characteristics. However, improvements in the precision of SPR measurements and of their theoretical description may soon lead to new approaches for ex-

tracting fundamental information about biomolecular interactions using SPR sensors with receptors with varying degrees of restricted mobility.

3 Mass Transport Effects

In SPR biosensors, the rate of biomolecular interactions at the surface depends on the free analyte transport toward (association stage) or away from (dissociation stage) the active zone. The stepwise free analyte concentration changes discussed above are only an idealization, because the free analyte transport is always limited. The influence of analyte transport on the reactions at the sensor surface is given by comparing the transport throughput to the kinetic rates. Slow analyte transport causes a decrease in its concentration when it is consumed during the association phase and an increase when it is produced during the dissociation phase. As a result, both reactions are slowed down.

This effect is illustrated in Fig. 6 where the kinetics of a simple pseudo first-order reaction are calculated assuming that analyte transport is propor-

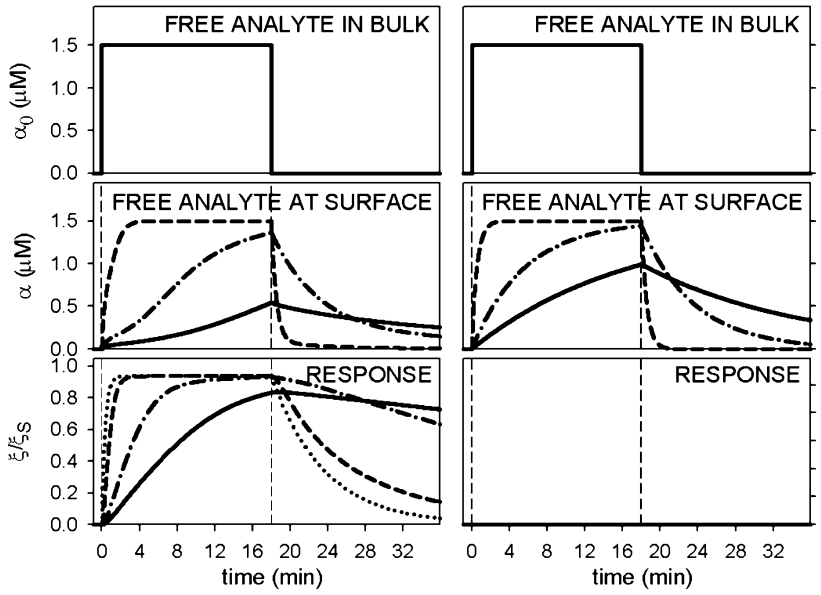

Fig. 6 Free analyte concentrations in the active layer and sensorgrams for the pseudo first-order reaction and two-compartment model of the analyte transport. Parameters: α_0 = 1.5 μM, β = 1 nM cm. *Left* $k_a = 0.03\ M^{-1}\ s^{-1}$, $k_d = 0.003\ s^{-1}$; *right* no binding of analyte to receptor. Rate constant of the analyte diffusion flux (Eq. 32) $k_M/h_{layer} = 3 \times 10^{-5}\ s^{-1}\ cm^{-1}$ (*dashed line*), $3 \times 10^{-6}\ s^{-1}\ cm^{-1}$ (*dash-and-dot*), and $10^{-6}\ s^{-1}\ cm^{-1}$ (*solid*). *Dotted line* no limitations of the analyte transport

tional to the concentration difference between the bulk analyte solution and the active sensor layer (two-compartment model, discussed in greater detail later). In addition to the effect on analyte binding kinetics, the figure also clearly illustrates that the reaction between the receptor and analyte influences, i.e., significantly reduces the free analyte concentration. If the reaction does not occur (right-hand figures), the free analyte concentration reaches its equilibrium value more rapidly.

3.1 Analyte Transport in a Flow Cell

The flow cell shape is typically rectangular with its length l (dimension along the flow) and width w (dimension perpendicular to the flow and parallel to the sensor surface) in the range 10^{-0}–10^{-2} cm, and a substantially lower height h (dimension perpendicular to the sensor surface) measuring 10^{-2}–10^{-3} cm. Flow characteristics can be described by the Reynolds number:

$$\mathrm{Re} = \frac{\rho \Phi}{\eta h} , \tag{34}$$

where ρ and η are the density and viscosity of the fluid, and Φ is the flow rate (volume of fluid passing through the cell per unit time interval). The flow is expected to be laminar (without turbulence) if $\mathrm{Re} < 2100$ [15]. For water at 20 °C, $\mathrm{Re} = (\Phi/h) \cdot 0.998\ \mathrm{mm^2\ s^{-1}}$. Considering typical flow cell dimensions and flow rates, the Reynolds number does not exceed several hundreds. The distance between the active sensor surface and both the inlet and outlet is as a rule far enough that the laminar flow profile is fully developed in the active sensor region [16]. The velocity profile is therefore considered as constant over the sensor active zone.

Let us introduce spatial coordinates in the flow-cell interior: x in direction of the length, y in direction of the height, and z in direction of the width. The magnitude of the velocity (its direction is uniformly parallel to the x-axis) depends mainly on y. The velocity profile is parabolic, with the maximum velocity $v_{\max}$ at the mid-point of the cell height and zero velocity at the cell walls. In contrast, the velocity dependence on z is negligible (except for the regions very close to the cell walls, which are sufficiently far from the active region) [17]. The total fluid flux through the flow cell can thus be obtained by integrating over the y coordinate from zero to h. This provides a relation between $v_{\max}$, the cell dimensions, and Φ:

$$v_{\max} = \frac{3}{2} \frac{\Phi}{hw} . \tag{35}$$

Similarly to the flow velocity, other parameters characterizing analyte transport are also constant in the z-direction. This allows us to reduce the transport problem to two spatial dimensions described by the coordinates x and y.

The actual analyte concentration, which is of course no longer constant, is then described as a function of these two coordinates, $\alpha = \alpha\left(x, y, t\right)$. The time dependence of the analyte concentration is given by the continuity equation. If no transport mechanism other than the laminar flow is considered, a partial differential equation is obtained:

$$\frac{\partial\alpha\left(x,y,t\right)}{\partial t} = -\,v\left(y\right)\frac{\partial\alpha\left(x,y,t\right)}{\partial x} = -\,4v_{\max}\frac{y}{h}\left(1-\frac{y}{h}\right)\frac{\partial\alpha\left(x,y,t\right)}{\partial x}\,. \tag{36}$$

To model the effect of an analyte injection, the equation has to be solved for an initial condition of zero analyte concentration inside the flow cell at $t = 0$ and a boundary condition of analyte concentration α_0 at the entrance of the flow cell $\alpha\left(0, y, t\right) = \alpha_0$. Results are shown in Fig. 7. It can be seen that for the central part of the vertical profile the injected analyte concentration α_0 is achieved relatively rapidly (depending on the flow rate), but the analyte concentrations remains zero in close proximity of the cell walls. This is a direct consequence of laminar flow – analyte transport to the active surface layer by laminar flow alone is very ineffective.

The other transport mechanism, i.e., translational diffusion of the analyte, becomes therefore highly important in the vicinity of the active sensor layer. Translational diffusion is a mechanism that leads to concentration uniformity in non-mixed solutions. It is described by the first Fick's law that states proportionality between the rate of diffusion and the concentration gradient.

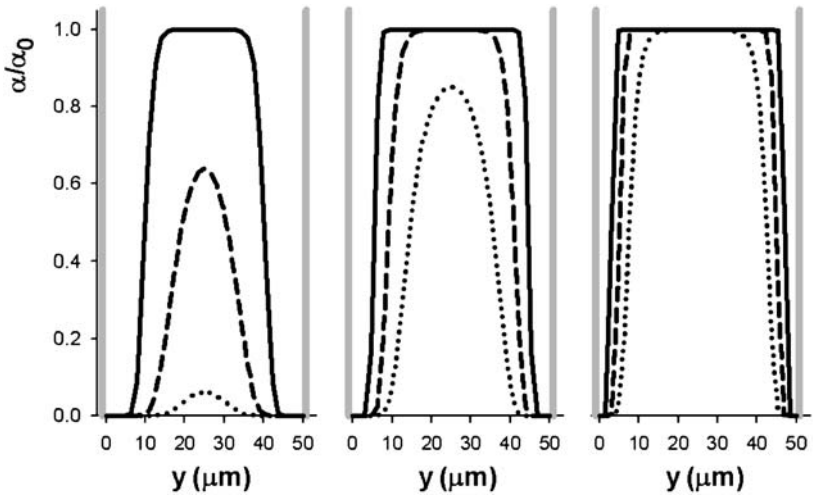

Fig. 7 Analyte concentration in a flow cell at 10 mm distance from the injection entrance reached 3 s (*dotted line*), 6 s (*dashed*), and 15 s (*solid*) after beginning of the injection as a consequence of pure laminar flow (diffusion not considered). Flow rates were 10 μL min^{-1} (*left*), 30 μL min^{-1} (*middle*), and 90 μL min^{-1} (*right*). Cell dimensions: 20 mm (length) × 2.7 mm (width) × 0.05 mm (height)

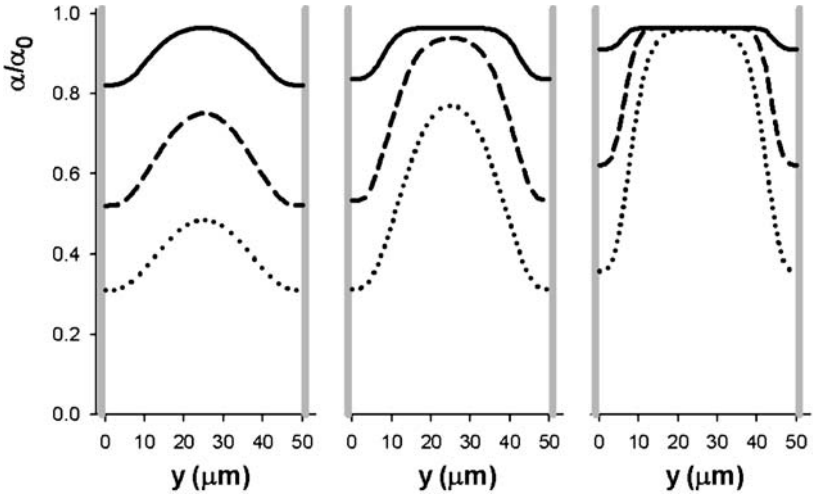

Fig. 8 Analyte concentration in a flow cell at 10 mm distance from the injection entrance reached 3 s (*dotted line*), 6 s (*dashed*), and 15 s (*solid*) after beginning of the injection as a consequence of laminar flow and diffusion. Flow rates were 10 μL min^{-1} (*left*), 30 μL min^{-1} (*middle*), and 90 μL min^{-1} (*right*), diffusion coefficient 10^{-6} cm^2 s^{-1}. Cell dimensions: 20 mm (length) × 2.7 mm (width) × 0.05 mm (height)

The proportionality constant D is called the diffusion coefficient and quantifies the chaotic translation motion of the molecules in solution. Its basic evaluation is given by the Stokes formula (Eq. 33). The diffusion coefficient decreases as the size of the molecule increases. For typical biomolecules in aqueous medium, D is usually between 10^{-7} cm^2 s^{-1} and 10^{-6} cm^2 s^{-1}. Temperature dependence of the diffusion coefficient follows T/η, where T is absolute temperature and η viscosity of the solvent, unless the temperature change does not alter the molecular shape.

If the translation diffusion is taken into account, the equation of the analyte transport will become:

$$\frac{\partial\alpha\left(x,y,t\right)}{\partial t} = D\left(\frac{\partial^2\alpha\left(x,y,t\right)}{\partial x^2} + \frac{\partial^2\alpha\left(x,y,t\right)}{\partial y^2}\right) - 4v_{\max}\frac{y}{h}\left(1-\frac{y}{h}\right)\frac{\partial\alpha\left(x,y,t\right)}{\partial x}\,. \tag{37}$$

The effect of diffusion on the analyte distribution is shown in Fig. 8, where Eq. 37 was solved using the same boundary conditions that were applied to Eq. 35 to generate Fig. 7. Note the significant increase in analyte concentration near the cell walls, thanks to diffusion.

3.2
Full Model of Mass Transport

A rigorous approach to modeling the reaction kinetics at the sensor surface, including the mass transport effects, requires solving the fundamental par-

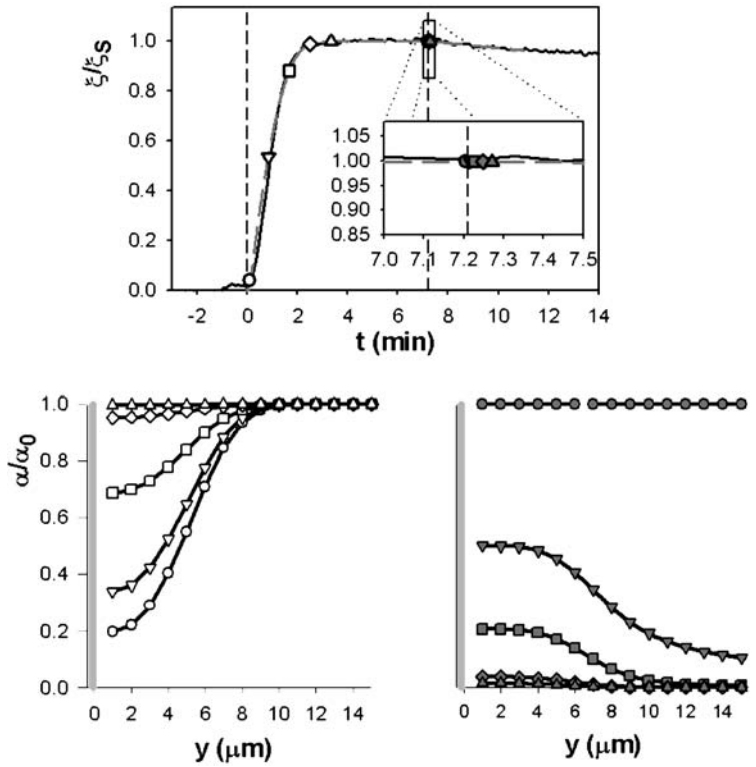

Fig. 9 Results of the full model of the analyte transport coupled to pseudo first-order reaction kinetics. The model fitted to experimental sensorgram of DNA 23-mer binding to its immobilized complementary DNA chain. The experimental sensorgram (*upper graph, black solid line* with the association and dissociation periods indicated by *vertical dashed lines*) is very well fitted by the theoretical course of the relative sensor response (*gray long dashes*). The *graphs below* show the free analyte concentration in the close vicinity of the active sensor layer as it is distributed 6, 50, 100, 150, and 200 s after the injection (on the *left*, from the *bottom up*) and 0, 0.5, 1.12, 2.4, and 3.75 s after stopping the injection (on the *right*, from the *top down*). The times corresponding to particular concentration profiles are indicated in the *upper graph* by same *graphical symbols*. In the case of the dissociation phase they can be resolved only after expansion of the time axis (*insert*). Parameters: $\alpha_0 = 10^{-7}$ M, $\beta = 1.84 \times 10^{-9}$ M cm, $\Phi = 70$ mL min^{-1}, $D = 2.5 \times 10^{-6}$ cm^2 s^{-1}, $k_a = 5.6 \times 10^5$ M^{-1} s^{-1}, $k_d = 2.5 \times 10^{-6}$ s^{-1}. The model was applied to the central part of the flow cell (*xy* coordinates corresponding to the active zone of the sensor) with dimensions of 2.5 mm × 2.7 mm × 0.04 mm

tial differential (Eq. 37, PDE) coupled with the relevant kinetic equations. The coupling is twofold. First, we have to apply the actual analyte concentration at the given point on the sensor surface. As this value varies along the x-coordinate, the concentration of analyte/receptor complexes can no longer be considered as only time dependent – it must be described as a function of t and x: $\gamma = \gamma(x, t)$. The kinetic equations need to be modified accordingly; for instance, the equation of simple first-order kinetics (Eq. 12) is modified as follows:

$$\frac{\mathrm{d}\gamma(x,t)}{\mathrm{d}t} = k_\mathrm{a}\alpha(x,0,t)\,[\beta - \gamma(x,t)] - k_\mathrm{d}\gamma(x,t)\,. \tag{38}$$

Secondly, we have to introduce the consumption or production of the free analyte due to the interaction with receptors to the PDE. It is usually performed [18–20] via a specific boundary condition that in the case of single reaction kinetics is:

$$D\frac{\partial\alpha(x,0,t)}{\partial y} = \frac{\partial\gamma(x,t)}{\partial t}\,. \tag{39}$$

For more complex reaction kinetics the right side of the equation must comprise all kinds of complexes (the formation of which requires consumption of the analyte) multiplied by respective stoichiometric factors. Analogously to Eq. 39, a boundary condition of:

$$\frac{\partial\alpha(x,h,t)}{\partial y} = 0 \tag{40}$$

is introduced for the flow-cell wall opposite to the sensor surface.

Equation Eq. 37 can be solved only numerically. Most often a finite element method with various grids in the xy region of the flow cell is employed [18], but other approaches have also been tested [19]. An illustration of the full model results is given in Fig. 9.

The enormously time-consuming nature of full model calculations prevents this approach from being used for complete fits of experimental data. As a rule, it is employed to verify simpler models and/or to confirm the reasonability of rate constants by comparison with experimental data. To enable more convenient and routine analysis of measured sensorgrams, simpler models of mass transport effects have been derived.

3.3 Simplified Models of Mass Transport

The first simplification of Eq. 37 is based on the assumption that the analyte transport in the x direction is mainly conductive, i.e., it is controlled by the flow in the cell. The relation between conductive transport and diffusion in y direction is often characterized by the Peclét number, which reflects the ratio of the ideal time required for an analyte molecule to diffuse from the cell

middle ($y = h/2$) to the cell wall, to the minimal time required for that same molecule to pass through the cell by the laminar flow:

$$\mathrm{Pe} = \frac{v_{\max} h^2}{Dl} \,. \tag{41}$$

If the Peclét number is high compared to 1 ($\mathrm{Pe} \gg 1$), Eq. 37 can be simplified by omitting the diffusion term in the x direction and by linearizing the flow velocity dependence on y, because we can limit calculations of the analyte concentration to a region close to the sensor surface ($y \ll h$) [20–22]. We find:

$$\frac{\partial \alpha\left(x,y,t\right)}{\partial t} = D\frac{\partial^2 \alpha\left(x,y,t\right)}{\partial y^2} - 4v_{\max}\frac{y}{h}\frac{\partial \alpha\left(x,y,t\right)}{\partial x} \,. \tag{42}$$

For a pseudo first-order analyte-to-receptor reaction this equation coupled with the reaction kinetics Eq. 38 via Eq. 39 can be solved so that an equation for only $\gamma(x,t)$ is obtained:

$$\begin{aligned}\frac{\partial \gamma(x,t)}{\partial t} = {} & k_\mathrm{a}\alpha_0\left[\beta - \gamma(x,t)\right] \\ & \times \left[1 - \frac{Fh}{\alpha_0 Dl \mathrm{Pe}^{1/3}} \int_0^x \frac{\partial \gamma(u,t)}{\partial t}(x-u)^{2/3}\mathrm{d}u\right] - k_\mathrm{d}\gamma(x,t)\end{aligned} \tag{43}$$

$$F = \frac{1}{12^{1/3}\Gamma(2/3)} \approx 0.32256 \,.$$

Equation 43, which is much easier to solve than the full model, can be further simplified in order to eliminate the integral term. This approximation can be applied when the dependence of $\frac{\partial \gamma(x,t)}{\partial t}$ on x is rather weak and can be assumed to be linear. This linearization allows the integral term to be evaluated explicitly. The result can be written formally in a form analogous to the original kinetic equation (Eq. 12):

$$\frac{\mathrm{d}\gamma(x,t)}{\mathrm{d}t} = k_\mathrm{a}^\mathrm{ef}(x,t)\alpha_0\left[\beta - \gamma(x,t)\right] - k_\mathrm{d}^\mathrm{ef}(x,t)\gamma(x,t) \,, \tag{44}$$

where the "effective" rate constants, however, are both space- and time-dependent:

$$k_\mathrm{a}^\mathrm{ef} = \frac{k_\mathrm{a}}{1 + k_\mathrm{a}\left[\beta - \gamma(x,t)\right]/k_\mathrm{M}(x)} \quad k_\mathrm{d}^\mathrm{ef} = \frac{k_\mathrm{d}}{1 + k_\mathrm{a}\left[\beta - \gamma(x,t)\right]/k_\mathrm{M}(x)} \tag{45}$$

$$k_\mathrm{M}(x) \approx 1.034\left(\frac{v_{\max} D^2}{hx}\right)^{1/3} \,.$$

Thanks to the previously applied assumption that $\gamma(x,t)$ is linearly dependent on x, it is also possible to integrate it over the active sensor region. As a result, we obtain equations analogous to Eq. 44, where $\gamma(x,t)$ is replaced by the

average concentration of complexes $\langle\gamma\rangle(t)$:

$$\frac{\mathrm{d}\langle\gamma\rangle(t)}{\mathrm{d}t} = k_{\mathrm{a}}^{\mathrm{ef}}(t)\alpha_0\left[\beta - \langle\gamma\rangle(t)\right] - k_{\mathrm{d}}^{\mathrm{ef}}(t)\langle\gamma\rangle(t)$$
$$k_{\mathrm{a}}^{\mathrm{ef}} = \frac{k_{\mathrm{a}}}{1 + k_{\mathrm{a}}\left[\beta - \langle\gamma\rangle(t)\right]/k_{\mathrm{M}}} \quad k_{\mathrm{d}}^{\mathrm{ef}} = \frac{k_{\mathrm{d}}}{1 + k_{\mathrm{a}}\left[\beta - \langle\gamma\rangle(t)\right]/k_{\mathrm{M}}} \tag{46}$$
$$k_{\mathrm{M}} \approx 1.378\left(\frac{\nu_{\max}D^2}{hl}\right)^{1/3}.$$

Equations 46 have been directly derived from the full model in [19]. On the other hand, they are almost identical with the relations obtained from the so-called two-compartment model (the only difference is that the numerical coefficient k_{M} is a little bit lower). The two-compartment model was first developed for sensors with receptors placed on small spheres [23]. In [24–26] it was adapted for the SPR flow cell and in [18] it was approved and verified by comparison of numerical results with those obtained from the full model. The two-compartment model approximates the analyte distribution in the vicinity of the receptors by considering two distinct regions. The first is a thin layer around the active receptor zone of effective thickness h_{layer}, and the second is the remaining volume with the analyte concentration equal to the injected one, i.e., α_0. While the analyte concentration in the bulk is constant (within a given compartment), analyte transport to the inner compartment is controlled by diffusion. The actual analyte concentration at the sensor surface is then given by the difference between the diffusion flow and the consumption/production of the analyte via interaction with receptors. For the simple pseudo first-order interaction model we obtain:

$$\frac{\mathrm{d}\alpha}{\mathrm{d}t} = \frac{1}{h_{\mathrm{layer}}}\left[k_{\mathrm{M}}\left(\alpha_0 - \alpha\right) - \frac{\mathrm{d}\gamma}{\mathrm{d}t}\right]. \tag{47}$$

The constant k_{M} can be approximated as [22, 27]:

$$k_{\mathrm{M}} \approx 1.282\left(\frac{\nu_{\max}D^2}{hl}\right)^{1/3}. \tag{48}$$

For a quasi-steady-state approximation where $\frac{\mathrm{d}\alpha}{\mathrm{d}t}$ is set to zero in Eq. 47, equations analogous to Eq. 46 are obtained from Eqs. 12 and 47.

The k_{M} value can be considered as a measure of the mass transport. Its effect on the SPR response can be evaluated by the maximal difference of the denominator in Eq. 46 from unity [16]. It is equal to the ratio of the reaction velocity to the diffusion flux of the analyte at the beginning of the association stage:

$$\mathrm{denom.}_{\max} - 1 = \frac{k_{\mathrm{a}}\beta}{k_{\mathrm{M}}} \approx 0.780 \quad k_{\mathrm{a}}\beta\left(\frac{\nu_{\max}D^2}{hl}\right)^{-1/3}. \tag{49}$$

This ratio (excluding the numerical constants) is called Damköhler number (Da):

$$\mathrm{Da} = k_a \beta \left(\frac{v_{max} D^2}{hl} \right)^{-1/3} = \frac{k_a \beta h}{D \sqrt[3]{\mathrm{Pe}}} . \tag{50}$$

For small Damköhler numbers (Da $\ll$ 1) the mass transport is much faster than the surface reaction itself and therefore the mass transport effect may be ignored. On the other hand, if the Damköhler number is high (Da $\gg$ 1) the sensorgram profile is completely controlled by the diffusion mass transfer and is it not possible to determine rate constants of the surface reaction.

All of the transport models presented so far assume that the diffusion mobility of the analyte in the active sensor zone is the same as in the bulk. In case of the sensors using a thick skeleton to fix the receptors, such as a dextran matrix, solgel, or MIPs, it might be useful to take into account varying analyte diffusion mobility inside the active sensor layer. Detail analysis and proposed models can be found in [28].

4 Summary

A constant and homogeneous concentration of free analyte represents the ideal condition for modeling molecular interactions at the surface of an SPR biosensor. In the most frequent case where an analyte binds to an immobilized receptor with 1 : 1 stoichiometry, the interaction follows the pseudo first-order kinetic model. Adequate interaction models can be built up to describe more complex molecular interactions; some of them have been presented and explained above.

The effect of mass transport on molecular binding in the SPR sensor active layer can be evaluated by means of the Damköhler number (Eq. 50). Except for cases of a very low Damköhler number, mass transport has to be regarded in theoretical models by means of the aforementioned equations.

References

1. Ward LD, Winzor DJ (2000) Anal Biochem 285:179
2. de Mol NJ, Plomp E, Fischer MJE, Ruijtenbeek R (2000) Anal Biochem 279:61
3. Fisher RD, Wang B, Alam SL, Higginson DS, Robinson H, Sundquist WI, Hill CP (2003) J Biol Chem 278:28976
4. McDonnell JM (2001) Curr Opin Chem Biol 5:572
5. Oshannessy DJ, Brighamburke M, Soneson KK, Hensley P, Brooks I (1993) Anal Biochem 212:457
6. Rich RL, Myszka DG (2005) J Mol Recog 18:431
7. Rich RL, Myszka DG (2005) J Mol Recog 18:1

8. Morton TA, Myszka DG (1998) Methods Enzymol: Energetics of biological macromolecules, Pt B 295:268
9. Kamimori H, Unabia S, Thomas WG, Aguilar MI (2005) Anal Sci 21:171
10. Shen BJ, Shimmon S, Smith MM, Ghosh P (2003) J Pharm Biomed Anal 31:83
11. Karlsson R, Falt A (1997) J Immunol Methods 200:121
12. Muller KM, Arndt KM, Pluckthun A (1998) Anal Biochem 261:149
13. Yoo SH, Lewis MS (1995) Biochemistry 34:632
14. Day YSN, Baird CL, Rich RL, Myszka DG (2002) Protein Sci 11:1017
15. Bird RB, Stewart WE, Lightfoot EE (2002) Transport phenomena. Wiley, New York
16. Edwards DA (2000) Stud Appl Math 105:1
17. Brody JP, Yager P, Goldstein RE, Austin RH (1996) Biophys J 71:3430
18. Myszka DG, He X, Dembo M, Morton TA, Goldstein B (1998) Biophys J 75:583
19. Mason T, Pineda AR, Wofsy C, Goldstein B (1999) Math Biosci 159:123
20. Edwards DA (1999) IMA J Appl Math 63:89
21. Edwards DA, Goldstein B, Cohen DS (1999) J Math Biol 39:533
22. Lok BK, Cheng YL, Robertson CR (1983) J Colloid Interface Sci 91:104
23. Glaser RW (1993) Anal Biochem 213:152
24. Myszka DG, Morton TA, Doyle ML, Chaiken IM (1997) Biophys Chem 64:127
25. Schuck P, Minton AP (1996) Anal Biochem 240:262
26. Schuck P (1996) Biophys J 70:1230
27. Sjolander S, Urbaniczky C (1991) Anal Chem 63:2338
28. Edwards DA (2001) Bull Math Biol 63:301